Design of Smart Catheter Systems for the Prevention of Infection

Charnete Casimero

BSc

Faculty of Computing, Engineering and the Built Environment

of Ulster University

Thesis submitted for the degree of

Doctor of Philosophy

January 2021

I confirm that the word count of this thesis is less than 100,000 words

Contents

List of Figures IX

List of Tables XVI

Acknowledgements XVIII

Copyright / Credit Notices XX

Abstract XXII

Abbreviations XXIV

Notes on Access to Contents XXVII

Chapter 1 Introduction and Project Aims

1.1 Introduction 2

1.2 Project Aims and Objectives 5

1.3 Chapter Summaries 6

Chapter 2 Literature Review

2.1 History of Intravenous Therapy 9

2.2 Central Venous Catheters 11

2.3 Healthcare Associated Infections 14

2.4 Catheter Related Bloodstream Infection 15

2.4.1 Pathology and Risk Factors of Catheter-Related Bloodstream Infection 16

2.4.2 Biofilm 21

2.4.3 Current Practice 24

2.4.4 Preventative Measures 27

2.4.4.1 Disinfection 28

2.4.4.2 Barrier Caps 29

2.4.4.3 Catheter Material 31

2.4.4.4 Anticoagulants 34

2.4.4.5 Antiseptic Impregnated Catheters 34

2.4.4.6 Lock Solutions 37

2.5 Emerging Technologies 42

2.5.1 Reactive Oxygen Species 42

2.5.2 Enhanced Catheter Systems 45

2.6 Electrochemical Methods 47

2.6.1 pH Sensing 47

2.6.2 Inhibition of Pathogen Growth 51

2.7 Conclusions 53

Chapter 3 Experimental Details and Methodologies

3.1 Materials and Instrumentation 57

3.2 Electrochemical Instrumentation 57

3.3 Electrochemical Cells 58

3.3.1 Working Electrode 58

3.3.2 Reference Electrode 59

3.3.3 Counter Electrode 61

3.3.4 Buffer Solutions 62

3.4 Mass Transport Mechanism 62

3.4.1 Diffusion 63

3.4.2 Convection 64

3.4.3 Migration 65

3.5 Electrochemical Techniques 65

3.5.1 Cyclic Voltammetry 66

3.5.2 Square Wave Voltammetry 69

3.5.3 Amperometry 72

3.5.4 Potentiometry 73

3.6 Characterisation Methods 73

3.6.1 Scanning Electron Microscopy 74

3.6.2 X-Ray Photoelectron Spectroscopy 76

3.6.3 Raman Spectroscopy 78

3.6.4 UV-Vis Spectroscopy 80

3.7 Surface Modification 82

3.7.1 Electrochemical Anodisation 82

3.7.2 Electropolymerisation 83

Chapter 4 Effect of the Co-Application of Ultrasound and Electrochemical Anodisation on Carbon Fibre's Electroanalytical Performance

4.1 Introduction 85

4.2 Experimental Details 87

4.2.1 Materials 87

4.2.2 Electrode Design 87

4.2.3 Electrochemical Configuration 88

4.2.4 XPS 88

4.2.5 Raman 89

4.3 Results and Discussion 89

4.3.1 Preliminary Electrochemical Assessment 89

4.3.2 Raman Spectroscopy Examination 93

4.3.3 Effect of Anodisation and Sonoanodisation on Surface Hydrophobicity 95

4.3.4 Effect of Ultrasound on Carbon Fibre Morphology 96

4.3.5 Influence of Anodisation on Carbon-Oxygen Functionalities 99

4.3.6 Carbon-Quinone Electrochemistry 102

4.4 Conclusions 104

Chapter 5 Flavin-Phenol Modified Electrode for In Situ pH Measurements

5.1 Introduction 107

5.2 Experimental Details 111

5.2.1 Materials 111

5.2.2 Electrochemical Configuration 112

5.2.3 Electrode Design and Modification 112

5.2.4 NMR Analysis 112

5.3 Results and Discussion 113

5.3.1 Characterisation of the Flavin-Phenol Moiety 113

5.3.2 Evaluation of Flavin-Modified Carbon Fibre Mesh as a pH Sensor 116

5.3.3 Challenging the Electrode's pH Sensitivity in a Microbial Reactor 119

5.4 Conclusions 123

Chapter 6 Flavin-Modified Carbon Loaded Polyethylene Film as a pH Sensitive Membrane

6.1 Introduction 125

6.2 Experimental Details 127

6.2.1 Materials 127

6.2.2 Electrochemical Configuration 127

6.2.3 Preparation and Characterisation of Modified Film 128

6.2.4 Electrode Design and Modification 130

6.2.5 Ethics Approval and Compliance 130

6.3 Results and Discussion 130

6.3.1 Electrochemical Evaluation of Flavin-Modified pH Sensitive Electrode 130

6.3.2 Mechanical Flexibility Assessment 136

6.3.3 Electroanalytical Capabilities within a Biofluid 138

6.4 Conclusions 140

Chapter 7 Integration of Riboflavin-Modified Carbon Fibre and Screen Printed Electrode Systems in Customised 3D Printed Hub

7.1 Introduction 142

7.2 Experimental Details 146

7.2.1 Materials 146

7.2.2 Electrochemical Configuration and Electrode Modification 146

7.2.3 Screen Printed Electrode Manufacture 146

7.2.4 Counter and Reference Electrode in 3D Printed Hub 147

7.2.5 Needle Free Hub Design 148

7.3 Results and Discussion – Carbon Fibre Mesh System 150

7.3.1 Electroanalytical Evaluation of Riboflavin-Modified Carbon Fibre Electrode 150

7.3.2 Assessment in TPN and Laked Horse Blood 154

7.4 Results and Discussion – Screen Printed Electrode System 157

7.4.1 Preliminary Electrochemical Characterisation 157

7.4.2 Integration within 3D Printed Catheter Hub 160

7.5 Hydrogen Peroxide 165

7.6 Conclusions 167

Chapter 8 Conclusions and Recommendations for Future Work

8.1 Conclusions 169

8.2 Recommendations for Future Work 173

References 175

Publications Resulting from this Research 217

List of Figures

Figure 1.1.1 An example of a catheter needle free hub (ICU Medical Clave™ connector) and CT scan of its internal components.

Figure 2.1.1 Typical components common to a peripheral venous catheter.

Figure 2.2.1 Types of IV catheters and typical insertion sites. Adapted from [35].

Figure 2.2.2 Seldinger Technique. Adapted from [38].

Figure 2.4.1 Potential pathogenic routes of catheter-related bloodstream infection.

Figure 2.4.2 Needle free connectors based on A) simple split septum, B) mechanical spring compression and C) blunt cannula. CT scans of the internal components of an ICU Medical Clave™ connector D) before and E) after connection to a giving set with a luer connector.

Figure 2.4.3 Biofilm life cycle. Adapted from [92].

Figure 2.4.4 Diagnosis flowchart for patients with CVC experiencing acute febrile episode. Adapted from [5]. DTP = differential time to positivity.

Figure 2.4.5 Designs of NFC barrier caps based on A) a simple foam insert, B) an encapsulating split septum and C) the ClearGuard® terminal cap.

Figure 2.4.6 A summary highlighting various research on suitable materials to prevent catheter contamination.

Figure 2.5.1 Plumbagin mechanism of action to release ROS [188].

Figure 2.6.1 Bioelectric effect - a net negative surface charge repels bacterial attachment thus prevents biofilm formation.

Figure 3.3.1 Configuration of a conventional silver/silver chloride reference electrode. Adapted from [245].

Figure 3.4.1 Simplified illustration of the diffusion pathway in an electrolytical cell. Adapted from [246].

Figure 3.4.2 Influence of mechanical convection on the transport of particles.

Figure 3.4.3 A simplified diagram of charge migration change as result of potential application.

Figure 3.5.1 Typical A) triangular waveform and B) cyclic voltammogram trace produced in cyclic voltammetry. Adapted from [245].

Figure 3.5.2 Cyclic voltammograms displaying different types of electron transfer systems.

Figure 3.5.3 Voltammetric profiles highlighting the A) staircase shape and B) resultant square wave voltammogram. Adapted from [246].

Figure 3.5.4 Common amperometric parameter profiles: A) potential and B) current as a function of time. C) Influence of time and distance to electrode surface on the concentration gradient of analyte. Adapted from [246].

Figure 3.6.1 Simplified schematic diagram of a typical scanning electron microscope. Adapted from [249].

Figure 3.6.2 Schematic diagram of photo-ionisation of an atom through XPS process. Adapted from [251].

Figure 3.6.3 A) Types of radiation and B) corresponding electron energy levels attributed to Raman spectroscopy. Adapted from [253,254].

Figure 3.6.4 A) Schematic diagram of a typical UV-Vis spectrometer. B) Possible electron jumps caused by visible light. Adapted from [256,257].

Figure 4.1.1 Summary of different oxygen functional groups present on the surface of carbon fibre generated through oxidation (adapted from [282]).

Figure 4.2.1 Carbon fibre mesh working electrode assembly.

Figure 4.3.1 Cyclic voltammograms highlighting the carbon fibre mesh electrode response after various anodisation periods without ultrasound towards A) ferrocyanide and B) ruthenium hexamine, both of which are at 2 mM concentration in 0.1 M KCl. C) Effect of anodisation time on the peak separation of ferrocyanide and ruthenium hexamine. Scan rate: 50 mV s^{-1}.

Figure 4.3.2 Influence of square root of scan rate on the anodised carbon mesh electrode response in the absence of ultrasound towards A) ferrocyanide and B) ruthenium hexamine.

Figure 4.3.3 A) Cyclic voltammograms detailing the response of a carbon fibre electrode towards ferrocyanide (2 mM, 0.1 M KCl) after anodisation with and without the application of ultrasound. B) Cyclic voltammograms highlighting the effect of prolonged sonoanodisation on the carbon mesh electrode response towards ferrocyanide. Scan rate: 50 mV/s.

Figure 4.3.4 A) Representative Raman spectra of the carbon fibre surface before and after various anodisation periods in the absence of ultrasound. B) Influence of anodisation with and without ultrasound on the degree of disorder within the carbon fibre lattice.

Figure 4.3.5 Contact angle measurements and corresponding representative images detailing the effect of anodisation, with and without the presence of ultrasound, on the surface wettability of carbon fibre.

Each bar is an average 6 measurements and error bars represent mean standard deviation.

Figure 4.3.6 Scanning electron micrographs highlighting the surface morphology of the carbon fibre A) before and after B-D) silent and F-H) ultrasound-aided anodisation. E) Comparison of carbon fibre diameter as a result of anodisation (N = 50).

Figure 4.3.7 XPS analysis of the A) C1s and B) O1s spectra before and after anodisation of carbon fibre mesh without ultrasound.

Figure 4.3.8 Summary of the net changes in carbon functionality on the carbon fibre electrode as a consequence of anodisation being conducted in the A) absence and B) presence of ultrasound. Error bars represent mean standard deviation.

Figure 4.3.9 Square wave voltammograms highlighting the carbon fibre electrode response in pH 3 BR buffer after various silent anodisation time periods.

Figure 4.3.10 Redox transition of simple quinone groups (A) and those spatially distant along the carbon lattice (B) on carbon fibre surfaces.

Figure 5.1.1 Redox transitions of the flavin unit (I→ II→I) and the electro-oxidation of the phenolic substituent leading to the production of a polyphenylene oxide polymer (I→III).

Figure 5.2.1 Summarised scheme highlighting the preparation of the custom synthesised phenolic flavin derivative.

Figure 5.3.1 A) Cyclic voltammograms comparing the response of a glassy carbon electrode towards riboflavin (red line) and the flavin-phenol derivative (black line) in pH 7 BR buffer. B) Five consecutive cyclic voltammograms detailing the electropolymerisation of flavin-phenol derivative in pH 7 BR buffer. Scan rate: 50 mV/s.

Figure 5.3.2 Cyclic voltammograms detailing the flavin-modified glassy carbon electrode response with increasing scan rate in fresh pH 7 BR buffer.

Figure 5.3.3 Variation of polyflavin peak heights with scan rate recorded on a glassy carbon electrode in pH 7 BR buffer.

Figure 5.3.4 A) Square wave voltammograms and B) corresponding linear regression calibration graph exhibiting the shift in oxidation peaks of the flavin-modified anodised carbon fibre mesh in BR buffers of various pH. Each point is an average of three scans and mean standard deviation error bars are added but too small to be observed.

Figure 5.3.5 Influence of pH on the oxidation peak potential of flavin-modified anodised carbon fibre mesh over three cycles in BR buffers of varying pH. Each pH is analysed in triplicate, totalling 63 scans, with each point on the graph representing the third scan of each cycle.

Figure 5.3.6 Square wave voltammograms comparing the response of a bare anodised carbon fibre electrode and polyflavin-modified anodised carbon fibre electrode in kefir-inoculated milk at the start and end of the fermentation cycle.

Figure 5.3.7 Comparison of pH measured between the conventional glass pH probe and the flavin-modified anodised carbon fibre mesh electrode within the kefir mixture over a period of 51 hours. Each point is the average of 3 scans.

Figure 5.3.8 Scanning electron micrographs of the carbon fibre network after incubation in kefir mixture (SU5000 FE-SEM, Hitachi, Japan).

Figure 6.1.1 Process of producing an electrically conductive carbon-loaded polyethylene film via laser etching.

Figure 6.1.2 Redox transition of the flavin unit (I→II→I) and the electro-oxidation of the phenolic substituent leading to the production of a polyphenylene oxide polymer (I→III) on exposed carbon surfaces at the carbon-polyethylene film interface.

Figure 6.2.1 Dektak surface profile of the laser-modified carbon-polyethylene film displaying the typical depth profile of areas receiving a single and double pass. Insert: photograph of the C-PE film after laser treatment.

Figure 6.2.2 Scanning electron micrographs of the carbon-polyethylene mesh after laser processing. A) Low magnification highlighting the direction of the laser raster and creation of holes within the film. B) Comparison of the laser etched track and unmodified C-PE film. C & D) Removal of the polyethylene at the pore edge as a consequence of laser double pass.

Figure 6.3.1 Cyclic voltammogram traces exhibiting the response of the anodised laser-modified carbon-polyethylene composite electrode towards the flavin-phenol derivative in pH 7 Britton Robinson buffer. Scan rate: 50 mV s^{-1}.

Figure 6.3.2 Square wave voltammograms displaying the pH sensitive response of a flavin-modified anodised C-PE mesh electrode in various pH Britton Robinson buffer solutions.

Figure 6.3.3 Corresponding calibration plot detailing the linear response between pH and peak positions over a total of 21 scans, recorded using flavin-modified anodised C-PE electrode. Each point is an average of 3 scans. Mean standard deviation error bars are included but are too small to be observed.

Figure 6.3.4 A) Variation of peak potential with pH over three consecutive pH series with each point being an average of 3 scans, B) effect of repetitive pH series cycling on the oxidation peak magnitude and C) corresponding linear regression calibration graph displaying the average peak positions for each pH, all recorded at the flavin-modified

anodised carbon-polyethylene mesh over 63 scans. Mean standard deviation bars are included but are too small to be observed.

Figure 6.3.5 Square wave voltammograms detailing the effect of 90° mechanical flexing on the analytical response of the flavin-coated anodised C-PE electrode A) after repetitive cycling and B) after fixedly bent at 90°. Scatter graphs displaying the changes in the flavin oxidation C) peak potentials and D) peak heights, attributable to repeated bending of the flavin-modified anodised C-PE electrode. Each point represents the 3rd scan.

Figure 6.3.6 Square wave voltammograms presenting the analytical signals taken from flavin-modified anodised C-PE electrode in each human urine sample. Insert: representative square wave voltammogram highlighting the broad second peak observed if potential is swept towards a more positive range.

Figure 7.1.1 Reaction scheme detailing the electrochemical redox reactions of riboflavin at the electrode and the catalysis of oxygen reduction leading to the generation of peroxide.

Figure 7.2.1 Three screen printed electrode configuration used within the customised catheter hub.

Figure 7.2.2 Representative A) potentiometric trace and B) calibration curve ($N_{electrodes}$ = 3) detailing the stability of the Ag/AgCl-modified carbon screen printed reference electrodes. Error bars represent mean standard deviation.

Figure 7.2.3 Initial design of the catheter hub extension showcasing its capability to be readily integrated with existing catheter lines.

Figure 7.2.4 External (A & C) and internal (B & D) designs of the suggested flow through catheter needle free connector.

Figure 7.2.5 Two carbon mesh electrode system assembly.

Figure 7.3.1 Cyclic voltammetry traces comparing the riboflavin (3.19 µM, pH 6.21) redox reaction at an anodised carbon fibre mesh electrode with and without solution degassing. Scan rate: 50 mV/s.

Figure 7.3.2 A) Representative square wave voltammetry scans of the physisorbed riboflavin-modified anodised carbon fibre electrode within the 3D printed hub to BR buffers of varying pH. B) Corresponding linear regression calibration line with each point of the calibration curve being an average of 5 scans and error bars represent the mean standard deviation.

Figure 7.3.3 Changes in A) peak potential and B) current magnitude of the physisorbed riboflavin-modified anodised carbon fibre electrode as a result of serial scanning in BR buffers of varying pH. C) Calibration

curve displaying the average peak potential for each pH (N_{total} = 54). Error bars represent mean standard deviation.

Figure 7.3.4 Square wave voltammograms showcasing the changes in peak potential using physisorbed riboflavin-modified anodised carbon fibre electrode: A) continuously kept in kefir-inoculated TPN, B) continuously submerged in TPN without kefir, C) periodically inserted in kefir-inoculated TPN and D) periodically placed in TPN without kefir.

Figure 7.3.5 Square wave voltammograms showcasing the changes in peak potential using physisorbed riboflavin-modified anodised carbon fibre electrode: A) continuously kept in kefir-inoculated laked horse blood, B) continuously submerged in laked horse blood without kefir, C) periodically inserted in kefir-inoculated laked horse blood and D) periodically placed in laked horse blood without kefir.

Figure 7.4.1 Cyclic voltammograms detailing the influence of scan rate on the redox processes of a physisorbed riboflavin-modified anodised screen printed electrode in pH 7 Britton Robinson buffer.

Figure 7.4.2 Variation of riboflavin peak heights as a function of scan rate recorded using physisorbed riboflavin-modified anodised carbon screen printed electrode.

Figure 7.4.3 A) Square wave voltammograms of a physisorbed riboflavin-modified anodised carbon screen printed electrode in Britton Robinson buffers of varying pH. B) Corresponding calibration curve (each point is an average of three scans) showing the effect of pH on peak potential. Mean standard deviation error bars are included but are too small to be observed.

Figure 7.4.4 A) Square wave voltammograms displaying the response of the physisorbed riboflavin-modified anodised SPE system in Britton Robinson buffers of varying pH and B) influence of pH on the oxidation peak potential over three cycles (total of 54 scans with each point representing an average of 3 scans).

Figure 7.4.5 Square wave voltammograms representing the response of physisorbed riboflavin-modified SPE and unmodified SPE in TPN (20^{th} scan).

Figure 7.4.6 Variation of A) magnitude and B) potential of the oxidation peak of the physisorbed riboflavin-modified anodised SPE as a result of repetitive square wave scans in TPN (N_{scans} = 20).

Figure 7.4.7 The effect of repetitive square wave voltammetry scanning in TPN on peak A) height and B) position of the Nafion-coated riboflavin-modified anodised screen printed electrode.

Figure 7.5.1 Simplified Fe^{3+}-xylenol orange reaction scheme in the presence of peroxide.

Figure 7.5.2 Linear relationship between hydrogen peroxide concentration and Fe(II)/Fe(III) assay absorbance (λmax = 585 nm) value. Each point is an average of 2 scans and the error bars represent mean standard deviation.

List of Tables

Table 2.1.1 A summarised version of significant events leading to current intravenous therapy. Information acquired from [23-28].

Table 2.2.1 Details of the four types of central intravenous catheters [5,31,34].

Table 2.4.1 Common biofilm forming microorganisms found in catheters [72, 78, 79, 83,84].

Table 2.4.2 Microbiological techniques to diagnose CRBSI [5,9].

Table 2.4.3 A summarised information on common antiseptic/antimicrobial components used in catheter impregnation.

Table 2.7.1 A summary of current practices and emerging technologies in the prevention of CRBSI.

Table 5.3.1 Detailed raw data obtained from repetitive scanning of flavin-modified anodised carbon fibre mesh electrode in BR buffers of varying pH; N_{scans} = 63.

Table 5.3.2 Comparison of electrode modifiers/pH detection methodologies.

Table 6.3.1 Detailed raw data obtained from repetitive scanning of polyflavin-modified anodised C-PE electrode in Britton Robinson buffers of various pH. N_{scans} = 63.

Table 6.3.2 Raw data highlighting the quantitative changes in peak positions of the polyflavin-modified anodised C-PE electrode resulting from mechanical flexing cycles and when electrode is fixed perpendicularly at 90°.

Table 6.3.3 Peak potentials of the flavin-modified anodised C-PE mesh in human urine and their equivalent pH measurements against conventional pH probe.

Table 7.1.1 Typical components of TPN solution.

Table 7.3.1 Detailed raw data obtained from repetitive square wave voltammetric series scanning of the physisorbed riboflavin-modified anodised carbon fibre electrode in Britton Robinson buffers of varying pH; N_{scans} = 54.

Table 7.3.2 Raw data obtained from the physisorbed riboflavin-modified carbon fibre electrode: A) continuously submerged in kefir-cultured TPN, B) periodically inserted in kefir-cultured TPN, C) continuously submerged in kefir-cultured laked horse blood and D) periodically inserted in kefir-cultured laked horse blood.

Table 7.4.1 Average atomic concentration percentages of unmodified and physisorbed riboflavin-modified SPE using XPS.

Table 7.5.1 Average absorbance value (λmax = 585 nm) and calculated peroxide concentration following on from electrochemical riboflavin reduction (-0.450 V) using an anodised carbon fibre mesh electrode at different time periods.

Acknowledgements

First and foremost, I would like to express my heartfelt thanks and gratitude to my supervisor Professor James Davis. Without his unending patience, encouragement, wacky ideas and sarcastic humour, my PhD life would not have been as enjoyable and meaningful as it was. Thank you for everything James, especially for tolerating me being an angry wee pleb, and for being the best supervisor I could ever ask for (proven by the Best Supervisor Award 2020)!

Many thanks also to Kimal PLC for sponsoring this work through a Cooperative Award in Science and Technology with the Department for the Economy Northern Ireland and providing invaluable assistance and support throughout the entirety of the project. My sincere gratitude to Mr. Steve Minett and the rest of the team for all your help and insights. This project could not have been completed without your assistance.

A special thank you to Mr. Declan Brown – without him I wouldn't have even chosen a science-related career path. Many thanks to all the NIBEC staff and academics who have provided support and contributed to my PhD including: Miss Ruth Holman, Mr. Damian McDonald, Mr. Brian McGrath, Mr. Andrew Toye and Mrs. Ann Blair.

I would also like to extend my thanks to my lab fam - both past and present. Michael, Aidan, Ruairi, Anna, Ashleigh, Sean and Jordan – thank you for all your support and sharing your knowledge. To our future doctorates Robert, Amy, Sarah and Teri – thank you for all the laughs, gossips and encouragement. It has been a great pleasure working with you all!

To Dr. Aaron McConville, you were such an inspiration and no amount of words could ever express how much you have positively influenced myself and the whole team. Thank you for all the knowledge, insights and memorable stories that you have shared with me. You are, and always will be, forever in our hearts.

A special thank you also to Dr. Alexander Martin for without him I wouldn't have had the courage to pursue a postgraduate study. Thank you for always lending me your ears and giving words of encouragement and support when I need it the most.

My most heartfelt thank you to Dr. Catherine Hegarty who have journeyed with me every step, bumps, inclines, hurdles and breakdowns throughout this adventure. I truly thank you for your relentless help and emotional support, for all the laughs, the eye roll moments and for the strong friendship we've built - I could not have completed this thesis without you.

Last but certainly not the least, I would like to thank my family and friends who I'm sure will be overwhelmed with joy when I finally submit this thesis. Thank you Auntie Teray and Danielle for always being there for me and baking me sugary treats whenever I wanted.

The greatest and wholehearted thank you to Papa, Mama, Ate Charmagne and PJ for your infinite love, support and understanding even throughout all my temper tantrums. You have been my source of inspiration and strength and are the pillars of my success – without you I would not be where I am today. Human na gayud ko og eskwela. Gihigugma gayud ko kamo tanan!

Copyright / Credit Notices

Within this thesis material (like text, figures, or tables) from the author's publications is reprinted. The copyright / credit notices are listed at this place in common for all the related chapters, paragraphs or sections. The material might have been modified slightly, however these copyright / credit notices still apply.

Acknowledgement is given to the original source of publication for:

McLister A, **Casimero C**, McConville A, Taylor C, Lawrence C, Smith R et al. Design of a smart sensor mesh for the measurement of pH in ostomy applications. Journal of Materials Science. 2019;54(14):10410-10419.

The final publication is available at Springer Link via doi: 10.1007/s10853-019-03600-x.

Abstract

At present, the main diagnostic for catheter related bloodstream infection is the presence of fever, often coupled with rigors, which is highly unspecific, unreliable and relies heavily on subjective decision on behalf of the patient or clinical staff to raise an alert. It is clearly imperative therefore to develop readily integratable in situ sensors which could monitor the condition of the catheter line and warn the patient/clinical professionals of the early onset of biofilm formation. The ability to eradicate pathogen contamination would also be an ideal prerequisite for such systems in order to fully minimise the risk of infection, undoubtedly reducing mortality and morbidity rates caused by the infection.

This research project has focused on the use of pH as an indirect method in detecting line contamination. Various carbon-based materials (carbon fibre mesh, carbon-loaded polyethylene film and carbon screen printed electrodes) were used as electrode substrates due to their versatility, mass manufacturability, scalability as well as relatively low production cost – a prerequisite given the emphasis on cost reductions within healthcare systems.

Surface modifications through electrochemical anodisation, electropolymerisation of a custom flavin-phenol derivative as well as adsorption of riboflavin were investigated and their purpose in enhancing the proposed sensor's electroanalytical performance towards pH detection were critically assessed. A microbial reactor, total parenteral nutrition (TPN) and laked horse blood – all of which present complex media containing a range of potential interferences, were employed to examine the sensitivity, selectivity and repeatability of the various sensor designs. The design and development of a flavin-modified polymer was found to exhibit Nernstian behaviour (55 mV/pH) over pH 2.55 to pH 8.12. This approach was further updated to exploit physisorbed riboflavin (vitamin B2) with similar characteristics (61 mV/pH) but which was intrinsically biocompatible. The riboflavin system was employed with authentic TPN formulations and found to exhibit reversible pH monitoring capabilities (repeated cycling in over 20 scans) with minimal drift (4 mV).

The dual capability of riboflavin in detecting pH as well as electro-generating reactive oxygen species was also exploited and studied. Through the generation of the reactive oxygen species, it was envisaged that the eradication of catheter-contaminating pathogens could be

feasible. Ultimately, a riboflavin-based smart catheter system is proposed as a suitable solution to the challenging problem of catheter-related bloodstream infection.

Abbreviations

Ag	Silver
AgCl	Silver Chloride
ALS	Antibiotic Lock Solution
ALT	Antibiotic Lock Therapy
BR	Britton Robinson
BSI	Bloodstream Infection
C. albicans	*Candida Albicans*
C-PE	Carbon - Polyethylene
CAUTI	Catheter Associated Urinary Tract Infection
CDC	United States Centre for Disease Control and Prevention
CE	Counter Electrode
CFM	Carbon Fibre Mesh
CFU	Colony Forming Unit
ChSSD	Chlorhexidine-Silver Sulfadiazine
CLABSI	Central Line Associated Bloodstream Infection
CRBSI	Catheter Related Bloodstream Infection
CV	Cyclic Voltammetry
CVC	Central Venous Catheter
E	Electrode Potential
ECDC	European Centre for Disease Prevention and Control
ECM	Extracellular Matrix
EDTA	Ethylenediaminetetraacetic Acid
emf	Electromotive Force
EPS	Extracellular Polymeric Substances
ESPEN	European Society for Clinical Nutrition and Metabolism
EtOH	Ethanol
FAD	Flavin Adenine Nucleotide
FMN	Flavin Mononucleotide
H_2O_2	Hydrogen Peroxide
HCAI	Healthcare Associated Infection
HICPAC	Healthcare Infection Control Practices Advisory Committee
ICU	Intensive Care Unit

IPA	Isopropyl Alcohol
IV	Intravenous
KCl	Potassium Chloride
K. pneumoniae	*Klebsiella Pneumoniae*
MIC	Minimum Inhibitory Concentration
MinR	Minocycline-Rifampicin
mV	Millivolts
MWCNT	Multi-Walled Carbon Nanotubes
$NaHCO_3$	Sodium Bicarbonate
NaOH	Sodium Hydroxide
NFC	Needle Free Connector
NO	Nitric Oxide
P. aeruginosa	*Pseudomonas Aeruginosa*
PAN	Polyacrylonitrile
PICC	Peripherally Inserted Central Catheter
PMF	Proton Motive Force
PVC	Peripheral Venous Catheter
RE	Reference Electrode
RM	Rifampicin-Miconazole
ROS	Reactive Oxygen Species
RNS	Reactive Nitrogen Species
S. aureus	*Staphylococcus Aureus*
S. epidermidis	*Staphylococcus Epidermidis*
SWCNT	Single Walled Carbon Nanotubes
SEM	Scanning Electron Microscope
SPE	Screen Printed Electrode
SQWV	Square Wave Voltammogram
TC	Taurolidine-Citrate
TCH	Taurolidine-Citrate-Heparin
TLS	Taurolidine Lock Solution
TPN	Total Parenteral Nutrition
TSC	Trisodium Citrate
UK	United Kingdom
US	United States

UV-Vis	Ultraviolet-Visible
V	Volts
VAP	Ventilator Associated Pneumonia
WE	Working Electrode
WHO	World Health Organisation
XPS	X-Ray Photoelectron Spectroscopy

Notes on Access to Contents

“I hereby declare that with effect from the date on which the thesis is deposited in Research Student Administration of Ulster University, I permit

1. the Librarian of the University to allow the thesis to be copied in whole or in part without reference to me on the understanding that such authority applies to the provision of single copies made for study purposes or for inclusion within the stock of another library.

2. the thesis to be made available through the Ulster Institutional Repository and/or EThOS under the terms of the Ulster eTheses Deposit Agreement which I have signed.

IT IS A CONDITION OF USE OF THIS THESIS THAT ANYONE WHO CONSULTS IT MUST RECOGNISE THAT THE COPYRIGHT RESTS WITH THE AUTHOR AND THAT NO QUOTATION FROM THE THESIS AND NO INFORMATION DERIVED FROM IT MAY BE PUBLISHED UNLESS THE SOURCE IS PROPERLY ACKNOWLEDGED".

Chapter 1

Introduction and Project Aims

Overview

There is a pressing need for a smart sensor system that can identify and monitor catheter contamination and ultimately the onset of catheter-related bloodstream infection. Efficient and timely intervention could lead to a significant reduction in morbidity and mortality rates relating to this ubiquitous nosocomial infection. This chapter introduces the research conducted and summarises the overall aim and objectives of the project.

1.1 Introduction

Nosocomial infection, or healthcare-associated infection (HCAI), is described by the World Health Organisation (WHO) as an infection that was absent during admission and which occurred while the patient is under the care of a hospital or other similar facility [(1)]. It is highlighted as the leading adverse event in healthcare. Although it is difficult to obtain reliable global data to determine the significance or severity of HCAI due to the lack of surveillance as well as the complexity and absence of standards for determining nosocomial infections, studies suggest that hundreds of millions of patients around the world are affected by HCAI annually [(1)]. Despite several efforts and precautions to reduce the risk of HCAI, there is still no solution to the problem.

Hospital-acquired infections can be caused by a myriad of factors. Clinical determinants include: immunosuppression, extended and unnecessary use of antibiotics and invasive devices, as well as going through complex and high-risk procedures [(1)]. Other socioeconomic factors are due to resource-limited settings which are common in developing countries. Some examples of these are overcrowding, limited knowledge and application of basic antiseptic and aseptic techniques, inadequate equipment and the lack of knowledge in proper hygienic conditions and correct waste disposal [(1)].

It is inevitable that the longer patients stay in the hospital, the higher the risk of acquiring a HCAI. Hospital-acquired infection leads to a multitude of problems including but not limited to: increased duration of hospital stays, augmented hospital bills for patients and their guardians, higher risk of antimicrobial resistance, additional cost for health care systems, and more importantly, it causes unnecessary deaths [(1)].

Patients who have had invasive devices inserted, such as catheters, have a higher risk of acquiring a HCAI [(1)]. Although catheters and other indwelling devices are integral to modern medical procedures, they proffer perfect conditions for biofilm-forming bacterial colonisation which increases the risk to not only antibiotic resistance but also for catheter-related blood stream infections (CRBSI). There are two types of CRBSI: central line-associated bloodstream infection (CLABSI) and non-CLABSI (i.e. catheter associated urinary tract infection). Central lines are described by the United States Centers for Disease Control and Prevention (CDC) as an intravascular catheter that is employed for blood withdrawal,

infusion or haemodynamic monitoring and which concludes at or near the heart or in one of the following major vessels: umbilical artery/vein in neonates, internal jugular veins, subclavian veins, aorta, superior/inferior vena cava, pulmonary artery, common/external iliac veins, brachiocephalic veins and/or femoral veins [2]. Intravenous catheters vary depending on its entry site into the vein. This includes tunnelled and non-tunnelled catheters, totally implantable catheters and peripherally inserted central catheters (PICC). In comparison to other medical devices, central venous catheters (CVC) lead to more device-related infections, are one of the leading causes of mortality, morbidity as well as the major source of septicaemia in hospitalised patients [3]. In addition, CVCs are said to have up to 64-fold greater relative risk when compared to peripheral venous catheters [3]. It is important to note that there are two major types of catheters: urinary and intravenous (IV) catheters. The primary focus of this thesis will be on the latter.

Each year in the United States (US) alone, an estimate of 250,000 cases of CLABSI are reported, making this one of the most prevalent cause of nosocomial infection [4,5]. Among those affected, the mortality rate is approximately 24% [5] which results to around 28,000 patient deaths in intensive care units (ICUs) in the US annually [6]. With an attributable average cost of around $45,000 per patient, CRBSI costs up to $2.3 billion each year in addition to these life-threatening complications [6,7]. Moreover, studies [7,8] have shown that there is an increased hospital length of stay of up to 22 days and up to 20 day extended ICU admission. Hence, CRBSI is the most expensive and lethal complication arising from central venous catheterisation [3].

At present, the main diagnostic method for CRBSI are CVC patients with fever which can be accompanied by rigors. Other symptoms include nausea, inexplicable hypotension, malaise and vomiting [3]. The appearance of swelling, erythema and oozing drainage around the catheter exit site are also indicators of CRBSI [3] but these are largely subjective and unreliable. As such, several clinical/laboratory tests are completed to exclude alternative sources of infection. In addition to the aforementioned clinical indicators, at least one positive peripheral blood culture with a definitive proof that there is no other possible source of infection apart from the catheter must be obtained [3]. Furthermore, for a patient to be diagnosed with CRBSI, they need to have a positive quantitative or semi-quantitative culture from the catheter tip, which is contaminated with the same pathogen as that in culture obtained from the peripheral vein and a catheter segment [3,9]. Although necessary, these

tests take up time and other clinical/laboratory resources which adds to the economic healthcare burden and could increase risk of patient morbidity.

Currently, the most effective solution to catheter-related infection, especially to immunocompromised patients or those who have any local or systemic infection, is the removal of the catheter. There is a higher probability of recurring infection if the catheter is kept than if it is removed [3]. However, this is costly and may not always be feasible due to limited insertion sites. For catheter salvage, the intake of systemic antibiotics in conjunction with lock therapy, specifically antibiotic lock therapy (ALT), is a common method. This involves saturating the catheter lumen with supra-therapeutic concentrations of antibiotic(s) such as vancomycin and gentamycin. This increases the chances of eradicating pathogens growing in biofilms. Nevertheless, antibiotic lock therapy also has its downfalls. Firstly, it increases the risk of antibiotic resistance and secondly, the likelihood of success varies. Microorganisms such as *Staphylococcus aureus* (*S. aureus*) are infamously unsusceptible to ALT [3,10,11]. Other lock therapies which exploits the antimicrobial properties of substances such as ethanol and citrate have also been discovered and used [12–19]. Similar to ALT however, their efficacy can be contentious and some studies have indicated that they do not fully eradicate all pathogens, may affect the catheter material integrity and can lead to additional physiological complications.

Numerous preventative measures for reducing the incidence of CRBSI have been implemented and include: choice of catheter material, antimicrobial impregnation of catheters and improved training in the use of aseptic techniques. However it is evident that there is no permanent solution at present. Additionally, current diagnostic methods are costly, unreliable and highly subjective. The existence of various internal and external pathological pathways can also often lead to challenges in providing a suitable method in eradicating CRBSI-causing pathogens.

The most ubiquitous source of CRBSI is the catheter hub. This is due its frequent manipulation by healthcare workers, carers as well as patients themselves thus increasing the risk of catheter contamination. There are many hub designs in use and an example is shown in **Figure 1.1.1**. In this case, the hub is composed of an outer cap with internal female thread where a needleless syringe is inserted. A blunt cannula pierces through the silicone septum upon insertion of the syringe and allows the solution to flow into the catheter line.

Although aseptic techniques are performed, microbial colonisation still occurs. If the hub is compromised, the injection of solution through it allows the free movement of sessile microorganisms along the catheter line thus increasing the risk of CRBSI. As such, there is a pressing need for the development of a novel 'smart' hub which can detect contamination and enable swift replacement minimising the onset of biofilm formation. It could also be envisaged that the hub could be integrated into a more holistic connected health network where it could serve as an early warning alert to the patient/caregiver/clinicians enabling more timely interventions that lead to more positive outcomes and reduce likelihood of further, systemic complications. This thesis lays the foundations for an electrochemical monitoring system that can address some of these needs and showcases the development pathway and how new approaches to the design of a smart catheter hub could be implemented in practice.

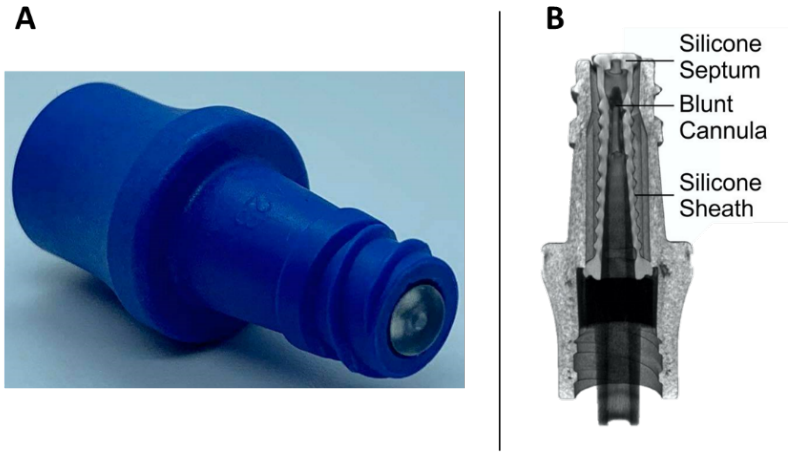

Figure 1.1.1 An example of a catheter needle free hub (ICU Medical Clave™ connector) and CT scan of its internal components.

1.2 Project Aims and Objectives

The aim of this project was to investigate the design and development of a 'smart' carbon-based sensor that could not only monitor the line condition but which could, ultimately, act autonomously to counter an emerging infection threat via the generation of reactive oxygen species. It was envisaged that this would eventually be amalgamated into already existing catheter systems thereby providing a quick and effective method of alerting relevant clinicians about the onset of biofilm formation. The present investigation sought to develop the technology for a radical approach to preserve line integrity, improving patient's quality of life and decrease economic healthcare burden.

The objectives of this project were:

- To develop and employ a modified carbon-based electrode capable of feedback control through monitoring pH as indirect markers of biofouling;
- To design and develop a catheter hub extension case that can easily be integrated into existing catheter systems;
- To characterise the surface morphologies of the electrically conductive material and optimise their electrochemical properties using conventional methods;
- To assess the modified system's ability to generate reactive oxygen species 'on demand';
- To ensure robustness of the sensor through repetitive scanning;
- To demonstrate the electrode's ability to monitor pH within a more complex setting.

1.3 Chapter Summaries

In attempting to fulfil the project objectives, the thesis documents the approaches taken, the corresponding outcomes of the various investigations and provides a critical analysis of the practical applicability of the resulting technological advances. The thesis consists of 8 chapters and a summary of each is given in turn:

Chapter 2 details an overview of the relevant literature and emerging research trends necessary for considering the development of new tools for addressing catheter-related bloodstream infection. Existing approaches (technical and clinical) and the challenges faced in attempting to minimise the onset of CRBSI and subsequent treatments are discussed. Developments in smart materials and new clinical procedures are critically considered.

Chapter 3 outlines the experimental methods and the underlying principles utilised throughout this research project. It should be noted that the peculiarities of the various experiments are detailed in each individual chapter.

Chapter 4 discusses carbon fibre as a versatile, scalable material often used as a sensor substrate. It is relatively common to employ electrochemical anodisation to improve the electrode's response and anodised carbon fibre mesh was therefore envisaged to be a

suitable foundation in developing a smart catheter probe. This chapter examines the effect of anodisation along with ultrasonic forces in exfoliating carbon fibre surfaces. Electrochemical measurements and surface characterisation were completed wherein the efficacy of the technique in enhancing the conductive electrode's sensing capabilities was examined.

Chapter 5 focuses on the addition of an electrode modifier which was used to enhance the sensor's ability to detect the required variable which, in this project, is pH – exploited as a method in detecting the presence of microorganisms. Although there is a variety of pH sensitive modifiers, their application in real matrices often comes as a challenge. This chapter describes the use of a customised flavin-modified carbon mesh and its ability to indirectly detect pH changes using potentiometric techniques. Its function was then challenged in a more complex, relevant in situ setting of a microbial bioreactor.

Chapter 6 details the employment of flavin-phenol polymer on a carbon-polyethylene film. The developed sensor is mechanically flexible and electrochemically active which are both suitable requisites to pH-sensitive smart systems.

Chapter 7 employs screen printed electrode as a cheaper, more readily mass reproducible and disposable alternative to carbon fibre mesh. This chapter examines the functionality of carbon-based screen printed electrode modified with riboflavin, vitamin B2, in detecting pH changes. A 3D printed catheter hub was created, used as an extension and its purpose was evaluated. Additionally, this chapter highlights the use of a revised catheter hub system using carbon fibre mesh as the working, counter and reference electrode. Preliminary work on the generation of hydrogen peroxide using amperometric techniques was also discussed.

Chapter 8 summarises and concludes the research conducted within this project. Recommendations for further work are also discussed here.

Chapter 2

Literature Review

Overview

There is undoubtedly a pressing need to identify as well as inhibit the onset of catheter contamination to provide valuable information for clinicians when consulting a catheterised, febrile patient. This would enable more rapid and efficient clinical interventions to eliminate catheter related bloodstream infection and improve patient outcomes. The introduction of a smart system that could readily be integrated into existing intravenous lines and which could detect as well as eradicate pathogens would be an ideal response to the need. The primary aim of this literature review is to concisely provide a critical assessment of the pivotal and emerging research pathway leading to the underpinning principles and eventually, the development of future devices.

Aspects of the work detailed in this chapter is published as the cover article in:
Casimero C, Ruddock T, Hegarty C, Barber R, Devine A, Davis J. Minimising Blood Stream Infection: Developing New Materials for Intravascular Catheters. Medicines. 2020;7(9):49.

2.1 History of Intravenous Therapy

Intravenous (IV) therapy is one of the most ubiquitous, standard medical procedures in modern medicine. A walk through any hospital setting will reveal patients with some form of intravascular access device and, as they form the basis of most treatments, such systems will be among the first medical interventions upon being admitted to hospital. Within the media (print or screen), an image of a patient connected to an intravenous drip bag is almost inevitably used to depict hospitals. Yet only a few are aware of the climactic events that belie its evolution from antiquity to the present day. In simple terms, IV therapy is a treatment that delivers and/or extracts fluid directly from a vein. The most common device is the peripheral venous catheter (PVC) which employs a small, hollow and flexible tube (cannula), which is inserted through the skin into the vein and is typically placed at the back of the hand or in the arm and it has been estimated that some 330 million are inserted in US hospitals each year [20,21]. A conventional PVC device is highlighted in **Figure 2.1.1** and comprises of a removable needle which guides the catheter into the vein. Such intravascular devices are typically used to deliver fluids straight into the bloodstream and can also be used to extract blood for sampling.

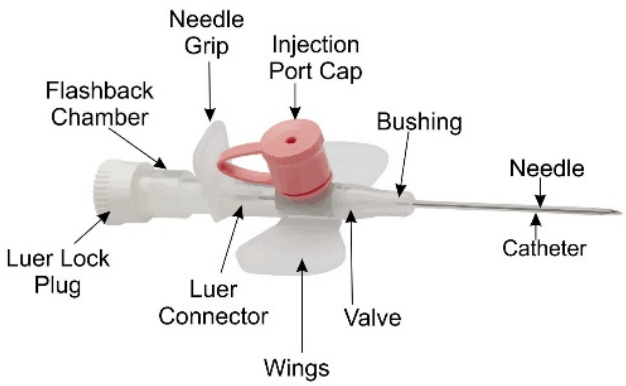

Figure 2.1.1 Typical components common to a peripheral venous catheter.

Derived from the ancient Greek word 'kathiénai', translating to 'to send down', catheters were first used as treatment for male urinary retention [22]. The evolutionary pathway of IV therapy is punctuated with revolutionary changes in medical practice. While IV therapy has been known from antiquity, it has been suggested that the first recorded application can be found in Greek mythology involving Jason and the golden fleece [23]. In short, after retrieving the golden fleece, Jason was met by his ailing father Aeson who was too unwell and weak to join him in his celebrations. Upon noticing this, the enchantress Medea 'took' Aeson's blood,

mixed it with some herbs and returned it into his veins which reinvigorated him [23]. This procedure has hints of the modern blood transfusion we now know and use today. A brief summary of the significant, real-life scientific events that led to current intravenous therapy methods are exhibited in **Table 2.1.1**.

Table 2.1.1 A summarised version of significant events leading to current intravenous therapy. Information acquired from [23–28].

Year	Event
1492	First attempt at blood transfusion to Pope Innocent VII who fell into a stroke-induced coma. However, blood could have actually been given orally as per custom of the time.
1615	Andreas Libavius of Saxony first provides the description of blood transfusion.
1628	William Harvey discovers blood circulation.
1654	Francis Folly completes the first successful animal to animal transfusion.
1656	First intravenous injection from animal to animal. Sir Christopher Wren famously used a quill and a pig's bladder to intoxicate a dog.
1662	First IV injection to a human is described by Johann D. Major.
1665	Richard Lower accomplished the first animal to human transfusion. In the same year, Lower transfused sheep blood to a man suffering from a case of insanity.
1818	First recorded successful human to human blood transfusion by William Blundell.
1827	Cholera epidemic ensues from India and reached England in 1831.
1831	William Brooke O'Shaughnessy coined the term 'black blood' and first describes the primary pathology of cholera.
1833	With the help of O'Shaughnessy, Thomas Latta was the first to successfully infuse saline solution which formed the basis of current solutions.
1844	Francis Rynd develops the first hollow metal needle and subsequently performed the first subcutaneous injection. In the same year, Claude Bernard employed the early modern application of cardiac catheterisation and which formed the basis of current methods used by surgeons today.
1853	Charles Gabriel Pravaz and Alexander Wood independently produced the first designs of metal hypodermic syringe.
1857	Louis Pasteur defines the relationship between germs and disease.
1867	Joseph Lister used and applied Pasteur's theory of disease and developed of the use of antiseptic surgical methods.
1894	Sir Almroth Wright first discovered citrate as an anticoagulant.
1901	Karl Landsteiner identified 3 out of 4 of the now known blood groups and final AB blood group was discovered a year later.
1914	Citrated blood was first used for transfusion.
1932	The first blood bank was founded in Leningrad.
1939	Discovery of the Rh system.
1940s	David Sheridan pioneered the modern disposable catheter upon the second world war advent.
1945	Introduction of plastic IV catheters in hospitals.
1950	David Masa developed the Rochester plastic needle, creating the first modern disposable IV catheter system and inadvertently exploded the use of intravenous fluids.
1950	William Murphy and Carl Walter replaced the problematic glass bottles and introduced the use of plastic bags for blood collection and IV transfusion.
1969	Development and introduction of current total parenteral nutrition solution.
1970	Beldig H. Scribner and Wayne Everett Quinton invented the first designs of the Scribner-Quinton central venous catheter.
1973	The Broviac catheter was originally developed by Robert C. Atkins but was more famously use for catheterisation by John Walter Broviac.
1975	Verne L. Hoshal Jr., Tommy Thompson, the Thompson and Baxter company, and Millie Lawson of the MD Anderson Cancer centre all contributed to the development and popularity of modern peripherally inserted central catheters.
1979	Both Robert O Hickman and James Sisley were responsible for creating and commercialising the Hickman catheter.
1988	Due to the increasing cases of catheter-related bloodstream infection, particularly in home parenteral patients, Dr. Bernard Messing and his team were the first to report the use of antibiotic lock therapy.
1997	Silver loaded catheter was first employed by Nina Gatter and her team as a preventative method and an alternative to antibiotic use.
2009	The Infectious Diseases Society of America recommended antibiotic lock therapy as a standard for certain central venous access device infections.

From this, it evident that the curiosity coupled with dedication of scientists have allowed the establishment of IV therapy – a method that is considered to be one of the most vital and ubiquitous prerequisites in modern healthcare settings.

2.2 Central Venous Catheters

The estimated global central venous catheters (CVC) market was around US$ 647 million in 2015 [29] with up to an estimate of 5 million CVCs inserted annually in the US alone [21,30]. Central venous catheters are samples of lifesaving indwelling devices that are usually used for monitoring, therapeutic and/or diagnostic purposes. There are four different types of central intravenous catheters: totally implantable catheters, peripherally inserted catheters, tunnelled and non-tunnelled catheters, as detailed in **Table 2.2.1**. Central venous access is usually through the dexter (left side) of the patient as this provides a shorter, easier and a more direct route to the superior vena cava [31]. **Figure 2.2.1** displays common access sites for CVC placement. Typically, CVCs are used for long term-access to administer parenteral nutrition, fluids and various medications, especially those that are harmful to the peripheral veins, through the bloodstream. Additionally, CVCs are inserted for patients who require frequent blood tests, haemodialysis, chemotherapy and long-term antibiotics. The measuring and monitoring of central venous pressure are also completed through CVCs [30,32].

The choice of central venous catheter type is dependent on the frequency and severity of complications as well as risk of failure that may arise with each type [33]. The associated risks and ease of access with individual insertion sites must also be considered. Mechanical difficulties, thrombosis, local haematoma, vessel laceration as well as catheter related bloodstream infection are common adverse effects of catheter placement. Further discussion about risk factors of infection are detailed in **Section 2.4**.

Table 2.2.1 Details of the four types of central intravenous catheters [5,31,34].

Line type	Duration of use	Examples of use	Advantages
Totally implantable ports	Months to years	Delivery of chemotherapy and other irritant drugs as well as long-term intermittent access.	Less interference with daily activities; minimal flushing; lower risk of infection.
PICC-line	6 weeks to 6 months	Administration of irritant drugs, antibiotics and total parenteral nutrition; blood sampling.	Low complication rate; easier to insert and lower insertion hazard – important especially to more vulnerable patients i.e. immunocompromised patients.
Tunnelled (Broviac and Hickman)	Months to years	Long term infusion of chemotherapy and other irritant drugs.	Reduced risk of infection due to distance between vein entrance site and skin exit site.
Non-tunnelled	Less than 3 weeks	Short term administration of TPN; delivery of irritant drugs, vasopressors and inotropes.	Multi lumen access; can be replaced in non-surgical setting through resitting or replacement over guidewire.

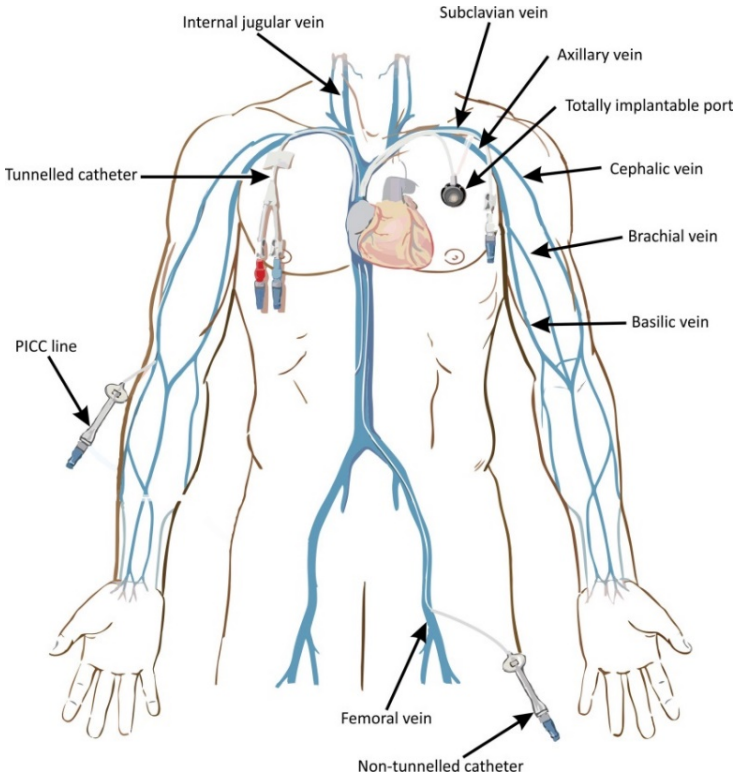

Figure 2.2.1 Types of IV catheters and typical insertion sites. Adapted from [35].

The recommended approach to catheter placement typically involves the employment of ultrasound guidance. Some emergency situations however prohibit the use of ultrasound. This includes the absence of equipment as well as difficulty in placing the ultrasound probe due to the lack of space, primarily while inserting the needle through the subclavian access site [36]. In these cases, anatomical surface landmarks are professionally detected and used to orient the cannulating needle and thus catheter placement [36]. Clinicians also consider contraindications such as the presence of thrombus in the chosen vein, existing infection along the access route and trauma in the anatomic surrounding [36]. Understandably, catheter placement is completed in sterile, aseptic conditions.

Depending on the line type, there are different techniques used to insert a catheter: Seldinger and cut-down approach. Initially established in the 1950s, the modified Seldinger technique is used in most cases of catheter placement [21]. It was first used as an innovative approach for arteriography and, in spite of its advantages over previous catheter placement methods (i.e. through the needle and needle alone technique), it was the early 1980s before its use became routine [37]. The method involves inserting a flexible guidewire into a punctured vein through the needle, threading the catheter and removal of the guidewire (**Figure 2.2.2**). Its primary advantage is that it allows a catheter to be introduced into a vessel through an aperture that is only the size of the catheter itself which reduces the injury caused to the patient [37].

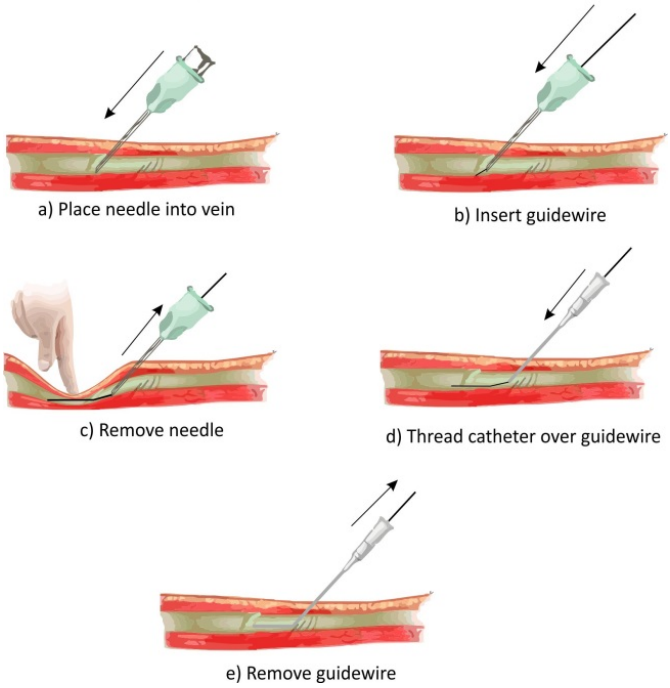

Figure 2.2.2 Seldinger Technique. Adapted from [38].

2.3 Healthcare Associated Infections

As the name suggests, healthcare associated infections (HCAI) are infections that weren't present during initial patient diagnosis and which patients attain while receiving care for other health issues in a hospital or other healthcare institutions. The United States Center for Disease Control and Prevention (CDC) states that around 1.7 million hospitalised patients are affected by a HCAI with mortality rate of 1 in 17 [1,2,39]. Nosocomial infections are described as the common adverse effect of healthcare and belongs to the top 10 leading causes of fatality in the US [1,39]. It is also estimated that up to 15% of hospitalised patients in developed countries obtain a HCAI, affecting up to 37% of those in intensive care units (ICUs) [39]. The risk of acquiring a HCAI is even greater in lower income countries with up to 20 times higher risk than developed countries [39]. Patients in intensive care are more susceptible to infection as they are critically ill and are commonly immunocompromised. It is estimated that around half a million cases of HCAIs are diagnosed annually in ICUs alone [39–41]. Nosocomial infections predictably increase morbidity, mortality as well as costs. Approximately 90,000 deaths in the US are due to HCAIs and annually costs up to US$45 billion in the US alone [39]. As such, HCAIs are a major concern not only for the patients but also on the healthcare industry.

Nosocomial infections affect patients in both developed and developing countries. In the US, the CDC reported an estimated morbidity rate of 4.5% [1]. According to a surveillance report by the European Centre for Disease Prevention and Control (ECDC) in 2013, HCAI has an average prevalence of 5.7% (1 in 18 patients), translating to an estimated 80,000 patients in European countries [42,43]. The World Health Organisation (WHO) also reported that up to 51% of European ICU patients are infected and around 30% will be affected by at least one episode of nosocomial infections [1].

In developing countries, the average prevalence of hospital-acquired infection varies between 5.7% and 19.1% [1]. It is also estimated that an overall frequency of 42.7 episodes per 1000 patients days occur in ICU patients which is nearly three times more than those in developed countries [1]. Additionally, it is reported that in some low- and middle-income countries, patients using ventilators, central lines and other invasive devices, have a higher risk - up to 19-fold increase than patients in the US and Germany [1]. In countries with inadequate resources, infection due to surgery is regarded as the most common HCAI where

up to 67% of patients have been found to be affected and an incidence rate of up to 9 times greater than in higher income countries [1]. Noteworthily, nosocomial infections are said to be the cause of up to 56% death in neonatal period among babies born in resource-limited hospitals, which increases to up to 75% in South-East Asian countries and Sub-Saharan Africa [1].

Apart from infections attributable to surgical intervention and the common spread of infection between patients and health care workers, most HCAIs are due to invasive, indwelling devices. These are categorised into catheter-related bloodstream infection (CRBSI), catheter-associated urinary tract infections (CAUTIs) and ventilator-associated pneumonia (VAP). For the purpose of this literature review, CRBSIs will be the primary topic in discussion, focusing mainly on central venous catheters.

2.4 Catheter-Related Bloodstream Infection

Although catheter use is advantageous, it is not without its complications. Catheter related bloodstream infection, also known as catheter-related sepsis, is defined as the presence of bacteraemia and/or fungaemia as a direct result of intravenous catheterisation. It is the most common, expensive and fatal complication caused by central venous catheters and has been estimated to account for a mortality rate approaching 25% [3,44]. Additionally, it is the most common source of nosocomial infection, accounting for up to 20% in the United Kingdom (UK) [3]. Though there is a reduced incidence rate of 46% between 2008 and 2013 in the US, over thirty thousand cases of central-line associated bloodstream infection are still reported annually in intensive care units and facilities wards in the US alone [44].

The main difference between CRBSI and CLABSI definitions are simply the settings where they were developed. The former is typically used in research settings where it is imperative that an objective and unambiguous information regarding the risk factors and pathogenesis of bloodstream infection as a result of vascular catheters are obtained [45]. In contrast, CLABSI is used in a non-research environment, usually for surveillance purposes of healthcare-associated bloodstream infection, where standardised, clear and definite results can't be determined due to different diagnostic laboratory investigations completed in individual healthcare establishments [45]. As such, CLABSI is essentially employed as a surrogate measure of CRBSI [45]. In this project however, both phrases are used interchangeably.

The use of intravascular devices such as CVCs have significantly increased over the past couple of decades which has led to an increased rate of indwelling device-related bloodstream infection. Of this, catheter related blood stream infection affects up to 250,000 patients and cause up to 15 million CVC days in the US alone yearly [1,32]. The infection leads to up to 28,000 deaths and costs up to approximately $2.3 billion annually [4,6], with each patient roughly costing an additional $45,000 [6,7], in the US alone. The majority of patients with CRBSI are chronically catheterised i.e. those who are in clinical care, with cancer and those who undergo haemodialysis [47]. Around 22,000 – 100,000 of these CRBSI cases are in the haemodialysis population and costs over US$500 million annually [47].

In the UK, CRBSI leads to an additional cost of up to £6,200 per episode with an annual cost of up to £36.2 million for the healthcare system [48]. This infection can also lead to up to 14 days additional length of stay with up to 33,600 ICU days recorded per year [48]. In a 2011 UK survey, around 40% of primary bloodstream infection was related to CVC [34]. More than half of ICU patients already have at least one central line and generally around 20% - 30% of these are eventually colonized by microorganisms [49]. In a study by Tacconelli et al. (2009), an associated cost of between €36 million and €164 million are annually spent in each of four European countries namely the UK, France, Italy and Germany [48]. The same study estimates 14,400 CRBSI cases causing up to over 201,000 ICU days and an upper approximate of 1,584 deaths per annum [48]. According to the report by the National Nosocomial Infections Surveillance system published in 2004, the median rate of bloodstream infection (BSI) caused by central lines varied from 0.38 to 0.79 per 1000 catheter in different ICU types [50]. Although the attributable mortality rate of CRBSI can vary (12-25%) [5], the morbidity caused by the infection is well studied including thrombophlebitis, sepsis and septic shock. The variance in numbers between each research can be explained by the diversified quantity and quality of individual epidemiological studies as well as discrepancies between clinical practices worldwide [48].

2.4.1 Pathology and Risk Factors of Catheter-Related Bloodstream Infection

There are four major pathogenic pathways of CRBSI as displayed in **Figure 2.4.1**. First, the bloodstream infection can originate from the catheter insertion site where microbial

colonisation of the catheter tip and cutaneous tract can readily occur [3]. This is the most common extraluminal infection pathway for short-term catheters [21]. Central venous catheters are readily coated with plasma proteins after insertion and skin flora can promptly embed in the protein as they move along the catheter and down it's lumen, hence colonizing the catheter [51].

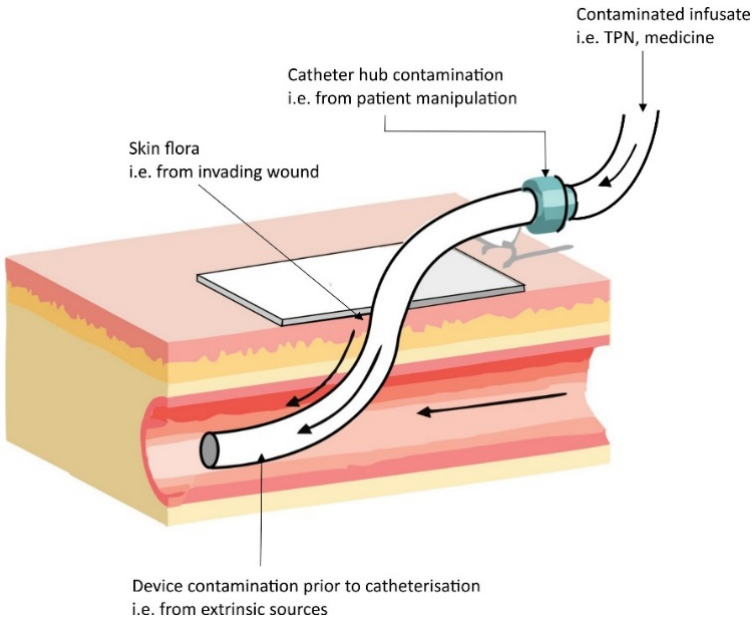

Figure 2.4.1 Potential pathogenic routes of catheter-related blood stream infection.

A study of 2,595 patients by Lorente et al. (2005) found that femoral access correlated to a higher incidence than both jugular and subclavian venous access [52]. This is further supported by a randomised control trial of 289 adult patients within intensive care units completed by Merrer et al. (2001) where it was concluded that subclavian catheterisation was associated with lower risk of complications in comparison to femoral catheterisation [53]. Similarly, central venous insertion through the femoral or jugular vein is not advised for adult patients, especially for non-tunnelled CVCs [21,52–57]. It is stated that a subclavian access would significantly reduce the risk of CRBSI [9,52,58] however, the risk of mechanical complications can sometimes outweigh the benefits of using this site, particularly evident in haemodialysis patients [56]. For instance, in a comparative study by Trerotola et al. (2000), of 279 catheters placed, no significant difference in infection rates between subclavian and internal jugular access was found yet 13% of patients with catheterisation through the former suffered from symptomatic venous thrombosis in comparison to 3% with the latter [59]. Furthermore, post catheterisation subclavian stenosis can be avoided by placing the catheter through the

preferred internal jugular route [56,60,61]. As such, deciding for the correct and suitable catheter placement must consider the risk and benefits of each insertion site.

Catheter related bloodstream infection could also originate from catheter lumen contamination prior to insertion or through a hematogenous route from a separate infection site. Similarly, the introduction of infusate, such as total parenteral nutrition (TPN) and dialysate, leads to an increase risk of CRBSI. In fact, the major cause is the frequent manipulation of the line allowing the internal migration of the colonising microorganisms along the catheter lumen. Previously thought to subsequently cause CRBSI exclusively in long-term catheters, hub colonisation and migration has been acknowledged to be the most common source of infection for both short- and long-term catheters [45]. Chernecky and Waller (2011) state that fifty percent of CRBSI cases are caused by intraluminal migration of microorganisms through the catheter connector and hub, which can be easily colonised within 24 hours of insertion [62]. Similarly, a review by Moureau and Flynn (2015) state that needle free connectors (NFC) are the greatest risk for contamination of the catheter, after insertion, with up to 45% of NFCs contaminated [63].

System manipulation usually occurs through the needle free connector and, as such, is the most common nidus in the catheter system leading to CRBSI. Though there are a variety of commercially available NFCs, most share common access port design. Commonly the hub has an outer cap that allows a male luer needleless syringe/connector to be inserted which leads to the compression of a silicone septum which then allows the solution to flow into the catheter lumen [64,65] (**Figure 2.4.2**). While there are differences in internal mechanism, most designs rely on a split septum which acts as a physical barrier to pathogen entry when disconnected. Another septum design involves the use of solid sealed silicone surfaces (BD Max Zero™) which potentially minimises the number of surface crevices through which contaminants can adhere to. However, this still relies on the luer activated deformation of the silicone cap within the device to enable fluid flow. If planktonic microorganisms are already present in the hub, these are then able to freely migrate through the catheter line, leading to infection. The design of the catheter needless connectors must therefore be thoroughly considered.

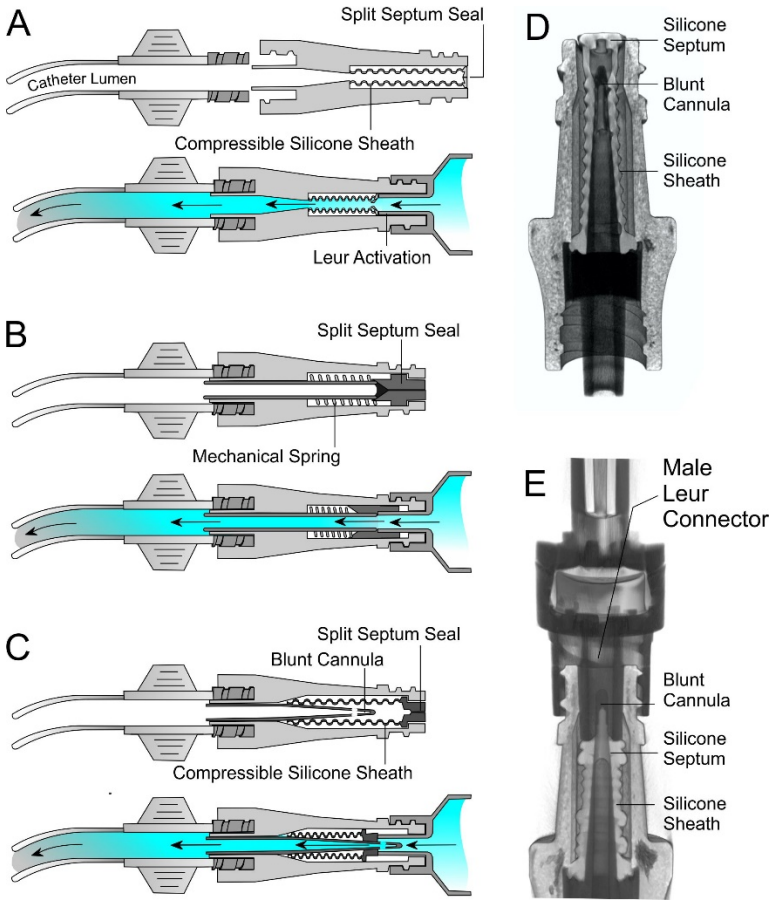

Figure 2.4.2 Needle free connectors based on A) simple split septum, B) mechanical spring compression and C) blunt cannula. CT scans of the internal components of an ICU Medical Clave™ connector D) before and E) after connection to a giving set with a luer connector.

In a study by Chernecky and Waller (2011), wherein a comparison between commercially available antimicrobial and non-antimicrobial connectors was completed, an antimicrobial connector produced up to 8.8 times more colony forming units (CFU) than the latter type [(62)]. It is suggested that this could be due to the variation in design, with there being three types of fluid displacement in conventional needleless intravenous connectors: zero/neutral, positive and negative. Positive displacement refers to the forced movement of a minute solution volume into the end of the catheter after disconnection, as a safety precaution to prevent occlusion due to blood [(66)]. Negative pressure luer access refers to the opposite i.e. there is blood reflux to the catheter, and where a neutral valve type is supposedly designed to prevent any backflow of fluid into the catheter [(66)]. Additionally, there is a variety of antimicrobial components that could be used to impregnate connectors and hubs, hence adding to the discrepancy between antimicrobial properties. It is known that the presence of blood (as minute as 4-30 µL) within the needle-free catheter hub would lead to haemolysis of red blood cells thus leading to fibrin clots, occlusion and eventually inhibits fluid flow [(67)].

Moreover, blood is also a significant source of nutrients that would enhance bacterial growth and their interaction with fibrin further leads to adhesion and biofilm formation thus ultimately leading to CRBSI [67]. It is the complex external surface designs and intricate interiors of catheter hubs and other needleless connectors that causes complications in flushing and disinfection which, in turn, increases susceptibility to contamination. Furthermore, the presence of gaps, such as those in between septum and solution pathway, as well as dead spaces inside the hub proffers the perfect nidus for pathogen invasion and thus a major source of CRBSI [62,66]. There is a need therefore to design a hub where less is better.

Independent from the insertion site, another risk factor is the number of lumens present in the catheter system. Multi-lumens are used to administer multiple, usually incompatible, intravenous fluids such as medicines and TPN simultaneously. An observational study by Khanna et al. (2013) found that in comparison to single lumen, double and triple lumen catheters are associated to higher CRBSI incidence (23.1% vs 37% vs 39.8%, respectively) [68]. Additionally, Frasca et al. (2010) described five randomised studies where it was concluded that, although a significant increase in contamination was observed in both single- and multi-lumen catheters, a higher risk of infection was associated with multiple lumen catheters [21]. For patients with indwelling catheters who require TPN, 13.1% of patients with bloodstream infection had multiple lumens which is significantly greater than only 2.6% of single-lumen catheterised patients affected [21]. Likewise, a surveillance study of 1,369 CVCs showed that each additional lumen increased the risk of infection [57]. Therefore, the use of multi-lumen catheters should, where possible, be limited. Lipid-containing solutions should be administered through a specific lumen, and unnecessary lumens should be permanently closed in cases where a catheter can't be removed [57]. For catheters with triple- or double-lumen, CLABSI will be missed if more than one lumen is not tested for blood culture up to 15.8% and 27.2% of the time, respectively [69].

Unsurprisingly, the increased duration of catheter use is associated with an increased risk of catheter related bloodstream infection. Studies completed in the 1990s have shown that catheter use between 5-7 days corresponds to higher risk of infection but a study in 2013 has revealed that only after 12 days of catheter use was there a significant risk [68]. It states that patients with in situ catheterisation greater than 12 days have 2.21 times more chance of being affected by CRBSI in comparison to those who have shorter-term catheters [68]. A

more recent surveillance by Pandit et al. (2019) supports this study as they observed that of 107 patients, 65 of them did not attain CRBSI with an average catheterisation period of only 8.43 ± 1.28 days while the other 42 patients was affected by CRBSI with average catheterisation duration of 12.19 ± 1.89 days [70]. The difference may be explained by various variables in individual studies including the number of patients involved and choice of characteristic inclusions.

Certain patient characteristics, such as low serum albumin levels can also predispose a patient to CRBSI. For instance, studies show that patients with lower albumin levels, compared to those that are in normal range, had a greater risk of nosocomial infection [71,72]. This is said to be due to albumin having an anti-adhesive property against the attachment of bacteria, like *Staphylococcus aureus*, to cells in vitro [72]. Thus, a low albumin level leads to an increase in bacterial colonization which, in turn, increases the risk of CRBSI. Additional risk factors include, but are not limited to: age, poor personal hygiene, moisture around insertion site and other morbidities like diabetes mellitus, low haemoglobin level and peripheral atherosclerosis [3].

Additionally, patients who receive total parenteral nutrition have been found to have a higher risk of developing CRBSI compared to those who don't (60.7% vs 34.4%) [73]. Patients with morbidities like intestinal failure rely heavily on the administration of TPN and other intravenous fluids through the catheter in order to receive the required fluids and nutrition [74,75]. Although necessary, this leads to an increased risk of catheter-related bloodstream infection and catheter malfunction since the line is used more frequently and for over a long period each time. Dibb et al. (2016) identified 588 patients administered with home parenteral nutrition and, of these, 137 patients acquired 297 cases of CRBSI [76]. This correlation is unsurprising as TPN contains various components such as amino acids, dextrose and lipids that proffer an idyllic environment for the proliferation of CRBSI-causing microorganisms [77].

2.4.2 Biofilm

Catheter contamination readily leads to the formation of biofilm – bacterial or fungal. Biofilm-forming microorganisms commonly isolated from CVCs are described in **Table 2.4.1**. The individual prevalence detailed below are based on a study by Marcos et al. (2011) where

they recorded 1129 episodes of CRBSI [78]. However, it is important to note that the prevalence of organisms vary from each study and are dependent on various factors including the chosen application i.e. haemodialysis and chemotherapy [3,45,79–81]. Upon the insertion of a catheter, the device is instantaneously enveloped with a conditioning film composed of organic macromolecules such as fibrinogen, pyruvate and glucose, which, in turn, further aids pathogen surface adhesion [9,82]. Pathogens will more readily adhere to this film than to the bare catheter material itself and, once attached to the luminal surface, will rapidly establish a biofilm [9]. As early as 24 hours after catheter placement, device contamination and biofilm formation onset can occur [9].

Table 2.4.1 Common biofilm forming microorganisms found in catheters [72,78,79,83,84].

Pathogen	Gram stain	Common source	Prevalence
Coagulase negative staphylococci (i.e. *S. epidermidis*)	Gram positive bacteria	Skin	44.9%
Staphylococcus aureus (*S. aureus*)	Gram positive bacteria	Nose, respiratory tract, and on the skin	19.8%
Pseudomonas aeruginosa (P. aeruginosa)	Gram negative bacteria	Environment mainly in soil and water	7.1%
Klebsiella pneumoniae (K. pneumoniae)	Gram negative bacteria	Intestines	5.0%
Escherichia coli (*E. coli*)	Gram negative bacteria	Lower intestines	3.6%
Enterococcus faecalis	Gram positive bacteria	Gastrointestinal tract	3.4%
Candida albicans	Gram negative fungi	Gastrointestinal tract	2.7%

A biofilm is an accumulation of microbial organisms that are associated to a substratum and releases extracellular matrix (ECM) that can shelter it from antimicrobial treatments [9,85,86]. Around 65 - 80% of all microbial and chronic infections are caused by biofilms [87,88]. Biofilm formation is said to occur in four main stages: surface attachment and cell division, micro colony formation, maturation of biofilm, and dispersion, as summarised in **Figure 2.4.3**. A biofilm is defined by the release of extracellular polymeric substances (EPS), composed of

mostly nucleic acid, protein and exopolysaccharides, which forms the ECM surrounding the cells [89]. Biofilm structures are integrated with fluid-filled channels that allow the transport and exchange of nutrients and oxygen to the cells developing underneath. In addition, this encasement provides biofilms with their mechanical stability by producing glue-like connections between cells and to the substratum [86], improving their irreversible adhesion to catheter surfaces [9]. This protective layer can also limit the diffusion of antimicrobial agents, by creating a barrier or simply binding directly to the agents, towards cells in the deeper layer which inadvertently reduce the effect of antibiotics thus ultimately leading to antibiotic resistance [87,90]. This hallmark resistance, or at least tolerance, to antibiotic therapy plays a significant role in the appearance of bacteraemia [3]. In comparison to antibiotic concentrations required to eliminate bacteria in solution, biofilm eradication demands minimum inhibitory concentrations of 100 to 1000 times greater [91]. After maturation, the biofilm life cycle then continues with microorganism detachment and dispersion which is crucial for bacterial survival and transmission of disease. A myriad of factors including overpopulation (due to continuous cell division), competition, and nutrient deficiency causes planktonic cells to detach from the biofilm colony which can then readily disperse, form new biofilm colonies and cause systemic infection [87,89,90].

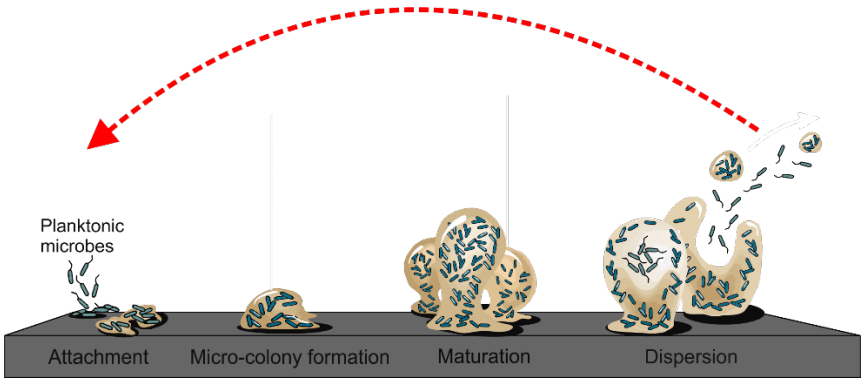

Figure 2.4.3 Biofilm life cycle. Adapted from [92].

Microbial properties such as the presence of fimbriae and flagella as well as surface-associated proteins can also increase the rate of bacterial attachment [9]. Repulsive forces found in most environmental materials, at about 10 – 20 nm from the surface, can help deter microbial attachment however, these appendages along with attractive van der Waals forces, enable the cells to remain in place prior to enforcing a more stable and permanent attachment mechanism [87,90]. Another factor that enhances microbial attachment is the physicochemical properties of the catheter material used i.e. hydrophobicity, porosity and

surface roughness [9]. Lee et al. (2017) studied the development of various biofilm forming microbes on different types of catheter materials. They found that the smooth, less porous silicone-based catheters had 1.5 times less biofilm count than the corresponding latex-based catheters [93]. This is due to rough surfaces having greater surface area than smooth surfaces thus enhancing surface adhesion [82,94]. Additionally, the presence of grooves and trenches on rough surfaces could reduce the effect of shear forces on the microbe, which would therefore lead to better attachment [82]. Adherence to the surface is a key stage in colonisation and it is said that hydrophobic, non-polar surfaces such as those used in catheters lead to more biofilm formation compared to its counterpart [82,89].

2.4.3 Current Practice

Currently, the most sensitive and main diagnostic in determining CRBSI is the significant increase of patient temperature and presence of rigors (periodic onset of cold shivering and sweating) which are highly unspecific, insensitive and unreliable [34]. **Figure 2.4.4** displays the diagnostic process applied when a CVC patient experiences an acute febrile episode. Local inflammation around the catheter site, erythema, purulent discharge and presence of phlebitis can also be used to determine CRBSI [5,95]. However, these are reported to occur even without CRBSI or local infection and thus their use for indicative purposes can be subjective [5,95]. As such, microbiological data linking the catheter to BSI is required. There are various approaches to attain this data and they can be divided into two: requiring catheter removal and catheter-salvage method as summarised in **Table 2.4.2**.

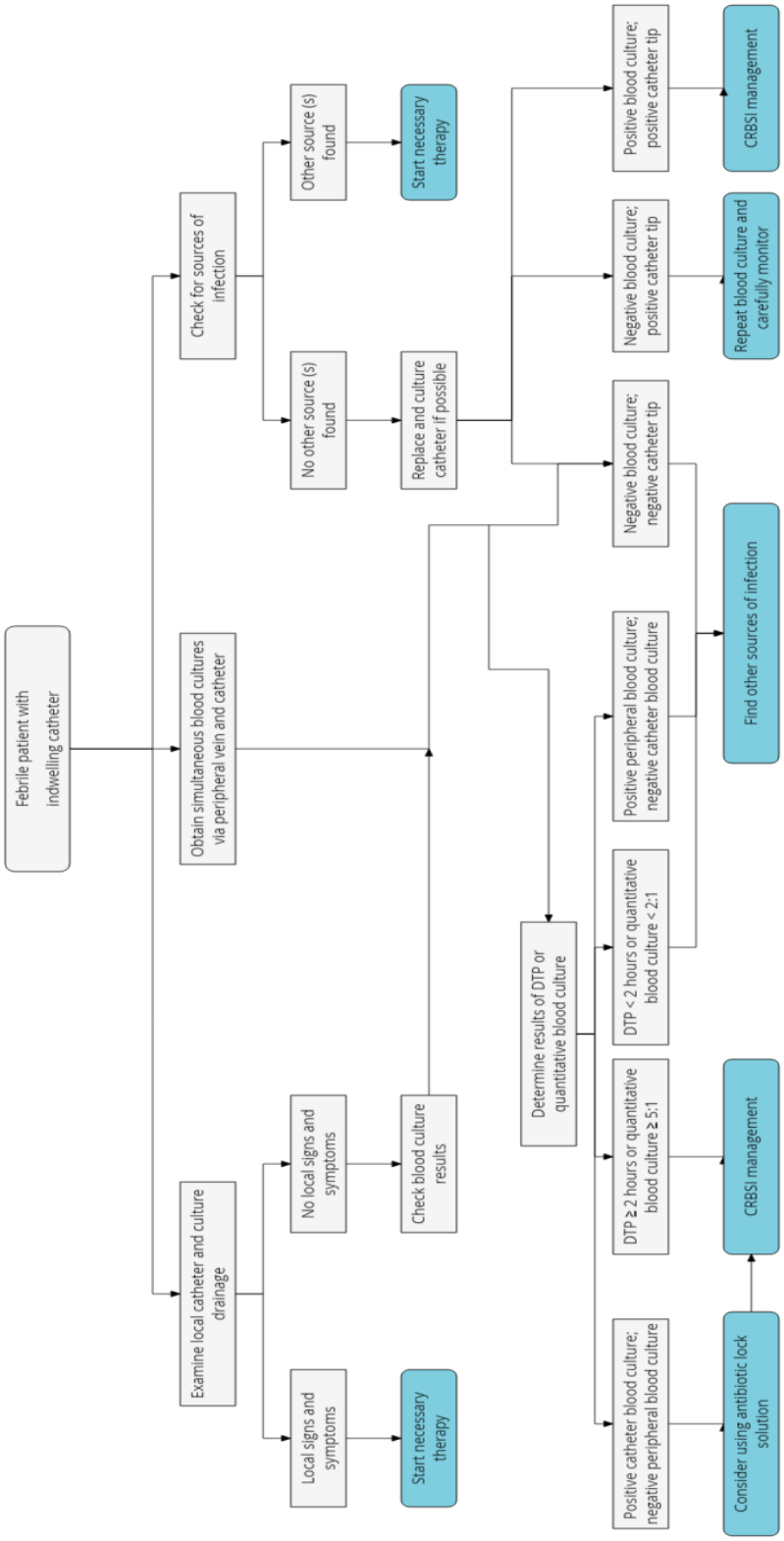

Figure 2.4.4 Diagnosis flowchart for patients with CVC experiencing acute febrile episode. Adapted from [5]. DTP = differential time to positivity.

Table 2.4.2 Microbiological techniques to diagnose CRBSI [5,9].

Procedure	Diagnostic criteria	Sensitivity	Specificity	Disadvantages
Catheter - salvage techniques				
Simultaneous quantitative blood cultures	Quantitative central blood culture results to colony forming unit (CFU) count of ≥ 5-fold more than CFU count from simultaneously drawn blood from peripheral vein	93%	97% - 100%	Costly and labour intensive.
Differential time to positivity	Non-quantitative blood culture drawn from CVC becomes positive ≥2 h before simultaneously drawn blood culture from peripheral vein	89% - 90%	72% - 87%	Interpretation can be difficult due to blood culture contamination or if antibiotics are delivered through catheter line.
CVC-drawn quantitative blood culture	Quantitative blood culture from CVC is ≥100 CFU/mL	81% - 86%	85% - 96%	Cannot differentiate between CRBSI and high-grade bacteraemia.
Acridine orange leucocyte cytospin	Bacteria presence	87%	94%	Not commonly used or tested.
Endoluminal brush	Quantitative culture with >100 CFU/mL	95%	84%	Bacteraemia, arrhythmia and/or embolization may occur.
Requiring catheter removal techniques				
Maki's roll plate, semi-quantitative CVC tip culture	≥15 CFU/mL from a 5 cm CVC tip	45% - 84%	85%	Only detects extra luminal and distal colonisation. Unable to detect microorganisms strongly embedded in biofilm.
Quantitative CVC culture: centrifugation, vortexing, sonication	$\geq 10^3$ CFU from CVC tip	82% - 83%	89-97%	The cut-off points of $\geq 10^3$ CFU vs $\geq 10^2$ CFU is not well defined.
Microscopy of stained CVC: Gram stain and acridine orange staining	Direct visualisation of the microorganisms	84% -100%	97% - 100%	Impractical and labour intensive

As previously noted, CRBSI diagnosis mostly relies on the association of clinical signs and laboratory result synergy. It is important to note that if a positive result is obtained from the catheter but a negative outcome results from the percutaneous blood sample, then it

signifies catheter colonisation rather than CRBSI [3]. Microbiological testing, with or without line removal, provides a much clearer analysis, however, quantitative blood cultures are not always readily accessible.

Currently, patients with CRBSI are treated with antibiotics such as vancomycin, teicoplanin and cefazolin [96]. However the eradication of line contamination by antibiotics can be unreliable and international guidelines, such as those from the Infectious Diseases Society of America, have highly recommended catheter removal - especially when the presence of *Staphylococcus aureus* is detected due to its association to treatment failures and further complications [97]. The impermeable biofilm requires higher concentrations of antibiotics and for a longer period which in turn increases costs. Infection relapse may also occur as an initial culture may find a false negative result, since biofilms can be in a dormant but viable state, thus allowing the microorganisms under the biofilm to regenerate and cause infection [75].

A second method is the total removal of catheter. This is often the primary route for patients suffering from immunodeficiency, however, the build-up of scar tissue means that alternative insertion sites are needed which is not always viable. Additionally, patients suffering from comorbidities, including thrombocytopenia and coagulopathies, and those with clinical needs like intravenous drips and TPN, complicates the catheter removal decision further [98]. Moreover, this can incur a significant amount of resources both for patients and healthcare systems. It is therefore imperative to salvage the vascular line as much as possible. As such, not only is there a total absence of a suitable diagnostic approach, there is also a need for a better treatment method to CRBSI.

2.4.4 Preventative Measures

Due to an increasing prevalence of pathogen colonisation and biofilm formation in indwelling devices - leading to an increased number of CRBSI cases, various protocols, guidelines and technologies have been implemented. Examples of commonly used systems are detailed in turn in the following sections.

2.4.4.1 Disinfection

In order to reduce the risk of biofilm formation and infection, organisations like the CDC and Healthcare Infection Control Practices Advisory Committee (HICPAC) have provided various guidelines and protocols. Precautions are made prior to insertion which includes skin cleansing preparation with an antiseptic (i.e. 70% alcohol, povidone iodine or 2% chlorhexidine gluconate). Continuous training for healthcare staff, having a dedicated infusion therapy team and routine monitoring of CRBSI rates within each institution are also suggested [9,58]. Central venous catheters carry a more substantial risk of infection compared to PICC lines and more stringent, maximal sterile protective precautions are required such as sterile gloves, gown and drapes [9,58]. Moreover, dressing choice such as placing a chlorhexidine gluconate-impregnated sponge (Biopatch ™) in contact with the catheter insertion site and covered with transparent polyurethane film helps reduce microbial colonisation [9,58]. In order to reduce risk of infection, catheters are also typically placed and secured using a suture-less securement device [56]. Likewise, a set of guidelines are provided for the catheterised patients and/or their caregivers for the maintenance of the catheters. This includes daily/routine skin washing with alcohol-based soap or antibacterial products, specifically 2% chlorhexidine for ensuring hygienic, cleansed hands which is associated to the reduction of CRBSI [99–101].

As aforementioned, aseptic techniques including the rubbing of 70% isopropyl alcohol (IPA) are used to reduce the risk of contamination. Alcohol-based wipes are the most commonly used tools to manage and decontaminate catheter lines and needleless connectors since the alcohol dehydrates bacterial cell both during application and as the solution evaporates [102,103]. The addition of a suitable antimicrobial agent such as chlorhexidine or povidone iodine is commonly applied to enhance the potency of this anticontamination technique as it prolongs the required disinfection effect, relying on the immediacy of alcohol and sustained action of the antimicrobial [63,64,104–106]. However, this is not completely effective since it relies on human factors (force applied, procedure duration, etc.) and compliance. Device design issues also have a part to play where the presence of crevices may hinder the penetration of the disinfectant thus reducing the success of complete pathogen eradication. An in vitro study by Menyhay and Maki (2008) discovered that of 30 needleless connectors disinfected with the standard 70% IPA, 67% remained able to transmit the infecting pathogens with up to 25,000 CFU detected [103]. Moreover, there remains a question on the

most effective duration of alcohol rubbing with there being conflicting results from different studies. Some studies [107,108] found that relatively short scrubbing (3-15 seconds) was adequate to disinfect needleless catheter connectors. In contrast, a study by Kaler and Chinn (2007) has found that longer disinfection durations of 15-60 seconds was required to effectively do so [105]. The UK EPIC3 recommendations supports the latter and, based on an expert panel, it is recommended to disinfect such hubs by scrubbing with 70% alcoholic-chlorhexidine pre- and post-manipulation for at least 30 seconds [109]. While 'scrubbing the hub' is internationally recognised as a critical step in attempting to reduce CRBSI cases, it depends heavily on compliance and there remains an issue with disinfecting the entirety of the needle-free connectors (NFC) where penetration to gaps may not be possible.

Additionally, for patients who require frequent blood tests or administration of drug and/or TPN, it means that the catheter hub is frequently manipulated thus leading to a higher risk of contamination. The transition of TPN administration from a healthcare environment to a home-based setting enhances the risk of non-compliance to aseptic guidelines and techniques however, even in hospitals with well-trained healthcare workers, microbial colonisation can still occur. A study by Holroyd et al. (2017) in an intensive care unit setting, showed that catheter hub contamination occurred 44% of the time [69]. Indwelling catheters are known to have a greater risk of CRBSI in comparison to short-term catheters and the increased hub manipulation associated with it may contribute to the reason. Studies [69,110–113] have revealed that if a negative culture is taken from the catheter hub, then it is unlikely that CVC colonisation will occur. This further corroborates the pressing demand for the development of a novel catheter hub which can detect pathogen contamination to reduce the risk of CRBSI.

2.4.4.2 Barrier Caps

The silicone septum previously highlighted in **Figure 2.4.2** is commonly the primary barrier between the lumen of the catheter and external contamination, therefore it plays a key role in preventing pathogens from entering the line. In recent years, passive NFC barrier caps have been developed to provide continuous disinfection whilst the catheter is not in use which, in turn, allows further protection and attempts to reduce CRBSI cases [114–118]. Several design concepts, as well as various operation modes, have been used in creating such barrier caps as highlighted in **Figure 2.4.5**. The basic method is the integration of a foam/gauze

saturated with 70% IPA (i.e. 3M Curos™, SwabCap®, Site-Scrub®) or an antimicrobial (povidone iodine or alcoholic chlorhexidine) which is then threaded onto the luer connector once the catheter is inactive. When the foam comes in contact with the silicone septum, the twisting of the cap provides a degree of friction which can aid in the removal of bacteria. In a revised version, Menyhay and Maki (2008) developed a two-part system where upon threading the antiseptic barrier cap onto the luer connector, an internal spike pierces the capsule containing 2% chlorhexidine gluconate in 70% IPA which only then leads to the saturation of the sponge (**Figure 2.4.5A**) [(103)]. A critical advantage of these systems is their relative independence from NFC manufacturer as it simply requires a conventional luer connector.

Buchman et al. (2009) proposed a contrasting system whereby the barrier cap encapsulates the entire terminal end of the NFC (**Figure 2.4.5B**) which is intended to remain threaded onto the luer connector during flush procedures [(119)]. Supporting this method is a study by Mariyaselvam et al. (2015) where the team stated that syringe tip contamination is often a forgotten factor that leads to CRBSI and thus the retention of the antiseptic foam as a secondary septum could effectively aid in the disinfection of the tips prior to insertion onto the NFC [(120)]. Their alternative to the barrier cap approach was to use syringes with a coated antiseptic tip during flushing and observed a significant eradication of contaminants in comparison to control, non-coated syringe [(120)]. The combination of both strategies could clearly be advantageous were it not for the increased cost.

Although these barrier cap designs do not directly interact with the catheter lumen, they allow the disinfection of the silicone septum and surrounding area, which therefore act as a preventative measure specifically intended for applications where frequent manipulation of the hub is required. In contrast to these, Brunelli et al. (2018) employed ClearGuard® which uses a chlorhexidine-impregnated rod that directly interacts with the catheter lumen and replaces the NFC connector (**Figure 2.4.5C**) [(121)]. The antiseptic diffuses into the intraluminal space which has been shown to be highly effective at reducing CRBSI rates within patients undergoing haemodialysis – a cohort notoriously known to have high rates of infection [(121)].

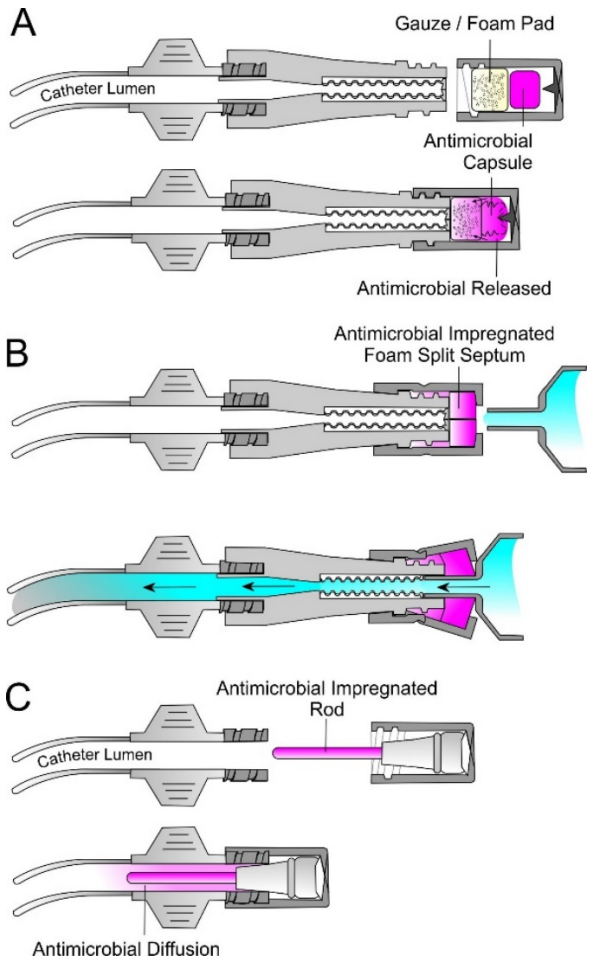

Figure 2.4.5 Designs of NFC barrier caps based on A) a simple foam insert, B) an encapsulating split septum and C) the ClearGuard® terminal cap.

2.4.4.3 Catheter Material

A more prominent method currently used in preventing infection is the choice of catheter material. It has been long recognised that the development and deployment of materials with antimicrobial and antifouling properties is a possible pathway in eradicating catheter contamination, biofilm formation and essentially eliminate the risk of catheter related bloodstream infection. Various research strategies on viable materials are summarised in **Figure 2.4.6**. The catheter material must have properties that would reduce protein adhesion and, as such, the polymer's hydrophilicity, surface energy and material coating are taken into consideration. Historically polyethylene glycol derivatives were tethered at the polymer-solution interface to create a tightly bound water interface which would inevitably make it more arduous to adsorb protein. Catheters were then modified with a protein (albumin) coat which, albeit seemingly counterintuitive, has been shown to significantly reduce protein

deposition that would otherwise adhere and contribute to biofilm formation [122,123]. However, this method provides only a short-term solution as prolonged and continuous interaction with blood eventually causes albumin detachment and removal as it is replaced by higher substrate affinity adhesive proteins found in blood (i.e. fibrinogen) [123]. Ideally, the choice of catheter material is one that doesn't require pre-modification but can effectively minimise adhesion. As such, depending on the duration of use, various materials are used to make catheters but the most commonly used are low surface energy (<25 mN/m) polymers such as silicone and polytetrafluoroethylene (Teflon®) [123–125]. The latter has been associated with a decreased infection rate compared to other materials such as polyvinyl chloride and polyethylene [58]. However, rather than the polymer substrate's intrinsically low surface energy, it has been suggested that passivation by albumin is effectively the main cause of inhibiting non-specific adhesion [123,125]. Manipulating surface topography has also been suggested in that increasing surface roughness or the addition of specific patterning based on biological materials (i.e. Sharklet) would provide superhydrophobic layers which in turn, would effectively impede bacterial growth (i.e. *E. coli* and *S. aureus*) [126]. Moreover, minimising platelet adhesion as well as inhibiting fibrin sheath formation can also be achieved through the introduction of biologically inspired patterning and therefore the translation of such technologies to catheter systems would be markedly beneficial in preventing extra- and intraluminal contamination. However, this approach may be more challenging and currently remains to be a speculative concept.

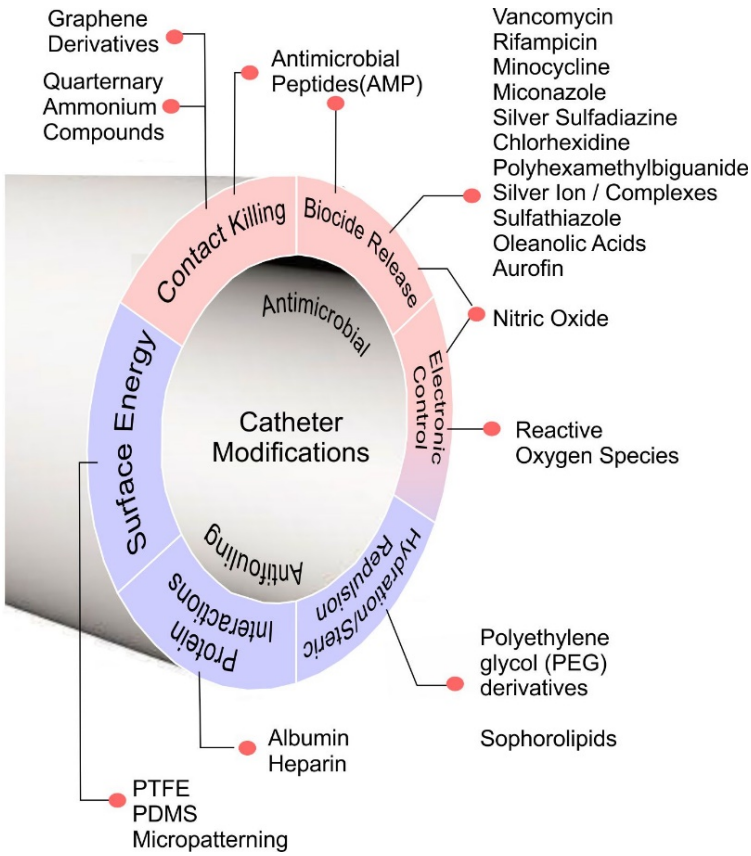

Figure 2.4.6 A summary highlighting various research on suitable materials to prevent catheter contamination.

Furthermore, studies have shown that the use of subcutaneous and silver impregnated cuffs have lowered the risk of infection [127]. Subcutaneous Dacron® (polyethylene terephthalate) cuffs are incorporated on Hickman and Broviac catheters which produces a barrier against skin flora invasion by allowing host tissue to grow over it [127]. A systematic review by Maki et al. (2006) showed that cuffed and tunnelled CVCs decrease the risk of CRBSI by nearly half (1.6 per 1000 catheter days) compared to non-cuffed, non-tunnelled CVCs (2.7 per 1000 catheter days) [128]. Similarly, attachable silver impregnated cuffs are used for short-term catheters [128]. The silver ions act as antiseptic agents against both bacteria and fungi preventing their migration through the insertion tract [127,129]. Out of 234 catheters studied, the silver cuffs produced nearly 25% bacteria less than control catheters (1.0% vs 3.7%) [130]. The main disadvantage of cuffs is their inability to prevent infection from other sources such as already existing microorganisms in the catheter hub, poor home care techniques and frequent manipulation of catheters [129].

2.4.4.4 Anticoagulants

The presence of thrombus is widely associated with septic thrombophlebitis but, importantly, also serves as a nidus of CRBSI [51,131]. Presently, catheters are prophylactically infused with anticoagulant agents such as heparin to decrease the occurrence of catheter thrombosis, however, this may also have the additional benefit of reducing CRBSI. In a meta-analysis study of 14 randomised trials by Randolph et al. (1998), it was suggested that heparin bonding and heparin prophylaxis reduce the risk of microbial contamination as well as thrombosis caused by central venous catheters [132]. However, this didn't clearly define the effect of heparin in the reduction of CRBSI and CDC guidelines encourage the avoidance of routine employment of anticoagulant therapy [58,131]. Nonetheless, prophylactic heparin is still employed for deep vein thrombosis and could be helpful to maintain line integrity. Other contradicting explanations have also been suggested to elucidate the mechanisms of heparin coating and how it increases resistance to non-specific protein fouling (i.e. protein specific interaction, inhibition of bacterial adhesion, electrostatic repulsion, etc.), however, further studies are needed to determine whether these suggestions perform collectively or a specific mode of action predominates.

2.4.4.5 Antiseptic Impregnated Catheters

Another preventative measure currently used is the antimicrobial coating or impregnation of catheters which minimises microbial colonisation. There are 3 types of antiseptic/antimicrobial agents currently used in catheters: chlorhexidine-silver sulfadiazine (ChSSD), minocycline-rifampicin (MinR) and rifampicin-miconazole (RM) [58,133]. **Table 2.4.3** summarises the properties and functionality of each compound components.

Table 2.4.3 Summarised information on common antiseptic/antimicrobial components used in catheter impregnation.

Nomenclature	Structure	Mechanism of action	Classification	Ref.
Chlorhexidine	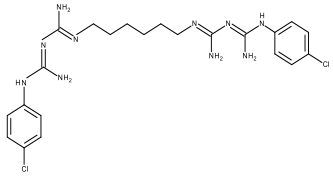	Initiates cell death through cell wall binding and disruption of cytoplasmic membrane leading to outflow of cell contents.	Antiseptic Antibacterial Antifungal	(134,135)
Silver sulfadiazine	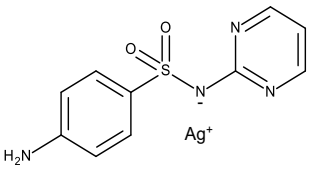	The slow release of silver ions, triggered by the interaction with sodium chloride-containing fluids, initiates disulphide bond formation causing changes to protein structure and inactivation of certain enzymes. It also disrupts DNA syntheses through inhibiting folic acid metabolism.	Antibacterial Antifungal	(136)
Minocycline	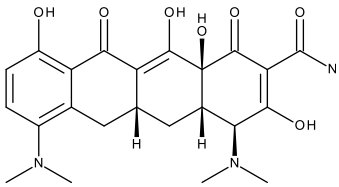	Beneficial effect via calcium chelation, antioxidant functionalities as well as tissue penetration leading to protein synthesis inhibition.	Antibacterial	(137,138)
Rifampicin	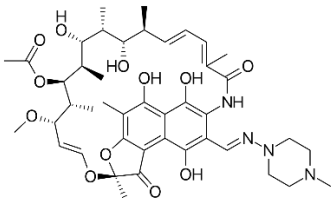	Binds to RNA polymerase which physically blocks RNA synthesis therefore inhibiting transcription and synthesis of proteins.	Antibacterial	(139)
Miconazole	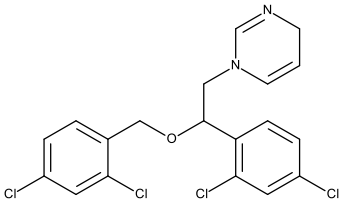	Initiates an internal release of reactive oxygen species within the fungal specimen, causing oxidative stress and eventually cell death.	Antifungal	(140–142)

In a clinical trial comparing 403 catheters, those externally coated with ChSSD against bare catheters, showed a decrease in colonisation rate when the former was used (13.5 vs 24.1 per 100 catheters) [143]. The same study stated that the use of ChSSD-impregnated catheters resulted in nearly a fivefold reduction in producing CRBSI with 1.6 incident per 1000 catheters compared to 7.6 [143]. Comparing the first generation of catheters impregnated with ChSSD with that of MinR-impregnated catheters, the latter was found to be associated with a lower infection rate. In a study of 738 catheters, there was a 14.9% decrease in colonisation of catheters impregnated with MinR compared to ChSSD. The difference remained roughly constant when the duration of catheter use was also compared (6.0% vs 21.4% with catheters placed for less than 7 days; 10.8% vs 24.4% for those placed for more than 7 days). The difference in efficacy between the two could be due to the fact that catheters are coated with MinR both internally and externally whilst those with ChSSD are only externally coated. Similarly, in a study conducted by Lorente et al. (2016), RM-impregnated catheters also resulted in a significant decrease in CRBSI rate. Of the 227 patients with RM-coated catheters, corresponding to 2,009 CVC days, no cases of CRBSI was reported whilst 18 reports were registered in 245 patients using standard catheters [144].

A multivariate cost-effectiveness analysis by Veenstra et al. (1999) stated that an antiseptic-impregnated catheter is expected to save approximately US $196 in direct medical costs (i.e. additional costs for medical interventions attributable to CRSBI including specialist and nursing care) per catheter, with an upper limit estimate of US $391 saving compared to a standard catheter [145]. Additionally, CRBSI incidence is predicted to decrease by 2.2% (relative decrease of 42%) and local infection incidence to decrease from 12.4% to 7.5%, when an impregnated catheter is used in comparison to a bare catheter [145]. Although antiseptic impregnation of catheters is an efficient and beneficial method in minimising the risk of CRBSI, impregnated catheters are said to lose their function after around 14 days and as such are only suitable for short term use [9,58]. The use of antibiotics can also add to the ever-increasing resistance to antibiotics. Attributable to the ever-increasing antimicrobial resistance, the urge to find novel alternative methods to tackle infection caused by biofilm-forming microorganisms are intensifying.

2.4.4.6 Lock Solutions

Lock solutions have also been widely practiced as a preventative measure of CRBSI and which also increase the chance of salvaging the venous access line for long-term CVC patients. During periods in which the line is dormant, the European Society for Clinical Nutrition and Metabolism (ESPEN) recommend solutions containing saline to be flushed and locked after TPN administration [146,147]. This not only prevents blood reflux back to the line, but it also maintains catheter patency. Depending on guidelines generated by catheter manufacturer, heparin lock solutions may be required which reduces blood clot formation. Although heparin is known for its anticoagulant as well as antimicrobial properties, a contradicting study by Shanks et al. (2005) have shown the contentious nature of heparin in that it may actually promote staphylococcal biofilm formation at clinically relevant concentrations [5,148]. In instances where heparin is mandatory, saline lock solution must be introduced prior to locking the catheter lumen with heparinised solutions [146,147].

As a recent approach in tackling CRBSI, antimicrobial catheter lock solutions applied within the catheter lumen are used. There are two types: antibiotic and antimicrobial (non-antibiotic) locks. This is an important therapeutic solution especially in cases where the salvage of a previously infected catheter is possible and desirable. The principal purpose of an antibiotic lock solution (ALS) is to eradicate early biofilm formation [10,11,149,150] inside the catheter lumen by using a small volume of highly concentrated antibiotics such as vancomycin and gentamycin for a period of 12 – 72 hours [11]. However antibiotic lock solutions are not ideal as they can lead to the emergence antibiotic-resistant organisms. The use of glycopeptide antibiotics such vancomycin should particularly be avoided to prevent the development of vancomycin-resistant Gram-positive microbes. These antibiotics are currently the only available treatment to infections caused by penicillin-resistant enterococci and methicillin-resistant staphylococci [49]. Additionally, ALS reduces access to the catheter for 7-14 days as it is necessary for the long-term catheter to be locked for this length of time which could result in patient distress especially for those who have limited venous access [10,11]. Lastly, the removal of catheter is still recommended for cases involving *S. aureus* and *P. aeruginosa* since there is still a high risk of ALS failure in eradicating these pathogens [10,11]. Thus, this is not an efficient way of eradicating biofilms and there is a need for a solution that requires less time of catheter unavailability [11].

Non-antibiotic substances such as ethylenediaminetetraacetic acid (EDTA), ethanol and citrate have also been discovered to reduce the risk of CRBSI. Chelators like citrate and EDTA can be used as alternatives to heparin as they have both anticoagulant and antimicrobial capabilities [5]. Cell membranes appear to be degraded when calcium and magnesium ions are chelated, causing an increase in their permeability, ultimately leading to cell death [17]. Bookstaver et al. (2009) showed that a 4-hour time point, the synergy between gentamicin and EDTA showcased a 3.98 log unit reduction of methicillin-susceptible *S.aureus,* a significantly greater decrease than other lock solutions and even more so in solutions without EDTA [150] . In addition, gentamicin-EDTA solutions have been proven to reduce biofilm-producing strains of *E. coli* and *P. aeruginosa* [10]. Similarly, a study by Lebeaux et al. (2015) disclosed that EDTA improves the effect of gentamicin in eliminating bacteria by up to 3 log units [11]. They also found that EDTA alone was better at eradicating *S. aureus* in comparison to vancomycin. The addition of EDTA to vancomycin and amikacin, used for Gram-positive and Gram-negative bacteria respectively, resulted in an increased rate of eliminating most strains of biofilm-forming bacteria by up to 50% [11]. However, this method still requires the use of antibiotics which, as mentioned above, is not a suitable solution.

Correspondingly, citrate has been shown to significantly lower bacterial colonisation compared with heparin locks [96]. Weijmer et al. (2005) studied the effect of using 30% trisodium citrate (TSC) against heparin lock solutions in haemodialysis patients. In comparison to a total of 33 episodes of CRBSI in patients administered with heparin lock solution, only 9 patients assigned to TSC suffered CRSBI [151]. Bloodstream infection rates decreased with TSC in both tunnelled, cuffed and untunnelled, uncuffed catheters compared to heparin. Additionally, this suggested that fewer patients would die due to sepsis as a result of using TSC, with no increased risk of catheter malfunction for discontinuing the use of heparin. Similarly, the recommended 46.7% TSC also significantly reduced CRBSI cases and catheter days at risk, reportedly due to the significant decrease in staphylococcal infection [17]. However, citrate is said to support the growth of other biofilm-forming microorganisms, specifically *E. coli* and *K. pneumoniae*, leading to CRSBSI risk [152]. Similar to heparin use, this too highlights the contentious properties of citrate lock solutions which could possibly be explained by the lack of standardisation in the assessment of effectiveness as well as the different approaches or observation methods in varying studies.

Another substance used as lock solution is taurolidine. Studies [19,152–154] have shown the effectiveness of 2% taurolidine as well as 1.34% taurolidine-citrate (TC) and 1.34% taurolidine-citrate-heparin (TCH) in eradicating bacteria and fungi [154]. Olthof et al. (2015) showed that lock solutions containing taurolidine efficiently reduced the growth of *S. aureus* and *E. coli* [152]. It was found that even after 60 hours of culture, no microbial growth was observed. Additionally, the study concluded that the more concentrated (2%) taurolidine lock solution (TLS) allowed the inhibition of growth of both bacteria for ten hours longer in comparison to the commercially available diluted solutions. Moreover, it seems that citrate does not contribute to the antimicrobial activity [152,154]. This was discovered when the commercially available 2% taurolidine was diluted to 1.34% (concentration of taurolidine in TC and TCH lock solutions) and no significant difference in bacterial growth inhibition was seen between each parameter [152]. The effectiveness of taurolidine in inhibiting growth can be explained by its involvement in the chemical reaction with endotoxins, exotoxins and microbial cell wall [152]. This leads to a decrease in the microorganism's pathogenicity and adhesion to various surfaces. Taurolidine is derived from formaldehyde and aminosulphonic acid taurinamide which are effective at eradicating a range of bacteria, fungi and biofilms [19,152,154]. The use of taurolidine therefore has many advantages including its non-toxicity (metabolised into water, carbon dioxide and taurine) and, equally as important, the absence of antibiotics means that it doesn't contribute to antimicrobial resistance [19,152]. A disadvantage of TLS is its cost – €300 more than heparin treatment (around €1,500 per year) and, as such, an analysis of its cost-effectiveness is required [145]. Additionally, another study by Olthof et al. (2014) reported that approximately 7% of their patients with TLS experienced side effects (i.e. mouth tingling sensation despite intravenous delivery) that made them retract the use of or swap to a different solution of taurolidine in the said patients [155].

Besides the aforementioned locks, ethanol solutions have also been suggested. Ethanol is known for its effectiveness in eradicating a wide variety of microorganisms including biofilm formation [9]. Peters et al. (2013) discovered that the metabolic activity of monomicrobial and polymicrobial biofilms made up of *C. albicans* and *S. aureus,* cultured on polystyrene and silicone, were inhibited using only 10% ethanol (EtOH) and were eradicated with ethanol concentrations greater than 20% when exposed for at least 2 hours [98]. However, they found that regrowth was still possible at smaller concentrations of EtOH. It was also observed that 30% and 50% of ethanol exposure was required to prevent biofilm regrowth of *C. albicans* and *S. aureus,* respectively [98]. Similarly, an in vitro study by Rane et al. (2012) discovered

cell regrowth of *C. albicans* in silicone disks after administering EtOH concentrations below 35% for 2 and 4 hours [156]. This suggests that ethanol solution ≥ 35% along with a treatment time of at least 4 hours is necessary for adequate sterilization and biofilm removal [156]. A study by Balestrino et al. (2009) cultured biofilms composed of *C. albicans*, *S. epidermidis, K. pneumoniae* and *P. aeruginosa* on silicone catheter fragments for 4 hours and 24 hours [13]. They showed that a 20 minute exposure to 60% ethanol solution fully eradicated the biofilms irrespective of incubation time, with the exception of *S. epidermidis,* which required an extra 10 minutes before complete eradication [13].

Ethanol has been widely used as an effective disinfectant against bacteria and fungi with little to no adverse effect and, as per the previously mentioned studies, it is an attractive efficacious solution to biofilm formation in catheters. However, the effects of high EtOH concentrations on the catheter and catheter material should also be considered. Laird et al. (2005) administered 3 mL of 100% ethanol lock solution for 24 hours in three cases of CVCs inhabited by coagulase negative staphylococci [157]. Precipitated material was noticeably visible upon line aspiration and all three CVCs rapidly occluded, with one being completely sealed that it could not be spared and had to be removed [157]. Removal due to occlusion after a short period of time is not ideal for long-term indwelling devices such as CVCs. Furthermore, a systematic review by Mermel and Alang (2014) presented twenty clinical and eight in vitro studies of ethanol lock solutions with adverse effects [158]. The effects varied and included catheter fracture, dysfunction, occlusion and catheter removal [158]. A more recent study by Meckmongkol et al. (2018) also revealed that due to EtOH lock therapy, there was an increased catheter breakage rate from 0 to 13.7 and thrombosis rate from 0 to 3, both per 1,000 catheter days [159]. This further question the efficiency of ethanol lock solution in catheter salvage. Contradicting studies were also mentioned which showed an increase in biofilm formation of *S. epidermidis* [160] and *S. aureus* [161] in the presence of ethanol. Moreover, it is important to remember that ethanol does not have anticoagulant properties and thus can lead to other unwanted effects i.e. thrombosis.

An alternative lock solution component is sodium bicarbonate ($NaHCO_3$). Sodium bicarbonate has the ability to inhibit fibrin formation, and thus reduce blood clot development, through the chelation of calcium ions [162]. Apart from this, it also has the ability to hinder bacterial adherence thus inhibiting biofilm formation [162,163]. Farha et al. (2018) provided an extensive research on the properties, mechanism and antibacterial effect of

bicarbonate. The work states that bicarbonate selectively dissipates the pH gradient found in the transmembrane which, in addition to the membrane potential, completes the proton motive force (PMF) of bacteria [163]. This is significant as the efficiency of antibiotics as well as several components of bacteria's distinct immunity are dependent on the uptake and/or kinetics of PMF [163]. Moreover, the team found that by employing the bicarbonate system, superfluous protons are consumed thus causing the proton gradient of the bacterial transmembrane to short-circuit leading to microorganism complications/growth disruption which in turn could reduce the risk of CBRSI [163].

Biofilm formation of *P. aeruginosa* as well as growth of several planktonic bacteria were seen to be impeded by the presence of concentrated bicarbonate [164]. A recent study by El-Hennawy et al. (2020) found that 15 out of 226 catheterised patients who received normal saline lock solution had catheter removal due to CRBSI [162]. On the other hand, only 1 out of 225 patients who had been given a $NaHCO_3$ lock solution had catheter loss due CRBSI, translating to a significant comparison of 6.6% to 0.4%, respectively [162]. Its effects on fungal activity were also studied by Letscher-Bru et al. (2013), where they discovered that 10 g/L concentration of $NaHCO_3$ impeded 80% growth of all fungal specimens in vitro and fully inhibited the growth of 19 out of 24 fungoid infected clinical samples ex vivo [165]. The presence of bicarbonate in the bloodstream as well as in several tissues allows the exploration of $NaHCO_3$ lock solution as a safe method of reducing CRBSI. Still, additional studies are required to further prove the efficacy of sodium bicarbonate on the in situ susceptibility of biofilm-forming microorganisms. Moreover, research on the effect of bicarbonate on intravenous fluids as well as the catheter line integrity should be considered.

One potentially major disadvantage of using a lock solution is its transfer from the catheter line into the circulation at injection and in inter-dialytic sessions [96]. The parabolic flow distribution during injection and the gravity induced discharge, due to fluid (blood and lock solution) density differences from the distal end of the catheter, can cause the leakage of lock solution contents into the bloodstream [96]. This could then cause various events from allergic reactions to arrhythmias and toxicity. In addition, antibiotic lock spillage can emerge as the source of resistance [96]. It is also unlikely that a general, standardised lock solution will be generated due to the variance in epidemiological data, the diverging requirements to eradicate specific pathogens and in addition, the existence of patient-specific complications.

Although these are all adequate preventative measures, and should still be continued to use, they do not fully eliminate the risk of microbial infection. Therefore, in order to eradicate microbial colonisation and thus reduce the risk of CRBSI to zero, a coordinated and simultaneous adherence to aseptic techniques and introduction of novel technology is necessary.

2.5 Emerging Technologies

2.5.1 Reactive Oxygen Species

Another pathway in eradicating biofilm formation, especially those formed by drug-resistant microorganisms, is the production and exploitation of reactive oxygen species (ROS). The term reactive oxygen species encompasses agents such as: hydrogen peroxide (H_2O_2), peroxide (O_2^{-2}), hydroxyl radicals ($OH\cdot$), hydroxyl ions (OH^-), superoxide anion (O_2^-) and singlet oxygen ($^1O_2$) [166,167]. These are normally generated as by-products of cellular biological processes specifically during electron transport/oxidative metabolism in the mitochondria or as a response to bacterial contamination, cytokines and xenobiotics [168].

Through its activity in cellular processes, ROS are able to induce oxidative stress when its concentration goes beyond the capacity of the cell to mount an adequate antioxidant counteraction, leading to an imbalance in the equilibrium [168]. This leads to cellular adverse effects like damaging cellular structures such as deoxyribonucleic acid and cell membrane, which eventually leads to cell death [169]. Reactive oxygen species are known for their effectiveness against infection-causing Gram-positive and Gram-negative pathogens and more importantly, multi-drug resistant organisms [166]. Additionally, biofilm-forming microorganisms commonly isolated from CVCs include *C. albicans* and *S. aureus.* These are notoriously opportunistic pathogens that can, not only cause diseases on their own, but can also co-infect leading to morbidities such as biofilm associated infection and sepsis [169]. What makes them more formidable is their ability to resist existing antifungal and antibacterial agents, respectively. A solution to this problem, as well as alleviating the drawbacks from previously mentioned methods, may be the employment of reactive oxygen species.

The effect of reactive oxygen species on the elimination of pathogens and biofilms inhabiting superficial and chronic wounds, internal soft tissues and epithelial surfaces are currently

being researched [166,170,171]. It is stated that the employment of the mechanistic action of ROS in controlling and eradicating microorganisms is the first fully novel antimicrobial system used for early clinical intervention for a number of decades [172]. An example of this approach is the application of honey which has been known for its curative and antiseptic functionalities for over a millennium. Medical grade honey is an example of this (i.e. manuka honey) which is composed of sugar, methylglyoxal and ROS hydrogen peroxide [171,173]. Several studies have shown its antibacterial [174–177], antifungal [178–180] and more importantly, anti-biofilm [181–183] properties. An engineered honey, known as Surgihoney™, was developed which, through controlled-ROS release, eliminates bacterial contamination and prevents biofilm formation on wounds [172]. Surgihoney™ is based on organic, natural honey (which produces inconsistent, low levels of hydrogen peroxide) that has underwent a bioengineered process whereby its antimicrobial potency is enhanced and managed through controlling/intensifying its hydrogen peroxide activity and allowing the consistent release of ROS [184,185]. Subsequent investigations [184–187] have evidently disclosed that Surgihoney™ has a greater potency in eliminating bacteria, fungi and biofilms compared to other types of honey. This enhanced efficiency is mainly explained by the increased production of ROS thus signifying its potential importance in reducing CRBSI cases. Although it is clear that Surgihoney™ is an effective method in eradicating microorganisms and a suitable alternative which does not add to antimicrobial resistance, it is unfortunately not applicable to CVC systems. Challenges would arise in integrating the gel within the catheter line and problems with leaching as well as damage to the line may also become problematic. However, the employment of ROS mechanisms in preventing biofilm formation continues to be a valuable method.

Nair et al. (2016) studied several phytochemicals and discovered plumbagin as a naturally occurring quinone that has inhibitory antimicrobial properties that can eradicate catheter-colonising pathogens [169]. They found that plumbagin-treated *C. albicans* and *S. aureus* respectively produced 1.5 and 2.5 times more reactive oxygen species (ROS) in comparison to the non-treated pathogens while hydrogen peroxide, a known inducer of ROS, caused 3- and 3.5-fold increase, respectively [169]. **Figure 2.5.1** displays the release of ROS from plumbagin. The same study showed that plumbagin effectively disrupted both the 24-hour old mono and polymicrobial biofilms produced by the said microorganisms cultured in glass tubes. The minimum inhibitory concentration (MIC) of plumbagin (5 µg/mL) decreased biofilm formation of *C. albicans* and *S. aureus* by 58% and 67% respectively while 4X MIC

reduced this by 67% and 92.5%. However, plumbagin treatment was less efficient at eradicating the polymicrobial biofilm and even less so when the pathogens were adhered onto urinary catheter silicone tubes and later treated with the quinone. Additionally, at 50 µg/disc, plumbagin did not show any inhibitory action against other common pathogens found in catheters such as *P. aeruginosa* and *K. pneumoniae.*

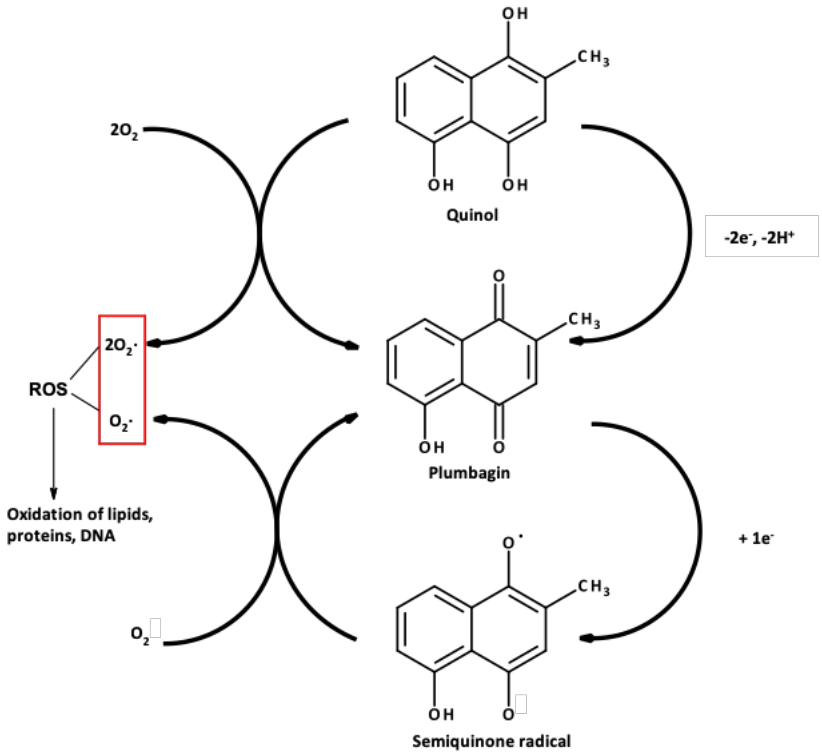

Figure 2.5.1 Plumbagin mechanism of action to release ROS [188].

Davis et al. (2013) successfully electropolymerised plumbagin on to carbon fibre and exploited its pH-dependent redox properties as a basis of a pH sensitive probe [189]. It is evident therefore that plumbagin can have a dual purpose in CVC systems wherein it could potentially aid in the eradication of contaminants whilst also being capable of monitoring the condition of the line. However, although effective at killing some microorganisms, plumbagin's ability to damage DNA, cause instability of genome and trigger telomere dysfunction [190,191] can alternatively cause adverse effects if healthy cells are unintentionally targeted. The ability to covalently tether plumbagin to the catheter would offer a solution however, the possibility of leaching remains to be a challenge. As such, the question lies on whether the benefits of using plumbagin for eradicating biofilm formation outweigh the risk of potentially attaining the unwanted secondary effect.

Nevertheless, the key takeaway from this section is the underlying principle of ROS release and its potency in eradicating formidable pathogens. This knowledge can be exploited to design and develop methods in eradicating pathogen colonisation and biofilm development in catheter systems and thus eliminate the risk of catheter-related bloodstream infection.

2.5.2 Enhanced Catheter Systems

Previous methodologies primarily focus on decreasing the rate of CRBSI by actively eliminating pathogens that are already present in the catheter system. In spite of some successes, there is still a need for a vigorous diagnostic and therapeutic method that completely impedes (or eradicates) central line pathogen contamination.

As mentioned in **Section 2.4.1**, the catheter hub is most common nidus related to CRBSI. It is therefore predictable that new hub designs are developed to help reduce the risk of infection. Perhaps one of the first instances of this was in 1996 where Segura et al. (1996) designed and employed a catheter hub which enclosed an antiseptic chamber saturated with 3% iodinated alcohol [(192)]. Of the 151 patients included in the study, 73 patients had catheters with the control hub design while 78 received the new design [(192)]. In comparison to the control, there was a four-fold decrease in catheter sepsis rate and a reduced catheter hub contamination in patients who received the alcohol-filled hub. A contradicting study was however completed by Luna et al. (2000). They found no significant difference between the control and new product group and have stated that the employment of the antiseptic chamber had similar effects as standard good clinical practices [(193)]. Nonetheless, this does not hinder the need for the development of a new hub design that would significantly and efficiently tackle hub contamination and consequently, catheter-related bloodstream infection.

A more recent technological advancement is the development of a smart central venous port by Paredes et al. (2014). Their miniaturised system is composed of an antenna, electronics and a biosensor for the rapid and early detection of biofilm onset [(194)]. The two former components are fundamentally required for the operation and long-range data transmission of the product, respectively [(194)]. The system is powered via a 50 mAh coin-cell battery which, it was reported can be active for 11 months [(194)]. The label-free interdigitated biosensor is composed of a three-inch oxidised silicon wafer array which is functionalised through the

deposition of radio frequency sputtered gold film. Through conducting impedimetric methods, the microelectrode is able to analyse the condition of the port's chamber and therein provide an assessment of the condition of the line. The team has successfully evaluated the effect of varying frequency on the impedance and equivalent serial capacitance measurements in the presence of *S. epidermidis* [194]. The results demonstrated that in the presence of bacteria, then consequently biofilm formation, the capacitance measurements increase while the impedance signals decrease, with significant changes detected as early as 10 hours after bacteria introduction. Additionally, the lowest frequency of 10 Hz has displayed better measurement changes and hence sensitivity to bacterial contamination.

While the system's advantages rest on detecting bacterial colonisation, validation of the system in complex solutions is absent and it lacks the much-needed therapeutic effect. The in vitro detection also depends on pathogen concentration and location which typically vary in each case of CRBSI. Flaws may also be observed with the trigger process of the device as it relies on a sequence pattern stimulated by an external signal. Moreover, the system requires improvements on its ability to decipher between steady and non-steady stages during electrical analysis. Although electronic compensations for minor and/or long-term changes were made, it is stated that false positive results can nonetheless occur and thus still requires medical staff intervention [194]. Further enhancement of this system along with the integration of a biofilm-eradicating component could nevertheless assist in combatting catheter-related bloodstream infection.

It should be noted that an electro-modulated smart catheter system was reported and ostensibly was at early stage development by Dr. Dipankar Koley and his team in 2012. He stated that the system chemically detects pH changes which in turn activates the release of therapeutic nitric oxide (NO). The smart activation and deactivation of the anti-biofilm compound allows its preservation and therefore the design can theoretically be used for over a week [195] . As of writing, no further information and commercial availability have been presented. Although this is the case, the release of NO as an effective eradication method has continued to be studied by others [196,197]. In catheter applications, the reactive nitrogen species (RNS) plays a key role in not only reducing platelet adhesion, but it also possesses antifouling properties suitable for in situ purposes. A study by Pant et al. (2018) found that by covalently linking N-acetyl penicillamine on silicone catheters where the thiol group can

be further functionalised to become a NO donor, the RNS can be stored and then released to provide anti-fouling characteristics which remains to be effective even after the NO biocides have been distributed [196].

In a separate study by Mihu et al. (2017), the team exploited the thermal reaction between nitrite and glucose during sol-gel formation process to entrap and then later generate NO directly from the nanoparticles [197]. The team notes that the adhesion of methicillin-resistant *S. aureus* is hindered significantly upon incubation with 2.5 mg/mL and >5 mg/mL concentrations of nitric oxide nanoparticles - reducing cell growth by 40% and 50%, respectively. More importantly in this case, the latter condition reduced the pathogen's biofilm viability by 51.8%. Additionally, bacterial growth was reduced by half after 8 hours of exposure without incubation with only 2.5 mg/mL concentration of NO and which remained even after 24 hours. This means that the interaction of the nanoparticle with the pathogen has a similar effect to that of antibiotic lock solutions while offering reduced dwell times [197]. This therefore indicates that the impregnation of catheters with NO-releasing nanoparticles is a viable route to replace, or an alternative to, prophylactic locking and provides a pathway where antibiotics are no longer required. However, further research into the in vivo effect of NO nanoparticle release is required.

2.6 Electrochemical Methods

The accessibility and availability of other electrochemical methodologies as a potential pathway to monitoring catheter lines and reducing catheter related bloodstream infection are briefly discussed in this section.

2.6.1 pH Sensing

Due to the products and by-products produced by biofilm metabolism, commonly lactic acid, acetic acid and ammonia, the presence of biofilm can induce changes to its local pH environment and, as such, pH can be an indirect method of detecting the presence of bacteria. Detecting pH electrochemically has been widely used for its ease of use and fast analysis. The most ubiquitous form of electrochemical pH sensing is the variety of commercially available pH sensors. In general, commercial glass pH sensors contain an electrode whose voltage varies relative to the concentration of hydrogen ions (H^+) and a

reference electrode that is non-polarisable and is unaffected by H^+ activity. Hence, the sensor can measure the change in H^+ ion concentrations and thereby pH changes. However, traditional glass pH sensors are rigid and have been gradually incompatible in miniaturised systems – especially when considering the physical dimensions of most CVC lines. Conventional glass pH probes also often require calibration to reduce potential drifts caused by the dehydration of the membrane, leading to a decreased sensitivity towards hydrogen activities [(198)]. This can become problematic in many applications where the probe is expected to accurately measure pH over a long period of time without intervention i.e. oceanographic, aquifer and source water network monitoring. Additionally, higher alkaline levels would normally affect the accuracy of glass probes since alkali ions (similarly sized to hydrogen ions) can permeate through the glass membrane causing a false increased measurement of hydrogen activities [(198)]. Thus, several, more flexible and readily scaled down materials have been characterised and employed as new pH sensing electrodes.

The most common reason for commercial pH probes requiring frequent recalibration is due to reference electrode drifts [(199)]. Throughout the years, parts of the sensor have been enhanced to try and overcome this issue. A primary example is the use of double junction probes which requires two junction to get through to the test solution which, in turn, delays electrolyte poisoning and help maintain the stability of the reference electrode [(199)]. If the test solution and conditions/environment remain the same, algorithms can be used to predict reference electrode drift [(199)]. Although predicting and delaying drift is useful, this does not stop the need for calibration. As such, a more recent and novel technology developed by ANB Sensors has negated the need for manual reference recalibration by creating a sensor that can self-calibrate. Their technology employs a second electrode into the reference chamber alongside the reference electrode [(199)]. The former reference tracking electrode is exploited to periodically track and measure any drift in the latter and automatically offsets the pH measurement [(199)]. In addition, their device can be integrated into existing conventional glass pH probes and eliminates the requirement for frequent, manual calibration [(199)].

The main issue in developing miniaturised systems – whether based on potentiometric or voltammetric detection also relates to the reference electrode. As with the glass electrode, the inclusion of a silver-silver chloride half cell with a predetermined chloride reservoir is not practical for the given application. As such, the common recourse is to use a solid state silver-

silver chloride pseudo reference in which the potential is determined by the chloride concentration within the sample. In the case of physiological solutions, it can be anticipated that the chloride concentration will be tightly regulated by the homeostatic checks and balances of the body's metabolism and should be relatively constant (typically 0.1 M).

A study by Robinson and Lawrence (2006) were among the first to explore an alternative to the pseudo reference approach through the use of a vinylferrocene and vinylanthracene-containing copolymer as a pH sensitive modifier [(200)]. The former moiety is pH insensitive and therefore acts as an internal reference while anthracene is purposed as the pH sensitive component due to its pH dependent redox activity. The copolymer was therefore exploited as the basis of a single component pH sensor. The pH was measured through employing square wave voltammetry and using the oxidation potential of anthracene with respect to that of the ferrocene peak position. A near Nernstian behaviour of 54 mV/pH was observed (pH 4, 7 and 9). It should be noted that the probe is also capable of detecting sulphide under cyclic voltammetric conditions wherein the sulphide is subjected to an electrocatalytic reaction with the oxidation of ferrocene [(200)]. In a separate study, the team also investigated the effect of derivatised carbon nanotubes on the copolymer's ability to determine pH [(201)]. It was observed that the presence of the nanotubes led to a better Nernstian response (59 mV/pH vs 63.1 mV/pH) and the relationship between the peak potential and pH remained linear for a wider pH range - change in Nernstian response occurred at pH 11.7 compared to pH 9.5 in the absence of carbon nanotube [(201)].

Several studies including those completed by Lawrence at al. (2007) [(202)], Lafitte et al. (2008) [(203)], Compton et al. (2011) [(198)] and Gao et al. (2018) [(204)] have also used ferrocene as a non-pH dependent internal reference. These studies used varying pH sensitive compounds (i.e. anthraquinone, phenanthraquinone, nitrosophenyl and alizarin) but the core remit remains the same in that ferrocene is used as the pH insensitive internal reference. The primary advantage of this is that, in principle, the produced electrode would be calibrationless since the peak potential of ferrocene will remain consistent irrespective of the solution composition. Since ferrocene is unaffected by these issues, its employment as an internal reference can therefore provide a suitable solution. Lawrence et al (2016) [(205,206)] have also developed a novel approach to the reference system for systems in low buffered media where the use of appropriately functionalised quinone species can set the local environment pH (typically one pH unit above or below pH 7) as a consequence of their inherent acid/base

properties. The voltammetric response at the electrode is dictated by the chemistry of the redox species rather than the sampled solution [205,206]. It should be noted that in the present application however, the buffering capacity of the biological solutions explored is high and the pH inherent to those solution will dictate the local pH at the electrode.

Another pH sensitive sensor studied is the use of Fast Blue RR diazonium salt-modified carbon fibre electrode. Makos et al. (2010) showed that the carbon-based cylindrical microelectrode was functionalised through the voltammetric reduction of the diazonium salt [207]. By doing so, the redox mechanisms of the electrochemically active species' *p*-quinone, initiated through fast cyclic voltammetry and which are dependent on hydrogen ion concentration, are then exploited as basis of a pH probe [207]. The modified electrode was successfully tested in both in vitro and in vivo microenvironments, revealing its sensitivity to physiological pH changes and limit of detection to 0.005 pH units [207].

Mclister et al. (2015) have functionalised both oxidised polyamide [208] and anodised carbon fibre mesh [209] with the redox-active polytryptophan as a premise for pH detection specifically in wound dressings. The former study employed square wave voltammetry and the developed redox wire expressed a Nernstian behaviour of 59 mV/pH for the physiological range of pH 3 - pH 8 with a minute error of only 0.04 pH units [208]. Similarly, the latter research further proves the efficacy of the homopolymer in detecting pH as the modified carbon fibre sensor exhibited a sub-Nernstian behaviour of 51 mV/pH in the same aforementioned functional range [209]. The new pH probe was then tested in a complex biofluid solution of horse blood to simulate wound environment. Upon consecutive scanning, the oxidation peak of tryptophan had a marginal shift of ±5 mV corresponding to only ±0.1 pH unit [209]. This result is encouraging in that the sensor can continue to measure pH in a challenging milieu which is specifically crucial in catheter systems.

As previously mentioned, Davis et al. (2013) have also used plumbagin as a pH sensitive moiety capable of being electropolymerised on to carbon fibre for use in catheter systems [189]. The probe was found to have a sub-Nernstian behaviour of 51 mV shift per pH in the physiologically relevant range of pH 3 – pH 8 [189]. The ability of the probe to produce an unambiguous signal even in the complex medium of blood, where biological interferences are present, was also observed. The employment of polyplumbagin proved to be advantageous in that its redox signals are found in the cathodic region where it is devoid of

competing signals [189]. Again however, the possibility of plumbagin leaching and its direct access to the circulatory system may prove to be counterintuitive in CVC applications.

Urate has also been investigated as a pH sensitive analyte by Phair et al. (2014) [210]. Although uric acid is often known as an interferent in electrochemical sensing processes, the team used the biomarker's pH dependent redox characteristics as well as its inherent low oxidation potential as an effective, indirect method of determining local pH [210]. The study employed an anodised carbon fibre probe, which has a 10 µm diameter suitable for integration in most central line catheters, as the conductive substrate to detect urate (200 µM) in various pH buffer solutions. The observed response showed a Nernstian behaviour of 58 mV per pH shift in the range of pH 5 – pH 8, which is where any fluctuations in local pH due to biofilm presence is said to occur [210]. The system was further tested in whole blood and a mean pH of 7.40 was obtained (N = 8; relative standard deviation percentage = 0.38) which proves to conform with that expected of normal blood pH [210]. The team also noticed that urate accumulated on the anodised carbon surface through passive adsorption and further studies on this could be beneficial. This study therefore showcases the potential of urate to be exploited as a naturally occurring pH dependent redox biomarker.

Similar studies [205,211–218] using various types of electrodes modified with different electroactive species (i.e. iridium oxide [215,216], zinc oxide [217], salicylaldehyde [218] and salicylic acid [218]) for the purpose of creating a solid state potentiometric pH sensors have also been extensively reviewed. The research mentioned here demonstrates easily designed and manufactured stable microelectrode sensors capable of measuring real-time pH changes. These sensors are cheap, sensitive and scalable alternatives to traditional pH sensors. Miniaturised electrochemical pH sensing probe functionalised with a biocompatible molecule can therefore be integrated into a smart electrochemical system for the detection of contamination.

2.6.2 Inhibition of Pathogen Growth

Electroanalytical sensing of intracellular generation of reactive oxygen species has been well studied [219–223] and some have discussed the deliberate electrochemical release of ROS or oxygen reduction outside biological processes for anti-pathogen purposes [224,225]. The functionality of ROS in pathogen growth inhibition was discussed in **Section 2.5.1**.

Apart from this, electrochemistry is also known to render pathological growth by inducing surface polarisation, also known as the bioelectric effect (**Figure 2.6.1**). The role of applying controlled potential and/or current in inhibiting biofilm formation has been thoroughly reviewed [224,226–229]. Although there are differences in their membrane structure, both Gram-positive and Gram-negative bacteria are negatively charged due to the presence of anionic phospholipids in their cell wall and outer membrane, respectively [224,230,231]. Bacterial attachment could therefore be delayed through electrostatic or electrophoretic repulsion by employing a negative charge on the surface. On the other hand, a net positive polarized surface can generate reactive chlorine species (i.e. hypochlorous acid and sodium hypochlorite) which could also aid in eradicating contaminants [224,232]. The reaction sequence for the generation of hypochlorous acid (HOCl) is summarised in **Equation 2.6.1**.

$$2\,Cl^- \rightleftharpoons Cl_2 + 2e^-$$
$$Cl_2 + H_2O \rightleftharpoons HOCl + HCl$$

…Eq. 2.6.1

An example of this was completed by Sandvik et al. (2013) where the team studied the effect of direct electrical current in the viability of *S. epidermidis* and *P. aeruginosa* – both known biofilm-forming microorganisms found in catheters [232]. The bacteria were grown in a bioreactor containing normal saline concentration of sodium chloride and were exposed to current for 24 and 20 hours, respectively. A log reduction of up to 6.7 $\log_{10}$ CFU/cm^2 was recorded and no significant difference was found between the presence and absence of ciprofloxacin antibiotic [232]. Additionally, the team found a significant positive correlation between current density and generation of free chlorine which is likely the primary contributor to the effectiveness of direct current in diminishing bacterial growth [232]. Although the efficacy of this involves saline solution and thus would be useful for catheter systems, Sandvik et al. (2013) state that free chlorine would have cytotoxic adverse effect to surrounding tissues [232] and can also possibly affect the catheter material. Therefore, designs must be made to ensure that its release, similar to reactive oxygen species, is localised only where contamination occurs i.e. catheter hub, for it to be useful in real-life technologies.

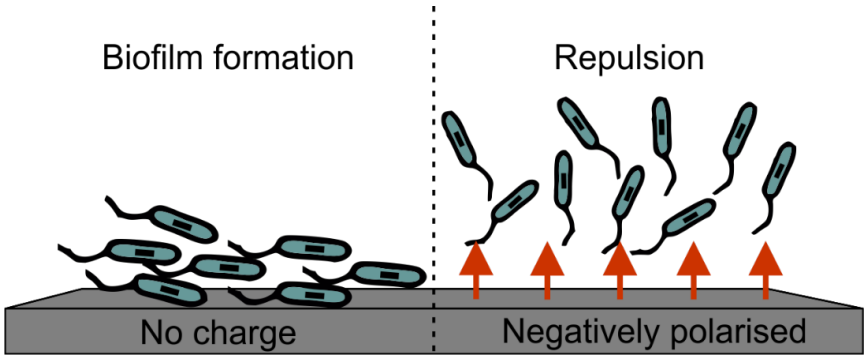

Figure 2.6.1 Bioelectric effect - a net negative surface charge repels bacterial attachment thus prevents biofilm formation.

The co-application of surface repulsion and electrochemical production of localised antimicrobial compounds is an attractive method that could be incorporated into existing technologies. With the correct design and a non-antibiotic based biocompatible compound, electrochemical techniques have great potential for exploitation to control and inhibit microorganism contamination in catheter systems.

2.7 Conclusions

The role of intravenous therapy and thus catheterisation are evidently imperative in modern healthcare settings. The importance of lifesaving indwelling devices is unquestionable, however, they can be a major source of nosocomial infections. The presence of contamination and biofilm formation hinders the functionalities of catheters. Consequently, healthcare associated blood stream infection poses a great threat to patient wellbeing as well as an added burden to healthcare providers.

Without an effective diagnostic and preventative modality, and the continuously increasing lifespan of indwelling devices like central venous catheters, catheter-related bloodstream infection will unceasingly pose as a challenge in the healthcare industry. Although there is extensive research around various techniques and treatments for CRBSI, as summarised in **Table 2.7.1**, there is still an urgent and pressing demand for a potent novel technology that can eradicate planktonic and biofilm-forming microbes in order to completely reduce the risk of CRBSI to nil.

Table 2.7.1 A summary of current practices and emerging technologies in the prevention of CRBSI.

Method	Advantage	Disadvantage
Catheter removal	Completely removes risk of CRBSI	Not always viable; requires plenty of resources
Blood culture	Determines cause of infection allowing correct CRBSI management to occur	Not easily and readily accessible; doesn't prevent CRBSI
Antibiotic treatment	Readily available and eliminates bacteria	Expensive; may lead to microbial resistance; not capable of fully eradicating biofilm-forming pathogens
Hand hygiene / aseptic technique	Easy to do and reduces risk of infection from healthcare personnel/patient	Inefficient
Catheter type and insertion sites	Reduces risk of CBRSI	CRBSI still occurs; inefficient
Coated / impregnated catheters	Effectively lowers rate of infection	Only effective for up to 14 days; expensive; can lead to antibiotic resistance
Lock solutions	Proven to eradicate biofilm-forming bacteria and fungi	Requires long-term catheters to be locked for up to 14 days; spillage may lead to other morbidities; can become source of antibiotic resistance; some solutions are only effective for certain microorganisms
Plumbagin	Does not require antibiotics and completely eradicates planktonic microorganisms and biofilms	Can cause cancer
Iodinated alcohol filled-catheter hub	Inhibits pathogen contamination at commonest source prior to entering the main catheter line	Contradicting efficacy results
Smart central venous port	Rapid and easy method of detecting the onset of biofilm formation	Lacks therapeutic requisite of a smart catheter system

The primary aims are therefore to produce a rapid and efficient system to not only reduce financial costs, but more importantly, to improve patient outcome without numerous professional healthcare interventions. It is widely acknowledged that the presence of a biofilm would inadvertently modify the local environment's pH as a result of pathogen metabolism. It is therefore envisaged that pH could be effectively exploited as a potential indicator of contamination within the catheter system. Although there are many pH sensitive modifiers/sensors, the issue lies in securing a biocompatible redox probe whose analytical signals are devoid of interferences that would normally hinder existing pH sensors. Ideally, the probe would not only monitor the line, but can also eradicate biofilm formation through the release of reactive oxygen species via the electroreduction of oxygen. The aim of this project was therefore to address these issues by investigating a suitable electrode modifier

whose redox characteristics are pH dependent and whose monomers/oligomers are biocompatible, which means leaching wouldn't become problematic. Additionally, it has the dual capability of electro-generating reactive oxygen species to actively combat pathogen contamination. Equally as important, the suggested system could be easily integrated into existing catheter lines.

Chapter 3

Experimental Details and Methodologies

Overview

The following section will provide information regarding the materials, methods and instruments used throughout the project. It will detail the underpinning reason for using certain techniques, their meaning and influence, as well as the analysis of data obtained. Broader discussions of specific experimental details are detailed in the appropriate individual results chapter.

3.1 Materials and Instrumentation

In general, the majority of the chemicals were purchased from Sigma-Aldrich (UK), were the highest grade available and were used without further purification, unless stated otherwise. Stock solutions of custom synthesised phenol flavin derivative and riboflavin (typically 250 μM) were dissolved with methanol and acetone. Britton-Robison (BR) buffers (0.04 M acetic, boric and phosphoric acids), with the addition of concentrated sodium hydroxide to adjust pH to desired value, were used to prepare all other solutions unless specified otherwise. A concentration of 0.1 M potassium chloride completed all BR buffer solutions which supplied ample electrolytes and defined potentials of pseudo-references. All solutions were prepared with deionised water from an Elgastat water system (Elga, UK). Total parenteral nutrition was provided by ITH pharma (London, UK).

Electrochemical analyses were completed using a μAutolab Type III potentiostat (Eco-Chemie, Utrecht, The Netherlands) at room temperature (22°C ± 2°C). A standard three-electrode system was generally employed with platinum wire as the counter electrode and a conventional silver/silver chloride half cell (3 M KCl, BASi, UK) serving as reference electrode. A range of materials acted as the working electrode throughout this work namely: carbon fibre mesh (Toray, TGP-H-30/TGP-H-60), glassy carbon, carbon-loaded polyethylene and carbon-based screen printed electrode. In instances where a two-electrode configuration was utilised, silver/silver chloride deposited onto carbon-based electrode acted as both the reference and counter electrode. Additional experimental details are specified in each chapter.

3.2 Electrochemical Instrumentation

Electrochemistry centres around the movement of electrons between the working electrode and electrolyte solution, driven by chemical processes. The qualitative and quantitative data provided by the resulting electric response also provides an insight to the kinetics and thermodynamics of the chemical reaction that occurred. In this instance, electrochemistry is exploited to indirectly detect the presence and, ultimately the eradication of contaminating microorganisms as a means of reducing catheter-related bloodstream infection. This is achieved through the use of redox probes capable of undergoing oxidation and reduction processes at the electrode interface.

The rising popularity of electrochemistry in the field of medicine, along with other industrial areas, is explicable for a myriad of reasons. For instance, it offers a quicker and cheaper mode of analysis in comparison to traditional laboratory methods such as spectroscopy. It also facilitates a straightforward modification method of electrode surfaces which may be necessary to increase their sensitivity, selectivity, efficiency and/or practicality. Additionally, the flexibility and compatibility of electrochemistry, in terms of being able to use different types of electrodes, regardless of size, cost, application etc., amplifies its advantages over current methods used as well as its applicability to a variety of fields.

3.3 Electrochemical Cells

A three-electrode system is generally used in electrochemical analyses. This is composed of a working electrode (WE), a counter electrode (CE) and a reference electrode (RE). The potential applied to a working electrode is controlled by a potentiostat and is a function of the reference electrode's fixed potential. Each type of electrode is further discussed in the following sections. A potentiostat is used to control the electrode system, specifically the voltage difference between the working and reference electrode and is a critical instrument in most electroanalytical experiments. The reader is directed to more comprehensive texts for information on the instrumentational and operational characteristics inherent to potentiostat design [233–236].

3.3.1 Working Electrode

In electrochemical analyses, the working electrode is the main point of interest as this is the site of all significant electrochemical reactions. Although the WE can be a plethora of compositions/configurations depending on requirements (e.g. potential window, catalytic functions, stability, cost, size), a common characteristic of a working electrode is its relative inertness allowing for the transfer of electrons from the induced redox reactions. Some examples are gold, carbon, graphene and palladium. Exceptions to this rule are copper and nickel electrodes whose surface oxidation within the electrolyte results in catalytic species (i.e. CuO, NiO) that can further catalyse the oxidation of other analytes (i.e. carbohydrates) that might not necessarily be accessible to the more inert electrode substrates [237,238].

Different materials can lead to different electrochemical responses but, in the context of electroanalytical applications, a material with fast electron transfer kinetics is generally preferred as a working electrode [235,237,239–241]. It is also a necessity that the WE's surface is clean and its surface area is clearly defined as these affect the resulting response. Depending on the electrode used, the surface may be cleaned through polishing and may also be modified electrochemically to enhance the signal response i.e. via anodisation, or to decrease the potential required to initiate a reaction [235,242–245]. Steps ensuring result reproducibility and repeatability is also a must.

3.3.2 Reference Electrode

Regardless of whether the electrolytic set-up is a two- or three-electrode system, a reference electrode is compulsory. The reference electrode's function is to provide a stable, constant potential which is used to monitor the working electrode's potential. There are three common types of reference electrodes used in aqueous solution: standard hydrogen, saturated calomel and silver/silver chloride (Ag/AgCl) electrode. This study uses a Ag/AgCl reference electrode and hence will be discussed further. Silver/silver chloride half cell reference electrodes are composed of a silver wire coated with silver chloride, encased in a glass cover typically filled with 3 M potassium chloride (KCl) solution. The KCl solution provides a stable environment, maintaining the constant potential of the reference electrode. Generally, reference electrodes have a potential independent of the electrolytic solution in the cell and is separated from the solution through a porous junction that is typically made from ceramic (i.e. Vycor®). The frit acts as a barrier restricting the transport of chloride ions from the internal solution to the sample matrix and, similarly, any contaminants from the latter into the sheath. Crucially it allows electrical conduction between electrode and solution. A typical Ag/AgCl reference electrode assembly is displayed in **Figure 3.3.1**.

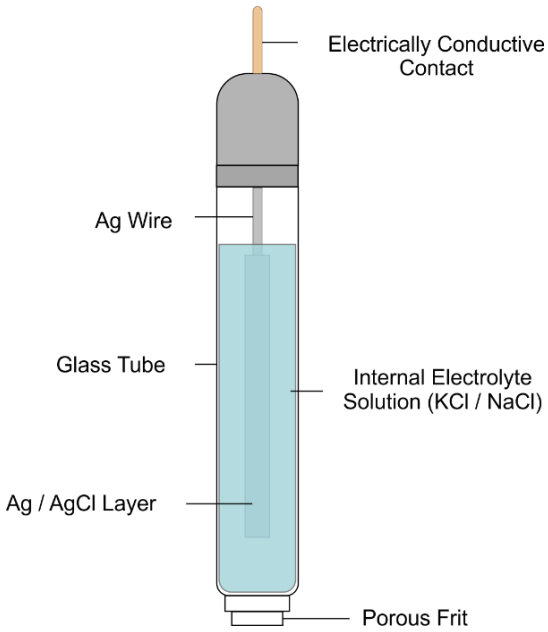

Figure 3.3.1 Configuration of a conventional silver/silver chloride reference electrode. Adapted from [245].

Reversible redox reactions occur within the cell at a fast rate allowing the rapid adjustment to changes in ionic activity in the working solution. The maximum difference between redox potentials is called the electromotive force (emf). Alongside the standard potential, the convention of emf is used to allow the computation of cell potentials from two half cell reactions to be easier and more straightforward. The relationship between the electrochemical cell potential, the relative redox activities and the standard potential in a cell reaction is mathematically expressed by the Nernst equation (**Eq. 3.1**). In a one-electron transfer, as in that occurring in a RE, n is set to 1 and the oxidation/reduction activities are replaced with their more experimentally accessible concentrations. It is important to note that the concentration of molecules in solely aqueous form can be measured.

$$AgCl_{(s)} + e^- \leftrightarrow Ag_{(s)} + Cl^-_{(aq)} \qquad E^0 = 0.222V$$

$$E = E^0 - \frac{2.303RT}{nF} * \log\frac{[B]}{[A]}$$

$$E = E^0 - \frac{0.05916}{1} * \log\frac{[Ag_{(s)}][Cl^-_{(aq)}]}{[AgCl_{(s)}]}$$

$$E = E^0 - 0.05916 * \log[Cl^-_{(aq)}]$$

…Eq. 3.1

where:

E = electrode potential

E^0 = standard electrode potential

R = gas constant (8.314 JK^{-1} mol^{-1})

T = temperature (298.15 K)

n = number of electrons transferred to electrode during reaction

F = Faraday constant (96485 C mol^{-1})

[A] and [B] = activities of the oxidised and reduced species, respectively.

From the equation above, the electrode potential due to the redox reaction occurring in a silver/silver chloride reference is solely dependent on the chloride ion concentration (assuming temperature is held constant). Hence, to maintain this directly proportional relationship, the employment of a stable, concentrated (typically 3 M) KCl solution is an integral part of the reference electrode system.

3.3.3 Counter Electrode

The ability of the reference electrode to quickly adjust to changes in ionic activity leaves it vulnerable to damages caused by large current densities and susceptible to losing their ideal, non-polarizable characteristics [(235)]. To prevent this, a three-electrode system is commonly used whereby a third electrode, the counter or auxiliary electrode, is added to the configuration. By doing so, current caused by the potential application to the WE to initiate analyte reduction or oxidation, will flow through the counter instead of the reference electrode thus completing the electrical circuit. As such, the flow of electrons between the two electrodes defines the corresponding current. An opposite reaction to that occurring in the working electrode transpires in the CE (i.e. if oxidation occurs at the WE, reduction occurs at the CE and vice-versa), therefore it is imperative that the CE is inert against the reactions taking place. Moreover, it is essential for a CE to have a larger surface area than the WE to

deter the inhibition of the reaction kinetics occurring in the former to those happening in the latter. Platinum-based electrodes are typically used as the CE within laboratory-based systems due to their inertness and high conductivity but carbon is frequently used in disposable screen printed systems where cost is an over-riding factor. For experiments producing large currents and to inhibit the generation of by-products from certain experiments, the counter electrode may be isolated in a separate cell and adjoins the circuit via a glass frit [235,245].

3.3.4 Buffer Solutions

A high concentration of supporting electrolyte(s) in an electrochemical cell is required to increase solution conductivity, limit analyte movement via migration, and attain charge balance which decreases solution resistance to charge transfer. Therefore, this allows electrochemical reactions and measurements to be recorded. Buffer solutions, such as Britton-Robinson (BR) buffers used in this work, provide sufficient electrolytes and are also inert allowing the detection of the electroactive species of interest. The use of buffer solution also minimises the change in local pH of the electrode surface caused by chemical processes where hydrogen ions (H^+)/hydroxides (OH^-) are generated or exhausted. Rearrangement of the Nernst equation to establish the change in potential due to the log change of H^+ concentration (1 pH unit) is displayed in **Eq. 3.2** below (all characters represent their common meaning as displayed previously). This shows that under standard conditions, a 59 mV potential shift should be seen per pH unit. If a process acts in such a way, it is said to have a Nernstian behaviour.

$$E = E^0 + \frac{2.303RT}{nF} * \log[H^+] + \log\frac{[B]}{[A]}$$

$$E = E^0 + 0.05916\text{V} * pH$$

…Eq. 3.2

3.4 Mass Transport Mechanism

A typical electrochemical reaction involves the interaction between electrode and electrolytic solution. Although the potential difference within the cell affects the electrolysis reaction rate, it is important to note that the rate of transport of analyte to the electrode

surface also plays a major role in influencing the rate of reaction. Such movements are categorised into three types of mass transport: diffusion, convection and migration. Details explaining each type is discussed in the following sections.

3.4.1 Diffusion

Most electrochemical experiments rely on molecular movement through diffusion. In fact, this is the only mode of transport that is included in theoretical treatments and modelling [245]. Diffusion occurs when there is a concentration difference between two points in a cell, causing the movement of electroactive species from an area of high concentration to a low concentration area. For instance, diffusion arises at electrode surface where the concentration of the analyte is less than in the bulk solution, and vice versa in terms of chemical reaction product, leading to a concentration gradient (**Figure 3.4.1**). Therefore, diffusion pushes the original material from the bulk solution towards the electrode surface and simultaneously moving the resulting product away from the electrode. Diffusion is defined by Fick's first law of diffusion as highlighted in **Eq. 3.3**.

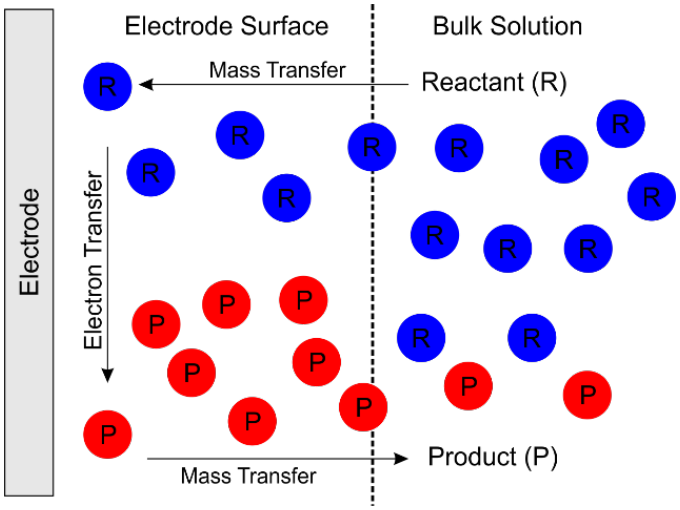

Figure 3.4.1 Simplified illustration of the diffusion pathway in an electrolytical cell. Adapted from [246].

$$\text{Flux} = -D_i \frac{\partial c_i}{\partial x}$$

…Eq. 3.3

where:

D_i = diffusion coefficient (cm^2/s) of particle i

$\frac{\partial c_i}{\partial x}$ = concentration gradient at distant x

Additionally, Fick's second law (**Eq. 3.4**) describes the change of concentration due to diffusion with respect to time. This now describes the relationship between concentration, time and distance [237].

$$\frac{\partial c}{\partial t} = D \frac{\partial^2 c}{\partial x^2}$$

…Eq. 3.4

3.4.2 Convection

In electrochemistry, convection is the hydrodynamic transport of particles in a solution via natural source i.e. heat, or mechanical forces such as stirring or vibration or through density gradients. It can also be induced through ultrasound where acoustic streaming and cavitation induce forced convection at the electrode – a topic covered in **Chapter 4**. If mechanically induced, convection precedes all other mode of mass transport. **Figure 3.4.2** displays the use of a stirring rod in a solution and the effect of convection.

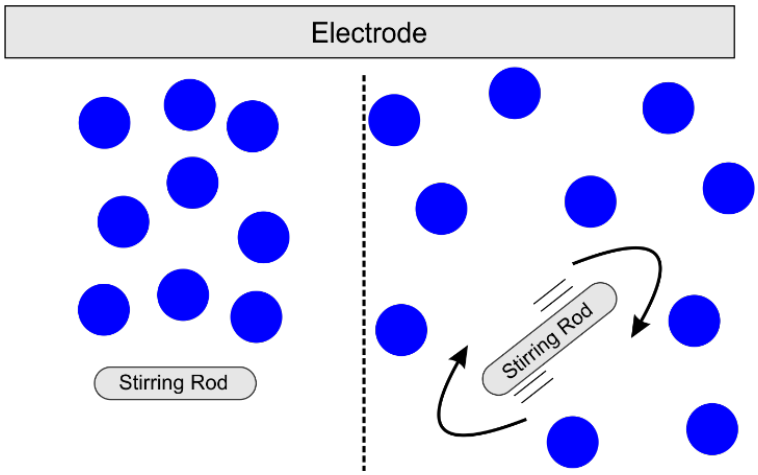

Figure 3.4.2 Influence of mechanical convection on the transport of particles.

3.4.3 Migration

Migration is the movement of ionic solutes as a result of a localised electric field, i.e. positively charged particles are attracted to negatively charged electrode and vice-versa. The application of potential to a solid electrode in an ionic solution changes the charge migration, as exemplified in **Figure 3.4.3**. The effect of migration in electrochemical analysis is reduced by the employment of solution containing highly concentrated inert analyte. The relatively higher concentration of electrolyte to analyte increases the statistical probability that the electrolyte will migrate and transport the charge to the electrode surface, thus leaving the electrochemically active species preserved and unaffected by migration.

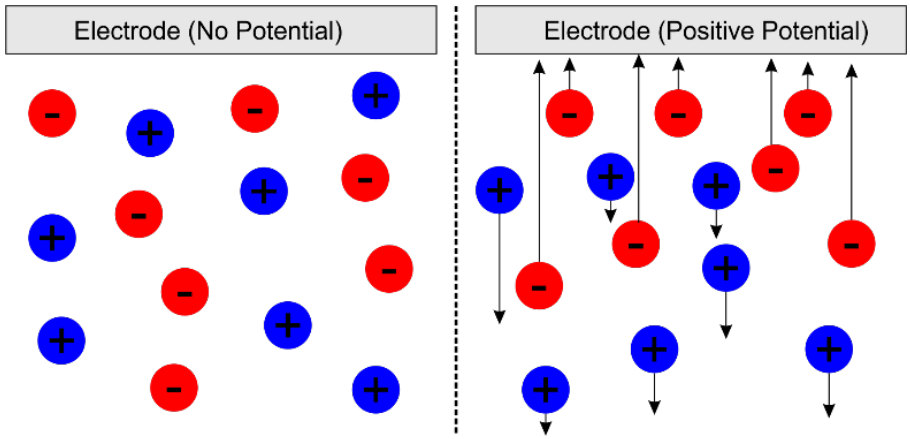

Figure 3.4.3 A simplified diagram of charge migration change as result of potential application.

3.5 Electrochemical Techniques

A variety of electrochemical techniques are available including voltammetry, amperometry and potentiometry. These methods are used throughout the project and will be further discussed in the following sections. Voltammetry is a common technique whereby a varying potential is applied to the working electrode and the current response due to the chemical reaction occurring at the electrode is measured. A voltammogram is used to display the relationship of current against voltage. Similar to voltammetry, amperometry is an electrochemical method wherein the corresponding current is quantified as a consequence of a fixed potential being applied to the working electrode instead. Finally, potentiometry is a technique where the potential difference between working and reference electrode in a cell is measured under zero current. Unless otherwise stated, the potentiostat used

throughout out this study is the computer-controlled µAutolab Type III potentiostat (Eco-Chemie, Utrecht, Netherlands).

3.5.1 Cyclic Voltammetry

One of the most prominent electrochemical techniques used to characterise the oxidation and reduction processes of an electroactive species is cyclic voltammetry (CV). It is a simple, quick and efficient method which provides sensitive and qualitative analysis of electrochemical behaviour or composition of the molecule of interest. This method imposes a potential on the working electrode which is swept linearly in a triangular form as in **Figure 3.5.1A**. The starting potential, E1, is usually set where no chemical process at the electrode occurs and is then linearly swept at a constant rate to the second potential, E2. The latter potential is typically selected to be greater than the potential required to induce the oxidation or reduction of the analyte under investigation to ensure the required reaction is recorded. In linear sweep voltammetry, the scan terminates at this point however in CV scans, the potential is linearly swept in the reverse direction and ends at the starting potential E1. The anodic trace is drawn when the potential is swept positively from E1 to E2 and reversely, the cathodic trace is defined by the negative linear sweep from E2 to E1. The trace resulting from this process is called a voltammogram or cyclic voltammogram. The resulting current is plotted as a function of the applied potential as in **Figure 3.5.1B**.

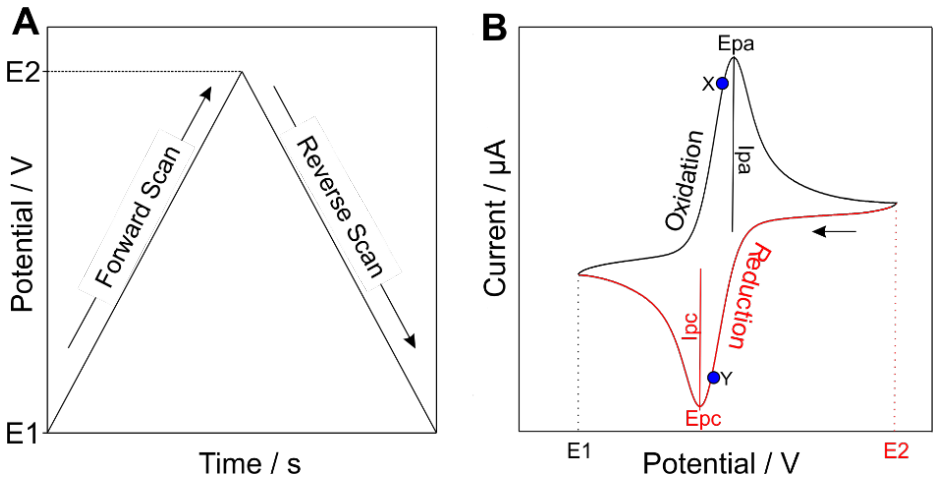

Figure 3.5.1 Typical A) triangular waveform and B) cyclic voltammogram trace produced in cyclic voltammetry. Adapted from [245].

As the potential is swept in the anodic direction, the rate at which the electroactive species of interest oxidises increases and the resulting current exponentially increases with the commencement of electron transfer. At the electrode surface, the concentration of the oxidised form of the analyte (Ox_a) increases throughout the forward scan and builds a growing diffusion layer which slows down the mass transport of the reduced form of the analyte (Red_a) to the electrode. Points X and Y represent the instants where there is equal balance between increased Ox_a concentration and the exhaustion of Red_a near the electrode surface, and vice-versa respectively, thus satisfying the Nernst equation E = $E_{1/2}$. At a certain potential (Epa) the increase in current reaches a maximum and this is called the peak anodic current. Beyond this peak, the resulting current relies on the diffusion of additional Red_a from the bulk solution as a result of the concentration gradient. Simplistically, the magnitude of the current depends on the rate at which 'fresh' material can diffuse through to the electrode surface instead of electrode kinetics. As the scan continues to more positive potentials, the current decreases as the distance to transport Red_a to the electrode surface increases due to the aforementioned diffusion layers hence decreasing the rate of diffusion (Epa$\rightarrow$ E2).

When the vertex (switching) potential (E2) is reached, the direction of the scan is reversed towards less positive potentials. During the reverse scan, the kinetics of reduction becomes more favourable and essentially converts the product generated at the surface of the electrode back to the original form, in this case from oxidised to reduced form. The reverse sweep completes the voltammogram and can be explained in the opposite direction but analogous to that described for the forward scan.

A wealth of diagnostic information can be obtained from the shape of the CV trace – starting with defining the reversibility of the system. **Figure 3.5.2** displays a variety of the more typical voltammetric traces that can be observed. The electron transfer kinetics between the electrode and analyte defines the electrochemical reversibility of the system. If there is little to no barrier of electron transfer, electrochemical reversibility occurs, and the Nernstian equilibrium is established immediately upon any potential change. On the other hand, if a system is quasi-reversible, it means that a greater positive or negative potential, often termed an overpotential, is required to induce oxidation or reduction, respectively, leading to an elongated CV trace. Similarly, an electrochemically irreversible system means that a larger overpotential is required to induce redox reaction. The CV trace of such systems display the maximum peak separation between oxidation and reduction peaks (if the latter

is at all visible). This shows that the electron kinetics are insufficient to maintain the equilibrium of redox species. It is also important to note that in the absence of electroactive species, no peaks are visible and only the capacitance background is observed.

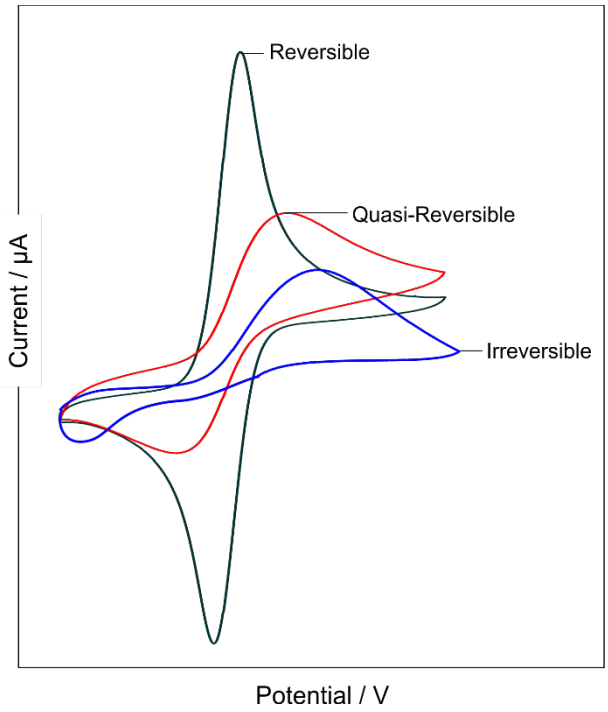

Figure 3.5.2 Cyclic voltammograms displaying different types of electron transfer systems.

For a system to be classified as electrochemically reversible, the following characteristics must be followed:

- The potential difference between the anodic and cathodic peak (peak-to-peak separation, ΔE_p) must equal to $\frac{59}{n}$ mV, where n is the number of electrons transferred during chemical reaction, independent of scan rate;
- The ratio between anodic and cathodic peak currents must equal to 1;
- And finally, the peak currents must be directly proportional to the square root of scan rate.

An important parameter to consider is the scan rate, υ, as it controls the speed at which the applied potential is scanned. Typically, higher resultant currents are detected with faster scan rates as this decreases the diffusion layer size. Additionally, the flux of electrons, and thus the current to the electrode surface increases with scan rate leading to a greater current magnitude. The relationship between the square root of scan rate and peak current (i_P) also

describes whether an electrochemically reversible system involves a freely diffusing analyte or if the electroactive species is adsorbed on to the surface of the electrode. This correlation is mathematically expressed by Randles-Ševčik equation (**Eq. 3.5**).

$$i_P = 0.446\ \mathrm{nFAC^0}\left(\frac{\mathrm{nF\upsilon D_o}}{\mathrm{RT}}\right)^{\frac{1}{2}}$$

…Eq. 3.5

where, under standard conditions:

n = number of electrons transferred

F = Faraday constant (96485 C mol^{-1})

A = electrode surface area (cm^2)

C^0 = concentration (mol cm^{-3})

υ = scan rate (V s^{-1})

D_o = diffusion coefficient of the oxidised analyte (cm^2 s^{-1})

R = gas constant (8.314 J K^{-1} mol^{-1})

T = temperature (298.15 K)

If the electroactive species is adsorbed on to the surface of the electrode i.e. not diffusion-limited, the derived current will have a linear relationship with scan rate. In this case, the analyte's surface concentration (Γ_c), in mol cm^{-2}, can be calculated from **Eq. 3.6** where all the characters have their usual meaning, as seen above.

$$i_p = \frac{\mathrm{n^2F^2A\Gamma_c}}{4\mathrm{RT}}$$

…Eq.3.6

3.5.2 Square Wave Voltammetry

Similar to cyclic voltammetry, square wave voltammetry (SQWV) records the current as a function of the linearly swept potential applied to the working electrode. The main difference is that the potential imposed in SQWV is swept in time over a set span of values by using a voltage ramp with a staircase shape instead of the triangular fashion that occurs in CV. In a square wave cycle, the current is measured twice, once at the end of the forward step direction and then again at the end of the reverse step direction, which consequently generates a peak for each process producing information about the oxidation or reduction

of the analyte under investigation [247]. Simplistically, the resulting current (ΔI) is calculated as the difference between the currents at the end of the forward pulse and at the end of the reverse pulse of each staircase step (**Figure 3.5.3A**) which is then plotted against the sweep potential to display a peak-shaped voltammogram [247], as illustrated in **Figure 3.5.3B**. The time to complete one staircase or square wave period is expressed as τ and the frequency in Hertz (Hz) is calculated as the reciprocal of τ. The two characteristics that determines a square wave are amplitude (E_{sw}), where 2 E_{sw} is the peak-to-peak amplitude, and width of the pulse (t_p). The scan rate, in mV/s, for this electrochemical technique can be calculated by dividing the step height in mV (ΔE) by the square wave period in seconds.

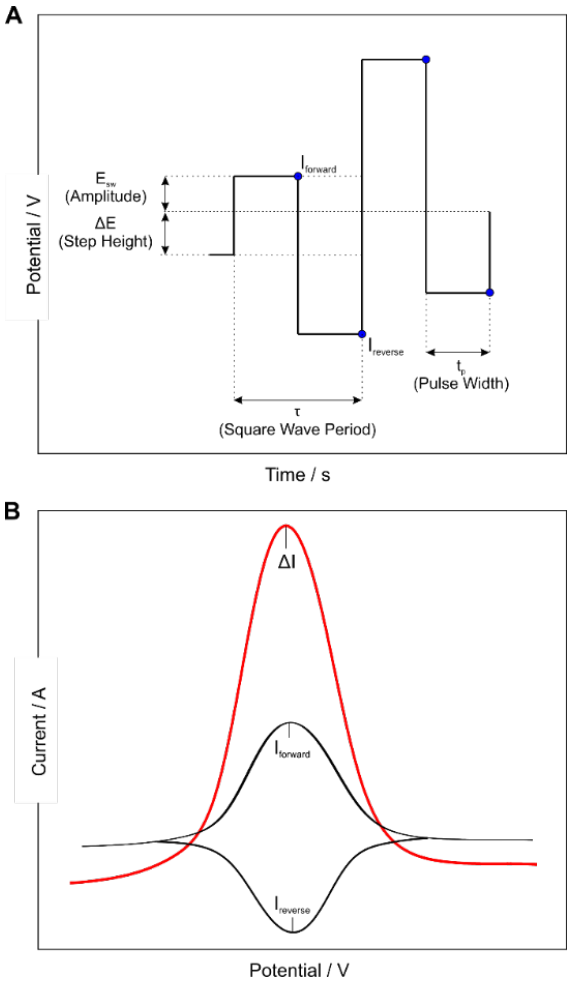

Figure 3.5.3 Voltammetric profiles highlighting the A) staircase shape and B) resultant square wave voltammogram. Adapted from [246].

It is noteworthy that the peak height/current of the resulting voltammogram is proportional to the concentration of the electroactive species in the solution, as mathematically expressed in **Eq. 3.7**.

$$\Delta i_p = \frac{\mathrm{nFAD}^{\frac{1}{2}}\mathrm{C}}{(\pi \mathrm{t}_p)^{\frac{1}{2}}}\Delta\psi_p$$

…Eq. 3.7

where:

Δi_p = differential peak current (A)

t_p = pulse width (s)

$\Delta\psi_p$ = dimensionless peak current

and all other symbols have their common meaning.

The main advantage of square wave voltammetry in comparison to CV is its ability to discriminate or minimise the influence of capacitive current on the total current reading [(247)]. Since current is recorded twice in each square wave pulse, there is a miniscule (a few milliseconds) but significant delay in current measurement. This delay allows the immediate reorganisation of ions at the electrode surface, attributable to potential changes at electrode surface, to be completed before measuring the current which leads to low capacitance current. In SQWV, the current due to electron transfer between analyte and electrode, known as the Faradaic current, is largely measured while in CV the sum of both Faradaic and capacitance current is recorded. Generally at trace (μM or less) levels of analyte, the former current tends to be overpowered by the capacitance background and hence greater concentrations of the analyte is required in CV than in SQWV. Subsequently, the ability to dissipate capacitance allows fast analysis of a myriad of electrochemically active species leading to a technique with higher sensitivity and hence a much improved detection limit than cyclic voltammetry. Furthermore, this technique eliminates the need to remove oxygen in the solution, unless it interferes with the chemical reaction, as the oxygen has no time to diffuse to the surface of the electrode.

It is important to note that capacitive charging currents are due to the accumulation of ions at the electrode surface caused by the electrochemical reaction [(248)]. These ions and the electrode's charged surface forms a double layer, or capacitor, which stores a charge depending on the potential applied [(248)]. In electrochemical techniques like CV or SQWV where the potential of the electrode is swept, and therefore changes continuously throughout the scan, the charge accumulated by the capacitor also changes and current with no chemical meaning flows through [(248)]. This capacitive charging current charges or discharges the capacitor and affects the results of CV. However as aforementioned, in SQWV,

the significant delay in current measurement allows the dissipation of capacitance current and only the more meaningful Faradaic current is measured.

3.5.3 Amperometry

Amperometry involves stepping the potential of the working electrode from a potential where no reaction takes place to a second potential which is then fixed and remains constant for a specified amount of time as exhibited by **Figure 3.5.4A**. The latter potential is chosen to induce the redox reaction of the electroactive analyte(s). **Figure 3.5.4B** demonstrates a typical amperometry profile showing the variation of current produced in response to time and the resulting change in concentration gradient is shown in **Figure 3.5.4C**.

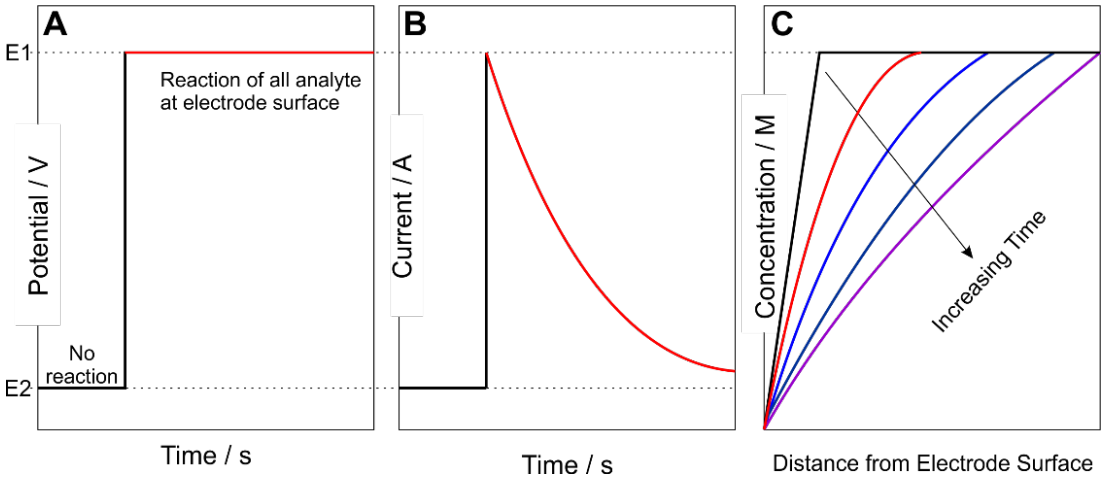

Figure 3.5.4 Common amperometric parameter profiles: A) potential and B) current as a function of time. C) Influence of time and distance to electrode surface on the concentration gradient of analyte. Adapted from [246].

This technique reveals the change in concentration gradient around the electrode surface which is useful in determining physical factors of the electrochemical system of interest such as diffusion coefficients and electrode surface area. The large potential shift driving the reaction causes a variation in the analyte's concentration at the electrode surface thus generating a concentration gradient which, in turn, leads to its diffusion from the bulk solution towards the electrode and ultimately expanding the diffusion layer with time. The reduction of analyte flux towards the electrode along with the growing diffusion layer decreases the current density thus explaining **Figure 3.5.4B**. The difference in analyte concentration with respect to time is explained by Fick's second law of diffusion (**Eq. 3.4**). Derived from this law, the Cottrell equation (**Eq. 3.8**) mathematically expresses the current decay in time, under large over potential conditions, and is typically employed to potential

step methods such as chronoamperometry. To use this equation however, the current must be limited by analyte diffusion to the electrode surface meaning that the solution must be unperturbed.

$$i = \frac{\mathrm{nFAC_a^0}\sqrt{\mathrm{D_a}}}{\sqrt{\pi \mathrm{t}}}$$

…Eq. 3.8

Where 'a' correlates to the analyte of interest and all other characters represent their common meaning as displayed previously.

3.5.4 Potentiometry

Another popular electroanalytical technique used is potentiometry. This method measures the working electrode's potential as a function of time relative to the reference electrode. In contrast with previously discussed methods, potentiometric measurements occur under zero net current i.e. no current flow in the cell. As such, there is no change in the arrangement and composition of the electrochemically active compound therefore quantitative potential measurements can be recorded which exhibits the activity of the analyte near the surface of the electrode. Potentiometry is used in this project to characterise the pseudo reference electrodes. In such cases, the scan is conducted over a period of 180 seconds during which the potential is allowed to stabilise and then the average value of the concluding ten seconds of the scan is typically recorded. In general, such scans are conducted for various concentrations of analyte (typically chloride ion or hydrogen ion) and the average potential plotted against the log of the concentration in accordance with the conventional Nernst type relationship normally used with ion selective electrodes [235,247].

3.6 Characterisation Methods

Throughout this work, a variety of techniques were used to characterise the physical, chemical and surface attributes of the electrode/system of interest. The following section will briefly explain each method and the basic principles behind them.

3.6.1 Scanning Electron Microscopy

Invented by Manfred von Ardenne in 1937, a scanning electron microscope (SEM) is a ubiquitous and powerful magnification tool which produces a high-resolution image of solid samples through raster scanning the surface with a demagnified, high energy focused beam of electrons - instead of light that is traditionally used. The electrons interact with the atoms on the specimen's surface allowing the generation of signals detailing the morphology and topography of the sample under investigation. **Figure 3.6.1** displays a typical configuration of a SEM and the electron's route of travel to the specimen surface. The SEMs used in this project are the SU5000 FE-SEM (Hitachi, Japan) and JSM-6010 (Jeol Ltd., Japan).

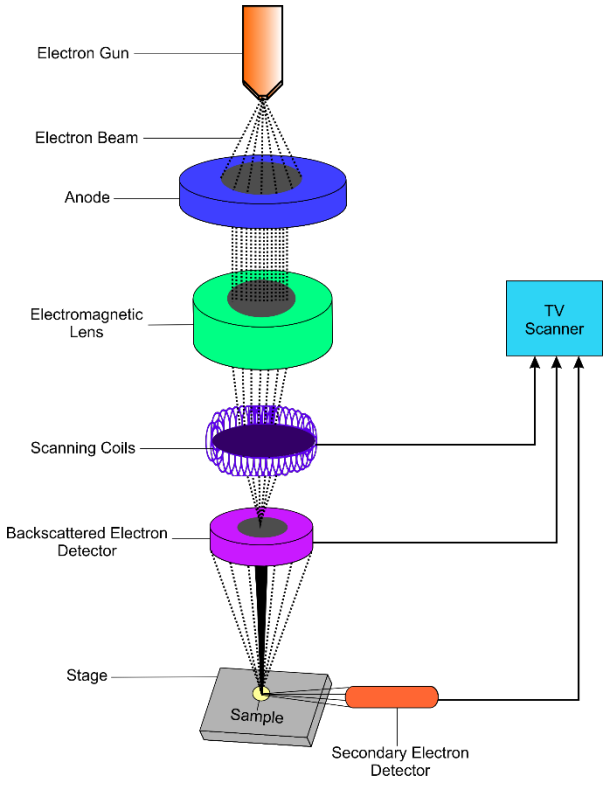

Figure 3.6.1 Simplified schematic diagram of a typical scanning electron microscope. Adapted from [249].

The major components of a SEM are the electron source, the column with electromagnetic lenses where electrons travel through, electron detector, sample chamber and the output display screen. Electrons are produced at the top of the column using an electron gun equipped with a tungsten source filament which is employed as a cathode. Tungsten is typically used in this application due to its low cost and highest melting point in comparison to other metals. As the potential is applied, the tungsten begins to heat thus thermionically

generating the electrons which then accelerate downwards to the anode through lenses and apertures. As the name suggests, the sample stage inside the chamber holds the sample of interest and, once the SEM is in operation, the sample is kept under vacuum within the column and chamber. With the additional use of scanning foils, the incident electron beam is focused towards the target allowing the beam to interact and scan over the surface of the sample.

Upon being decelerated on the surface of the specimen, the kinetic energy of the electrons dissipates thus leading to the emission of a range of electrons (secondary, backscattered and Auger electrons) and X-rays. Through the inelastic collision between the electron beam (primary) and the electrons in the outmost shell of the specimen's atoms, an energy transfer occurs leading to the excitement and ejection of loosely bound secondary electrons. Within the scanned region, the signal intensity of secondary electrons is dependent on surface morphology and topography thus giving information on such characteristics of the sample's surface. On the other hand, backscattered electrons are produced from the elastic scattering of the interaction. The signal it produces are used to determine the atomic number, and hence the element, as the absorbance of backscattered electrons increases with atomic number. The beam of electrons can also excite an electron in the inner shell of the sample's atoms causing the emission of X-rays. Upon doing so, the higher energy electron is forced to replace the detached electrode leading to energy emanation. This energy is then taken up by another electron, called an Auger electron, which is also released from the atom. The combination of X-ray and Auger electrons provide valuable data regarding the profusion of elements and superficial composition of the specimen of interest. The released signals are then identified by their respective electron detectors and an image is produced.

Samples under investigation must be conductive as electrons are used to produce signals which means that charging could occur if an insulated material was employed. To avoid the latter, sputter coating of conductive metals (i.e. gold, gold/palladium and carbon) onto the specimen are typically completed. Additionally, it is common sense, but vital, that the sample should be able to withstand being under vacuum over a period of time. It is also notable that the collisions between beam and sample do not cause sample volume loss, thus the same specimen can be reused and analysed repeatedly.

3.6.2 X-Ray Photoelectron Spectroscopy

Spectroscopic methods are dependent on the interaction between the sample and electromagnetic radiation. An example of this is X-ray photoelectron spectroscopy (XPS) which involves the use of a primary radiation source, an electron energy analyser, the sample under investigation and an ultra-high vacuum sealed chamber encasing the system [250]. Often, in addition to emitted photoelectrons, XPS analysis also instigates Auger electron emission and as such, both can be detected and measured in the same analytic instrument therefore basic principles of both will be summarised here. The XPS system used in this project is the Axis Ultra DLD Spectrometer (Kratos Analytical Ltd., UK).

As the name suggest, X-ray photoelectron spectroscopy involves the irradiation of the specimen being studied with X-ray photon energy. This energy must be sufficiently high to induce electron excitation, break surrounding attraction forces of the element and thus electron photoemission from the core bound state. Upon impact between X-ray and sample, some of the ejected electrons are inelastically scattered throughout the sample towards the surface whilst other electrons are promptly emitted into the vacuumed environment without energy loss (**Figure 3.6.2**). The kinetic energy of the freely ejected electrons is then collected and analysed by an electron energy-selective analyser, constituting the characteristic peaks found in XPS spectra. Conversely, excited electrons which suffered energy loss from inelastic scattering contributes to the spectra's background.

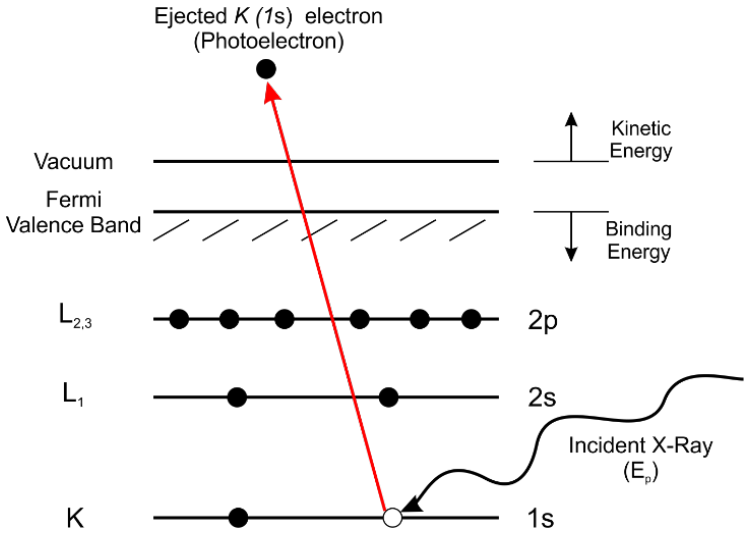

Figure 3.6.2 Schematic diagram of photo-ionisation of an atom through XPS process. Adapted from [251].

The kinetic energy of electrons measured by the spectrophotometer is dependent on the incident X-ray photon energy and therefore does not determine the intrinsic characteristics of the sample under investigation. The binding energy of the electron however provides specific information about the electron including its atomic energy level and thus identifying its parent element [250]. The relationship between the parameters involved in XPS are expressed in **Eq. 3.9**. Apart from the binding energy, all other factors are either known or measurable.

$$\mathrm{E}_b = \mathrm{E}_p - \mathrm{E}_k - \emptyset$$

…Eq. 3.9

where:

E_b = binding energy of electron

E_p = incident X-ray photon energy

E_k = kinetic energy of electron

$\emptyset$ = spectrometer work function

Upon the liberation of core-level electrons, the newly ionised element must restore back to its ground state. To do so, two possibilities can occur: X-ray photon emission, known as X-ray fluorescence, or Auger electron release. The latter happens when a higher energy level electron replaces the emitted core-level electron. Confirming with the conservation energy, the ejection of another electron from the atom ensues leading to Auger electron release. An estimated value of the kinetic energy of Auger electrons can be calculated as the difference between the energy levels of the outer electrons and the energy of the core hole left by the primarily emitted electron. This kinetic energy is independent of the incident beam energy or composition thus generating important quantitative chemical data about the atoms present in the studied specimen.

A typical XPS spectrum is displayed as a graph of intensity against binding energy of the photoemitted electrons. Individual energy peaks seen on an XPS spectrum are directly and uniquely related to a specific elemental core level transition, occurring at a specific binding energy, therefore is useful for specifically determining elements present in the material examined. Additionally, the peak intensity and peak area produce quantitative data regarding individual elements and number of atoms in each element, respectively. Through calculating the respective contribution of each peak area, the chemical composition and

state of the elements existing in the specimen can also be verified. Additionally, the slight shift due to photo-ejection of electrons from core levels provides information on the outer valence configuration of the sample. Moreover, the type of bond (i.e. single or double bond) connected to individual elements can be determined through analysis of each XPS peak. As such, XPS is a valuable analytical surface characterisation technique which determines not only the elements present in the sample but also the elemental bonds.

3.6.3 Raman Spectroscopy

Another spectroscopic method used in this project is Raman spectroscopy - a technique based on the frequency difference of the scattered radiation from the incident (primary) radiation, caused by the inelastic collision between the latter and the sample's vibrating molecules, also known as the Raman effect **(Figure 3.6.3A)**. This change, and thus the Raman shift, is unique to the molecule that produced it and hence useful for analytical purposes. It is a non-destructive method to characterise crystalline, nanocrystalline and amorphous carbons [(252)]. The Raman spectra in this project were obtained using a LabRAM 300 spectrometer (Horiba, Japan).

Raman spectroscopy involves the use of a monochromatic laser beam, in this case Helium-Neon laser, to produce the incident light. After its interaction with the molecules on the material, most radiation scatters with the same wavelength, and hence frequency, as that of the primary radiation which constitutes Rayleigh scattering. Only a small fraction of scattered radiation has Raman effect properties. With regards to electrons, the absorbance of energy from the incident photon causes them to rise to a virtual energy state and then falls back to a vibrational state as they lose energy. If the electrons return to their original vibrational state, these correspond to Rayleigh scattering, otherwise it is Raman scattering. Stoke lines in Raman spectra are produced when the incident radiation has a higher frequency than the scattered radiation whereas anti-Stokes lines are generated if the opposite happens, as displayed in **Figure 3.6.3B**.

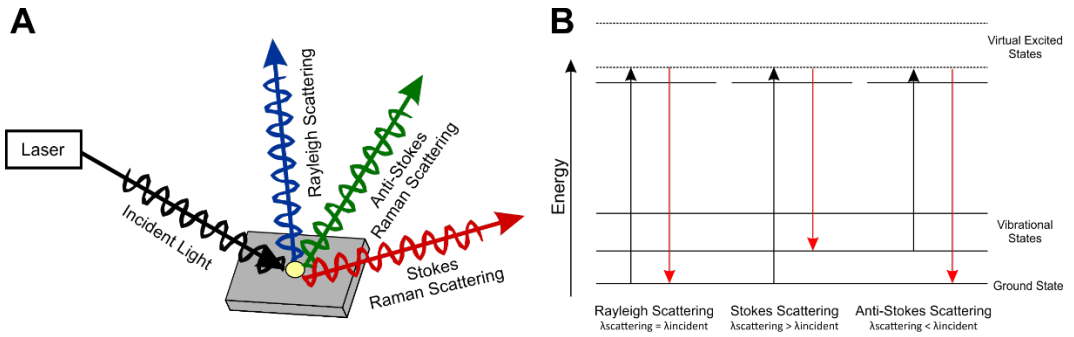

Figure 3.6.3 A) Types of radiation and B) corresponding electron energy levels attributed to Raman spectroscopy. Adapted from [253,254].

Conventional Raman spectroscopy primarily focuses on Stoke bands as these have higher intensity than anti-Stokes since it involves shifting from lower to higher energy states. The latter is used more with fluorescent samples as anti-Stoke lines are not affected by fluorescence while Stoke lines are. Of note, for a molecule to be Raman active, its charge distribution must able to distort from its norm upon the application of an external force, in simple terms its polarizability must change during molecular vibration.

Generally, Raman spectrometers use mirrors and lenses made with glass as optical components. Additionally, filters are used to isolate and focus the single laser beam whilst different types of notch filters and grating monochromators separate weak Raman radiation from Rayleigh radiation. The scattered photons are then converted into charge and detected by an array of charge transfer devices such as charge-coupled devices. The produced Raman spectrum is displayed as intensity against the shift in wavelength. Depending on the configuration of the spectrophotometer used, the spectra can cover wavenumber ranges of 400-5 cm^{-1} and 4000-3800 cm^{-1} thus allowing the detection of Raman induced molecular vibrations which transpire between 4000-400 cm^{-1} [255].

Disordered graphite typically generates a Raman spectrum consisting of two sharp modes: *D* peak (around 1350 cm^{-1}) and *G* peak (1580-1600 cm^{-1}). The former peak arises as a result of out-of-plane vibrations due to defects within the lattice structure and can therefore be used as an indicator of disorder. The *G* band on the other hand correlates to the graphitic in plane vibrations of sp^2 bonded carbon atoms and is due to the C-C bond stretching. Raman spectroscopy is a sensitive technique used to characterise the disorder as well as to determine sp^2 carbon systems. In the presence of impurities randomly dispersed in the lattice and/or any changes in the graphene surface, the *G* band may split into two peaks: *G*

peak and *D'* peak (1610 cm^{-1}). This is explained by the interaction between the extended phonon mode of graphene and the localised vibrational modes of impurities. The intensity ratio between the D and G bands (I(D/G)) corresponds to the number of defects present in the sample, i.e. higher I(D/G) means greater number of defects.

3.6.4 UV-Vis Spectroscopy

Ultraviolet-Visible spectroscopy (UV—Vis) refers to the study of absorption or reflection of light in the ultraviolet and visible range. Similar to previous methods, UV-VIS spectroscopy involves a light or electromagnetic radiation source (i.e. hollow cathode lamp such as tungsten lamp), a sample holder (i.e. quartz cuvette) and a detector. There are two types of absorbance spectrometers used in UV-Vis namely single beam and double beam. As the name suggests, the former uses a single beam of light which passes through the sample and a reference or blank scan must be measured prior to taking measurements to standardise and offset results attained from the absorbance of the sample cell and solvent/water. A reference solution is typically water or solvent used to dissolve the compound of interest. Alternatively, a double beam spectrometer splits the light beam into two so that one beam passes through a standard reference solution and the other through the sample thus eliminating the need for a blank scan. A monochromator is typically used between the light source and sample to isolate the spectral wavelength of interest as shown in **Figure 3.6.4A**. The detector then measures the energy absorbance of light.

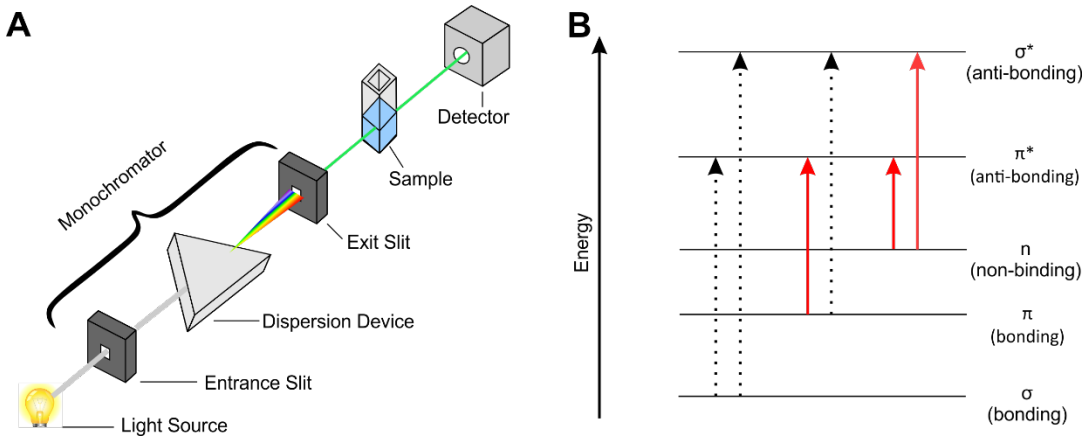

Figure 3.6.4 A) Schematic diagram of a typical UV-Vis spectrometer. B) Possible electron jumps caused by visible light. Adapted from [256,257].

As the light passes through the sample, the electrons absorb light energy and are excited from a binding or non-binding state to an empty anti-bonding orbital (**Figure 3.6.4B**). Since a typical UV-Vis spectrometer works at a range between 200 – 800 nm range, only a limited number of electron jumps are possible (red lines) while some occur when electrons absorb light outside the wavelength range (black dotted lines). The groups in a molecule which absorb light and therefore responsible for its colour are known as chromophores. Understandably, each jump needs a fixed amount of energy where bigger energy absorbance leads to a greater electron jump. Each wavelength, and thus frequency, of light corresponds to a specific energy value as detailed by Bohr-Einstein equation (**Eq. 3.10**). Electrons that excite easier require lower energy meaning they absorb the energy from light with a longer wavelength or a lower frequency while the opposite occurs with larger orbital jumps where a greater energy is needed.

$$v = \frac{c}{\lambda}$$

…Eq. 3.10A

$$E = E_2 - E_1 = hv$$

…Eq. 3.10B

where:

v = frequency of light

c = speed of light (2.998 x 10^8 ms^{-1})

λ = wavelength of light

E = energy of light

h = Planck's constant (6.626 x 10^{-34} Js)

In a typical UV-Vis configuration, a scan ranges from 200 to 800 nm thus covering near ultraviolet and approaching near infrared wavelengths. This narrow range means only specific energy absorbance and thus electron jumps can occur. From **Figure 3.6.4B** the red lines indicate the possible jumps in the UV-Vis range and reveals that a molecule must contain either pi bonds or atoms with non-bonding orbitals (i.e. lone pair in oxygen). A standard UV-Vis spectrum displays absorbance (a.u.) value against wavelength (nm).

Ultraviolet-Visible spectroscopy is ubiquitously employed in analytical environments, normally to gather concentration data of a particular compound. The relationship between absorbance and concentration of a molecule in a fixed path length (normally 1 cm) is expressed by Beer-Lambert's law (**Eq. 3.11**). Solutions containing increasing known

concentration of analyte of interest are employed to generate standard calibration curve where change in absorbance is measured as a function of concentration. This is then used as reference to determine concentration of analyte in unknown samples.

$$A = \log\frac{I_0}{I} = \varepsilon * c * L$$

…Eq. 3.11

where:

A = absorbance (a.u.)

I_0 = intensity of incident light at a given wavelength

I = intensity of transmitted light

ε = molar absorptivity of molecule/compound in solution (L mol^{-1} cm^{-1})

c = solution concentration (mol L^{-1})

L = pathlength (usually 1 cm)

It noteworthy that individual types of bonds in a molecule are correlated to a specific absorption peak wavelength and can thus be used to determine the functional groups present in the molecule under study. However, UV-Vis absorption spectra can be affected by a myriad of variables including solution pH, temperature, effective slit bandwidth and the presence of interfering substances. As such, these factors must be controlled and accounted for first in order to produce qualitative data identifying the specific compound/molecule present in the sample.

3.7 Surface Modification

Electrochemical techniques were used throughout the project to improve electrode response and/or modify electrode surfaces. These methods are briefly described in the following sections and will be further expanded upon in corresponding chapters.

3.7.1 Electrochemical Anodisation

Enhancing electrode surfaces, and thus electrode responses, are often necessary in electroanalytical methods. An example method is electrochemical anodisation. This can be achieved simply by using chronoamperometry, previously mentioned in Section **3.5.3**,

whereby the working electrode is submerged in 0.1 M sodium hydroxide (NaOH) solution and an oxidation potential of +2 V applied for a particular amount of time (typically between 60 and 300 seconds). This results in an increase in oxygen functionalities at the surface which can also lead to changes in the crystal structure of the sample's layers and its microscopic surface texture. As such, this process creates more edge plane sites which can allow faster electron transfer kinetics thus improving electrode sensitivity and voltammetric response [210,243,258,259]. Where necessary, anodisation details are described for each type of electrode employed in each chapter. **Chapter 4** will also further clarify the effects of anodisation as well as sonoanodisation.

3.7.2 Electropolymerisation

Electropolymerisation is a simple and efficient method to modify the surface of the electrode and therein change the properties and function of the sensor. This can be done to provide a permselective barrier against matrix interferences or to immobilise redox groups directly on the surface. In this project a flavin derivative functionalised with a phenol substituent was used as an electropolymerisable monomer through which to modify carbon-based electrodes. The electrochemical polymerisation is completed through inserting the working electrode in solution containing the required monomer and the application of potential or employment of cyclic voltammetry for a certain amount of cycles, which enables the oxidation of the phenolic group. This results in the formation of a film comprising of a non-conductive polyphenylene backbone but with pendant flavin redox centres. This work is described in more detail in **Chapter 5.**

Chapter 4

Effect of the Co-Application of Ultrasound and Electrochemical Anodisation on Carbon Fibre's Electroanalytical Performance

Abstract

Modification of carbonaceous surfaces through electrochemical oxidation processes are well known to enhance the electrochemical properties of carbon electrodes. In this case, a detailed study on both the influence of anodisation alone and with the co-application of ultrasound during electro-oxidation was performed. Chronoamperometry (+2 V) was employed to initiate electrochemical modification and the effect of prolonged anodisation periods in both experiments was examined. Surface sensitive techniques (SEM, Raman, and XPS) as well as electrochemical methods were employed to determine the resulting disparities generated by the presence and absence of ultrasound during anodisation. Ultrasonic cavitation and acoustic streaming led to greater physical deterioration and achieved contrasting net changes in various carbon-oxygen surface functional groups observed in the C1s spectra when compared to silent anodisation.

The work presented in this chapter forms the basis of a publication in:
Casimero C, Hegarty C, McGlynn R, Davis J. Ultrasonic exfoliation of carbon fibre: electroanalytical perspectives. Journal of Applied Electrochemistry. 2020;50(3):383-394.

4.1 Introduction

Carbon is one of the most ubiquitous electrode base materials used in electrochemical applications due to its versatility, extensive interfacial chemical properties, variance of physical form, and the electrodes which can be produced using carbon are relatively inexpensive and methodically simple to fabricate [260]. Carbon electrode fabrication techniques, beyond using solid graphite, include: screen printing [261–264], drop casting [265–267], pyrolysis of polymers formed via electrospinning [268,269] and polyacrylonitrile (PAN) fibre extrusions processes [244,270,271]. The interest in the latter, as well as other synthetic and bio-based equivalents, has been increasing over the last few years and is the commonest precursor (>90 %) in creating carbon cloth electrodes [244,272]. These electrodes can be made up of woven, aligned or randomly intertwined matrices of carbon fibre whose unique properties (i.e. vast surface area, electrical conductivity, chemically inertness and macro porosity) offer many advantages in electroanalytical applications.

Although carbon fibre systems possesses sufficient conductivity for some electrochemical applications, its unmodified form tends to have a relatively featureless surface and, as such, it is relatively common to modify the fibres via chemical, plasma or electrochemical methods to enhance electrode performance [243,244]. Surface modification was originally envisaged from engineering perspectives intended to improve mechanical and structural characteristics aimed for high load bearing purposes [273,274]. Such processes also generated a greater range of active functional groups and increased surface area that lead to augmented performance and adaptability of the carbon mesh when employed as an electrode. The effect of different surface modifiers and treatments along with their influence on electrode performance has been extensively reviewed [244,275–278] and, while there is a variety in technique, the end result typically involves surface oxidation which in turn amplifies the population and diversity of carbon-oxygen functional groups [242,275,279,280]. **Figure 4.1.1** summarises the various types of oxygen functionality typically generated through the oxidation of carbon fibre surfaces, reportedly analogous to those observed in graphene oxide fragments [281] though fixed to the body of the fibre structure instead. It is important to note that these are indicative solely of base functionality and a range of forms will arise as the graphitic plane is modified [282,283].

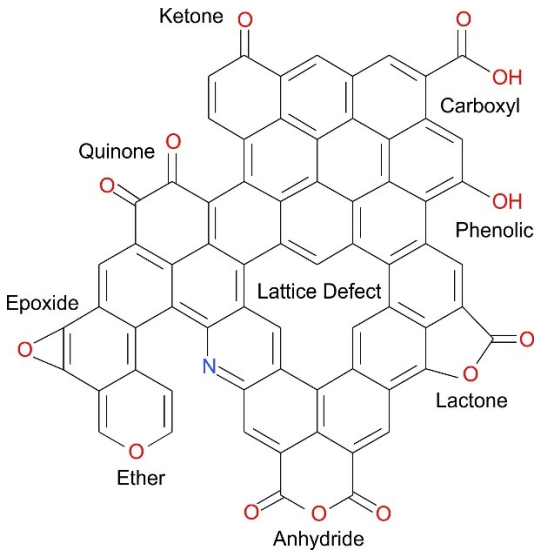

Figure 4.1.1 Summary of different oxygen functional groups present on the surface of carbon fibre generated through oxidation (adapted from [282]).

It should be noted that a representative nitrogen functionality has been added in the figure above as it was envisaged that a minute population (i.e. pyrrolic and pyridinic) would be present within the graphitic planes. In the absence of an external source of nitrogen, such occurrence can be explained by the incorporation of PAN nitrogen into the lattice during the carbonisation process of the carbon fibre production [284]. The majority of functional groups found in unmodified fibres however are sp^2 carbon and it is the oxidative destruction of the latter that results in the carbon-oxygen functionality. Electrochemical oxidation, also known as anodisation, is an effective method to allow surface etching along with generating oxygen groups through the application of a positive potential [242,275,279,280] and it's now common for carbon fibre-based electrodes to undergo this treatment to enhance electron transfer kinetics prior to employment [242–244].

This chapter focuses on the influence of the simultaneous application of electrochemical anodisation and ultrasonic activation in enhancing electrochemical properties of carbon mesh electrodes. It is known that the macro/micro acoustic streaming processes and cavitation caused by ultrasound can have a radically positive effect on its electrochemical activities [285,286] and has been proven to work in both porous and planar substrates [287,288]. It was envisaged that such effects could also enhance the influence of anodisation by facilitating further permeation of electrolyte through the fibre matrix, removing bubbles and accelerating delamination of mechanically weak carbonaceous layers [289]. Additionally, it was expected that this co-application would increase the manifestation of new graphitic layers, increase edge plane sites as well as alter the proportions of relevant functional groups.

4.2 Experimental Details

4.2.1 Materials

All chemicals were purchased from Sigma Aldrich (UK), were of the highest grade available and were used without further purification. Britton-Robinson buffers composed of phosphoric, acetic and boric acids, each at 0.04 M concentration, were used throughout the experiment, unless otherwise stated. Each BR buffer was adjusted to the correct pH unit by adding concentrated sodium hydroxide (NaOH). Toray carbon paper (TGPH-30, no wet proofing) was obtained from University of Surrey.

4.2.2 Electrode Design

Carbon fibre mesh was segmented and these sections were thermally sealed within a commercial polyester laminate [290], designed with a 4 x 4 mm window to establish a standardised geometric area which enables analogous comparisons before and after modification. The carbon film was connected to an electrically conductive copper adhesive tape, as shown in **Figure 4.2.1**, to allow connection to the potentiostat.

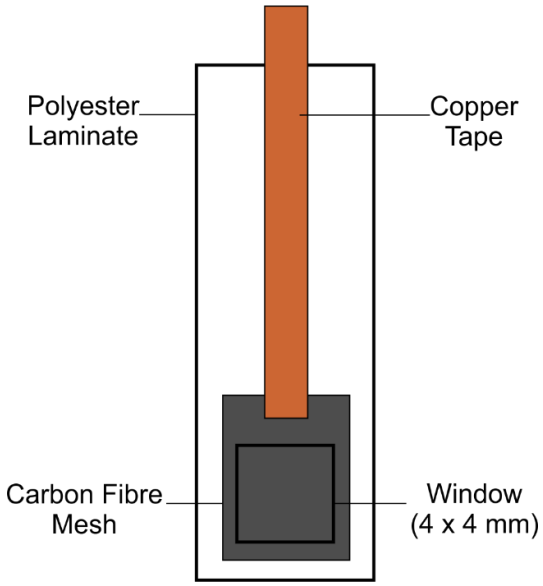

Figure 4.2.1 Carbon fibre mesh working electrode assembly.

4.2.3 Electrochemical Configuration

A µAutolab Type III computer-controlled potentiostat (Eco-Chemie, Utrecht, Netherlands) was used to execute all electrochemical analysis. A standard three-electrode set-up was used throughout with carbon fibre mesh acting as the working electrode, a Ag/AgCl commercial half cell (3 M NaCl, BASi Technicol, UK) as the reference electrode and a platinum wire completed the configuration as the counter electrode. Experiments involving sonoanodisation were conducted through submersing the electrochemical cell in a conventional laboratory ultrasonic bath operating at 40 kHz. All experimentations were carried out at room temperature (22 °C ± 2 °C).

4.2.4 XPS

The quantification of surface composition and acquirement of XPS spectra were completed using an Axis Ultra DLD Spectrometer (Kratos Analytical Ltd., UK). Spectra were analysed using monochromated Al Kα X-rays (hv = 1486.6 electron volts (eV)) operating at 15 kV and 10 mA (150W). A hybrid lens mode was employed (electrostatic and magnetic) during analysis with a 300 µm x 700 µm analysis area and a take-off angle of 90° with respect to the sample surface. Wide energy survey scans were collected across a range of -5 to 1200 eV binding energy, with a pass energy of 160 eV and step size of 1 eV. High-resolution spectra were collected with a pass energy of 20 eV with a 0.05 eV step size, a scan width of 25 eV, a dwell time of 150 milliseconds and at least 3 sweeps to reduce the signal noise. A Kratos charge neutraliser system with a filament current of 1.8 A and a charge balance of 3.6 V and a filament bias of 1.3 V was used for all samples. Charging effects on the binding energy positions were adjusted by setting the lowest binding energy for the C1s spectral envelope to 284.8 eV, which is commonly accepted as adventitious carbon surface contamination. Three measurements were analysed per sample, with a Shirley background subtracted from each XPS spectra. The peak areas of the most intense spectral lines for each elemental species were used to determine the percentage atomic concentration. Peak fitting of high-resolution spectra was carried out using Casa XPS software.

4.2.5 Raman

Raman spectra were obtained using a LabRAM 300 (Horiba, Japan) spectrometer employing a HeNe laser (632 nm, 50 X optical lens, spot approx. 30 µm, 10 % filter, laser power 2.59 W (25.9 * 10 %)). The carbon fibre samples were analysed over 100 - 3500cm^{-1} in 5 slices (energy per slice 38.85 J) to cover the range with 5 spots per sample.

4.3 Results and Discussion

4.3.1 Preliminary Electrochemical Assessment

The presence of various types of carbon in the electrode configuration inevitably corresponds to a vast range of interfacial structures. Simply put, graphitic carbon has two structural features, namely basal (hexagonal surface parallel to the graphite plane) and edge planes (edge surface perpendicular to the normal graphite layer), which possess significantly contrasting electrochemical characteristics. Although both are ubiquitous to carbon fibre, the former planar type is predominant in unmodified carbon fibre surfaces. Electron transfer kinetics is affected differently by each interfacial feature and is highly dependent on the nature of the redox probe used for examination. For instance, ferrocyanide and ruthenium hexamine are common redox species which offer different sensitivity to surface chemistry. Ferrocyanide is an inner sphere complex that is highly influenced by varying structural form, while the latter exhibits an outer sphere behaviour that is indifferent to such phenomena. In instances where edge plane sites are predominant along the carbon surface, a faster electron transfer kinetics is observed with ferrocyanide compared to those where basal layers are more prevalent [291–293]. Using the same electrode, it is clear that the unmodified carbon fibre exhibits irreversible behaviour (ΔEp = 300 mV) towards ferrocyanide (**Figure 4.3.1A**), while a reversible cyclic voltammogram trace is observed for ruthenium hexamine (**Figure 4.3.1B**).

Electrochemical anodisation, with or without ultrasonic treatment, significantly alters the graphitic plane formation with a substantial increase of carbon-oxygen functionality as well as carbon defect population, as depicted in **Figure 4.1.1**. The effect of various anodisation treatment periods on the cyclic voltammogram response of the carbon mesh electrode towards ferrocyanide and ruthenium hexamine (each at 2 mM dissolved with 0.1 M KCl) are highlighted in **Figure 4.3.1A** and **Figure 4.3.1B**, respectively. Noticeably, the irreversible

response, initially examined at the unmodified electrode, towards ferrocyanide is markedly transformed through the process of electrochemical oxidation and the electrode behaviour is subsequently changed to become reversible. Additionally, the peak separation drastically decreases as the anodisation time increases. The typical reversible system was observed at electrodes which have been anodised for 300 seconds or longer as highlighted in **Figure 4.3.1C**. There have been conflicting results regarding the role of surface oxides on electron transfer kinetics. On one hand, it is reported that anodised carbon-based electrodes have enhanced transfer kinetics for a range of redox probes ($Fe(CN)_6^{3-/4-}$, $Eu^{2+/3+}$, $Fe^{2+/3+}$ and $V^{2+/3+}$), with a 500 fold increase compared to its unanodised version [294,295]. On the other hand however, there have been contradicting reports which imply that carbon oxides only have a minor role of only 2 to 3 factor increase towards ferrocyanide [296].

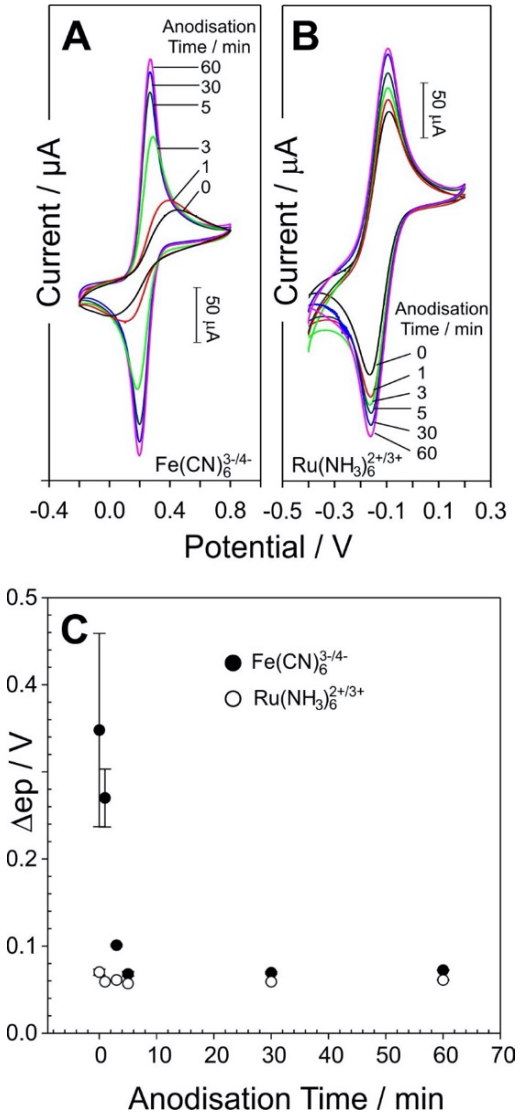

Figure 4.3.1 Cyclic voltammograms highlighting the carbon fibre mesh electrode response after various anodisation periods without ultrasound towards A) ferrocyanide and B) ruthenium hexamine, both of which are at 2 mM concentration in 0.1 M KCl. C) Effect of anodisation time on the peak separation of ferrocyanide and ruthenium hexamine. Error bars represent mean standard deviation. Scan rate: 50 mV s^{-1}.

As previously mentioned, ferrocyanide is recognised to be highly sensitive to surface chemistry [297,298] which helps explain the results attained. It was envisaged that the process of anodisation increased the surface concentration of oxygen functional groups and edge plane sites which, together, improves the electron transfer kinetics of the electrode towards ferrocyanide. This stands in agreement with the results by Gooding et al. (2005) where they determined the importance of oxygenated species on single walled carbon nanotubes (SWCNTs) to improve the electrode response to ferrocyanide [299]. The researchers amplified the population of oxygen functionalities at the SWCNT through using nitric acid as the oxidation medium. Compton et al. (2006) also established that through the addition of multi-walled carbon nanotubes (MWCNTs), whose exposed ends contain a large amount of oxygen functional groups, markedly improved the basal plane pyrolytic graphite's response to ferrocyanide albeit the surface being normally renowned for its poor response towards the latter [298]. Additionally, the group has determined that the generation of freshly cleaved edge plane pyrolytic graphite aids in enhancing ferrocyanide electron transfer kinetics and that oxygenated species actually impedes this which stands in contrast against previous outcomes [298]. In their case however, carbon was only oxidised in air and thus it is envisaged that the carbon-oxygen functionality engendered through this does not have the same effect as that produced through more rigorous oxidative procedures, be it chemical or electrochemical.

Upon assessing the carbon fibre electrode responses to ruthenium hexamine (**Figure 4.3.1B**), the latter's outer sphere characteristics and thus insensitivity to surface functionality is observed as highlighted by the reversible behaviour detected even at the unmodified carbon electrode. Notedly, peak separation as well as peak height ratio was unaffected by electrochemical oxidation. Similar to ferrocyanide however, it should be noted that the peak height evidently increases with anodisation time, attributable to slight enlargement of electrode surface area due to the increasing carbon fibre surface delamination. In addition, the influence of scan rate on the anodised (300 s) electrode response towards ferrocyanide and ruthenium hexamine was examined to determine if carbon surface modification led to defects that could, in turn, lead to the entrapment of the redox species. **Figure 4.3.2** displays the resultant linear relationship detected between peak current magnitude and square root of scan rate, confirming that both systems are diffusion limited.

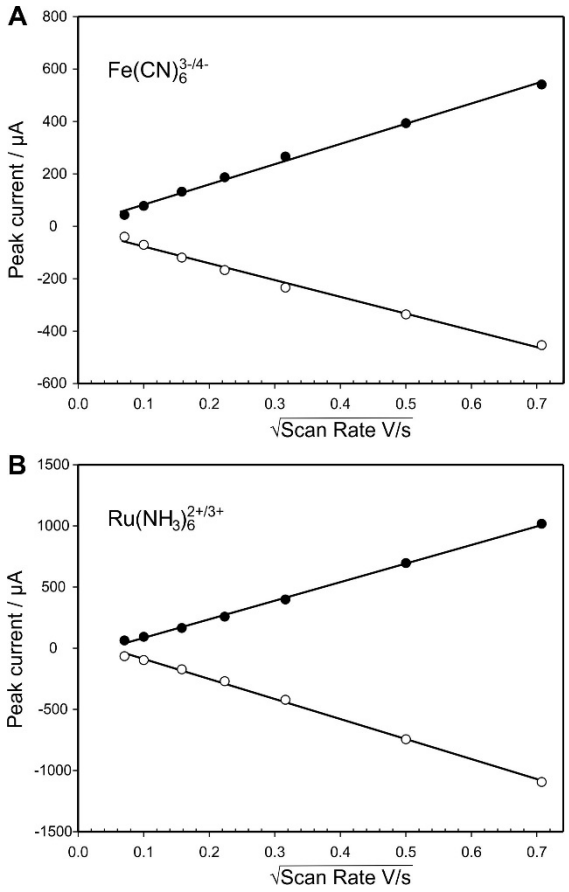

Figure 4.3.2 Influence of square root of scan rate on the anodised carbon mesh electrode response in the absence of ultrasound towards A) ferrocyanide and B) ruthenium hexamine.

Although a reversible behaviour was observed with ferrocyanide post carbon electrode anodisation, the combination of applying electrochemical oxidation and ultrasound achieved this reversibility quicker. Comparative cyclic voltammetry traces are shown in **Figure 4.3.3A**, revealing the response of unanodised, anodised (60 s) and sonoanodised (60 s) carbon fibre mesh electrodes. It is noteworthy that beyond 300 seconds of electrochemical oxidation, the presence of ultrasonic support had only minute influence in the voltammetric response (**Figure 4.3.3B**), having similar peak separations and peak heights to electrodes anodised in the absence of ultrasound - analogous to the behaviour previously exhibited in **Figure 4.3.1C**. The preliminary evaluation discussed here would imply that ultrasound has a kinetic influence on the electrode modification rather than any significant structural variation. The succeeding sections however discusses the likelihood that more factors could corroborate the responses attained.

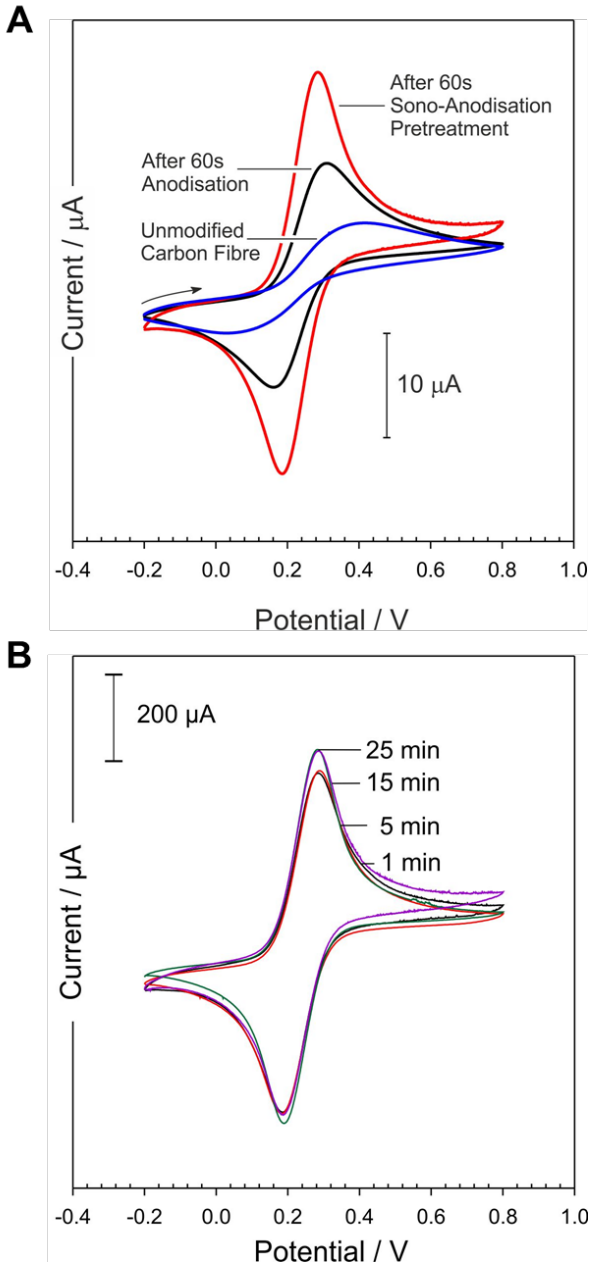

Figure 4.3.3 A) Cyclic voltammograms detailing the response of a carbon fibre electrode towards ferrocyanide (2 mM, 0.1 M KCl) after anodisation with and without the application of ultrasound. B) Cyclic voltammograms highlighting the effect of prolonged sonoanodisation on the carbon mesh electrode response towards ferrocyanide. Scan rate: 50 mV/s.

4.3.2 Raman Spectroscopy Examination

The difference in surface chemistry between unmodified (0 min) and anodised carbon fibre, with various treatment times without the aid of ultrasound, was initially assessed using Raman spectroscopy and representative spectra are presented in **Figure 4.3.4A**. The first order Raman spectra of the carbon fibre displays three relevant and distinguished peaks namely D band (1350 cm^{-1}), G band (1580 cm^{-1}) and D' band (1610 cm^{-1}). The G band

represents the graphitic in plane vibration with an E_{2g} symmetry whilst the D and D' bands complement the manifestation of out of plane vibrations corresponding to the generation of structural lattice defects and, as such, act as indicators of disorder as previously suggested by preceding investigations regarding oxidised carbon fibre [277,289,300]. Evidently, the greater the anodisation time, the greater the population of oxygen functionalities as well as defects within the lattice including grain boundaries, aliphatic components and in-plane heteroatoms (akin to **Figure 4.1.1**). As a result, the D and D' band peak heights intensify with treatment time as seen in **Figure 4.3.4A**.

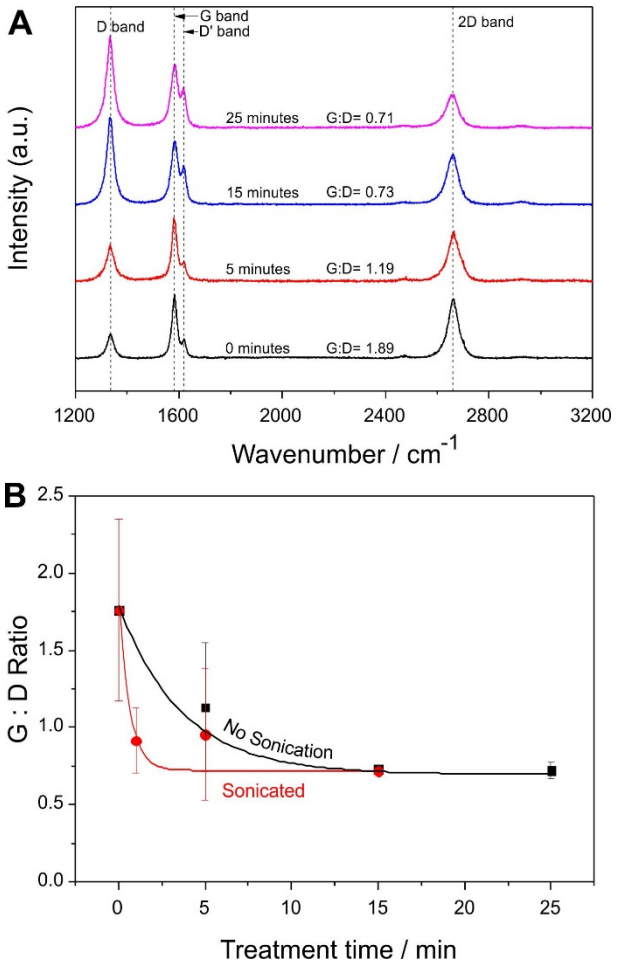

Figure 4.3.4 A) Representative Raman spectra of the carbon fibre surface before and after various anodisation periods in the absence of ultrasound. B) Influence of anodisation with and without ultrasound on the degree of disorder within the carbon fibre lattice. Error bars represent mean standard deviation.

By comparing the ratio of intensity of D and G bands for each anodisation period, further knowledge into the influence of electrochemical oxidation on the carbon structure can be attained. Although it is quicker to achieve graphitic lattice disorder through the co-application of ultrasound during anodisation, the former does not ultimately lead to any increase in disorder greater than those attained in its absence as exhibited in **Figure 4.3.4B**.

Analogous to the electrochemical responses observed previously in **Figure 4.3.3A**, sonoanodisation simply sped up the process at which the electrode response to ferrocyanide exhibited a reversible system. It was envisaged the application of ultrasound during anodisation aids the removal of oxygen bubbles generated by the imposition of the anodic potential (+2 V). The presence and entrapment of these bubbles within the interpenetrating carbon fibre mesh are expected to significantly deter the flow of electrolytes towards the electrode and, as such, reduces the effectiveness of the surface treatment. Essentially, the employment of ultrasonic waves serves to degas the electrode interface [(285)] and its subsequent cavitation effect should also aid in enhancing mass transport of fresh electrolyte (NaOH) to the carbon network which, in turn, promotes a faster interface remodelling.

4.3.3 Effect of Anodisation and Sonoanodisation on Surface Hydrophobicity

Contact angle measurements were used to briefly determine and compare the influence of anodisation and sonoanodisation on the surface hydrophobicity of carbon fibre. According to the contact angle measurements and the corresponding representative images shown in **Figure 4.3.5**, it is clear that the largely graphitic, unmodified carbon electrode was markedly more hydrophobic (>100°) in comparison to its anodised form, with or without ultrasound. Electrochemical oxidation on its own would have increased the number of hydrophilic C-OH and carboxyl functionality which would explain the improved the wettability of the surface [(301,302)]. However, the ultrasound-aided anodisation showed a greater augmentation in hydrophilicity compared to silent anodisation, attributable to the kinetic and physical effect of ultrasound-associated cavitation, as per previous discussion.

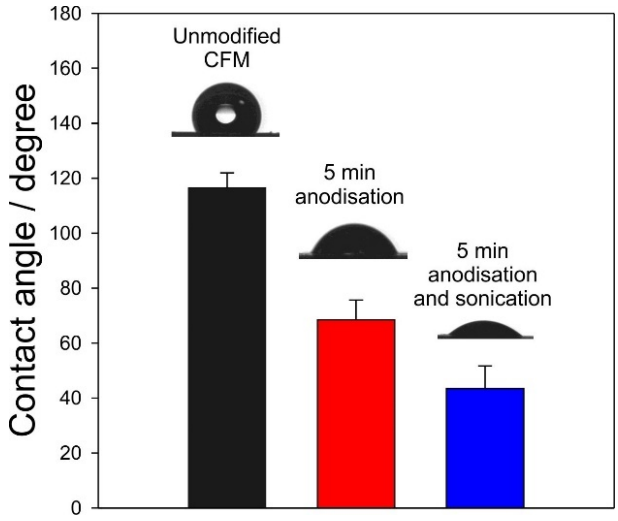

Figure 4.3.5 Contact angle measurements and corresponding representative images detailing the effect of anodisation, with and without the presence of ultrasound, on the surface wettability of carbon fibre. Each bar is an average 6 measurements and error bars represent mean standard deviation.

4.3.4 Effect of Ultrasound on Carbon Fibre Morphology

It is evident that in comparison to the Raman spectra obtained without ultrasound, no significant increase in lattice disorder was caused as a consequence of increasing anodisation times with the presence of ultrasonic waves. Although this is the case at the molecular scale, the application of sonoanodisation has a significant influence on the macro morphology of the carbon fibre. **Figure 4.3.6** displays the effect of various anodisation times, with and without ultrasonic force, on the physical structure of carbon fibre. It can be seen that prior to anodisation (**Figure 4.3.6A**), carbon fibre has striations parallel to its longitudinal axis which are attributed to the method of production. These striations then become more distinct after anodisation and the outer sheath begins to deteriorate after 5 minutes of electrochemical oxidation (**Figure 4.3.6B**). It is evident that longer anodisation times exert greater damage to the physical properties of the fibres with the delamination of graphitic shards becoming more apparent (**Figure 4.3.6C**). It was envisaged that the increasing presence of oxygen bubbles, generated through the anodisation process, under semi-delaminated sections of the carbon fibre causes such occurrences and further facilitates the erosion of the graphitic outer surface, which, in turn, inevitably decreases the fibre width (**Figure 4.3.6E**). However, **Figure 4.3.6D** highlights that the bulk physical condition of the carbon mesh remains mainly intact after anodisation in the absence of sonication.

With the application of ultrasound, the aforementioned changes occur at an accelerated pace. By comparing the scanning electron micrographs of electrodes with the same

anodisation times in the absence (**Figures 4.3.6B, 4.3.6C, 4.3.6D**) and presence of ultrasound (**Figures 4.3.6F, 4.3.6G, 4.3.6H**), it is clear that sonoanodisation causes greater physical deterioration than its silent alternative. This is further supported by **Figure 4.3.6E** which highlights the narrower diameter observed after the co-application of anodisation and ultrasound. This constant narrowing unsurprisingly leads to mechanical failure of the carbon mesh, thus causing the notable difference in the bulk structure (**Figure 4.3.6H**). These examinations are in clear disagreement with the Raman spectra (**Figure 4.3.4**) where no significant difference between the presence and absence of ultrasound was observed at anodisation periods longer than 15 minutes.

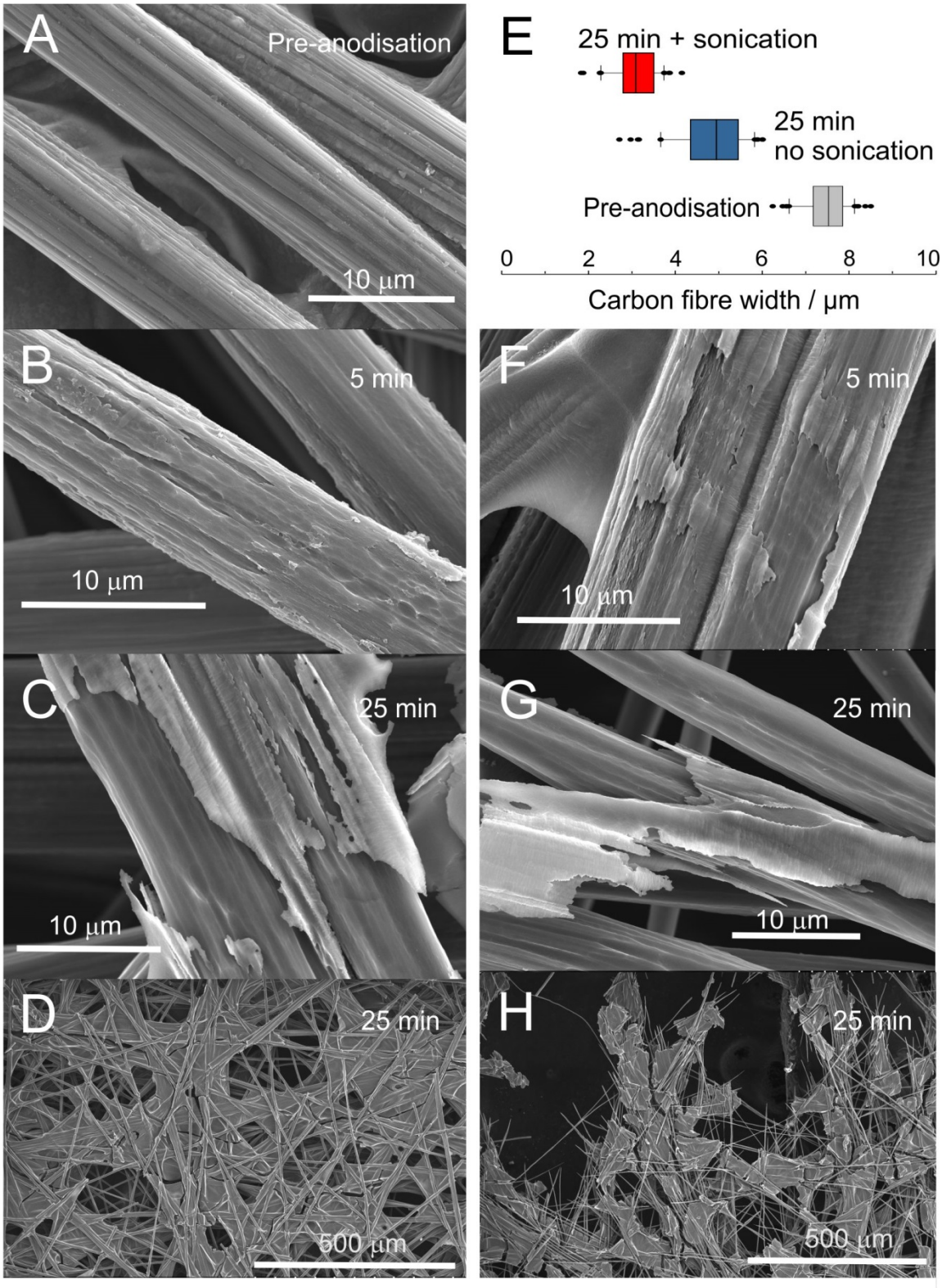

Figure 4.3.6 Scanning electron micrographs highlighting the surface morphology of the carbon fibre A) before and after B-D) silent and F-H) ultrasound-aided anodisation. E) Comparison of carbon fibre diameter as a result of anodisation (N = 50).

4.3.5 Influence of Anodisation on Carbon-Oxygen Functionalities

High resolution X-ray photoelectron spectroscopy, focused on the C1s and O1s spectra, was used to assess the effect of electrochemical oxidation in the population of carbon-oxygen functionalities. As detailed in **Figure 4.1.1**, there are main functional groups (C=C/C-C, C-OH/C-O-C, C=O and COOH) that will be generated as a result of anodisation and, as such, **Figure 4.3.7A** displays the C1s spectrum along with the deconvoluted/fitted peaks associated with the individual functionalities. The spectra clearly show that after 300 s of anodisation, there is a greater population of oxygen functionalities in comparison to those in unmodified fibre (**Inset Figure 4.3.7A**). This increase is further supported by the O1s spectra (**Figure 4.3.7B**) where the initial oxygen peak derived from the presence of carbonyl/ketone functionalities is fragmented to C-O group, implying the increase in phenolic functionality as a direct result of electrochemical oxidation.

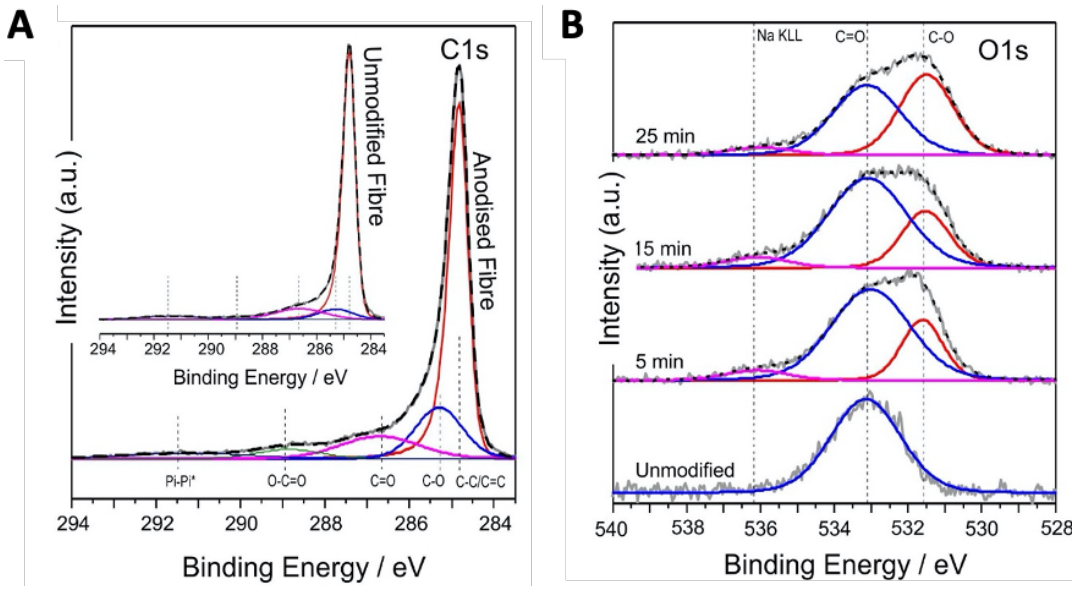

Figure 4.3.7 XPS analysis of the A) C1s and B) O1s spectra before and after anodisation of carbon fibre mesh without ultrasound.

Subsequently, a comparative study was completed to distinguish the difference in the effects of sonoanodisation and silent anodisation in the C1s and O1s spectra. Similar peaks were observed between both XPS spectra however, there were minute but distinct differences in the relative proportions of each group (**Figure 4.3.8**). The deconvoluted carbon functionality spectra, taken from carbon fibre electrodes with various anodisation periods without the aid of ultrasonic exfoliation (**Figure 4.3.8A**), illustrates that there is a significant change in the lattice upon the onset of electrochemical oxidation with a considerable decrease in C=C

population and appearance of C-O functionalities as well as materialisation of relatively minor proportions of carboxyl (COO) and carbonyl (C=O) groups. Prolonged anodisation resulted in no significant difference in the latter two groups but led to a markedly different percentage contribution of C-O and C=C sp^2 functionalities.

The latter observations can be interpreted in a number of ways, but a sense of caveat is imperative. First and foremost, it is unfeasible to reliably differentiate between sp^2 and sp^3 carbon peaks within the deconvoluted spectrum as their individual peaks are separated by only 0.3 eV. Although the former carbon type will be inevitably prevalent in the unanodised carbon fibre mesh, extended periods of electrochemical oxidation causes greater damage to the lattice which, in turn, could increase the population of the aliphatic sp^3 carbon forms. As such, the reduction of C=C groups should be offset by the surge in the C-C functionalities however, since both XPS signals are split by only 0.3 eV, the conversion of one carbon form to the other would mean diminutive change in the detected C-C/C=C peak. An alternative, and potentially complementary, explanation could be that the constant exposure of new graphitic layers as a result of the oxidation-aided exfoliation of the carbon sheath leads to minute changes to oxygen functionality instead of its population increasing with anodisation time. Simply, as the previously oxidised layers are desquamated, the prolonged anodisation process resets with a new graphitic layer (mainly sp^2 carbon) and the oxygen groups that was generated through electrochemical oxidation is essentially detached. Additionally, as a consequence of the diffusion-controlled electrolytic process, the pH of the local environment shifts which in turn could decrease the modifying effect of the electrochemical oxidation.

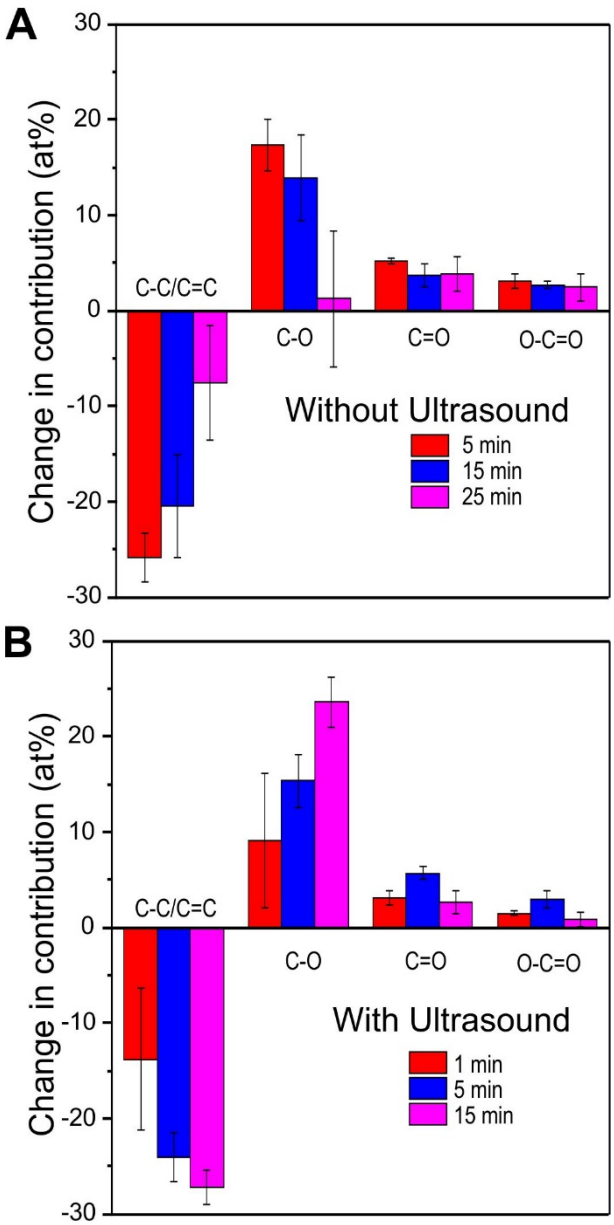

Figure 4.3.8 Summary of the net changes in carbon functionality on the carbon fibre electrode as a consequence of anodisation being conducted in the A) absence and B) presence of ultrasound. Error bars represent mean standard deviation.

On the contrary, anodisation in the presence of ultrasound (**Figure 4.3.8B**) gives rise to the opposite outcomes. In this case, prolonged oxidation periods lead to an increase in the modification of the lattice, essentially damaging the sp^2 carbon forms while populating C-O groups. The kinetic effect of anodisation discussed previously may also have an influence on the results observed here. Despite delamination clearly occurring at a faster rate in ultrasound-aided anodisation (**Figures 4.3.6F, 4.3.6G, 4.3.6H**) compared to silent anodisation (**Figures 4.3.6B, 4.3.6C, 4.3.6D**), it was envisaged that as the duration of the oxidative process increases, the fresh layers are immediately functionalised as soon as the preceding layers are

peeled. Moreover, it was anticipated that the ultrasonic cavitation allows the delivery of new electrolyte towards the carbon fibre electrode thus enhancing the oxidative modification.

Evidently, the results obtained from anodisation process in the presence of ultrasound differs to those observed in its absence. The major discrepancy between the two processes is the changes in percentage contribution of C-C/C=C and C-O functional groups but differences in carboxyl functionalities, although minor, are also observed. The latter groups are significant factors in the carbodiimide tethering of biological catalysts and, as such, the subtle changes in its production are also noteworthy. Carbon oxidation has been generally presumed to generate an abundance of carboxyl groups to be used for the coupling of biological agents however as per the outcomes attained here, although there is an increase, carboxyl functionalities are not the main output. In addition, sonoanodisation clearly produced less of these in comparison to anodisation alone which could be due to some other underlying physical effect of ultrasound or the constant exfoliation of carbon planes.

4.3.6 Carbon-Quinone Electrochemistry

Through the assessment of the unmodified carbon mesh's XPS spectra, it was revealed that the graphitic layers of the fibres already possess a range of carbon-oxygen functional groups even prior to anodisation. The occurrence of electroactive quinoid groups on the surface of carbon materials is well-known and their detection can be completed using sensitive electrochemical processes like square wave voltammetry [(243)]. The effect of various anodisation time periods without ultrasound assistance on the generation of such redox functionalities was therefore electrochemically assessed (**Figure 4.3.9**). A negative potential of -0.8 V was applied to initiate the reduction of the quinones to their hydroquinone form and the potential was then swept towards the more positive range to allow its re-oxidation (typically observed as a broad peak between -0.3 V and +0.3 V). The chronological voltammetric traces (**Figure 4.3.9**) reveal that the resultant peak formed at prolonged oxidation times are actually composed of various components which complements/replicates the heterogenous nature of the quinone functional groups that are present on the carbon surface produced by non-specific electrochemical oxidation process.

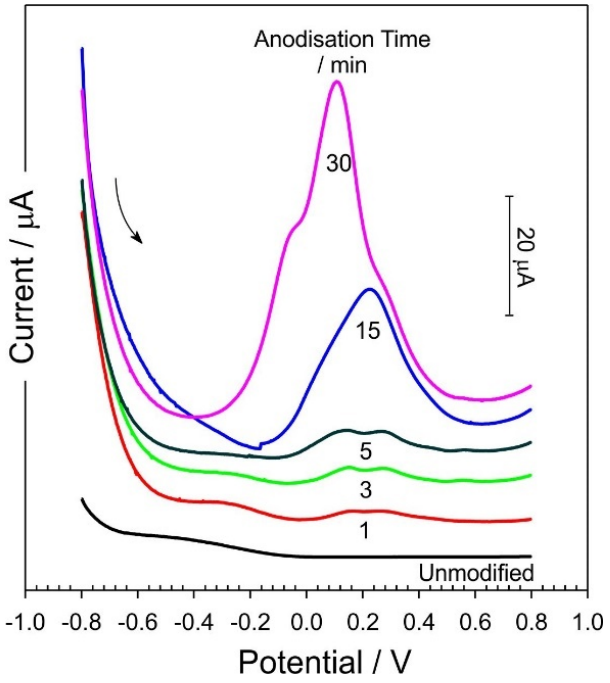

Figure 4.3.9 Square wave voltammograms highlighting the carbon fibre electrode response in pH 3 BR buffer after various silent anodisation time periods.

The C=O redox functional groups are known to be quinone constituents and, as previously discussed, longer anodisation times do not have much effect on their relative proportion. However, the square wave voltammograms highlighted in **Figure 4.3.9** stands in contrast to this and reveals that increasing the treatment time increases quinone activity. This could possibly be attributed to the chemical nature of quinone whereby its oxidised form possesses C=O functionality but its reduced form exhibits the C-O functional groups (**Figure 4.3.10A**). Therefore, the electrochemistry of the quinone is an amalgamation of both functionalities and does not completely complement the C=O peak observed in the XPS spectra. Furthermore, not only can these functional groups be modified to 1,2 or 1,4 dihydroxy moieties (**Figure 4.3.10A**), they can also have longitudinal quinone characteristics across the lattice as detailed in **Figure 4.3.10B**.

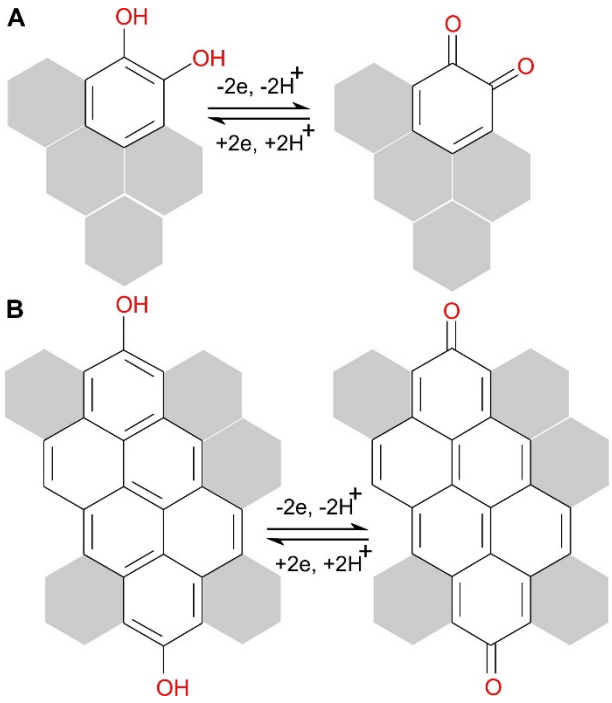

Figure 4.3.10 Redox transition of simple quinone groups (A) and those spatially distant along the carbon lattice (B) on carbon fibre surfaces.

4.4 Conclusions

Pre-treatment of carbon fibre and other carbonaceous surfaces has been long recognised to play a vital role in enhancing electrode properties. While a variety of surface modification techniques have been applied, no study has yet involved the employment of ultrasound as a means of augmenting the electrochemical anodisation method. This chapter revealed that ultrasonic cavitation and acoustic streaming enhanced the electron transfer kinetics of the electrochemical anodisation technique but has been shown to generate opposing net changes in the populace of C-C/C=C and C-O surface functionalities in comparison to unaided electro-oxidation. It was envisaged that the physical destruction of the carbon surface, as a direct result of sonoanodisation, is a possible cause of the observed disparity. Moreover, it was discovered that, both in the absence and presence of ultrasound, the population of carboxylic functional groups remains relatively constant even with prolonged anodisation times. This may have significant adverse effects for succeeding modification techniques where there is a need to covalently bind catalytic species to the carbon fibre surface. It should also be noted that although there are clear advantages in employing ultrasound, it simply speeds up the electrochemical processes that occur with anodisation alone and as such, the subsequent chapters effectively use the conventional silent electro-oxidation. The

results obtained here supports the application of anodisation in enhancing the electrochemical performance of carbon-based electrodes – the chosen substrate for this project. This is evidently useful in developing a smart catheter system that could provide electroanalytical information that could be exploited to monitor the condition of the line.

Chapter 5

Flavin-Phenol Modified Electrode for In Situ pH Measurements

Abstract

The ability to measure pH changes within the lumen of the catheter has been proposed as a potential route through which to monitor bacterial colonisation. Traditional glass pH sensors would be inappropriate in this context due to their rigid nature and their incompatibility with miniaturised environments. As such, a robust, inexpensive and scalable polymer-coated carbon fibre-based pH sensor has been developed and characterised. The probe's ability to measure pH changes in situ was tested through its application inside the challenging milieu of a microbial reactor. The latter represents an accessible approach in determining the influence of bacterial presence on the electrode response. The sensor was based on the electropolymerisation of a custom synthesized flavin-phenol moiety which demonstrated a pH sensitive redox response. The latter was investigated using square wave voltammetry wherein the oxidation peaks of the flavin film were found to provide a near Nernstian behaviour of 55 mV/pH with minimal drift. A key advantage of the system was that the oxidation peak processes were located within a potential region devoid of any common interferences that could hinder typical pH systems. The ability of the system to measure pH over a period of 51 hours within the bioreactor was demonstrated.

Part of the research described in this chapter is published as a cover/feature article in:
Casimero C, McConville A, Fearon J, Lawrence C, Taylor C, Smith R et al. Sensor systems for bacterial reactors: A new flavin-phenol composite film for the in situ voltammetric measurement of pH. Analytica Chimica Acta. 2018;1027:1-8.

5.1 Introduction

Following on from the examination of the effect of anodisation in enhancing the carbon fibre mesh's electrochemical characteristics, this chapter details the employment of an anodised carbon electrode as a pH sensor. Carbon fibre mesh was chosen as the initial substrate for the proposed sensor for its versatility, flexibility and scalability, which are prerequisites for miniaturised in situ monitoring. Research into replacing rigid, unadaptable traditional glass probes are underway by producing small, flexible and mechanically robust solid state pH sensors [216,303,304]. These characteristics are especially important in microfluidic and biomedical systems where disposability is often a requirement. In the present case, the pH sensitive electrode assembly involves a flavin-modified pressed carbon fibre mesh whose functionality was then tested in a challenging milieu of a microbial reactor intended to manufacture kefir-fermented milk products. This provided a simple route through which to assess the influence of a changing bacterial system, akin to that of a contaminated catheter system, on the electrode response without the issues associated with traditional microbiological testing. This includes the length of time taken for adequate bacterial growth and proliferation as well as the risk of contamination that could easily affect and skew the data obtained.

Riboflavin was first observed as a yellow-green fluorescent pigment found in milk by Alexander Wynter Blyth in 1872 and was the second B-vitamin characterised, hence it is also known as vitamin B2 [305,306]. Some food, such as fresh meat, leafy vegetables and milk, are natural sources of the vitamin whilst others are fortified with it [305,306]. Intracellularly, riboflavin is phosphorylated and is a precursor of flavin mononucleotide (FMN) and flavin adenine nucleotide (FAD) - both of which are important cofactors in numerous cellular processes including metabolism and other flavoprotein enzyme reaction [305–307], proving its key role in maintaining human health. Additionally, riboflavin has been suggested to have antimicrobial properties against catheter-related bloodstream-causing pathogens such as *E. coli*, *C. albicans* and *S. aureus* [308–311].

Apart from its detection [312–314], the more recent focus has been the exploitation of its redox-active flavin group as a sensor component which detects biomarkers linked with disease [315–323]. The flavin acts an electrochemical mediator and has evidently been able to aid the detection of several compounds such as glutamate [316] and persulfate [317] as well as maladies

like hepatitis C [318] and chorionic gonadotropin [319]. In these cases, either a chemical linker is used to covalently attach riboflavin to a base substrate, or it is directly electropolymerised on to the electrode surface. The polymerisation process occurs through the employment of large over-potentials but this aggressive oxidative activity is believed to significantly compromise the redox group and hence reduces its associated electrochemical signal. This chapter therefore details a newly engineered flavin-phenol moiety which, in comparison to riboflavin, can be electropolymerised without damaging the core redox flavin centre.

Similar to riboflavin [324,325], the customised flavin molecule (**Figure 5.1.1**) can undergo reduction and oxidation (**I** $\rightarrow$ **II** and **II** $\rightarrow$ **I**). As opposed to the polymerisation process occurring directly at the flavin, it was envisaged that through the addition of the phenol substituent, the monomer can be polymerised through a radical cation process via the attack of the phenol ring (**I** $\rightarrow$ **III**). In turn, this allows the preservation of the distinct redox transitions (**I** $\rightarrow$ **II** $\rightarrow$ **I**) which can then be exploited as the foundation of an electrochemical sensor. These transitions are dependent on H^+ ion concentrations and can therefore be utilised as an indirect method of measuring pH. The flavin oxidation peaks are envisioned to be within a potential range deprived of any competing reactions. The critical advantage of being able to electropolymerise the flavin monomer is that it can be directly and specifically deposited at appropriate conductive substrates, irrespective of shape or size.

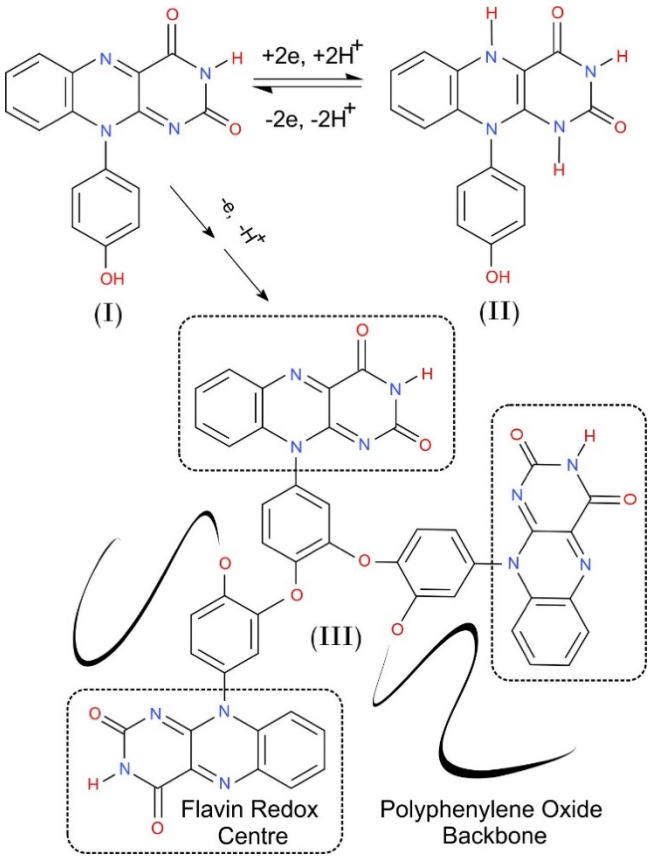

Figure 5.1.1 Redox transitions of the flavin unit (I→ II→I) and the electro-oxidation of the phenolic substituent leading to the production of a polyphenylene oxide polymer (I→III).

The commercialisation as well as home-based culturing of kefir-based probiotic milk products has been increasing since its first production from the late 19th century in the Caucasus mountains in Eastern Europe/Russia [326–328]. Despite its name and structure, kefir grains aren't simply grains but are clusters of exopolysaccharides (kefiran) encasing various heterogenous mixture of symbiotic bacteria and yeasts [326–328]. Kefiran is a water-soluble glucogalactan-based film composed of highly concentrated glucose and galactose and is known for its gel-like properties [327,329]. Microorganisms found inside the kefir consortium vary depending on origin country but the common, predominant isolates are lactic acid bacteria (i.e. *Lactobacillus* , *Streptococcus* species), yeast (i.e. *Candida*, *Saccharomyces* species) and acetic acid bacteria (*Acetobacter* species) [327,330,331]. The microbial count during production has an estimate range of 4.6×10^3 to 2.6×10^8 [327,330] - with lactic acid bacteria, yeast and acetic bacteria concentration approximately being 10^8 CFU/g, 10^7 CFU/g and 10^5 CFU/g, respectively [331]. It is inevitable that the microbial population will significantly vary depending on production method and will predictably proliferate with time.

Consumption of kefir milk products are known for its probiotic actions and health benefits including aiding in digestion as well as increasing milk tolerance [328]. Full fat cow milk has been traditionally used as the inoculation solution however milk from other animals like sheep and goat as well as non-animal sources like soy and rice are also being used. Independent from inoculation conditions (pH, temperature, fermentation duration) and source factors (species, location, season, etc.), which could vary the product's nutritional value and flavour outcome, the underlying characteristic acidic tang, similar to a carbonated beverage, remains constant – owing to the microbial production of lactic and acetic acid during fermentation [326,327,331,332]. However, the extent of the acidic taste affects the product palatability [333], therefore, pH monitoring within the reactor during the culturing procedure is vital. In turn this can significantly influence the final product characteristics and quality and thus there is considerable interest in the development of disposable sensors for monitoring the growth processes.

Although kefir-based microbial reactors do not predominantly involve CRBSI-causing microorganisms, its purpose in this case is to act as proof of concept and to test the ability of the flavin-phenol electrode to provide an unambiguous signal in a demanding milieu where biofouling can occur, similar to a catheter environment. Regardless of the manufacture process, the resultant medium is a thick, cream-like viscous concoction composed of proteins, sugar, lipids, minerals and naturally, an ever-expanding kefir grain biomass [326–328,332,333]. In relation to this project, this proffers an environment that is a substantially challenging setting for electrochemical sensors in that, as an interfacial technique, must obviously be in direct contact with the microbial nidus. Due to acid formation during fermentation, the inoculant milk's pH value will expectedly decrease – typically from pH 6.5 to pH 3.5. Additionally, the viscosity will inevitably inspissate which could possibly lead to surface fouling. It was envisaged that the matrix influence will be minimal as the flavin polymer will be directly anchored onto the electrode with a voltammetric approach allowing greater resolution of the peak processes. This electrochemical technique was envisaged to be preferable to conventional potentiometric methods in this case as the former offers greater selectivity to indirectly measure pH and have a fast response time while the latter is simpler and more readily corruptible [203,208,334,335]. Although the prevailing influence of proton concentration in the redox peak shifts of riboflavin has been extensively studied, this is the first investigation where an immobilised flavin moiety was employed as the primary component in determining pH.

5.2 Experimental Details

5.2.1 Materials

Chemicals were purchased from Sigma Aldrich (UK), were of the highest grade available and used without further purification. Unless otherwise stated, measurements were completed with Britton-Robinson buffer, modified with the addition of concentrated sodium hydroxide until the required pH value is achieved. Toray carbon paper (TGPH-30, no wet proofing) was obtained from University of Surrey. Live kefir grains (10 g) were acquired from commercial sources and were inoculated with 500 mL cow's milk at 22°C ± 2°C.

Riboflavin was obtained from commercial sources whereas the phenol derivative was custom synthesised and was a gift from Dr Robert Smith, University of Central Lancashire. The synthesis of the flavin derivative, 10-(4-hydroxyphenyl)benzo[g]pteridine-2,4(3H,10H)-dione, was accomplished via modifications to previous methods [336–338]. The reaction summary is highlighted in **Figure 5.2.1.** In summary, p-anisidine (**1**) was reacted with 2-fluoro-1-nitrobenezne (**2**) in the presence of potassium carbonate to yield 4-methoxy-2-nitrodiphenylamine (**3**) which was isolated at the pump in 78% yield. The crude material (**3**) was reduced using zinc dust under acidic conditions, and subsequently treated with alloxan monohydrate (**4**) in the presence of boric acid to yield the 10-(4-methoxyphenyl)benzo[g]pteridine-2,4(3H,10H)-dione intermediate in 93% yield which was demethylated using hydrobromic acid you yield the final derivative (**5**) in 98% yield.

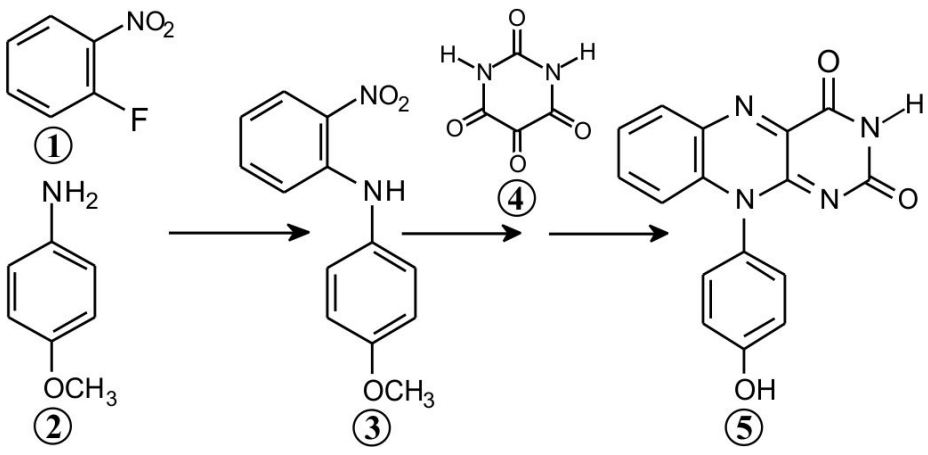

Figure 5.2.1 Summarised scheme highlighting the preparation of the custom synthesised phenolic flavin derivative.

5.2.2 Electrochemical Configuration

All electrochemical measurements were conducted at room temperature (22 °C ± 2 °C) using a μAutolab Type III potentiostat (Eco-Chemie, Utrecht, Netherlands) with a standard three-electrode system with either a glassy carbon or carbon fibre mesh as the working electrode. The circuit was completed with a conventional silver/silver chloride half cell reference electrode (3M KCl, BASi Technicol, UK) and a platinum wire serving as the counter electrode.

5.2.3 Electrode Design and Modification

Carbon fibre mesh was cut into suitable segments and were thermally sealed within a commercial polyester laminate [(290)], patterned with 4 x 4 mm window to establish a standardised area to enable comparisons before and after modification. The electrode was then electrochemically anodised (+2 V, 0.1 M NaOH, 300 s) which increases the exfoliation of the carbon fibre thus generating more edge plane sites and various oxygen functional groups, enhancing its electrochemical behaviour as discussed in **Chapter 4**.

The electropolymerisation of the flavin phenol derivative (150 μM, pH 7 BR buffer/methanol) was completed through placing the electrode (glassy carbon or carbon fibre mesh) into an aqueous solution containing the flavin moiety and running repetitive cyclic voltammetry scans (+0.2 V $\rightarrow$ -0.8 V $\rightarrow$ +0.1 V, 50 mV/s). The solution was degassed with nitrogen prior to electrochemical experiments and were then carried out under nitrogen blanket. The flavin-modified electrode was inserted in the kefir fermentation mixture and the pH of the microbial nidus was monitored in situ for up to 51 hours.

5.2.4 NMR Analysis

NMR spectra were recorded on a Bruker Fourier 300 (300 MHz) spectrometer. Chemical shifts are recorded in ppm relative to solvent residual (^{1}H NMR d_6-DMSO, 2.500 ppm and $CDCl_3$ ppm, 7.26; ^{13}C NMR d_6-DMSO, 39.520 ppm and $CDCl_3$, 77.16). Coupling constants are reported in Hertz (Hz) and are rounded to the nearest 0.5 Hz. Multiplicities are stated as singlets (s), doublets (d) and triplets (t) or a combination of these, peaks appeared broad are due to either H-bonding or restricted rotation are prefixed as broad (br). Low resolution mass spectra were recorded on a Finnigan™ LCQ™ Advantage MAX in ESI mode. Infra-red spectra

(1800-800 cm^{-1}) were recorded through a Perkin Elmer Spectrum RX 1 with a Specac Golden Gate™ ATR accessory and values are quoted in wavenumbers.

5.3 Results and Discussion

5.3.1 Characterisation of the Flavin-Phenol Moiety

A comparison between the electrochemical properties and voltammetric responses of riboflavin and the engineered flavin-phenol moiety was completed and observed using a conventional glassy carbon electrode in pH 7 BR buffer, shown in **Figure 5.3.1A**. Evidently, the flavin centre's redox process in both cases exhibit near reversible kinetics and displays well defined, distinct peaks. It can be seen that the reduction peak of the flavin-phenol compound occurs at a marginally less negative potential in comparison to riboflavin. This can be attributed to the latter containing methyl and sugar substituents which have a greater combined effect on the reduction potential required than that of the phenolic substituent altering its electron-releasing nature. Nevertheless, the primary difference between the voltammetric profiles is focused on the irreversible peak process observed at +0.81 V on the flavin-phenol moiety, which is noteworthily non-existent on the riboflavin scans. This irreversibility as well as the evident decrease of the peak height with increasing scan number (**Figure 5.3.1B**) is consistent with the phenol oxidation process.

The magnitude of the redox peaks observed at -0.3 V of the phenolic derivative are also visibly increasing with consecutive scans. As the potential is swept more positively, the phenol component is oxidised which, in turn, induces the formation of oligomeric and polymeric deposits on to the electrode, as forecasted in **Figure 5.1.1** (I $\rightarrow$ III). At a narrower cyclic potential range (+0.2 V $\rightarrow$ -0.8 V), the hydroxy functionality is not oxidised therefore no increase in the flavin current is observed. Thus, the increasing flavin peak magnitude is explained by the accumulation of deposited/polymerised flavin derivative on the electrode surface which only occurs via the oxidation of the phenol. Further investigation of the flavin's cyclic voltammogram traces reveals that the initial peak height increase seen on the second scan slows after a few cycles and ultimately ceases. This is explained by the lack of available electrode surface to be coated, which eventually hinders further polymerisation and film growth. It should be noted that the flavin peak processes continue to be well-defined and differs from indistinct peaks reported with the electropolymerisation of riboflavin [339].

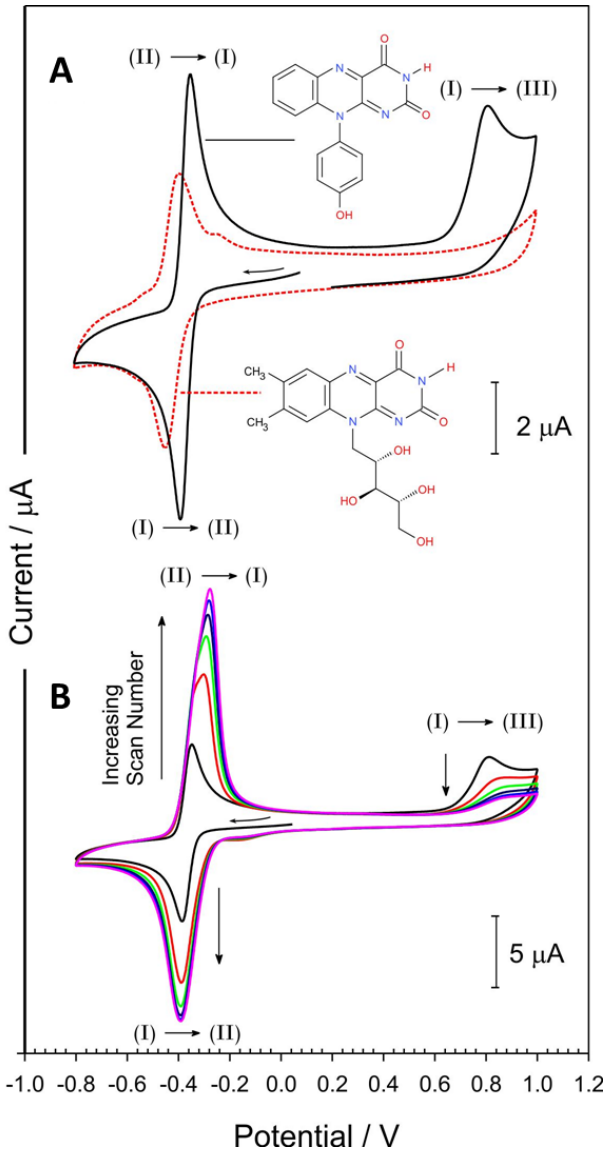

Figure 5.3.1 A) Cyclic voltammograms comparing the response of a glassy carbon electrode towards riboflavin (red line) and the flavin-phenol derivative (black line) in pH 7 BR buffer. B) Five consecutive cyclic voltammograms detailing the electropolymerisation of flavin-phenol derivative in pH 7 BR buffer. Scan rate: 50 mV/s.

To further prove the deposition of the polymer on the electrode surface, the electrode was thoroughly rinsed, placed in a fresh pH 7 BR buffer solution and cyclic voltammetry was again employed. Upon initial inspection, the characteristic flavin redox peaks remained, however, the slow transfer of counter ions into the flavin polymer significantly increases the film's redox peak separation with increasing scan rate (**Figure 5.3.2**).

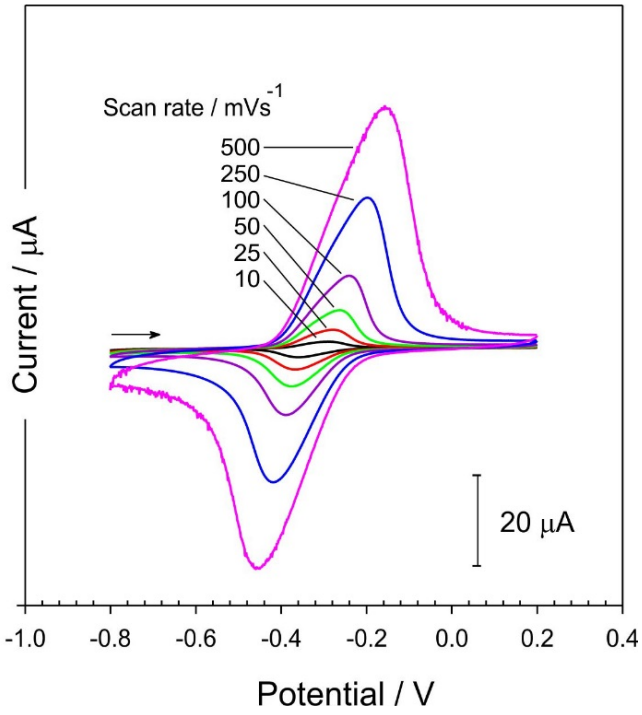

Figure 5.3.2 Cyclic voltammograms detailing the flavin-modified glassy carbon electrode response with increasing scan rate in fresh pH 7 BR buffer.

The relationship between the peak height response of the immobilised film to increasing scan rate is displayed in **Figure 5.3.3**. The positive linear relationship between scan rate (10 mVs^{-1} to 5 Vs^{-1}) and peak height also corroborates the initial suggestion that the flavin was immobilised on the electrode surface, as described by the Randles-Ševčik equation (**Chapter 3.5.1, Eq. 3.5**). The slope of the cathodic peak currents against scan rates allowed the calculation of the flavin polymer surface concentration on the glassy carbon electrode (surface area = 0.071 cm^2) which was revealed to be 1.32 x 10^{-10} cm^{-2}.

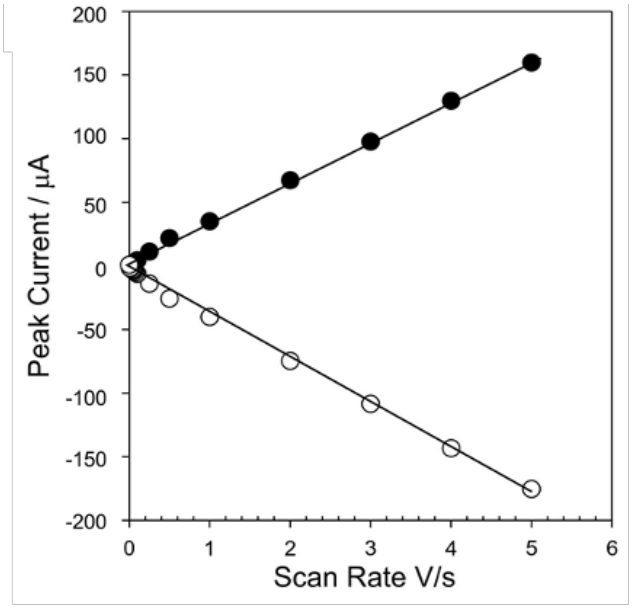

Figure 5.3.3 Variation of polyflavin peak heights with scan rate recorded on a glassy carbon electrode in pH 7 BR buffer.

5.3.2 Evaluation of Flavin-Modified Carbon Fibre Mesh as a pH Sensor

Upon the observed stability of the redox processes and their retainment after insertion in fresh BR buffer, the flavin was then electropolymerised on to the surface of a more flexible and scalable carbon fibre mesh electrode. It should be noted that the same electropolymerisation technique described in **Section 5.2.3** was employed in this case and with the glassy carbon electrode. The same voltammetric profiles were also observed as in **Figure 5.3.1B**. As per previous method, after confining the flavin polymer on the electrode surface, the electrode was rinsed and then placed in consecutive pH BR buffers to determine the influence of pH on the peak responses.

To minimise the effect of oxygen as well as to more accurately determine peak potentials, square wave voltammetry was employed. The scans were initiated at -0.8 V which is sufficiently negative to induce the reduction of the flavin centre and, as the potential is swept more positively, the core flavin is re-oxidised. **Figure 5.3.4** displays the shifts in oxidation peak due to varying pH and its corresponding calibration/linear regression graph. Evidently, distinct sharp peaks are observed with each pH and the oxidation peak moves towards more negative/less positive potentials as the pH becomes more alkaline. This relationship was found to be near Nernstian with a gradient of 55 mV/pH (E / V = 0.055 pH + 0.077; N_{total} = 21

(N_{pH} = 7, $N_{scans/pH}$= 3,); R^2 = 0.999), similar to that of a previous report by Roushani et al. (2014) on the use of riboflavin-graphene quantum dots [317].

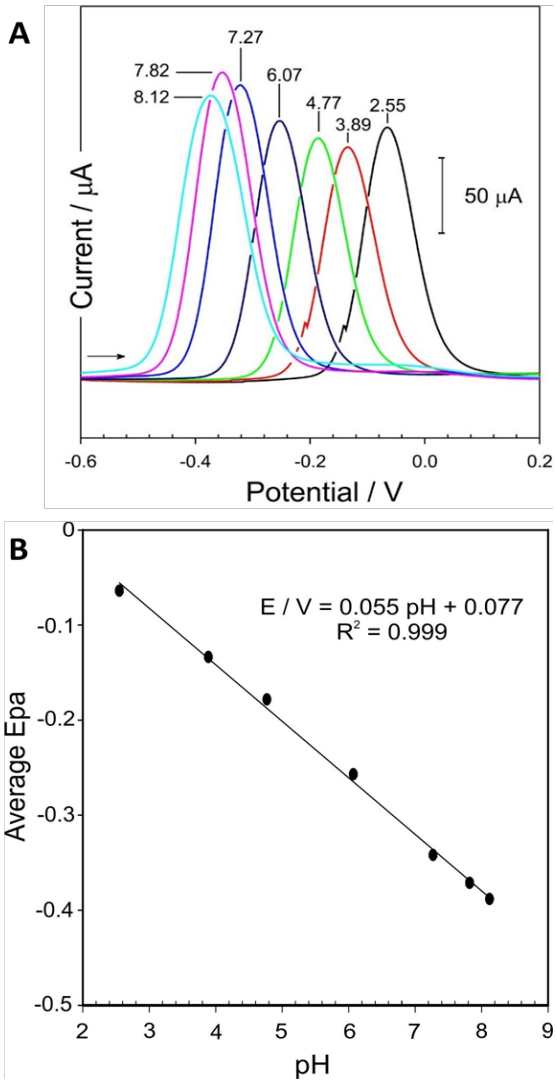

Figure 5.3.4 A) Square wave voltammograms and B) corresponding linear regression calibration graph exhibiting the shift in oxidation peaks of the flavin-modified anodised carbon fibre mesh in BR buffers of various pH. Each point is an average of three scans and mean standard deviation error bars are added but too small to be observed.

The ability to periodically scan and monitor the pH of the local environment is a prerequisite in not only kefir-microbial reactors where a batch takes at least 24 hours to process, but also in catheter systems which are used in a daily basis. The robustness of the flavin-modified electrode was therefore evaluated through successive cycling of the electrode in a series of three successive sequences with each ranging from pH 2.55 to pH 8.12 (**Figure 5.3.5**). In each pH BR buffer, square wave voltammograms were recorded in triplicate and the process was repeated a further two times as detailed in **Table 5.3.1**. This was completed to examine the reversibility of the phenolic-flavin's redox processes with pH changes going from low to high

and back. The process of repetitive cycling could, in turn, lead to potential drifts caused by a possible compromise on the integrity the flavin centre. This is typically common in quinoid systems where the oxidised centre can be susceptible to hydroxyl ion attacks in moderately alkaline conditions. In this case however, the pH sensing capability of the polymerised flavin is unambiguously reversible with a potential drift of only 4 mV (0.07 pH unit based on a 55 mV per pH shift) after 63 scans. Conversely, the peak height was observed to decrease in magnitude by around 20% over the repetitive scans.

Table 5.3.1 Detailed raw data obtained from repetitive scanning of flavin-modified anodised carbon fibre mesh electrode in BR buffers of varying pH; N_{scans} = 63.

	Scan number | Peak Potential / V									Average	Standard Deviation	Standard Error
	Series 1			**Series 2**			**Series 3**					
pH	**1**	**2**	**3**	**4**	**5**	**6**	**7**	**8**	**9**			
2.55	-0.076	-0.064	-0.062	-0.135	-0.072	-0.066	-0.088	-0.068	-0.066	**-0.077**	**0.023**	**0.0077**
3.89	-0.130	-0.135	-0.137	-0.134	-0.135	-0.137	-0.126	-0.132	-0.135	**-0.133**	**0.0036**	**0.0012**
4.77	-0.175	-0.179	-0.179	-0.175	-0.183	-0.183	-0.185	-0.185	-0.185	**-0.181**	**0.0041**	**0.0014**
6.07	-0.237	-0.249	-0.253	-0.253	-0.257	-0.258	-0.243	-0.249	-0.253	**-0.250**	**0.0067**	**0.0022**
7.27	-0.316	-0.320	-0.320	-0.316	-0.322	-0.322	-0.316	-0.320	-0.322	**-0.319**	**0.0026**	**0.0009**
7.82	-0.334	-0.344	-0.350	-0.342	-0.352	-0.352	-0.346	-0.352	-0.352	**-0.347**	**0.0063**	**0.0021**
8.12	-0.376	-0.376	-0.376	-0.368	-0.374	-0.374	-0.370	-0.374	-0.374	**-0.374**	**0.0028**	**0.0009**

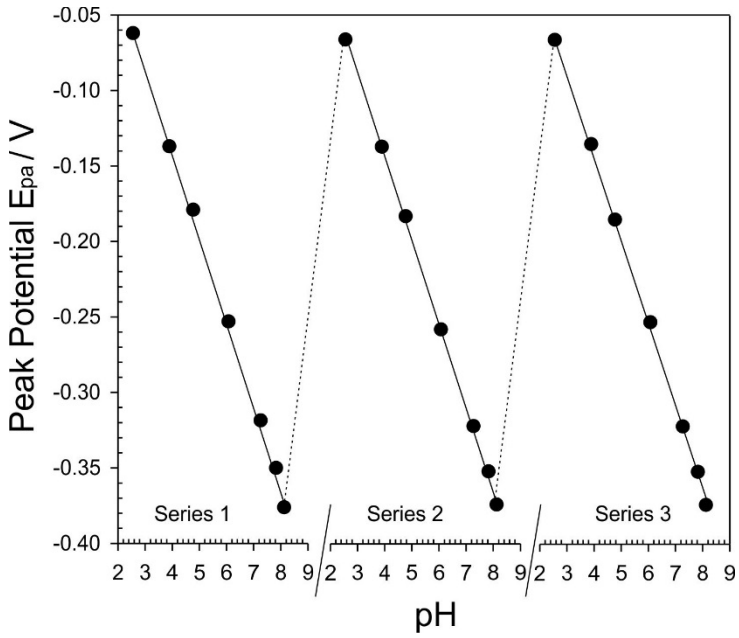

Figure 5.3.5 Influence of pH on the oxidation peak potential of flavin-modified anodised carbon fibre mesh over three cycles in BR buffers of varying pH. Each pH is analysed in triplicate, totalling 63 scans, with each point on the graph representing the third scan of each cycle.

5.3.3 Challenging the Electrode's pH Sensitivity in a Microbial Reactor

The pH sensing capabilities of the flavin film was further challenged by inserting the electrode in a kefir matrix. Kefir grains were inoculated with milk and was left to ferment over 51 hours. **Figure 5.3.6** displays the comparison between square wave voltammograms of anodised carbon fibre electrodes with and without the polymeric flavin film, attained at the start of inoculation and at the end of the fermentation process. The small but distinct peaks (initially at -0.413 V and shifted to -0.231 V) exhibited by the electrode without the polymer are attributed to the presence of natural riboflavin in milk. In comparison, the flavin-modified electrode displays a relatively larger, distinguished peak which has similarly shifted from -0.281 V to -0.114 V as the reactor's pH shifts from the initial pH of pH 6.18 to pH 3.68 at the end of production.

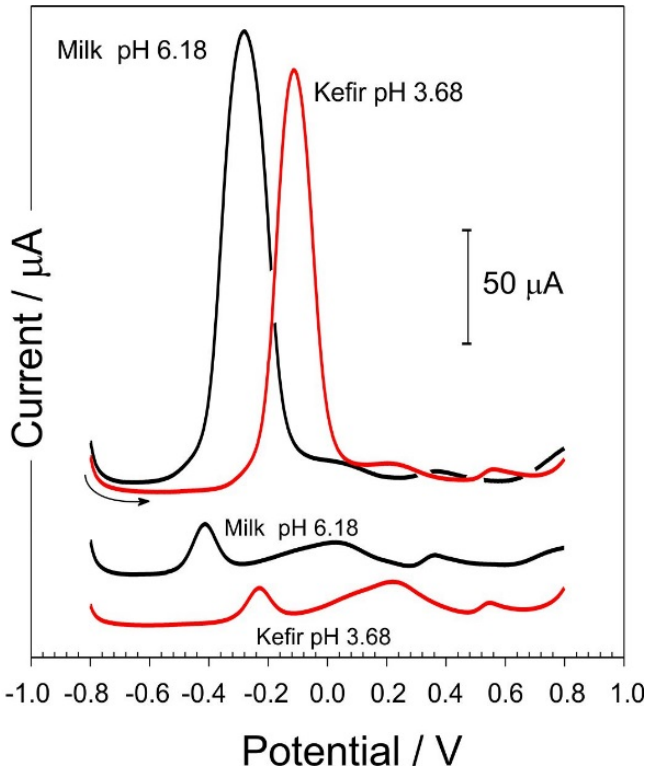

Figure 5.3.6 Square wave voltammograms comparing the response of a bare anodised carbon fibre electrode and polyflavin-modified anodised carbon fibre electrode in kefir-inoculated milk at the start and end of the fermentation cycle.

The calculated pH from the calibration curve was then compared to that recorded using a standard pH glass probe (**Figure 5.3.7**). The consequential pH measurements from the flavin-carbon electrode wherein the delay between each repetitive scan is short, are in close

agreement with the conventional pH sensor. It is evident however, that at both 21 and 47 hours after inoculation, anomalies which significantly differ from that of the control pH probe are detected. It should be noted that these deviations occur only after the electrode has been dormant in the microbial reactor for a period of over 12 hours.

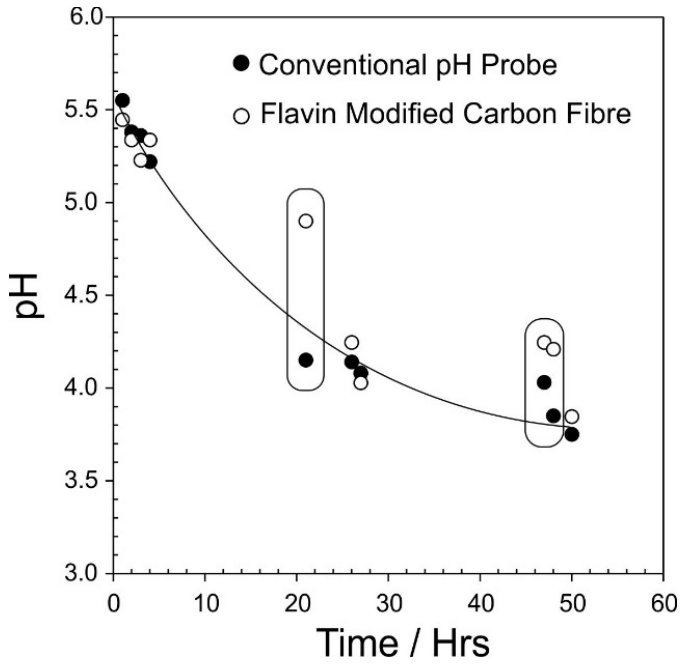

Figure 5.3.7 Comparison of pH measured between the conventional glass pH probe and the flavin-modified anodised carbon fibre mesh electrode within the kefir mixture over a period of 51 hours. Each point is the average of 3 scans.

During periods of no use, it is probable that the electrode is colonised by microbes present in the matrix which leads to the nonconformity and the pH measured is actually that of the local environment created by the biofilm at the electrode surface, not the bulk matrix pH. The former was confirmed via scanning electron microscopy photographs of the carbon fibre mesh after 51 hours of fermentation (**Figure 5.3.8**). It was envisaged that a significant increase in kefir biomass would be produced with time which would then foul the electrode. It could be envisaged that permselective barriers may be effective in inhibiting microbial attachment to the surface of the electrode which will sequentially minimise fouling. However, biofilm formation on the barrier may still lead to inconsistency in pH measurements between the bulk and internal void.

Upon recommencing measurements after the two aforementioned time points, the flavin response soon returns to matching the pH data of the standard probe. In this case, the frequent scanning minimises the discrepancy and negates the need for a barrier. This could

be ascribed to the redox transitions occurring at the surface which induces physical swelling through the flux of counter ions. Nonetheless, biofilm formation is obvious after a fermentation phase of 51 hours (**Figure 5.3.8**). This is arguably beyond the typical period used for kefir-based products but could be problematic when other microbial systems, including microbial fuel cells [340], are taken into consideration.

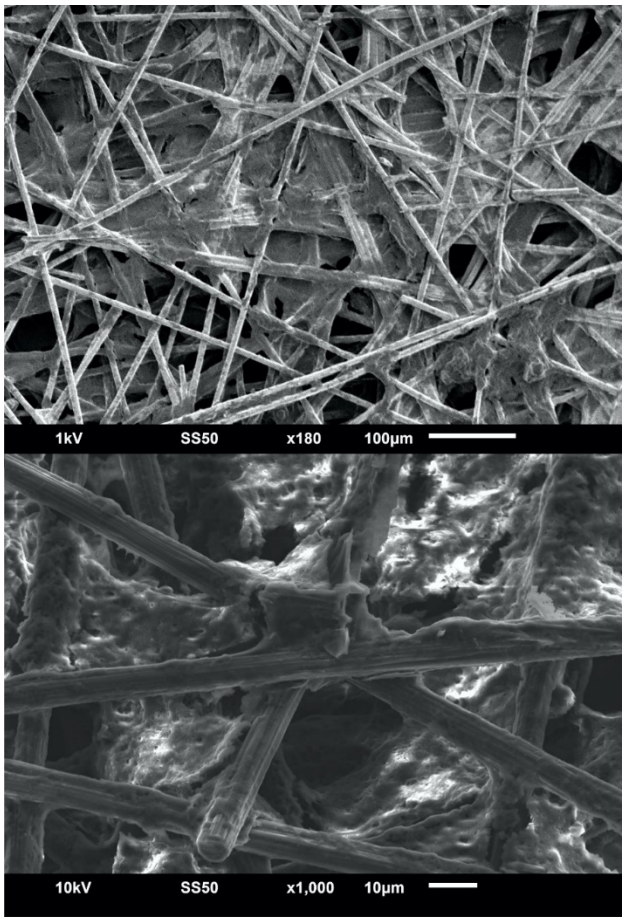

Figure 5.3.8 Scanning electron micrographs of the carbon fibre network after incubation in kefir mixture (SU5000 FE-SEM, Hitachi, Japan).

In principle, an anodised carbon fibre without further modification may be used as a way to directly measure riboflavin endogenous to the milk-kefir concoction and exploit the dependence of its oxidation process on H^+ ion concentration as the basis of a pH sensor. As seen in **Figure 5.3.6**, riboflavin oxidation peaks shift with pH. However, this approach assumes that riboflavin will always be present in milk feedstock and will be at an easily detected concentration. But in cases where there may be less riboflavin, i.e. other milk sources like coconut or soy, or more importantly where it is non-existent such as within the catheter lumen during IV fluid transfer, this method will be invalidated [332,341]. **Figure 5.3.6**

also reveals that although riboflavin has a separate, well-defined peak, its magnitude is similar to other kefir mixture constituents (broad peak at +0.25 V) which may further decrease the former's peak intensity. Changes to the composition of the milk source, like the introduction of additives or flavouring, could also conceal the peak produced by the present riboflavin. In contrast, the film modifier is polymerised on to the electrode surface and the intensity of the engineered flavin's oxidation peak is much greater than the constituents present in the kefir mixture. These characteristics should therefore overcome the aforementioned issues.

As previously mentioned, there is an ever-increasing need for the development of new pH sensing methods and electrode modifiers capable of monitoring pH in challenging environments. As such, several researches have focused on developing such technology as summarised in **Table 5.3.2**. Although there is evidently a variety of modifiers, it is also clear that validation through real matrix application can be difficult. The flavin-modified carbon-based system here exhibits near Nernstian behaviour and, in comparison to techniques whose underlying principles are similar to the aforementioned, the flavin-functionalised electrode was critically assessed within a microbial reactor which is a real, complex and changing medium.

Table 5.3.2 Comparison of electrode modifiers/pH detection methodologies.

Modifier	Type[a]	Sensitivity mV/pH	pH Range	Test Medium	Ref.
$CeTi_xO_y$	P	89.8	2-12	N/A	(342)
RuO_2/Nafion	P	55.2	2-6	Beverages	(343)
IrO_x/Pt	P	64	1-13	Corrosion	(344)
ERGO Polyaniline/Nafion	P	55	2-9	Fermentation	(345)
CuO nanorods	C	0.64 µF/pH	5-8.5	N/A	(346)
Graphite/polyurethane	P	11.13	5-9	Sweat	(347)
WO_4/WO_3	P	56	2-10	N/A	(348)
Graphene - Polyaniline	A	139 µA/pH	1-5, 7-11	N/A	(349)
NiO	P	63	1-13	N/A	(350)
ZnO/W	P	46	2-9	CSF	(351)
$Ni_3(PO_4)_2{\cdot}8H_2O$	P	34.8	4-7	Sweat	(352)
Carbon-quinone	V	73	2-8	Saliva	(211)
Pt-IrO_x	P	56	4-9	Biofilm	(353)
Si EGFET	P	56	2-12	N/A	(354)
ZnO	P	43	2-9	Tumour Cells	(303)
Polyaniline	V	50	4-10	Wound fluid	(355)
Poly Dopamine	V	58	1-12	N/A	(356)
Poly Flavin	V	55	2-8	Fermentation Reactor	This Work

[a] where C = capacitance; P = potentiometric; V = voltammetric; A = amperometric;
EGFET = extended gate field effect transistor; ERGO = electrochemically reduced graphene oxide.

5.4 Conclusions

This chapter detailed the use of a scalable, inexpensive, anodised carbon mesh that was further functionalised by an engineered flavin-phenol redox polymer as a solid-state pH sensor. The oxidation peak of the flavin derivative was found to occur within a potential range devoid of any typical interferences that may affect other pH sensors. Additionally, the probe was tested in a chemically complex medium of a microbial reactor where it was evident that the system provides a clear, unambiguous signal which shifts with pH. The analytical peaks exhibit reversible characteristics over a physiologically relevant pH range without requiring the solution to be degassed - an essential quality for in situ applications such as in catheter systems.

In spite of proving the reagentless system's capability of measuring pH in the presence of bacteria and fungi, there is a need to examine its functionalities in a more biologically relevant medium characteristic of that commonly utilised in IV therapy applications.

Chapter 6

Flavin-Modified Carbon Loaded Polyethylene Film as a pH Sensitive Membrane

Abstract

The customised flavin-phenol moiety was electropolymerised onto a mechanically flexible carbon-loaded polyethylene film to produce an adaptable electroanalytical sensor capable of measuring pH. This material was initially assessed as an alternative to the more brittle structure of the carbon fibre. The reagentless flavin system again exhibits its Nernstian-like behaviour of 60 mV per pH shift over a physiologically relevant pH range of pH 2.55 to pH 8.12. Its robustness was also assessed whilst under cyclic and/or constant perpendicular mechanical flexing and has proven to have less than 0.001 pH unit degree of error. Similarly, the stability, pH sensing capabilities and applicability of the proposed system was analytically evaluated by submerging the electrode in chemically complex human urine samples and successfully employing voltammetry to determine their corresponding pH.

Aspects of the work detailed in this chapter is published in:
McLister A, Casimero C, McConville A, Taylor C, Lawrence C, Smith R et al. Design of a smart sensor mesh for the measurement of pH in ostomy applications. Journal of Materials Science. 2019;54(14):10410-10419.

This work and corresponding publication was selected as the July finalist in the 2019 Springer Nature Cahn Prize.

6.1 Introduction

Following on from the last chapter, this section details the use of the same engineered novel phenolic-flavin derivative. Instead of polymerising the flavin on to carbon fibre however, an anodised and laser ablated carbon-loaded polyethylene (C-PE) film is used as the substrate of a pH sensitive probe. The use of carbon fibre mesh as an electrode substrate has potential drawbacks including its brittleness, cost and transferability limitations to large scale productions [357]. It was envisaged that a potential solution to these challenges could be the employment of a polyethylene based composite film that is inherently mechanically flexible and which is more amenable to mass manufacturing through conventional polymer processing techniques. Given the simplicity of the substrate, it has an additional advantage of being relatively low cost which is a prerequisite in healthcare devices given that there is an ever present focus on spending reduction.

In this case, the sensor is based on a polyethylene film infused with carbon particles to enhance the electrical conductivity of the film. It was anticipated that the electroanalytical properties of the carbon-polymer composite could be augmented through removing the outmost superficial polymeric layers, which in turn exposes more interfacial carbon [358]. It was anticipated that laser processing could be exploited at a level inadequate to break through the film but sufficient to generate etch tracks within the film, with pores produced where the tracks would intersect via rasterization through the X and Y planes. Subsequently, this would generate a porous, mesh-like structure as displayed in **Figure 6.1.1**. While exposing the underlying carbon would produce a conductive yet mechanically adaptable film as a basis of the sensor, it was envisioned that the carbon would not have any analytical selective/pH sensitive characteristic that is a prerequisite to the proposed application. Thus, the electrode would still require to be modified using the redox active flavin polymer (**Figure 6.1.2**) as described in **Chapter 5** (**Figure 5.1.1**).

The flavin polymer-coated polyethylene probe was tested in a range of matrices but, at the time of the study, it was not possible to acquire authentic IV fluids. Therefore, to test the analytical efficacy of the system with a complex biological fluid, human urine extracted from healthy volunteers was used. The latter was significant as it could be expected that the latter would contain a large range of molecules (i.e. ascorbate, urate) at relevant physiological

concentrations that could interfere with the flavin response thus hindering the sensor's ability to successfully sense pH.

The development of electrochemical biosensors for the analysis of urine are well established [359–361] and can allow the diagnosis of various clinical conditions that include: diabetes [362,363], cancer [364,365] and urinary tract infection [366,367] as well assessing urine pH [368,369]. Urine samples are compositionally complex and are naturally heterogenous thus providing a challenging matrix suitable for assessing the pH-sensing capabilities and reproducibility of the proposed system. The aim of this chapter therefore is to provide a detailed analysis of a mechanically flexible carbon-loaded polyethylene film modified with polyflavin and its ability to act as a pH sensor within a chemically complex media, which could ultimately be integrated within a smart sensing catheter system.

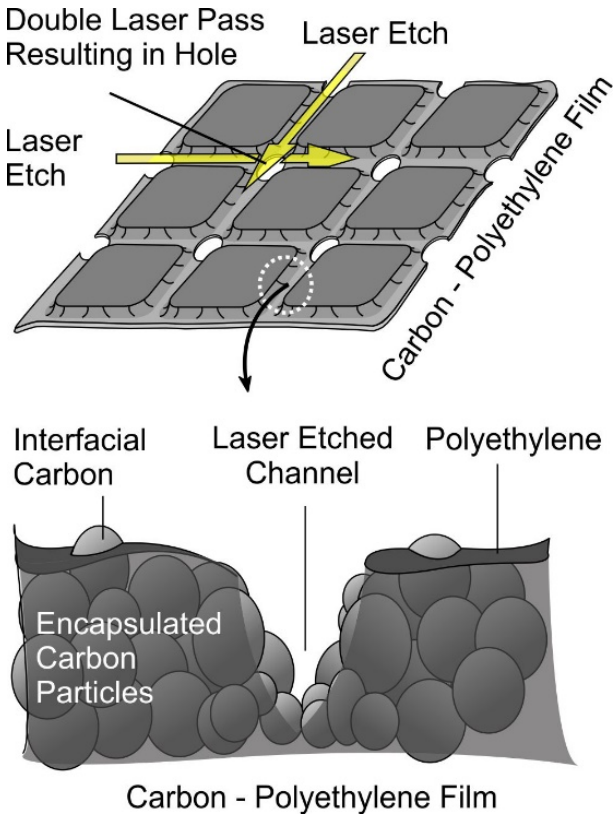

Figure 6.1.1 Process of producing an electrically conductive carbon-loaded polyethylene film via laser etching.

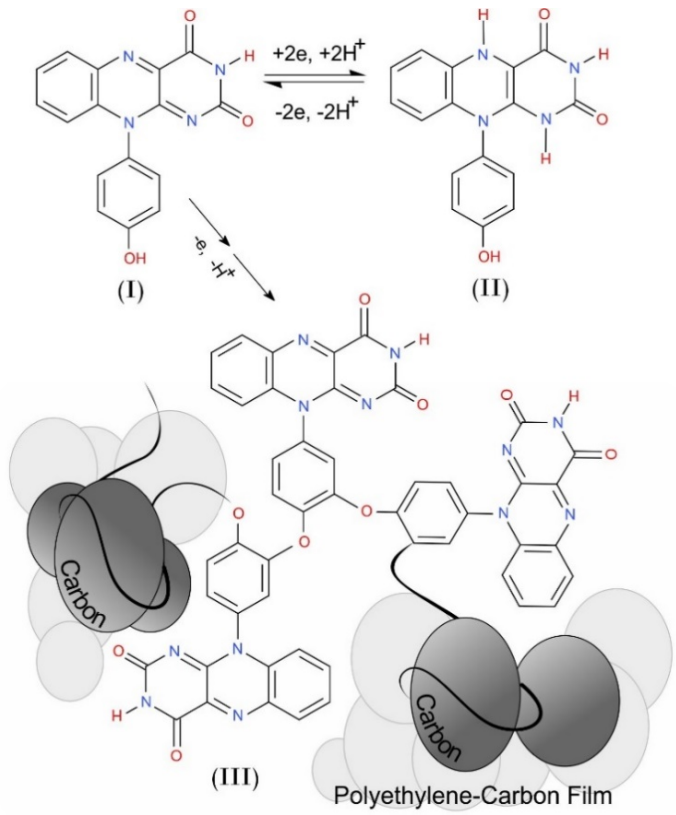

Figure 6.1.2 Redox transition of the flavin unit (I→II→I) and the electro-oxidation of the phenolic substituent leading to the production of a polyphenylene oxide polymer (I→III) on exposed carbon surfaces at the carbon-polyethylene film interface.

6.2 Experimental Details

6.2.1 Materials

All chemicals were purchased from Sigma Aldrich (UK), were the highest grade available and were therefore used without further refinement. Unless otherwise stated, Britton-Robinson buffers were amended to the appropriate pH by adding drops of concentrated NaOH and were used in electrochemical assessments. Butyl-grafted polyethylene films filled with carbon-black (80 μm thick, 100 Ωcm resistivity) were obtained from Goodfellow Research Materials (UK).

6.2.2 Electrochemical Configuration

Electrochemical measurements were executed using a VSP-300 Multichannel Potentiostat / Galvanostat / EIS (BioLogic Science Instruments, EC-Lab Ltd., France). A standard three-

electrode setup was employed, using either a glassy carbon or C-PE film, a conventional Ag/AgCl reference electrode (3M NaCl, BASi Technicol, UK) and platinum wire acting as the working, reference and counter electrode, respectively. All analytical assessments were carried out at 22 °C ± 2 °C.

6.2.3 Preparation and Characterisation of Modified Film

The carbon-polyethylene composite was laser patterned using a 30 W CO_2, air-cooled, computer-controlled FB400 series laser cutter (CadCam Technology Ltd., UK). The ApS-Ethos propriety software was used to control the laser's direction, raster/vector speed and output power, with a spatial resolution of 25 micron. The laser scanned along X and Y directions with a 2 mm distance between each pass. Dektak XT Stylus Profilometer (Bruker Corporation) was used to characterise the surface morphology and etch depth of the composite, with a single pass detailing 60 µm depth, as illustrated in **Figure 6.2.1**.

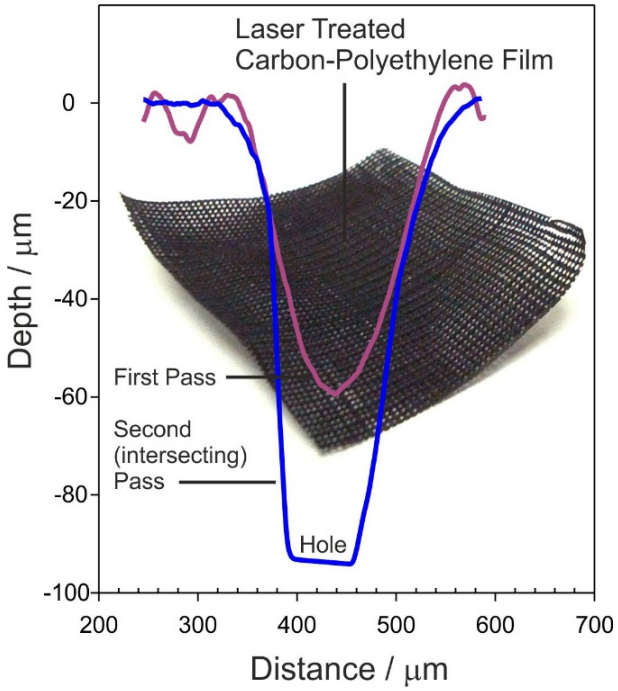

Figure 6.2.1 Dektak surface profile of the laser-modified carbon-polyethylene film displaying the typical depth profile of areas receiving a single and double pass. Insert: photograph of the C-PE film after laser treatment.

Macroscopic examination of the composite is able to clearly differentiate the permeable, mesh like structure of the film after laser procedures from the original non-porous and featureless film. The voids occur where the laser tracks perpendicularly intersect and are easily explained since the overlap means the relevant sections of the track undergo two laser

passes. Noteworthily, the polymeric film is only 80 µm thick and since one pass carves 60 µm, the second pass would effectively etch another 60 µm and cuts through the material.

Additionally, a scanning electron microscope (JSM-6010, Jeol Ltd., Japan) was employed to further characterise the surface of the mesh film as exhibited in **Figure 6.2.2**. The resulting images complement the visual investigation and further highlights the highly porous configuration produced through exposing residual carbon (**Figure 6.2.2B**) of the polyethylene polymer via laser etching, with **Figure 6.2.2C** displaying a point of intersection which further exhibits this permeable and porous structure as two laser passes occurred here. A comparison between untreated and laser-modified polyethylene in **Figure 6.2.2B** emphasizes the relatively featureless surface profile of the initial polymer, in which isolated accumulations of carbon particles are observed to penetrate through the film's surface, as hypothesised in **Figure 6.1.1**. It evidently proves that laser etching significantly increases the concentration of exposed carbon particles which would consequently, across the laser-treated tracks, enhance the electrochemical properties of the polymeric film.

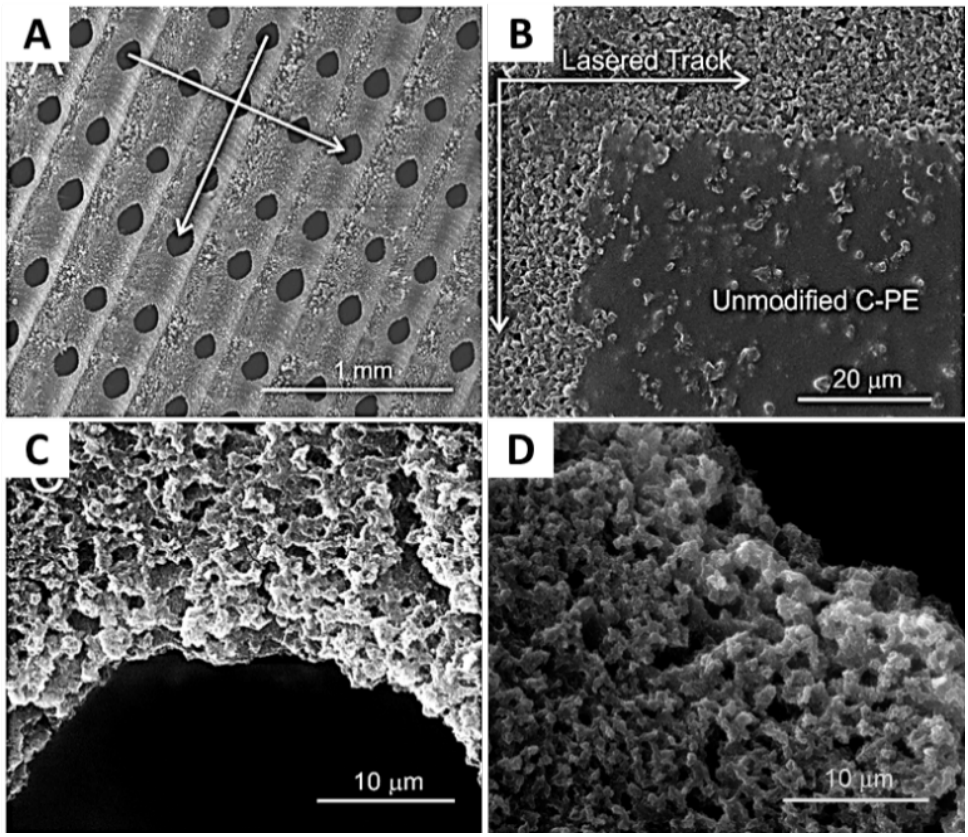

Figure 6.2.2 Scanning electron micrographs of the carbon-polyethylene mesh after laser processing. A) Low magnification highlighting the direction of the laser raster and creation of holes within the film. B) Comparison of the laser etched track and unmodified C-PE film. C & D) Removal of the polyethylene at the pore edge as a consequence of laser double pass.

6.2.4 Electrode Design and Modification

The laser modified C-PE film was sectioned and thermally enclosed in a polyester laminate with a fixed 4 mm x 4 mm window to enable comparative examination in a similar manner to that used with the carbon fibre in **Chapter 4** and **Chapter 5**. As per **Chapter 4**, the benefits of electrode anodisation in enhancing the electrochemical properties were also exploited in this case using chronoamperometric techniques (+2 V, 0.1 M NaOH). The synthesis of the phenol-flavin derivative was as described in **Chapter 5** (**Figure 5.2.1**). The moiety was polymerised onto the electrode surface via repetitive cyclic voltammetry scanning (+0.2 V $\rightarrow$ -0.8 V $\rightarrow$ +1 V, 50 mV s^{-1}) in an aqueous solution containing the derivative (150 µM, pH 7). In cases where the solution was degassed, nitrogen was used prior to commencing the experiment and was then run under a nitrogen blanket.

6.2.5 Ethics Approval and Compliance

The proposed flavin-modified laser etched carbon-polyethylene sensors were critically assessed in human urine. The bodily fluid was simply used as a relevant, multifarious matrix to test and assess the robustness of the electrode under investigation and to determine if electrode surface biofouling and/or electrochemical by-product generation occurs over time. Urine samples were obtained from three healthy volunteers (2 males and 1 female) who had not consumed any form of medication in the 24 hours preceding the collection. After sample collection and anonymisation, the fluids were stored at 4 °C until required and immediately after study conclusion, were appropriately flushed to waste. Ethical approval to use human urine samples was sanctioned through Ulster University Ethics Committee (UREC Ref: REC/16/0073) prior to the study.

6.3 Results and Discussion

6.3.1 Electrochemical Evaluation of Flavin-Modified pH Sensitive Electrode

The preceding chapter has successfully employed polyflavin onto carbon fibre mesh substrates and efficiently demonstrated its robustness as well as its ability to overcome

biofouling within a microbial reactor. In this case, it was necessary to assess and differentiate the electrochemical signature of the lasered carbon loaded polyethylene electrode in comparison to carbon fibre mesh electrodes. Despite improving the electroanalytical activity of the C-PE composite through the employment of laser etching, graphitic carbon would still be predominant and, as such, electrochemical anodisation in sodium hydroxide prior to commencing analytical experiments was carried out. Through this exfoliation process, more edge plane sites and oxygen functionalities are generated (**Chapter 4**) thus enhancing the electrode's electron transfer kinetics.

The same procedure detailed in **Chapter 5** (**Figure 5.3.1**) was conducted to electropolymerise the novel redox flavin moiety onto the surface of the C-PE mesh (**Figure 6.3.1**). Although the voltammetric profile of polyflavin on the C-PE electrode is similar to that of carbon fibre mesh, it is evident that the redox peaks are significantly less defined and have a larger peak separation on the composite mesh compared to the latter. Nonetheless, the three pertinent processes found on the flavin-modified carbon mesh are still clearly visible on the cyclic voltammogram response of C-PE moiety. In this case, polyflavin's increasing reduction and oxidation peaks (I $\rightarrow$ II an II $\rightarrow$ I, respectively, as highlighted in **Figure 6.1.2**) are observed at -0.65 V and -0.1 V, respectively, and the decreasing oxidation peak of the phenolic substituent can be seen at +0.81 V (I $\rightarrow$ III), thus following a similar trace to that with carbon fibre-based electrodes.

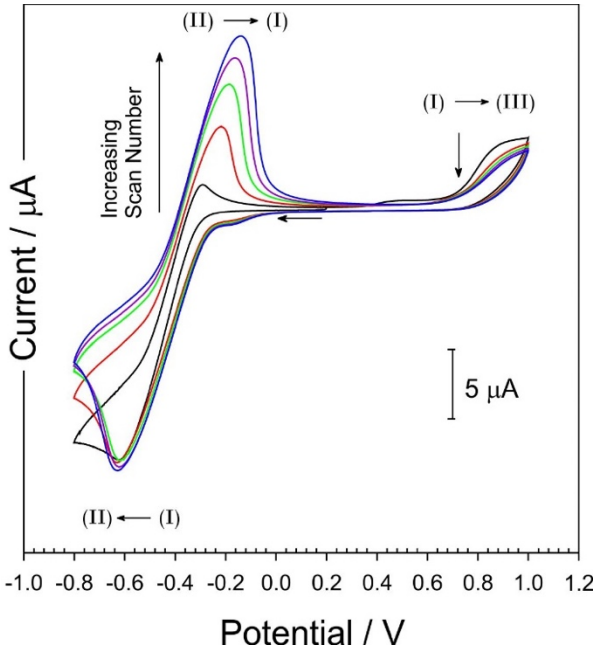

Figure 6.3.1 Cyclic voltammogram traces exhibiting the response of the anodised laser-modified carbon-polyethylene composite electrode towards the flavin-phenol derivative in pH 7 Britton Robinson buffer. Scan rate: 50 mV s^{-1}.

Similar to that in the former chapter, the electrode was removed from the phenolic flavin solution, thoroughly rinsed and then placed in fresh solutions buffered at various pH to not only determine the encapsulation of the polyflavin on the surface of the C-PE mesh but also to assess its pH sensing capabilities. **Figure 6.3.2** details the resulting square wave voltammograms comparable to carbon fibre-based electrodes with Nernstian behaviour of 59.5 mV per pH shift ($E / V = -0.0595\ pH + 0.0961$; $N_{total} = 21$ ($N_{pH} = 7$, $N_{scans/pH} = 3$); $R^2 = 0.9973$). It should be noted that each resultant point in the linear regression calibration graph (**Figure 6.3.3**) is an average of three analytical scans and that error bars are present, however, they are so minute (average standard deviation = 1.80 mV; average standard error = 0.601 mV) that they are not clearly visible within the larger y-scale of the figure. Analogous to the preceding chapter, the flavin oxidation peaks are within the negative potential range and are therefore devoid of other competing processes. The peaks are also insensitive to the presence of oxygen thus negating the need for solution degassing - a critical prerequisite for the implementation within a smart catheter hub.

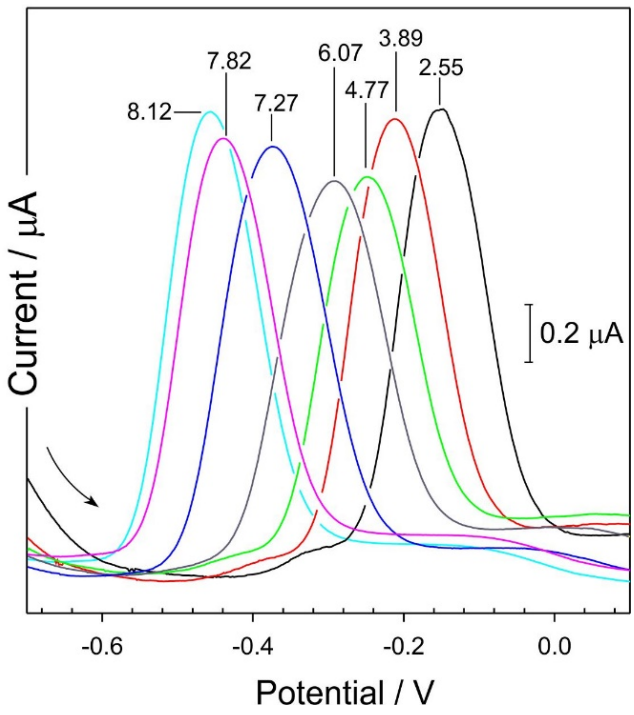

Figure 6.3.2 Square wave voltammograms displaying the pH sensitive response of a flavin-modified anodised C-PE mesh electrode in various pH Britton Robinson buffer solutions.

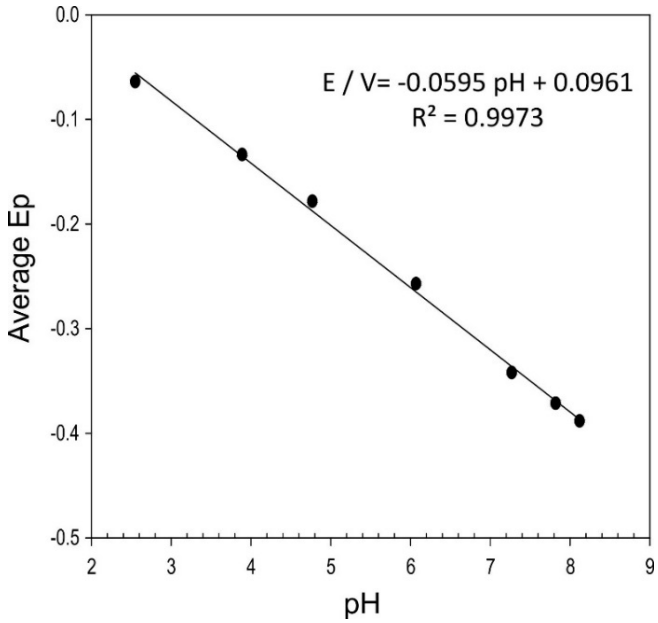

Figure 6.3.3 Corresponding calibration plot detailing the linear response between pH and peak positions over a total of 21 scans, recorded using flavin-modified anodised C-PE electrode. Each point is an average of 3 scans. Mean standard deviation error bars are included but are too small to be observed.

Subsequently, the robustness and reversibility of the sensor was examined through repetitive and sequential scanning in varying pH buffers. Simply put, the electrode was inserted into successive pH BR buffers, wherein the electrode completes three square wave voltammetric scans prior to being placed into the next BR buffer, and after completing the physiologically relevant pH series (pH 2.55 – pH 8.12), the whole sequence is repeated twice more, producing a total of 63 scans as detailed in **Table 6.3.1**. **Figure 6.3.4A** illustrates the corresponding pH vs peak position graphs while **Figure 6.3.4C** displays the linear calibration curve - both of which are acquired over the three consecutive sets, with each spot being an average of 3 and 9 scans respectively. Similar to the previous calibration graph, error bars were added for each data point but again are not visible due to their miniscule size (average standard deviation = 2.28 mV; average standard error = 0.253 mV) in relation to the graph scale. A similar Nernstian behaviour of 60 mV/pH was detected over the three sets (E / V = -0.060 pH + 0.0972; N_{total} = 63 (N_{pH} = 7, $N_{scans/pH/set}$ = 3); R^2 = 0.9977). Additionally, **Figure 6.3.4B** highlights the changes in peak height magnitude over the aforementioned scans.

Table 6.3.1 Detailed raw data obtained from repetitive scanning of polyflavin-modified anodised C-PE electrode in Britton Robinson buffers of various pH. N_{scans} = 63.

	Scan number | Peak Potential / V									Average	Standard Deviation	Standard Error
	Series 1			**Series 2**			**Series 3**					
pH	**1**	**2**	**3**	**4**	**5**	**6**	**7**	**8**	**9**			
2.55	-0.062	-0.066	-0.064	-0.062	-0.064	-0.062	-0.064	-0.064	-0.064	**-0.064**	**0.0013**	**0.0004**
3.89	-0.132	-0.134	-0.135	-0.134	-0.135	-0.137	-0.135	-0.135	-0.137	**-0.135**	**0.0015**	**0.0005**
4.77	-0.177	-0.179	-0.179	-0.181	-0.181	-0.183	-0.183	-0.183	-0.183	**-0.181**	**0.0022**	**0.0007**
6.07	-0.258	-0.258	-0.255	-0.260	-0.258	-0.258	-0.260	-0.258	-0.260	**-0.258**	**0.0016**	**0.0005**
7.27	-0.344	-0.342	-0.340	-0.340	-0.340	-0.344	-0.346	-0.346	-0.346	**-0.343**	**0.0027**	**0.0009**
7.82	-0.368	-0.372	-0.374	-0.372	-0.374	-0.376	-0.379	-0.378	-0.378	**-0.375**	**0.0036**	**0.0012**
8.12	-0.387	-0.389	-0.389	-0.395	-0.395	-0.393	-0.393	-0.395	-0.391	**-0.392**	**0.0030**	**0.0010**

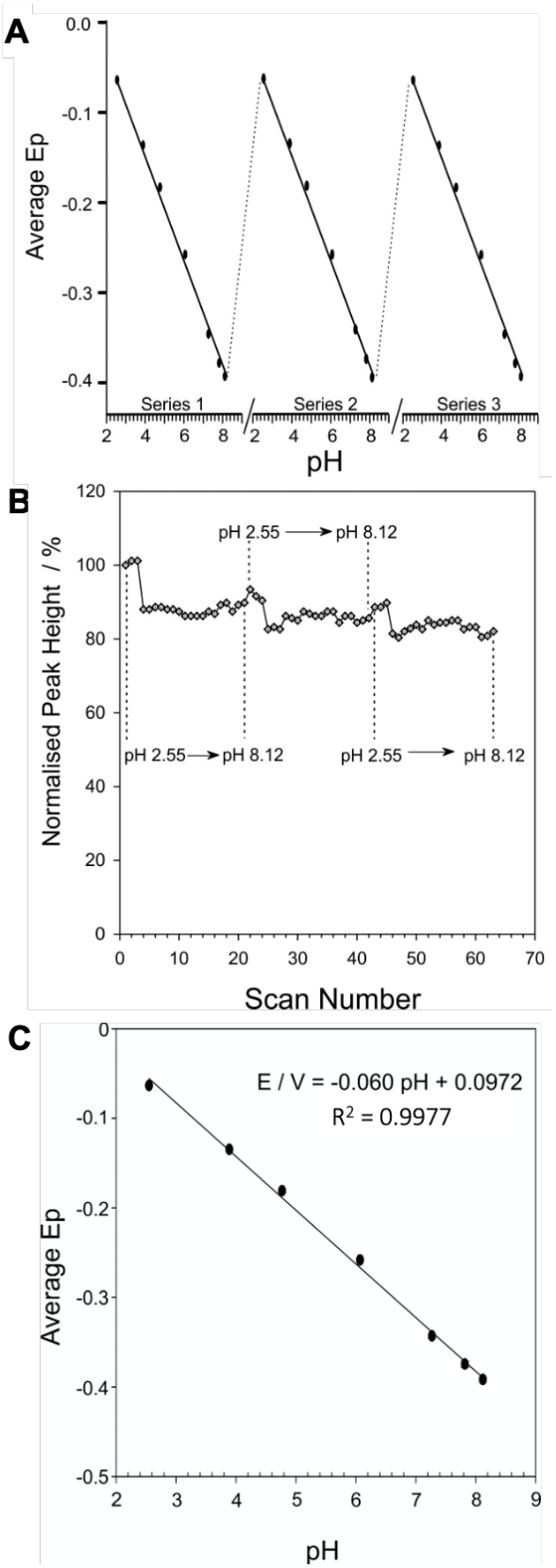

Figure 6.3.4 A) Variation of peak potential with pH over three consecutive pH series with each point being an average of 3 scans, B) effect of repetitive pH series cycling on the oxidation peak magnitude and C) corresponding linear regression calibration graph displaying the average peak positions for each pH, all recorded at the flavin-modified anodised carbon-polyethylene mesh over 63 scans. Mean standard deviation bars are included but are too small to be observed.

By normalising the peak heights (using the magnitude of the first scan as the base) and plotting this against related scan number (**Figure 6.3.4B**), it is evident that repetitive scanning affected the peak height but the retention of an unambiguous and distinct peak throughout the scans confirms the stability of the flavin polymer coating of the carbon-doped polyethylene film. After the scanning from low to high pH and repeating this action twice more, garnering a total of 63 data points, the inherent flavin oxidation peak height only diminishes by 18%. This is a specifically critical factor that is imperative for applications where periodic monitoring of physiological fluids for a relatively long period of time are ideal/desired, i.e. smart catheter devices.

6.3.2 Mechanical Flexibility Assessment

The primary advantage of using a carbon-doped polyethylene film against carbon fibre mesh is its mechanical flexibility while the latter has a more brittle characteristic. This is notably important for systems such as those used in ostomy applications where conformation to skin morphology is vital. As such, the effect of bending on the electroanalytical sensitivity of the electrode was assessed. The flavin-phenol derivative was electropolymerised onto the film surface as per previous and was then subjected to physical bending pressure prior to commencing square wave voltammetry scanning.

Electroanalytical responses of the anodised C-PE electrode functionalised with the redox flavin were conducted and recorded every fifth cycle of mechanical flexing at 90°, with a total of 50 bending cycles and 30 scans, as illustrated in **Table 6.3.2**. Subsequently, the same table summarises the film's ability to produce a signal while fixedly bent at 90°. The corresponding square wave voltammograms for the two experiments are displayed in **Figure 6.3.5**. It should be noted that an initial scan without bending was conducted prior to both experiments.

Table 6.3.2 Raw data highlighting the quantitative changes in peak positions of the polyflavin-modified anodised C-PE electrode resulting from mechanical flexing cycles and when electrode is fixed perpendicularly at 90°.

	Potential / V			Average	Standard Deviation	Standard Error
Bend Cycle	**1**	**2**	**3**			
0	-0.201	-0.199	-0.197	-0.199	0.00198	0.00115
10	-0.197	-0.195	-0.195	-0.196	0.00115	0.00066
15	-0.195	-0.195	-0.195	-0.195	0.00000	0.00000
20	-0.195	-0.193	-0.197	-0.195	0.00198	0.00115
25	-0.197	-0.195	-0.195	-0.196	0.00115	0.00066
30	-0.195	-0.195	-0.197	-0.196	0.00115	0.00066
35	-0.199	-0.199	-0.197	-0.198	0.00115	0.00066
40	-0.195	-0.199	-0.199	-0.198	0.00229	0.00132
45	-0.203	-0.195	-0.197	-0.198	0.00413	0.00238
50	-0.197	-0.199	-0.195	-0.197	0.00198	0.00115
Fixed at 90°	-0.199	-0.199	-0.199	-0.199	0.00000	0.00000

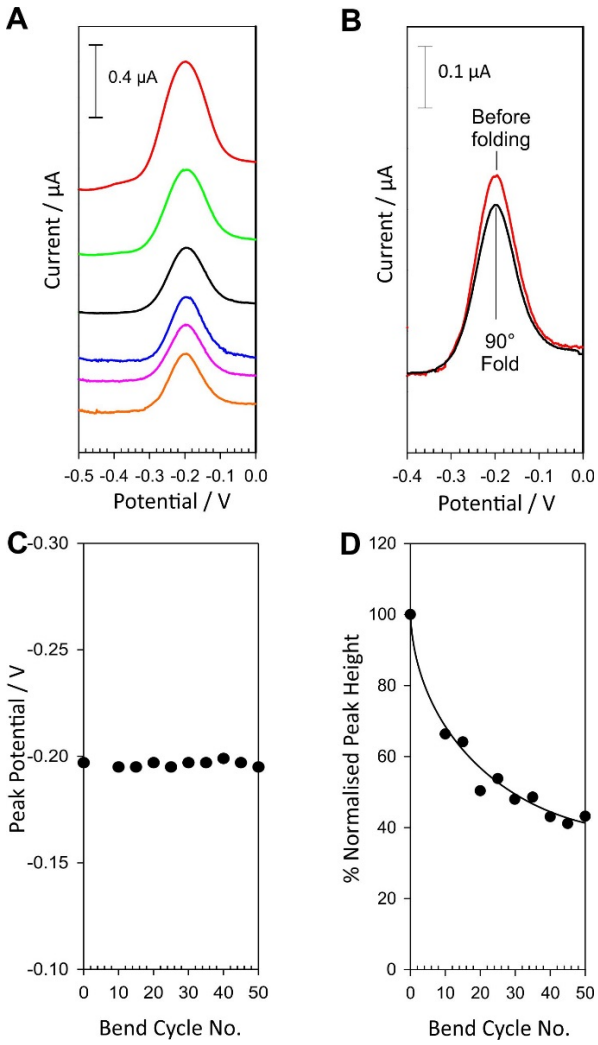

Figure 6.3.5 Square wave voltammograms detailing the effect of 90° mechanical flexing on the analytical response of the flavin-coated anodised C-PE electrode A) after repetitive cycling and B) after fixedly bent at 90°. Scatter graphs displaying the changes in the flavin oxidation C) peak potentials and D) peak heights, attributable to repeated bending of the flavin-modified anodised C-PE electrode. Each point represents the 3rd scan.

It is evident from **Figure 6.3.5** that there are differences between the initial scans and the subsequent scans. The principal change observed is the decrease in the oxidation peak height magnitude after both cases of cyclic bending and 90° fixed fold. The change in peak height is analogous to that highlighted in **Figure 6.3.4B** wherein repetitive scanning, conducted in the absence of mechanical bending, instigated the reduction of peak height magnitude - although at a slower rate. The former could be explained however by the possible loss of polyflavin from the electrode surface as the film is mechanically bent. Nevertheless, well-defined and unambiguous oxidation peaks of the flavin redox centre are still distinctly clear in the voltammograms - indicating that no significantly disastrous failure occurred throughout both studies. The second investigation where the electrode is fixed at an angle additionally proves the characteristic conductivity of the carbon-polyethylene composite upon physical distortion. Moreover, it is noteworthy that the oxidation peak position of the polyflavin remains constant with a relative standard deviation percentage of only 0.06% for both types of experiments, as detailed quantitatively in **Table 6.3.2**. The peak position determines the required electroanalytical signal and, as it has been proven to be unaffected by cyclic and set mechanical bending, is extensively important in several applications where flexibility is a primary need.

6.3.3 Electroanalytical Capabilities within a Biofluid

The functionality and accuracy of the flavin-modified anodised carbon polyethylene mesh was further assessed in human urine. The electrodes were submerged in the urine samples with each undergoing three consecutive square wave scans. The third square wave voltammograms of each urine specimen are presented in **Figure 6.3.6**. It is clear that the polymer composite electrodes retain their analytical characteristic in a more complex matrix. When the potential is swept towards less negative/more positive potentials, a second broader peak begins to develop (**Figure 6.3.6 insert**), which is instigated by the presence of other low weight components within urine – mostly likely attribute to excreted urate. The typical concentration of urate within urine ranges from 143 - 357 μM and 202 - 416 μM for a healthy female and male respectively [370]. As discussed in the preceding chapter, the key asset of the polyflavin is that its oxidation peak occurs at a lower potential range where it is devoid of any competing reactions.

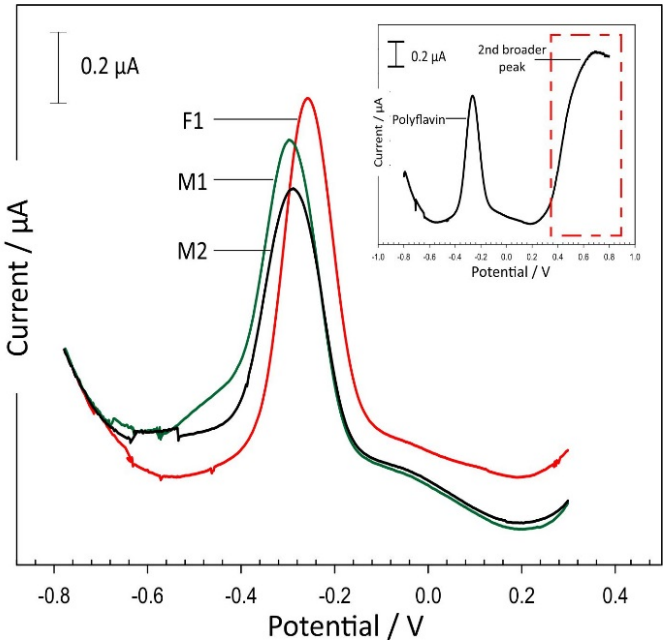

Figure 6.3.6 Square wave voltammograms presenting the analytical signals taken from flavin-modified anodised C-PE electrode in each human urine sample. Insert: representative square wave voltammogram highlighting the broad second peak observed if potential is swept towards a more positive range.

The oxidation potentials from each sample were taken and the linear regression equation attained from calibration graph generated in **Figure 6.3.4C** was exploited to calculate the urine pH from the peak positions. Measurements obtained from the flavin C-PE composite were then compared to those acquired from a conventional glass pH probe as shown in **Table 6.3.3**. This shows that the signals obtained from the manufactured electrode are only up to 2.2% different from that taken with the conventional probe. Again, the peak potential remains constant after consecutive scans and no biofouling has occurred when immersed in a relevant biofluid – an imperative function required in systems that will be used for days at a time. At more negative potentials, fewer processes that could potentially passivate the surface of the electrode can occur, including oxidation of tyrosine and tryptophan [358], thus the polymeric flavin has a great advantage against other modifiers as described in **Chapter 5.3.3**.

Table 6.3.3 Peak potentials of the flavin-modified anodised C-PE mesh in human urine and their equivalent pH measurements against conventional pH probe.

	Potential / mV			Average	Calculated pH	Commercial Probe pH	pH Unit Error
Sample	**1**	**2**	**3**				
F1	-0.258	-0.258	-0.258	-0.258	5.92	5.98	0.06
M1	-0.296	-0.296	-0.296	-0.296	6.55	6.48	0.07
M2	-0.294	-0.294	-0.288	-0.292	6.49	6.35	0.14

6.4 Conclusions

Electrochemical pH sensing using various modalities have already been explored, in this case however, a novel approach using a mechanically flexible anodised carbon-polyethylene film modified with polyflavin was investigated. The composite system was shown to provide a versatile sensor able to be employed in applications where flexibility, contouring and disposability are essential. The core redox flavin film clearly demonstrated its robustness upon continuous, repetitive scanning and is able to accurately determine pH even within a chemically complex urine biofluid. As per previous discussion, the potential required to oxidise the flavin centre, and thus the quantification of the electroanalytical oxidation peak potential, occurs in a cathodic range whereby there is no need for solution degassing and where it is also devoid of any common interferences. The flavin-modified carbon-polyethylene sensor described here evidently demonstrates its Nernst-like (60 mV/pH) behaviour that is robust and capable of performing under both constant and cyclic mechanical flexing as well as during normal measurements (without mechanical duress). The latter characteristic is advantageous in that it highlights only minute drifts in peak potential are observed under various types of pressure and with the degree of error being less than 0.001 pH unit, by far proves to be better than potentiometric system where drift commonly limits the usage of the sensor in real-life applications.

It is clear that the system could be used as an alternative to the carbon fibre detailed in **Chapter 5** but it also possesses a range of advantageous characteristics that could be transferable to other sensing applications. Although there are various spectroscopic methods of measuring urine pH, these are costly, unscalable, methodically complex and are therefore unsuitable for direct incorporation to conventional systems such as those used in ostomy as well as catheter applications. The configuration investigated here is proven to be the opposite as it is a thin, conductive, reagentless system that can not only be easily integrated due to its mechanical flexibility but is also inexpensive and has an ability to be mass produced. The underlying electronics necessary to operate the voltammetric methodologies, and hence method to obtain the corresponding electroanalytical signals, are well-known and can significantly be scaled down which enhances the capability of the flavin-C-PE sensor to be integrated into existing systems.

Chapter 7

Integration of Riboflavin-Modified Carbon Fibre and Screen Printed Electrode Systems in Customised 3D Printed Hub

Abstract

Riboflavin, vitamin B2, is a biocompatible chemical that possesses a redox active flavin core that is dependent on the presence of H^+ concentration and thus could be an ideal component within the proposed smart catheter system. As such this chapter details an investigation into its exploitation as the basis of a pH sensitive sensor. The sensing rationale is based on a riboflavin-modified electrode system integrated within a modified 3D printed catheter needle free connector (bionector) hub which, in turn, can be readily integrated into existing catheter lines and which can measure changes in lumen pH arising from microbial contamination. Carbon fibre mesh was initially used as a conductive substrate which was then replaced by a more disposable, inexpensive carbon-based screen printed electrode. Both systems exhibit near Nernstian behaviour of 63 mV/pH unit and 62 mV/pH unit, respectively, and are capable of monitoring pH within chemically complex solutions. The release of hydrogen peroxide from riboflavin is also briefly discussed as a means of eradicating biofilm formation prior to causing catheter-related bloodstream infection.

7.1 Introduction

The primary reason for employing the engineered flavin-phenol compound in initial investigations was its ability to be electropolymerised directly onto the electrode surface whilst preserving its characteristic redox transitions which, in turn, was exploited to produce electroanalytically sensitive sensors. Although there was evident success in employing the custom phenolic flavin derivative in measuring pH, its major drawback and limitation in central venous catheter applications is the non-biocompatible nature of its monomers/oligomers. In instances where polymer leaching could potentially occur, there is a possibility that the use of polyflavin could result in cytotoxic adverse effects and this is especially problematic as the fragments would have direct access to the vascular/circulatory system if implemented in venous catheter systems. Therefore, this chapter aims to provide an alternative route where electropolymerisation is not needed and the commercially available riboflavin can be used to replace the flavin-phenol moiety.

Needle free hub connectors (NFCs) were originally developed to reduce the risk of occupational injuries associated with needlestick events and which could potentially lead to the transmission of blood borne diseases [65]. These NFCs are essential extensions at the end of CVC lines which allows access for intravenous fluid in and/or out of the body [66]. They are designed to be gatekeepers to reduce catheter contamination, however, studies have shown that these catheter hubs are the most common source of infection [3,45,66,69,371,372]. This can be attributed to the presence of dead space in the core design between the septum seal and housing which proffers the perfect nidus for microorganism attachment, growth and proliferation thereby potentially leading to biofilm formation and eventually catheter-related bloodstream infection. The use of aseptic techniques, specifically scrubbing the NFCs with 70% isopropyl alcohol for 30 seconds [109,373], is suggested to reduce the risk of infection however, as stated in **Chapter 2**, contamination can still occur with user compliance being one of the main contributors to its ineffectiveness. As such, the vision for this project was the employment of a smart hub whereby the conventional design is enhanced to be devoid of empty spaces and can monitor the line. Additionally, it was hoped that the same redox species responsible for conferring the indirect measurement of pH could be harnessed as an electrocatalyst for the generation of reactive oxygen species and therein have the potential to proactively minimise the propensity for biofilm formation.

Carbon loaded polyethylene was initially considered as an alternative substrate to replace the brittle carbon fibre mesh but the availability of screen printed electrodes (SPEs) in the course of the project opened up another avenue of investigation. These represent a cost-effective solution given the ease with which they can be manufactured as evidenced by the commercial success of home glucose monitors. One possible limitation however would be whether or not they possessed the electrochemical characteristics necessary for facilitating the unambiguous identification of the riboflavin peak positions used as an indicator for pH. The employment of screen printed electrodes as an electrically conductive sensor has been widely used for several biomedical applications including detection of uric acid [374,375], salicylic acid [264], glucose [376,377] and hydrogen peroxide [378,379]. Modifications of SPEs are also common with graphene oxide [374,380,381], Prussian blue [378,379,382,383] and other nanoparticles [384–386] as primary samples of usual modifiers. In the present case, carbon-SPEs were functionalised with the pH-sensitive riboflavin.

The adsorption of riboflavin onto a conductive carbon-based electrode encased in a customised 3D-printed hub was the proposed development route. It was envisaged that the system would detect pH changes within the connector – the main site of contamination. Similar to the novel phenolic-flavin derivative, the redox transitions of the heterocyclic flavin core of riboflavin are highlighted in **Figure 7.1.1** where it can undergo reduction (**I** $\rightarrow$ **II**) and oxidation (**II** $\rightarrow$ **I)** based on a two electron/two proton transfer. Additionally, it was anticipated that the electroactive riboflavin core would also be capable of redox cycling in the presence of oxygen. In its natural state, riboflavin is present in its oxidised form (**I**) but upon reduction (**II**), it is capable of electron transfer to molecular oxygen resulting in the production of reactive oxygen species such as superoxide anion and peroxide. A core assumption was that the generation of the ROS could help prevent the establishment of biofilm within the access line. Although several studies [186,387–389] have shown that a significant amount of ROS (typically in millimolar range, ≥ 0.2 mM of hydrogen peroxide [186,387–389]) is required to eradicate bacteria, it was anticipated that within the small volume of the NFC, ROS electrogenerated from the riboflavin could be a potent antimicrobial, sufficient enough to overcome bacterial defences (i.e. superoxide dismutase or various peroxidases). It was also envisaged that in travelling down the catheter line, the ROS would dissipate and hence would be of little threat to the main vasculature.

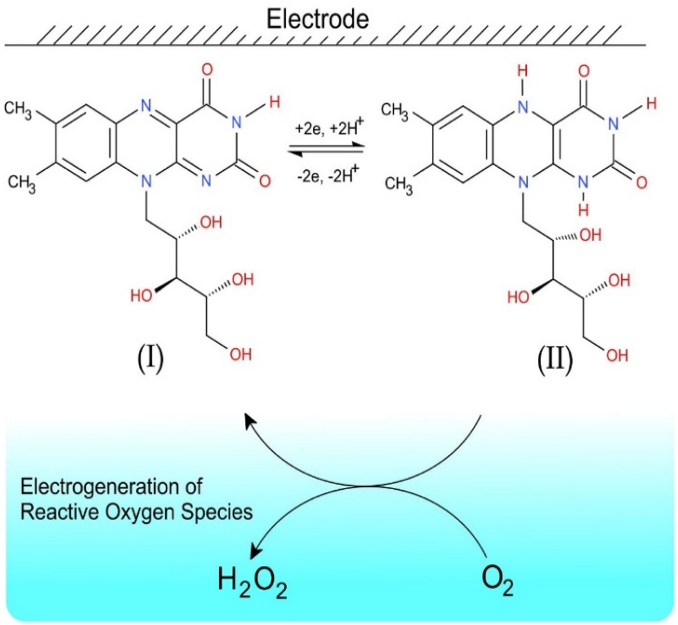

Figure 7.1.1 Reaction scheme detailing the electrochemical redox reactions of riboflavin at the electrode and the catalysis of oxygen reduction leading to the generation of peroxide.

As discussed in **Chapter 2**, there are many risk factors associated with catheter related blood stream infection (i.e. duration of use, presence of underlying disease, etc.). In particular, patients receiving total parenteral nutrition (TPN), and other intravenous fluids, are at a higher risk of infection as these solutions provide necessary nutrients for the patient but which can similarly provide a growth medium that enhances the proliferation of CRBSI-causing microorganisms [73,76,77]. A typical composition of TPN is detailed in **Table 7.1.1** highlighting the diverse range of carbohydrates, trace elements and amino acids critical for maintaining nutritional health. Some 26% of increased risk was observed in patients requiring TPN compared to those who don't and a study by Santarpia et al. (2016) highlights that, even with the lack of clinical symptoms, 50% of CVC tips used for TPN administration were infected [75]. Intravenous solutions like TPN are chemically complex and thus would provide a suitably challenging milieu for electrochemical sensors that are intended for catheter applications. Herein, the proposed sensor relies on carbon-based electrode as the underlying conductive substrate and riboflavin as the pH sensitive electroactive agent. It is noteworthy that riboflavin's oxidation peaks are observed at more negative potentials and as such, devoid of competing processes. In addition, this is of distinct advantage since the presence of amino acids such as tryptophan and tyrosine in TPN would mean that if the cyclic voltammetry or square wave sweep is too positive, these would be irreversibly oxidised leading to oligomeric/polymeric material that would potentially contaminate the electrode and thus affect electrode response.

Table 7.1.1 Typical components of TPN solution.

Total Calories	1210 KCal
Glucose	1000 KCal
Fat	0 KCal
Nitrogen	9 gram
Sodium	275 millimol
Potassium	60 millimol
Calcium	7.5 millimol
Magnesium	10 millimol
Non-Protein Calories	1000 KCal
Phosphate (excluding Fat)	10 millimol
Acetate	0 millimol
Chloride	324.19 millimol
Zinc	100 micromol
Copper	20 micromol
Selenium	400 nanomol
Iron	20 micromol
Water for Injection	2022.47 ml
Glucose 50%	500 ml
Magnesium Sulfate 50%	5 ml
Sodium Glycerophosphate 21.6%	10 ml
Additrace	10 ml
• Ferric Chloride, $6H_2O$	20 micromol
• Zinc Chloride	100 micromol
• Manganese Chloride, $4H_2O$	5 micromol
• Copper Chloride, $2H_2O$	20 micromol
• Chromic Chloride, $6H_2O$	0.2 micromol
• Sodium Selenite anhydrous	0.4 micromol
• Sodium molybdate, $2H_2O$	0.2 micromol
• Sodium fluoride	50 micromol
• Potassium Iodide	1 micromol
Cernevit (5ml WFI)	5 ml
• Retinol palmitate corresponding to Retinol (Vitamin A)	3500 IU
• Cholecalciferol (Vitamin D_3)	200 IU
• DL α-tocopherol	10.2 mg
- corresponding to α-tocopherol (Vitamin E)	11.2 IU
• Ascorbic Acid (Vitamin C)	125mg
• Nicotinamide (Vitamin B_3)	46 mg
• Dexpanthenol	16.15 g
- corresponding to pantothenic acid (Vitamin B5)	17.25 mg
• Pyridoxine Hydrochloride	5.5 mg
- corresponding to pyridoxine (Vitamin B_6)	4.53 mg
• Riboflavin sodium phosphate	5.67 mg
- Corresponding to riboflavin (Vitamin B2)	4.14 mg
• Cocarboxylase tetrahydrate	5.8 mg
- Corresponding to thiamine (Vitamin B1)	3.51 mg
• Folic Acid	414 mcg
• D-Biotin	60 mcg
• Cyanocobalamin (Vitamin B_{12})	5.5 mcg
Aminoven 25	350.19 ml
• Isoleucine	1.82 g
• Leucine	3.12 g
• Lysine Acetate	5.48 g
• = Lysine	3.89 g
• Methionine	1.33 g
• Phenylalanine	1.93 g
• Threonine	3.01 g
• Tryptophan	0.56 g
• Valine	1.93 g
• Arginine	7.00 g
• Histidine	2.56 g
• Alanine	8.75 g
• Glycine	6.48 g
• Proline	5.95 g
• Serine	3.36 g
• Tyrosine	0.14 g
• Taurine	0.70 g
Calcium Chloride 1 mMol/mL	7.5 ml
Sodium Chloride 30%	49.84 ml
Potassium Chloride 15%	30 ml
Ascorbic Acid 500 mg/5 mL	10 ml

7.2 Experimental Details

7.2.1 Materials

Chemicals were obtained from Sigma Aldrich (UK), were the highest grade available and were used without further purification. Toray carbon paper (TGP-H-60, 19 x 19 cm) and riboflavin were both purchased from Alfa Aesar (Thermo Fisher Scientific, UK). Similar to previous chapters, drops of concentrated NaOH was added to Britton-Robinson buffer until the appropriate pH unit was attained and the resultant buffers were used throughout the experiments unless otherwise stated.

7.2.2 Electrochemical Configuration and Electrode Modification

Electrochemical analysis was carried out using a μAutolab Type III potentiostat with a standard three-electrode configuration with a carbon fibre mesh (2.5 mm x 2.5 mm window) or a carbon screen printed electrode acting as the working electrode. These were modified via pre-anodisation (300 seconds and 180 seconds in 0.1 M NaOH, respectively) and were further functionalised through adsorption of riboflavin, completed through submersing the electrode in solution containing the latter (250 μM, pH 7, unless otherwise stated). Platinum wire served as the counter electrode and a conventional silver/silver chloride (3 M KCl, BASi Technicol, UK) reference electrode completed the set-up. All measurements were conducted at 22^{o}C ± 2^{o}C.

7.2.3 Screen Printed Electrode Manufacture

Carbon screen printed electrodes (SPEs) were fabricated using a DEK 240 Manual Screen Printer, a stainless-steel screen mesh and graphite ink (Gwent Electronic Materials, UK). The electrode was printed onto a Valox™ substrate which was heat cured at 70 °C for 90 minutes and the print had a typical height/thickness of 20 μm [264]. The electrode area of the carbon SPE was 0.1 cm^2.

7.2.4 Counter and Reference Electrode in 3D Printed Hub

Experiments involving the carbon fibre electrodes and 3D-printed catheter hub extension used a two-electrode system whereby a carbon mesh (8 x 4.5 mm window) modified with electrodeposited silver acted as both the reference and counter electrode. Silver electrodeposition was completed through chronoamperometric method employing -0.1 V for 300 seconds in 10 mM $AgNO_3$ in 0.1 M HNO_3. Subsequently, the electrodes were chlorodised through cyclic voltammetry (-1 V $\rightarrow$ 0.6 V $\rightarrow$ -1 V) in 0.1 M KCl electrolyte.

In experiments involving screen printed electrodes, the three-electrode configuration used within the hub is diagrammatically shown in **Figure 7.2.1**, where silver ink was added on to the third electrode to serve as the reference electrode. It should be noted that the working area was defined using a similar technique to that used with carbon fibre mesh where a polyester laminate was cut, and the electrode was thermally sealed.

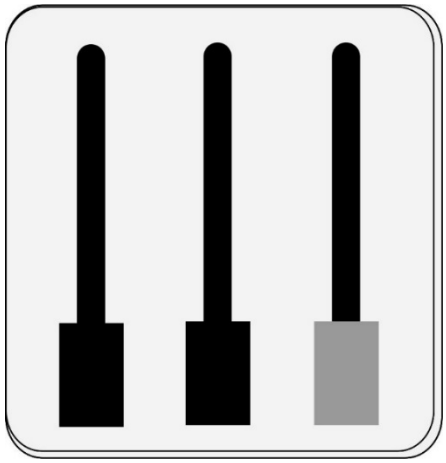

Figure 7.2.1 Three screen printed electrode configuration used within the customised catheter hub.

The stability of the produced reference electrodes was assessed using zero current potentiometry in logarithmically increasing concentrations (0.001 M to 1 M) of KCl for 180 seconds and recording the last 10 seconds for each concentration, as exhibited in **Figure 7.2.2**.

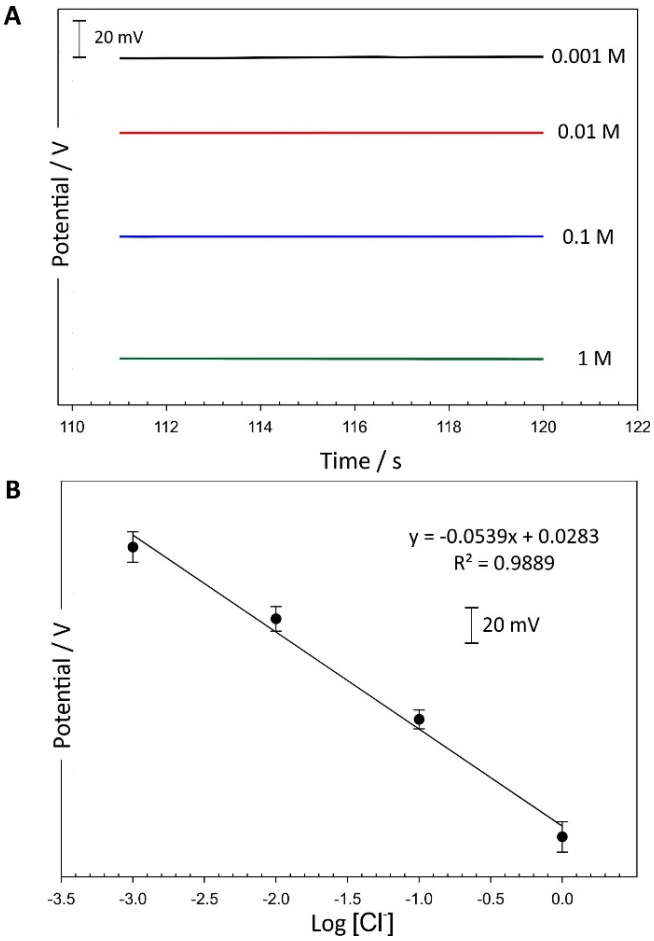

Figure 7.2.2 Representative A) potentiometric trace and B) linear regression calibration curve ($N_{electrodes}$ = 3) detailing the stability of the Ag/AgCl-modified carbon screen printed reference electrodes. Error bars represent mean standard deviation.

7.2.5 Needle Free Hub Design

The initial design of the suggested catheter hub system is presented in **Figure 7.2.3** wherein the 3D printed connector can be easily integrated into existing central venous lines. This was later enhanced (**Figure 7.2.4**) so that the solution flows through the two-electrode carbon fibre mesh sensor (**Figure 7.2.5**) to ensure that intravenous fluid is further filtered as reactive oxygen species are generated, and any changes in pH, as a consequence of the presence of microorganisms, could be detected to alert the patient or healthcare practitioner. **Figure 7.2.4D** highlights the flow through network inside the suggested hub. As discussed in **Chapter 2**, the design of the hub must remain simplistic and devoid of dead space in order to minimise the risk of the needle free connector becoming a pathogen nidus and ultimately the source of CRBSI. This was therefore taken into consideration and explains the straightforward nature of the design chosen. Luer connector ends were included to ensure that it can be integrated within existing catheter lines. Additionally, the application of 3D printing means

that it is easy to rapid prototype such a device and, it could be envisaged that the end results could therefore be easily augmented and reproduced with conventional moulding processes.

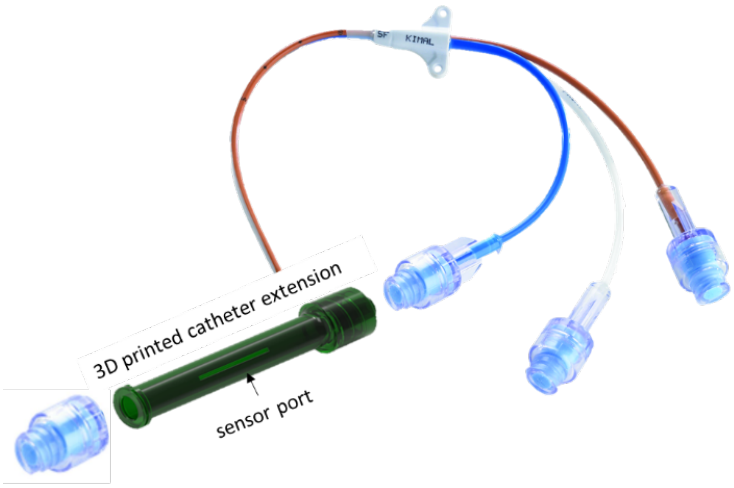

Figure 7.2.3 Initial design of the catheter hub extension showcasing its capability to be readily integrated with existing catheter lines.

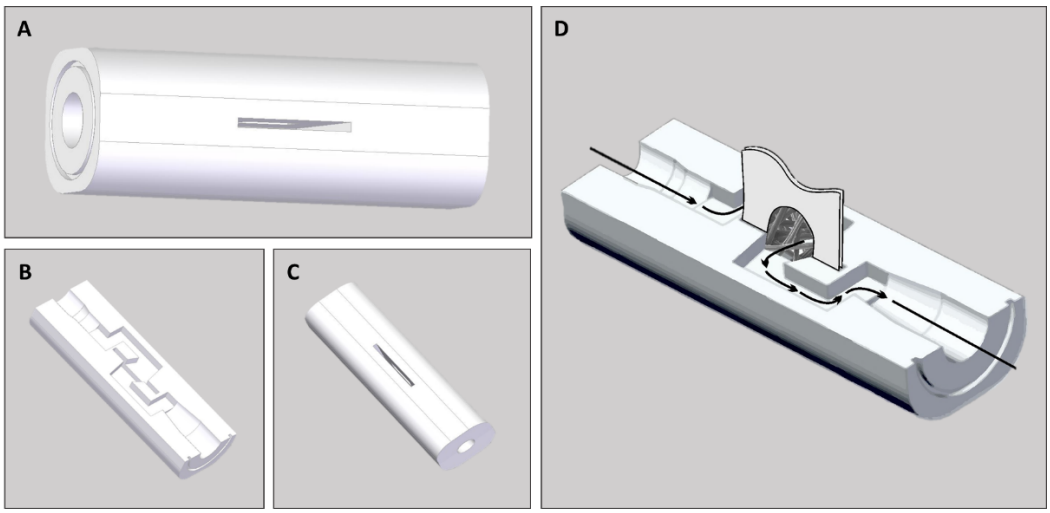

Figure 7.2.4 External (A & C) and internal (B & D) designs of the suggested flow through catheter needle free connector.

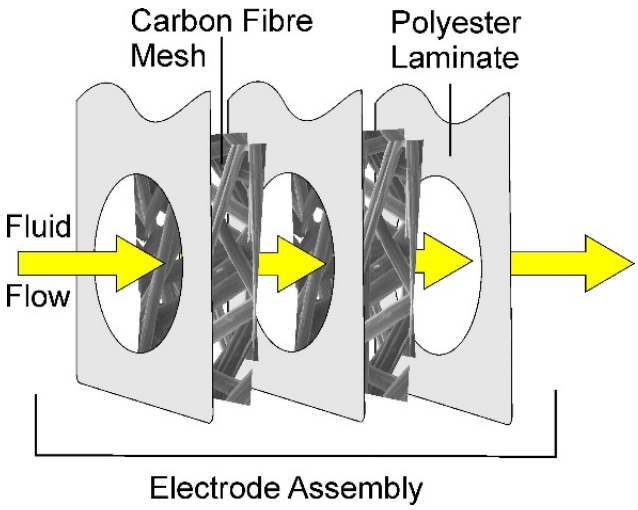

Figure 7.2.5 Two carbon mesh electrode system assembly.

7.3 Results and Discussion – Carbon Fibre Mesh System

7.3.1 Electroanalytical Evaluation of Riboflavin-Modified Carbon Fibre Electrode

Representative cyclic voltammogram traces of riboflavin (3.19 µM, pH 6.21) with and without solution degassing are highlighted in **Figure 7.3.1**. The oxygen peak observed at -0.722 V in the riboflavin CV trace is clearly absent when the solution is degassed. This is attributable to the presence of nitrogen which removes the oxygen in the solution. It can be seen however that both redox peaks of riboflavin are visibly distinct without the intervention of the latter and thus useful for in situ applications. Similar to the polymeric flavin, the peak potentials of riboflavin are also therefore easily measured for analytical purposes and exhibits a reversible system.

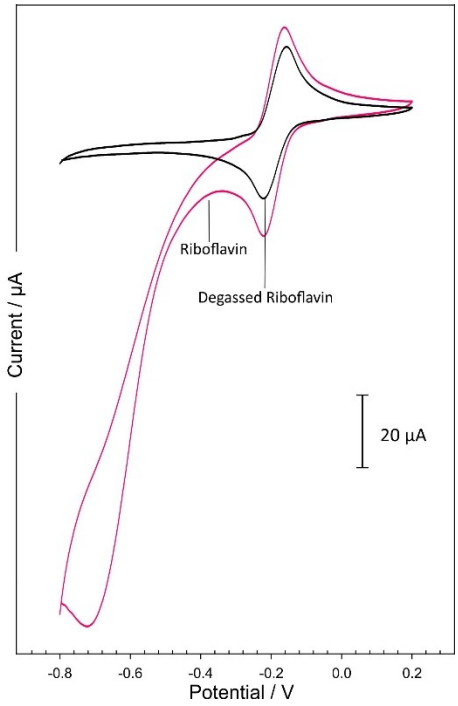

Figure 7.3.1 Cyclic voltammetry traces comparing the riboflavin (3.19 µM, pH 6.21) redox reaction at an anodised carbon fibre mesh electrode with and without solution degassing. Scan rate: 50 mV/s.

In contrast to previous chapters where the flavin component was electropolymerised onto the carbon substrate through the oxidation of the phenol component, in this case the electrode was modified by simple physisorption. The simple submersion of the carbon electrode into a solution containing the riboflavin (250 µM, pH 7) was sufficient to induce the adsorption of the flavin. Subsequent rinsing of the electrode with fresh electrolyte (or BR buffer) did not perturb the adsorbed species and the electrochemical properties were of little difference to those recorded with the riboflavin in solution (**Figure 7.3.1**). In order to test the efficacy of this simple modification procedure, the physisorbed riboflavin electrode was assessed in varying pH BR buffers. However, in this case, a two-carbon fibre mesh electrode system was employed directly within the 3D-printed catheter extension (detailed previously in **Figure 7.2.4D**). **Figure 7.3.2** showcases the shift of physisorbed riboflavin's oxidation peak towards less negative potentials with the presence of increasing H^+ concentrations. Square wave voltammetry was used to provide a more accurate measurement of peak potential as well as reduce the effect of oxygen. As with the phenolic flavin moiety (**Chapters 5** and **6**), the scan was initiated at a negative potential of -0.8 V which is enough to induce the reduction of riboflavin and is then swept towards more positive potentials to initiate its re-oxidation. The system is shown to have a near-Nernstian behaviour of 63 mV/pH unit (E / V = -0.0629 pH – 0.1189; N_{total} = 18 (N_{pH} = 6, $N_{scans/pH}$= 3); R^2 = 0.9933) which is broadly consistent with the results from the flavin phenol polymer.

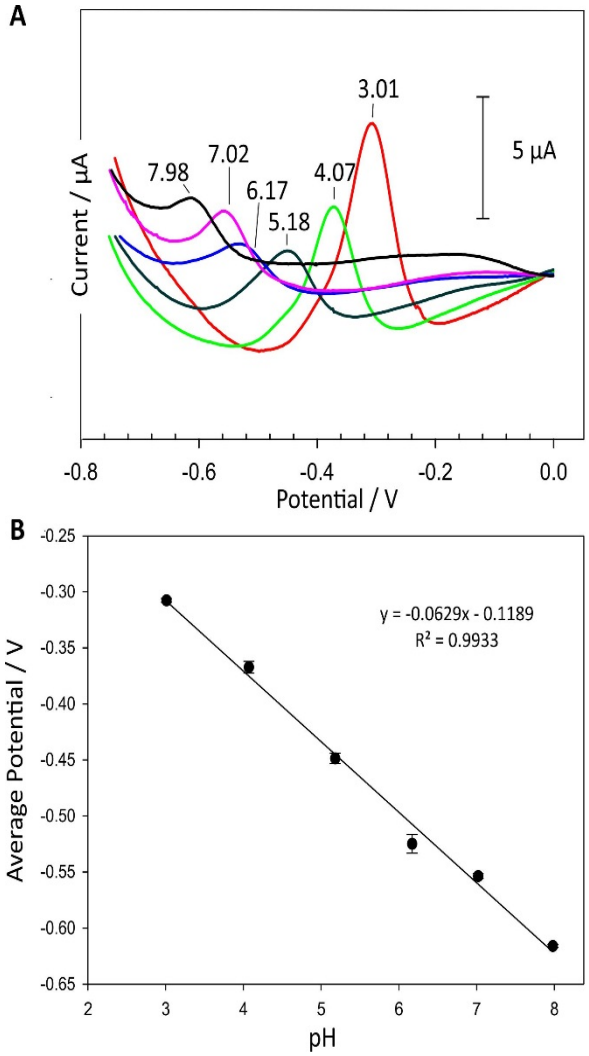

Figure 7.3.2 A) Representative square wave voltammetry scans of the physisorbed riboflavin-modified anodised carbon fibre electrode within the 3D printed hub to BR buffers of varying pH. B) Corresponding linear regression calibration line with each point of the calibration curve being an average of 5 scans and error bars represent the mean standard deviation.

Needle-free connectors are recommended by the CDC to be replaced no more than every 72 hours to reduce the risk of catheter related bloodstream infection [58,390]. As such, the smart hub system proposed here must be robust and able to perform multiple scans that could cover this period. As with the flavin-phenol film investigations, the physisorbed riboflavin-modified electrode was submerged in successive pH BR buffers (covering pH 3.10 to pH 8.07) and the series was repeated three times as shown in **Table 7.3.1**. The near Nernstian characteristic remained with a 57.8 mV/pH unit shift recorded (**Figure 7.3.3C**) (E / V = -0.0578 pH – 0.0221; N_{total} = 54 ($N_{pH\ buffers}$ = 6, $N_{scans/pH/set}$ = 3,); R^2 = 0.9989). The corresponding variation in peak potentials and changes in peak magnitude are displayed in **Figure 7.3.3**. An average potential drift of 11 mV (0.19 pH unit based on a 57.8 mV per pH shift) was observed

and a 42% difference in peak current magnitude was calculated at the end of 54 scans. Minimal drift as well as minute change in peak magnitude are imperative to applications where repetitive/continuous scanning is required such as in smart catheter bionector systems. Critically, there was relatively little loss of the physisorbed riboflavin despite the repetitive scan and frequent changes in pH (and associate rinses). The system presented here is therefore suitable for periodic scanning. Assuming that 12 scans are required per day (based on differential period of central line culture versus peripheral culture is ≥ 2hrs [5,9]), the proposed system would be viable for at least 4.5 days which is beyond the typical lifetime of needle free connectors of 3 days [58,390,391].

Table 7.3.1 Detailed raw data obtained from repetitive square wave voltammetric series scanning of the physisorbed riboflavin-modified anodised carbon fibre electrode in Britton Robinson buffers of varying pH; N_{scans} = 54.

	Scan number | Peak Potential / V									Average	Standard Deviation	Standard Error
	Series 1			**Series 2**			**Series 3**					
pH	**1**	**2**	**3**	**4**	**5**	**6**	**7**	**8**	**9**			
3.10	-0.196	-0.196	-0.196	-0.196	-0.196	-0.194	-0.220	-0.228	-0.232	-0.206	0.0158	0.0053
4.11	-0.252	-0.252	-0.252	-0.250	-0.250	-0.250	-0.264	-0.266	-0.268	-0.256	0.0076	0.0025
5.37	-0.328	-0.328	-0.328	-0.324	-0.324	-0.326	-0.332	-0.334	-0.334	-0.329	0.0039	0.0013
6.19	-0.376	-0.376	-0.378	-0.374	-0.376	-0.376	-0.380	-0.382	-0.382	-0.378	0.0029	0.0010
7.08	-0.436	-0.436	-0.436	-0.430	-0.430	-0.432	-0.434	-0.434	-0.434	-0.434	0.0024	0.0008
8.07	-0.488	-0.488	-0.490	-0.490	-0.490	-0.490	-0.490	-0.490	-0.490	-0.490	0.0009	0.0003

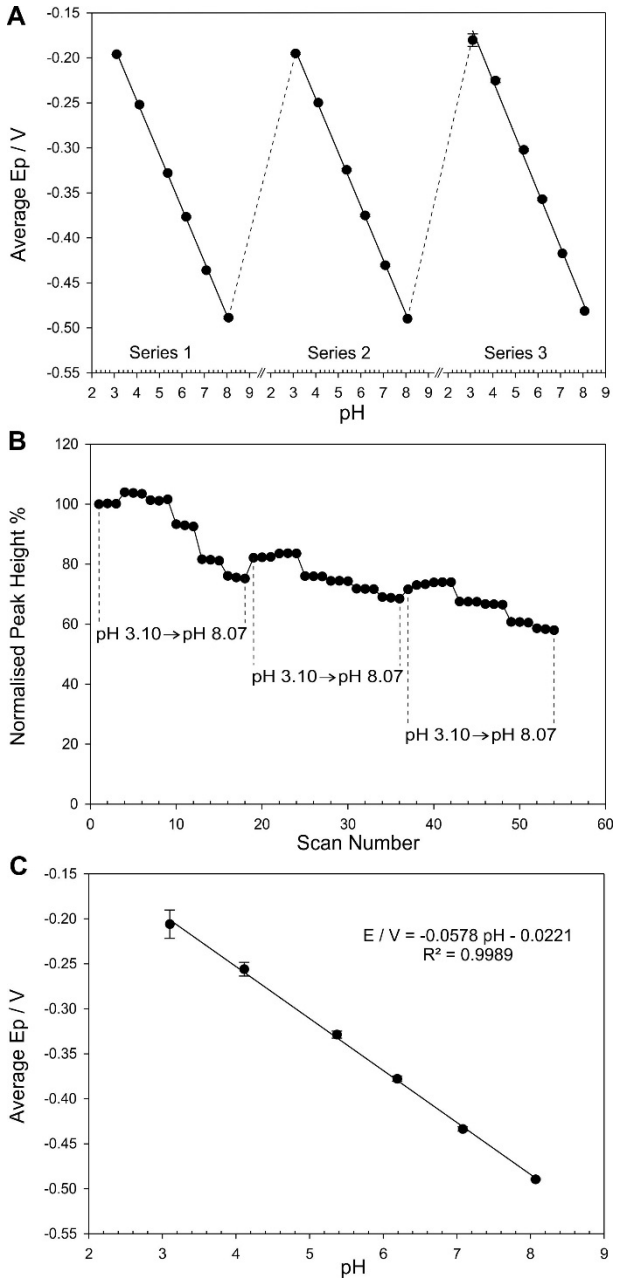

Figure 7.3.3 Changes in A) peak potential and B) current magnitude of the physisorbed riboflavin-modified anodised carbon fibre electrode as a result of serial scanning in BR buffers of varying pH. C) Calibration curve displaying the average peak potential for each pH (N_{total} = 54). Error bars represent mean standard deviation.

7.3.2 Assessment in TPN and Laked Horse Blood

It must be acknowledged that the simple Britton-Robinson buffers offer little challenge to the proposed system and, as such, relevant matrices that proffer a more complex milieu were used to assess the pH sensitive capabilities of the riboflavin-modified electrode. Total parental nutrition and laked horse blood both contain components that could be expected to hinder conventional electrochemical measurements and thus it was necessary to

determine if they would affect the redox activities (or indeed the stability) of the physisorbed riboflavin. Moreover, TPN is used as an intravenous fluid while laked horse blood was used as a more immediately accessible substitute for human blood. As noted in **Chapter 2,** reflux of blood into the NFC hub can occur and hence an investigation of its effect is of relevance for the purpose of this project. As in **Chapter 5**, kefir grains were used to alter the pH of both matrices and resulting square wave voltammograms are presented in **Figure 7.3.4** and **Figure 7.3.5**, respectively. It is clear that kefir inoculation had a greater effect in altering the pH of TPN compared to laked horse blood which could be attributed to the fact that the former would contain greater concentrations of available nutrients (i.e. glucose) that would significantly enhance the proliferation of the bacteria and yeast found in kefir grains.

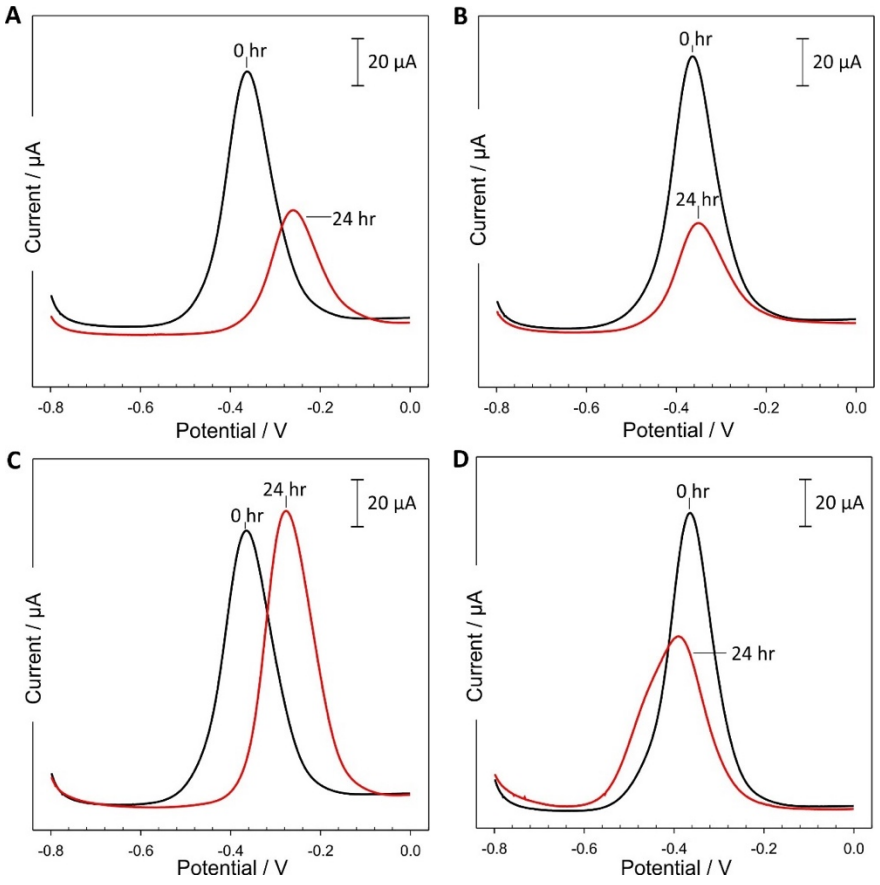

Figure 7.3.4 Square wave voltammograms showcasing the changes in peak potential using physisorbed riboflavin-modified anodised carbon fibre electrode: A) continuously kept in kefir-inoculated TPN, B) continuously submerged in TPN without kefir, C) periodically inserted in kefir-inoculated TPN and D) periodically placed in TPN without kefir.

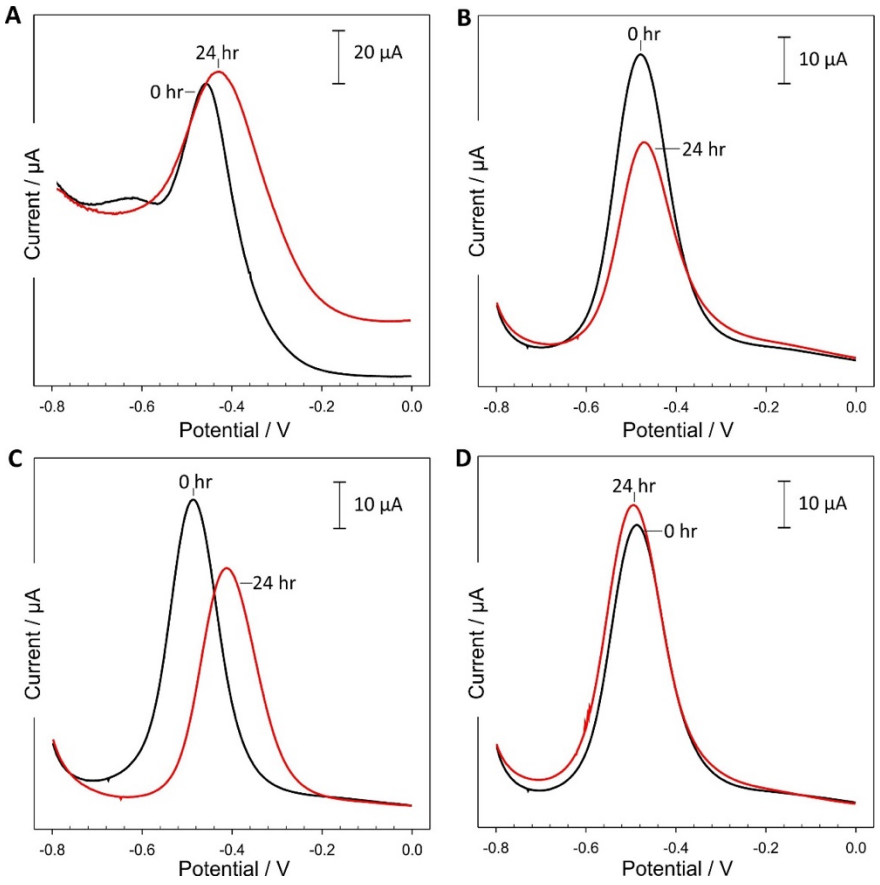

Figure 7.3.5 Square wave voltammograms showcasing the changes in peak potential using physisorbed riboflavin-modified anodised carbon fibre electrode: A) continuously kept in kefir-inoculated laked horse blood, B) continuously submerged in laked horse blood without kefir, C) periodically inserted in kefir-inoculated laked horse blood and D) periodically placed in laked horse blood without kefir.

Both figures show that the peak potential significantly changed only in the presence of kefir grains which continuously ferment throughout the experimental period, producing lactic and acetic acid, thus changing the pH to become more acidic [331,332,392,393]. This is analogous to the shifts found when BR pH buffers were used and by using the linear regression equation calculated from the calibration curve (**Figure 7.3.3C**), the pH of the TPN and laked horse blood cultured with kefir was determined as per **Table 7.3.2**. The difference between the results taken from the physisorbed riboflavin electrode continuously submerged in the solution and ones that were only inserted at each time period could be possibly explained by the biofouling of kefir, and thus biofilm formation on the former electrode surface is more viable than the latter. However, it is evident that data from both electrode protocols slightly deviated from the pH measured using the commercial pH probe. The maximum percentage difference was calculated to be less than 10% which was a result of the physisorbed riboflavin-electrode, inserted in the kefir-culturing TPN throughout the duration of the experiment, after a period of inactivity. This is somewhat similar to that found in **Chapter 5** (**Figure 5.3.7**) where a greater deviation was found after the electrode was left in the matrix

overnight and more frequent scanning reduced the discrepancy. It is also important to note that average peak potential is the mean of 3 consecutive scans and a total of 12 scans was completed for each riboflavin-functionalised electrode. This along with the peak magnitude shown in **Figure 7.3.4** and **Figure 7.3.5**, further suggests that the system is robust and useful for in situ applications.

Table 7.3.2 Raw data obtained from the physisorbed riboflavin-modified carbon fibre electrode: A) continuously submerged in kefir-cultured TPN, B) periodically inserted in kefir-cultured TPN, C) continuously submerged in kefir-cultured laked horse blood and D) periodically inserted in kefir-cultured laked horse blood.

A	**Commercial pH Probe**	**Average Ep**	**Calculated pH**	**pH Unit Error**	**B**	**Commercial pH Probe**	**Average Ep**	**Calculated pH**	**pH Unit Error**
0 hr	5.65	-0.363	5.89	0.24	**0 hr**	5.65	-0.369	6.01	0.36
4 hr	4.29	-0.259	4.10	0.19	**4 hr**	4.29	-0.277	4.42	0.13
23 hr	3.78	-0.220	3.42	0.36	**23 hr**	3.78	-0.229	3.58	0.20
24 hr	3.74	-0.230	3.60	0.14	**24 hr**	3.74	-0.229	3.58	0.16
C					**D**				
0 hr	7.52	-0.455	7.49	0.03	**0 hr**	7.52	-0.493	8.15	0.63
3 hr	7.21	-0.421	6.90	0.31	**3 hr**	7.21	-0.416	6.81	0.40
22 hr	7.15	-0.415	6.80	0.35	**22 hr**	7.15	-0.461	7.59	0.44
24 hr	7.28	-0.416	6.81	0.47	**24 hr**	7.28	-0.467	7.70	0.42

7.4 Results and Discussion – Screen Printed Electrode System

7.4.1 Preliminary Electrochemical Characterisation

The ease of deployment and replacement of the physisorbed riboflavin-carbon fibre system could be considered to be economically viable when considering the costs associated with CRBSI treatment (**Chapter 2**). Nevertheless, the translation of the proposed riboflavin technology to screen printed systems is recommended as the latter is easier to mass produce and offers a more inexpensive, disposable approach for employment in smart catheter systems. Therefore, a carbon-based screen printed electrode modified through the physisorption of riboflavin was investigated.

Similar to the previous technique used with the carbon fibre network, riboflavin (250 µM, pH 7) was adsorbed on to the screen printed electrode and its electrochemical response was assessed. **Figure 7.4.1** displays well defined peaks highlighting the redox profiles innate to

riboflavin and showcases the effect of scan rate on the riboflavin-modified anodised SPE. The redox peak separation increases with scan rate attributable to the decreasing transfer rate of counter ions. The peak visible at +0.06 V could be explained by the possible contamination of silver on the screen printed electrode surface.

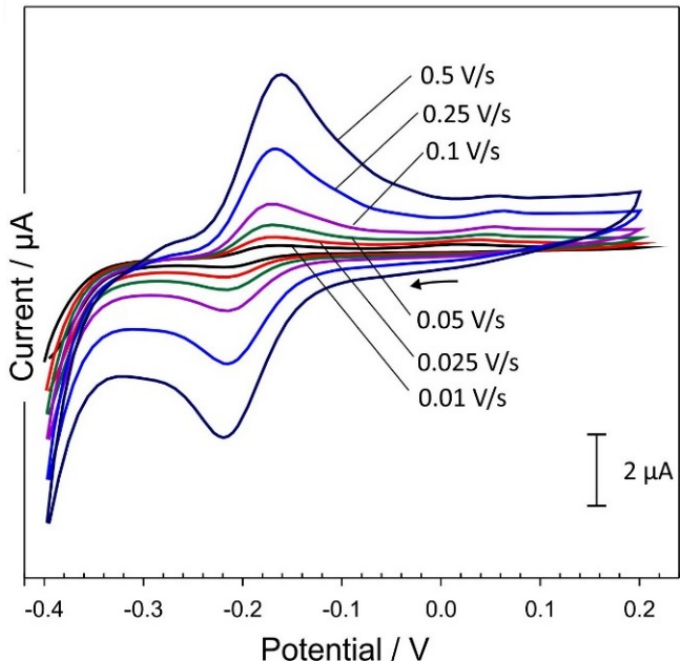

Figure 7.4.1 Cyclic voltammograms detailing the influence of scan rate on the redox processes of a physisorbed riboflavin-modified anodised screen printed electrode in pH 7 Britton Robinson buffer.

Likewise, **Figure 7.4.2** details the change in riboflavin peak height as a function of scan rate. The positive linear relationship between peak height and scan rate ascertains the confinement of the electroactive species on the surface of the electrode. To further assess the adsorption of riboflavin, the electrode was placed into fresh pH BR buffer after modification and square wave voltammetry was performed. As per the preceding section, the riboflavin oxidation peak remained present and shifts with pH as shown in **Figure 7.4.3**. The system shows a near Nernstian behaviour of 62 mV shift per pH (E / V = -0.0616 pH – 0.0646; N_{total} = 18 (N_{pH} = 6, $N_{scans/pH}$ = 3); R^2 = 0.9998).

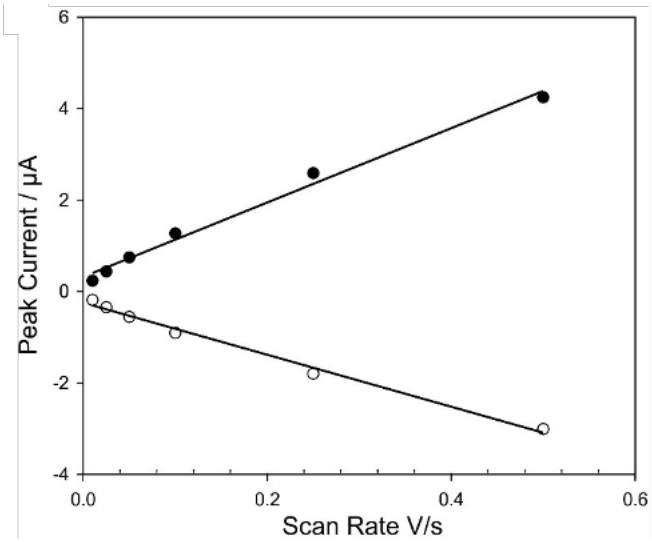

Figure 7.4.2 Variation of riboflavin peak heights as a function of scan rate recorded using physisorbed riboflavin-modified anodised carbon screen printed electrode.

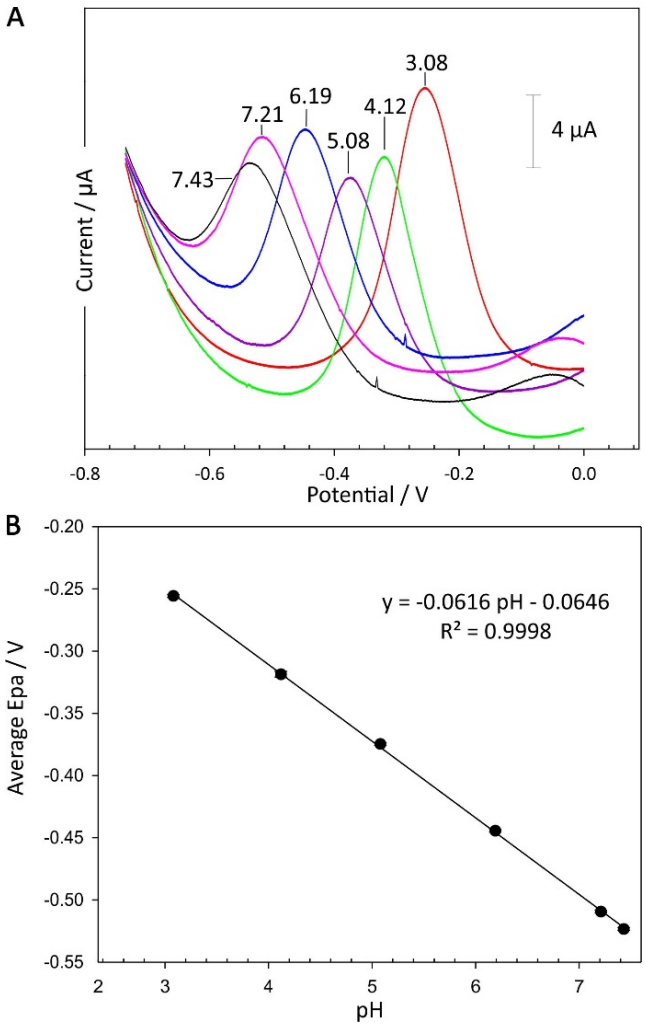

Figure 7.4.3 A) Square wave voltammograms of a physisorbed riboflavin-modified anodised carbon screen printed electrode in Britton Robinson buffers of varying pH. B) Corresponding calibration curve (each point is an average of three scans) showing the effect of pH on peak potential. Mean standard deviation error bars are included but are too small to be observed.

Additionally, X-ray photoelectron spectroscopy was also used to ensure riboflavin had been adsorbed. **Table 7.4.1** displays the average atomic concentration percentage of carbon, oxygen and nitrogen in an unmodified and physisorbed riboflavin-modified SPE. High resolution and wide energy survey scans both showed an increase of nitrogen in the physisorbed riboflavin-modified SPE compared to non-modified electrode - 2.48 and 2.21 times more, respectively. This increase is explained by the presence of nitrogen in riboflavin's chemical structure. It is assumed that although the carbon-graphite ink contains nitrogen, the adsorption of riboflavin significantly increased the atomic concentration percentage of nitrogen.

Table 7.4.1 Average atomic concentration percentages of unmodified and physisorbed riboflavin-modified SPE using XPS.

Average atomic concentration percentage (High resolution scans)

Element	**Non-modified SPE**	**Riboflavin-modified SPE**
O 1s	9.26	13.77
N 1s	0.81	2.01
C 1s	89.93	84.22

Average atomic concentration percentage (Wide energy survey scans)

Element	**Non-modified SPE**	**Riboflavin-modified SPE**
O 1s	9.53	10.83
N 1s	0.81	1.79
C 1s	81.93	79.47
Cl 2p	7.74	7.91

7.4.2 Integration within 3D Printed Catheter Hub

The influence of pH on the oxidation peak of the physisorbed riboflavin-modified SPE system was further assessed using various pH BR buffer solutions flushed into the 3D-printed catheter extension. The hub was modified to contain a slot for the screen printed electrode system instead of the two-electrode carbon fibre mesh configuration. As per previous investigations, square wave voltammetry was employed starting at a negative potential sweeping towards a more positive potential, which allows riboflavin to initially be reduced then re-oxidised. **Figure 7.4.4A** displays the distinct oxidation peaks obtained from the voltammetric scans. As the pH decreases, riboflavin's oxidation peak shifts towards a less negative potential. This relationship was found to display a near Nernstian behaviour with a

slope of 61 mV/pH unit (E / V = -0.061 pH - 0.085; N_{total} = 18 (N_{pH} = 6, $N_{scans/pH}$ = 3); R^2 = 0.9979) - analogous to previous result.

As previously mentioned, needleless components of catheters are typically changed every 72 hours [58,390]. This means that the electrode system must be robust enough to go through periodic scanning for up to three days. Robustness was therefore assessed by cycling the electrode system through a series of pH sequences with each sequence starting from a low of pH 3.07 to a high of pH 7.96. Square wave voltammograms of each pH BR buffer was completed in triplicates and the whole process was repeated three times (**Figure 7.4.4B**). An average drift of 31 mV (0.51 pH unit based on a 61 mV per pH shift) was found to have occurred after 54 scans which could possibly be due to hydroxyl ions attacking the oxidised riboflavin which, in turn, showcases a slightly irreversible characteristic. Equally, this could be due to the instability/degradation of the reference electrode. However, it should be noted that only a 12% decrease in peak height was seen after the repetitive cycling.

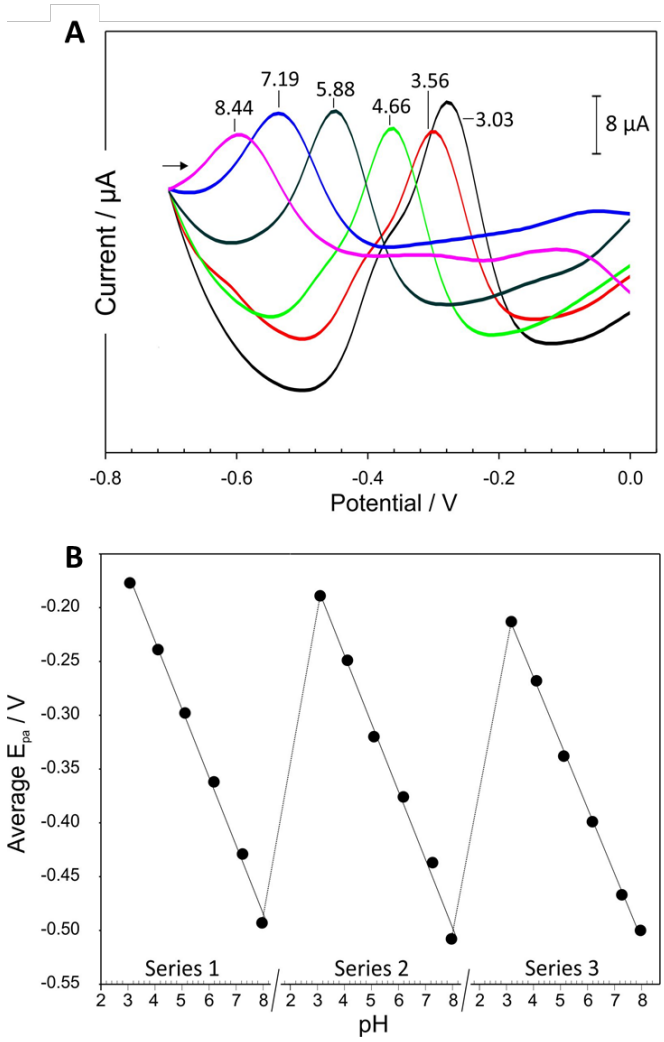

Figure 7.4.4 A) Square wave voltammograms displaying the response of the physisorbed riboflavin-modified anodised SPE system in Britton Robinson buffers of varying pH and B) influence of pH on the oxidation peak potential over three cycles (total of 54 scans with each point representing an average of 3 scans).

Figure 7.4.5 exhibits the representative cyclic voltammograms comparing the response of physisorbed riboflavin-modified SPE against a non-modified electrode in TPN. Analogous to previous chapters, it is also evident that the screen printed electrode is capable of electroanalytical measurements within a chemically complex media. Riboflavin is present in TPN (0.00138 mg/mL) thus explaining the small oxidation peak found using the unmodified SPE. It can be argued that a bare screen printed electrode can be used instead, however, it is evident that the modified riboflavin has a far greater peak response due to the riboflavin already adsorbed on the electrode. It must also be noted that the aim here is for the development of a sensing system that could be used across a range of applications and it is unlikely that riboflavin would be present in every infusion fluid. Hence modifying the electrode provides a generic action independent of the nature of the infusate.

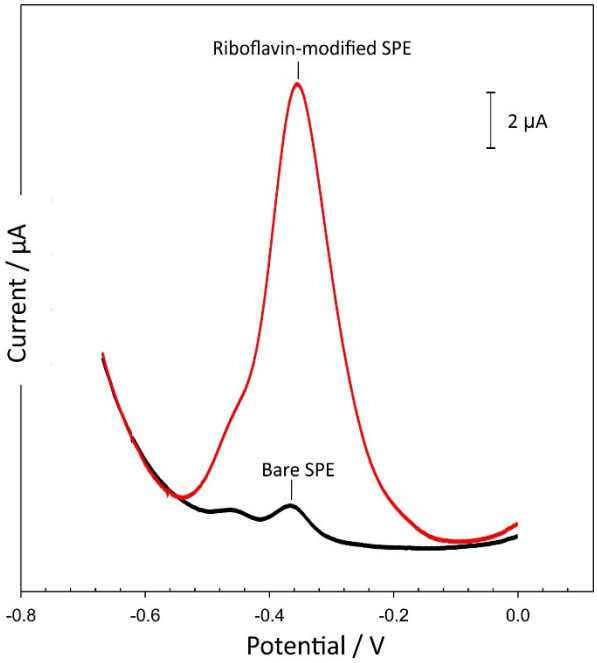

Figure 7.4.5 Square wave voltammograms representing the response of physisorbed riboflavin-modified SPE and unmodified SPE in TPN (20th scan).

Upon repetitive cycling (20 scans) in TPN, the peak potential remained steady (-0.356 V) with only a 4 mV potential drift (0.07 pH units based on the 61 mV/pH unit shift), however the magnitude of the oxidation peak decreased by 23% (**Figure 7.4.6**). Additionally, the modified three-SPE system was also assessed using TPN injected in the catheter extension after triplicate scans in each physiologically relevant pH BR buffer (pH 3.08 to pH 7.43; N_{pH} = 6; N_{total} = 18). The calculated pH was found to be pH 6.14 using the calibration graph from **Figure 7.4.3B** which is in good agreement with the actual TPN pH (pH 5.96). It must be noted that the peak current reduced significantly to only 42% of the original magnitude which does provide a query over the relative stability of the signal/strength of adsorption to the SPE graphite surfaces or the presence of components with the TPN that act to displace the riboflavin – competition for adsorption sites from other components.

Further experiments in ensuring a stronger adsorption of riboflavin is clearly necessary prior to clinical application though it should be recognised that the leaching of riboflavin from the surface would present no risk to the patient and stands in marked contrast to the flavin-phenol system investigated in previous chapters. The use of membranes that would hinder the diffusion of riboflavin out of the electrode could be a solution to the decreasing peak magnitude as well as improve the robustness of the modified electrode.

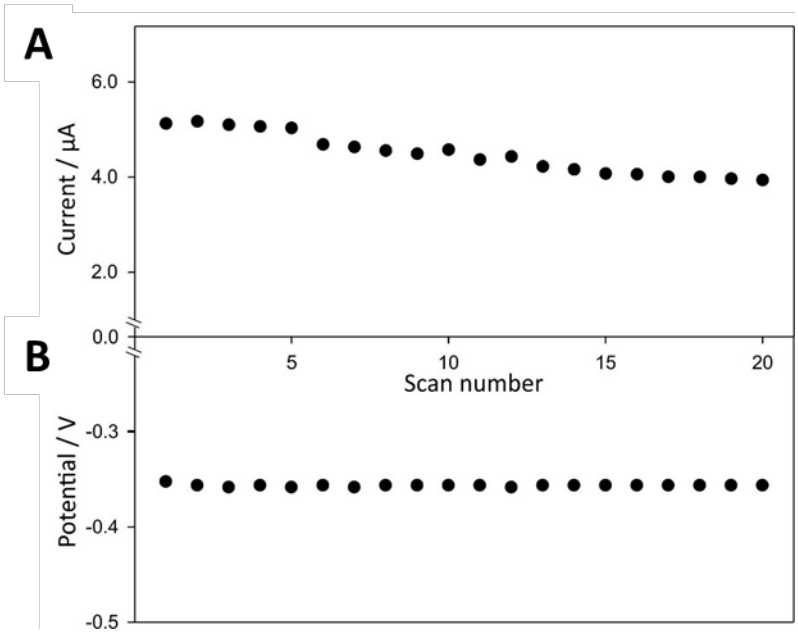

Figure 7.4.6 Variation of A) magnitude and B) potential of the oxidation peak of the physisorbed riboflavin-modified anodised SPE as a result of repetitive square wave scans in TPN (N_{scans} = 20).

With this in mind, the ion permeable Nafion™ membrane was utilised to impede the flow of riboflavin. The polymeric solution was cast on to the riboflavin-modified electrode by dropping a volume (30 µL) enough to cover the surface of the electrode and was left to dry. The resultant electrode was then inserted into TPN and underwent 40 square wave scans. It was noticed that the potential of the first 17 scans continued to fluctuate which may be explained by the fact that the polymer coating was still equilibrating to the pH of TPN. After this however, **Figure 7.4.7** demonstrates that the oxidation peak potential remained constant at around -0.383 mV and the peak height difference had a maximum 5% change with an average magnitude of 2.41 µA after the remaining 23 scans. This would therefore enhance the possibility of using inexpensive and disposable SPEs in existing catheter hub systems to monitor the condition of the line. As per **Figure 7.2.2B**, the slight shift in TPN peak potential could be attributable to the different Ag/AgCl SPE reference electrode used which would have a slightly shifted potential.

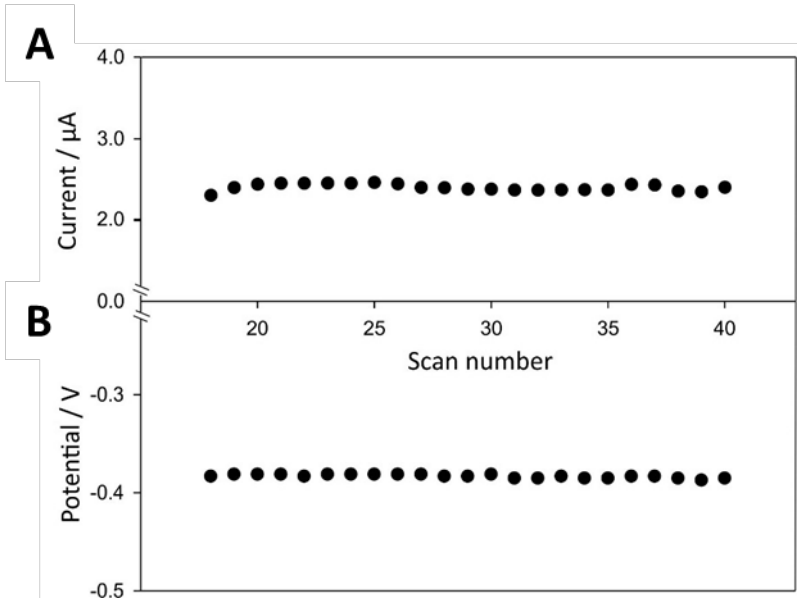

Figure 7.4.7 The effect of repetitive square wave voltammetry scanning in TPN on peak A) height and B) position of the Nafion-coated riboflavin-modified anodised screen printed electrode.

7.5 Hydrogen Peroxide

As mentioned in the introduction to the chapter, riboflavin has the ability to produce reactive oxygen species (superoxide anion, hydrogen peroxide) through catalysing the reduction of dissolved oxygen (**Figure 7.1.1**). Preliminary investigations examining the production of hydrogen peroxide through applying a suitable potential (-0.450 V) to reduce riboflavin (250 µM, pH 7) physisorbed onto a carbon fibre mesh electrode were conducted. A peroxide assay kit (Sigma Aldrich, UK) was used to validate the quantity of peroxide produced via the electrochemical processes. The latter relied on the Fe^{3+}-xylenol orange chromogenic reaction where a purple resultant is produced as Fe^{2+} is oxidised to Fe^{3+} due to the presence of peroxide in the sample (**Figure 7.5.1**) and, as such, the resulting colour intensity is directly proportional to the concentration of the latter [(394)]. **Figure 7.5.2** and **Table 7.5.1** showcases the calibration curve and subsequent calculated peroxide concentrations produced from the electrochemical reduction of riboflavin over varying electrolysis time periods. Each point was completed in duplicate.

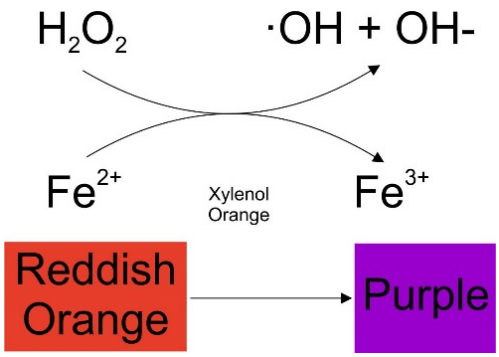

Figure 7.5.1 Simplified Fe^{3+}-xylenol orange reaction scheme in the presence of peroxide.

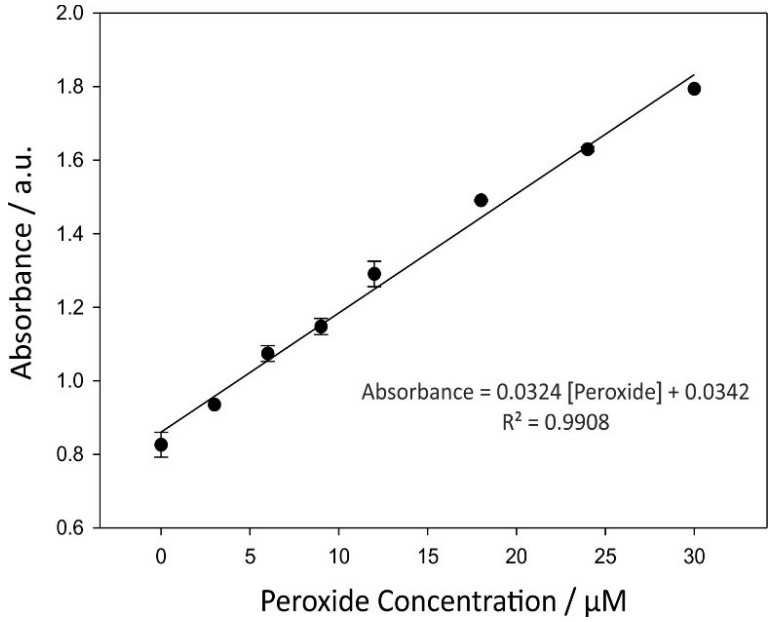

Figure 7.5.2 Linear relationship between hydrogen peroxide concentration and Fe(II)/Fe(III) assay absorbance (λmax = 585 nm) value. Each point is an average of 2 scans and the error bars represent mean standard deviation.

Table 7.5.1 Average absorbance value (λmax = 585 nm) and calculated peroxide concentration following on from electrochemical riboflavin reduction (-0.450 V) physisorbed on anodised carbon fibre mesh electrodes at different time periods.

Time (min)	Average Absorbance	Normalised Absorbance	Calculated Concentration (µM)
0	0.983	0	0
1	1.053	0.070	1.099
3	1.094	0.111	2.298
5	1.657	0.674	18.760
30	1.599	0.616	17.064

As highlighted in **Table 7.5.1**, there is a positive relationship between scan duration and peroxide concentration however it is noteworthy that the system plateaus essentially after 5 minutes with no significant difference recorded after 30 minutes. It is evident however that

employing chronoamperometry reduces riboflavin thus increasing the production of hydrogen peroxide. It is clear that the data presented here is preliminary however time constraints and complications due to the pandemic did not allow further work to be completed. The absorbance data however highlights that the production of hydrogen peroxide is promising. Evidently, further investigations are required to complete the study including, but not limited to, ROS generation within the customised 3D printed hub, its influence on CRBSI-causing microorganisms, the stability of the electrode substrate and the employment of miniaturised potentiostat/electronics, suitable for in situ use, to complete the required electrochemical techniques.

7.6 Conclusions

An inexpensive and disposable pH system, based on carbon fibre mesh and/or screen printed electrode, through the adsorption and manipulation of riboflavin has been described. The use of riboflavin solves the biocompatibility issues of earlier flavin polymer system, as vitamin B2 and its monomers are already present in the body. As observed with the phenolic flavin modifier, the oxidation peak of riboflavin provides an unambiguous signal free from typical interferences that could hinder conventional voltammetric pH measurements (i.e. those employing quinone based systems). Additionally, the system is capable of undergoing repetitive square wave voltammetry cycling in more chemically complex solutions (TPN/laked horse blood) whilst retaining its near Nernstian behaviour. The translation from carbon fibre mesh to screen printed electrodes is a critical advance as the latter would provide a cheaper, more disposable solution where mass production would be easier to achieve.

The proposed systems were also successfully integrated within a custom designed 3D printed needle free connector which in turn can be used as a smart extension that could be readily incorporated into existing CVC lines. The ability of riboflavin to generate hydrogen peroxide was also briefly assessed which suggests that riboflavin-modified carbon electrodes could not only monitor the condition of the line (detect contamination), but also has the potential in eradicating pathogen contamination through the release of reactive oxygen species. Therefore, the smart sensor could ultimately provide a novel, sustainable and efficient method in reducing catheter related bloodstream infection without the need for complex configurations.

Chapter 8

Conclusions and Recommendations for Future Work

8.1 Conclusions

The design, development and deployment of catheters for intravenous therapy can be considered as one of the key milestones that underpin modern healthcare. Catheters provide a bedrock and invaluable pathways for most medical treatments in modern medicine and are responsible for saving countless of patients suffering from various morbidities including but not limited to cancer, kidney failure and intestinal failure. Despite their indispensable benefits, catheters are prone to complications and can act as the gateway for life threatening infections. It is therefore necessary to ensure that the benefits outweigh the limitations prior to inserting an indwelling catheter. The most common drawback is the significant risk of catheter related bloodstream infection which is one of the most ubiquitous nosocomial infection. Currently, the onset of fever and presence of rigors are the primary diagnosis for CRBSI which remains to be highly unspecific, insensitive and unreliable.

Due to various reasons (limited insertion sites, presence of comorbidities, cost, etc.), catheter removal and replacement, although greatly effective, is not the preferred solution to this problem and, as such, a myriad of preventative measures have been researched and implemented throughout the years. The introduction of lock solutions, aseptic/disinfection techniques, barrier caps as well as thorough research on antiseptic impregnation and extensive developments on catheter material have all valuably aided in minimising CRBSI cases yet, they do not represent an infallible route to the effective eradication of the problem as infection, despite many decades of attention, still remains problematic. Some of these techniques provide protection only for a limited period and do not eliminate all contaminating microorganisms. It should also be noted that the use of antibiotics adds on to the ever-increasing risk of pathogen resistance, thus is not a suitable long-term solution. There is therefore a pressing need for the development of a smart sensor system that can be easily integrated into existing catheter lines which can ultimately detect and eradicate pathogen invasion before health-jeopardizing infection occurs. Thus, the suggested smart catheter system described here was developed as a response to that need. Rather than relying on subjective factors and prolonged waiting for clinical results, it is envisaged that employing a sensitive electrochemical sensor could provide a faster diagnostic alternative as well as a more efficient and effective method to eradicate contaminants which would ultimately prevent CRBSI. Furthermore, such system could be used as a conduit for routine and decentralised line monitoring for all patient cohorts.

Carbon is the most common electrode material used in electroanalysis and its modification through electrochemical oxidation is recognised to enhance its ability to perform in various applications. **Chapter 4** detailed the effect of the co-application of ultrasound during anodisation towards the generation of surface functionalities and ultimately its influence on carbon electrode performance. As with silent anodisation alone, ultrasound-aided anodisation increased the electron transfer kinetics of the carbon fibre mesh electrode and has improved its response towards ferrocyanide, effectively altering the irreversible behaviour of an unmodified carbon electrode to a reversible one. Through solely comparing cyclic voltammogram traces of silently anodised and sonoanodised electrode towards ferrocyanide, it was observed that ultrasound simply accelerated the process to which reversibility is achieved and that via the examination on the influence of prolonged anodisation periods (beyond 300 seconds), the latter provided only minimal improvement in the voltammetric response in comparison to the former, thus suggesting ultrasound had a kinetic effect rather than a structural influence. This was then corroborated with the data obtained from Raman spectroscopy which highlighted that the lattice disorder characteristics of sonoanodised electrode was analogous to that of its conventionally anodised counterpart.

However, sonoanodisation significantly enhanced electrode surface hydrophilicity and, through SEM assessments, had a clear influence on the morphology of the carbon fibre, resulting in markedly greater physical deterioration compared to silent oxidation which stands in contrast to the Raman spectra. Additionally, deconvoluted carbon functionality XPS analyses on the C1s and O1s spectra of both normal and ultrasound-aided anodisation revealed that there were major distinct disparities in the population of the C=C/C-C and C-O functional groups between the two conditions, and only diminutive differences were found in the percentage contribution of carboxyl functionalities even with prolonged anodisation. In spite of these discoveries, and with regards to the purpose of this project, sonoanodisation simply sped up the electrochemical processes which occur through silent anodisation alone and, as such, only the latter was used for the rest of the experimental work.

Subsequently, anodised carbon fibre mesh was used as a substrate for a scalable and disposable pH sensitive electrode in **Chapter 5**. A novel flavin-phenol moiety was custom synthesised and was electropolymerised on to the carbon base. Its distinct, hydrogen ion

concentration dependent redox reactions were then exploited as the basis of an electrochemical sensor. Unlike riboflavin, the phenolic flavin derivative can undergo electropolymerisation without damaging the core pH-sensitive flavin group as the presence of the phenol ring allows polymerisation to occur through a radical cation process attacking the phenolic substituent instead. When assessed in physiologically relevant pH BR buffers (pH 2.55 – pH 8.12), the oxidation peaks of the polymer occurred and shifted within the potential range where no other competing signals are present – a prerequisite for electrochemical sensors. The system exhibited a near Nernstian behaviour of 55 mV/pH with minimal drift of only 4 mV upon repetitive cycling. The sensor's ability to detect pH changes was further tested via insertion within a demanding milieu of a kefir-based microbial reactor. The shift in oxidation peak after 51 hours was in correlation with that observed in the less challenging pH BR buffers which suggests its applicability in microbial systems. However, in dormant periods, the presence of biofilm on the electrode surface was evident in the SEM images as well as the nonconformity of the calculated pH against the actual pH measured with a conventional pH probe, which could be problematic in other microbial systems and should therefore be thoroughly considered. However, upon continuous cycling with shorter periods of rest, the peak oxidation potentials soon returned to complement actual pH values.

Carbon loaded polyethylene film was then used as the base of a conductive yet mechanically flexible pH probe in **Chapter 6**. Through raster mode laser ablation, mesh like interfacial carbon pores were exposed where the tracks intersected. The redox active phenolic flavin was again polymerised as the pH sensitive layer and the reagentless system provided unambiguous signals which indirectly measure pH without the need for solution degassing. As with the previous chapter, a near Nernstian behaviour of 60 mV per pH shift was observed over the physiologically relevant pH range of pH 2.55 to pH 8.12. Upon repetitive 90° mechanical bending, it was observed that the oxidation peak height decreased but the signal remained unambiguous and more importantly, the peak potential was constant and unaffected by repetitive bends as well as when the sensor was fixed at a 90° bend. The decrease in signal amplitude was analogous to results obtained from repetitive scanning without flexing and may be explained by the possible loss of the flavin polymer from the electrode surface. The ability to detect pH was further assessed in chemically complex urine samples. With only a maximum pH difference of 0.07 pH units from results achieved via a conventional pH probe, the system proved to be useful in detecting biofluid pH changes without biofouling becoming a challenge. The potential range in which the signals are

observed remained advantageous in this case as it is barren of other competing signals that would be present in biofluids such as tryptophan and tyrosine.

Although there is evident success in employing the novel engineered flavin phenol derivative as the core remit of a pH sensitive sensor, its primary disadvantage in catheter application is the non-biocompatibility of its oligomers. Adverse cytotoxic events could occur upon the event of polymer leaching and, if implemented within a catheter system, this would have a direct route towards the vascular system. Riboflavin, vitamin B2, was therefore used as an alternative in **Chapter 7**. The primary reason for not using the latter initially was its inability to be electropolymerised without affecting the core redox flavin group however, it was observed that upon submersion of electrode into a riboflavin solution (250 μM, pH 7), the vitamin strongly adsorbed onto the electrode surface. The system was then inserted in a custom designed needle free connector hub and a two-electrode configuration was implemented. Riboflavin-modified carbon mesh was employed as the working electrode while a silver coated carbon fibre mesh served as the counter and reference electrode. Oxidation peaks shifted with pH and a near Nernstian behaviour of 58 mV/pH was observed upon repetitive cyclic scanning with a maximum standard error of only 0.005 was calculated. The system was further assessed in kefir inoculated TPN and laked horse blood and distinct, unambiguous riboflavin oxidation peaks were observed in both cases even after 24 hours of electrode immersion in respective solutions. The calculated shifts in pH had minimal discrepancy to those obtained from a commercial probe.

The system was successively translated to a more disposable, inexpensive and easily mass-produced screen printed electrodes. Analogous to previous, a 62 mV per pH shift was observed when integrated within the hub thus again displaying a near Nernstian characteristic. However, upon repetitive cycling, the oxidation peak magnitude decreased significantly and as such the ion permeable Nafion membrane was employed to minimise signal deterioration - only a 5% height decrease was observed after the implementation. Subsequently, chronoamperometry was employed to induce the reduction of riboflavin to release hydrogen peroxide. Prolonged reduction meant that a greater concentration of reactive oxygen species was produced. This mechanism could potentially be exploited to eliminate catheter contaminating pathogens and ultimately, significantly minimise the risk of catheter-related bloodstream infection. However, it is important to recognise the preliminary nature of the peroxide results and much more work is required to fully appraise

the efficacy of the methodology. Nevertheless, the dual capability of detecting the presence of pathogens as well as eradicating them suggests the system's marked advantages over existing preventative measures.

8.2 Recommendations for Future Work

The main scope of this work was to develop a smart sensor that can be readily integrated within existing catheter systems for the prevention of catheter related bloodstream infection. However, the simplicity, scalability and disposability of the suggested system can be easily transferred to other applications including smart bandages, ostomy applications and other invasive/indwelling medical devices requiring the detection and eradication of pathogens. The next key viable step would be the development of a miniscule, portable potentiostat that would allow autonomous, periodic monitoring of the line condition. The addition and implementation of such a device would minimise intervention beyond the initial placement and ultimately alert the relevant medical personnel if a shift in local pH, due to the onset of biofilm formation, is detected. It is envisaged that early intervention would significantly minimise the risk of bloodstream infection, reduce economic burden relating to CRBSI and more importantly, improve patient outcome. Although the work investigated here focused on the development of the sensor rather than the development and implementation of a miniature potentiostat, it is necessary for the latter to be investigated. In view of the ever-growing advancements in miniaturised electrical components as well as the pressing need for portable smart systems, the production of such a device is undoubtedly anticipated.

Further modification on the suggested catheter hub could also be studied where the focus would be on the elimination of gaps and dead spaces as well as the use of other manufacturing methods that could improve the final design of the hub. The flow of pertinent solutions including total parenteral nutrition and lock solutions through the hub and smart electrode configuration should also be thoroughly investigated. Eddie currents and retention of fluid (i.e. blood) that could encourage pathogen growth should be avoided and, as such, hub modifications may be necessary.

Surface fouling is an inevitable challenge for devices developed to function within complex biological fluids as it could eventually significantly decrease the accuracy and lifespan of the sensor. In this application however, central venous catheter hubs are expected to be replaced every 72 hours and it was evident that the proposed system, through continuous

cycling of up to 63 scans from pH 3 to pH 8, remained to produce reproducible, sensitive and distinct signals with minimal potential drift. It is therefore envisaged that such configuration could last beyond the conventional lifetime of a needle free connector thus avoiding further manipulation. However, amendments through the addition of size sensitive polymers could be further assessed to prevent polymer leaking specifically for the physisorbed riboflavin systems where the loss of redox core could occur at a faster rate.

Moreover, the sensor's ability to detect pathogen growth through pH changes should be further challenged via investigations involving microbiological methods. By culturing common CRBSI-causing microorganisms (*S. epidermidis, S. aureus, P. aeruginosa*, etc.) in normal catheter solutions and detecting pH changes using the suggested sensor configuration, the applicability of the device in real life situations could be assessed. Additionally, this could further assess the correlation between shift in pH and the presence of pathogens in needle free catheter hubs. In depth evaluation of the release of reactive oxygen species from riboflavin and its ability to eradicate aforementioned microbes could offer significant advantages and are potential directions for future development of the system described here. Nonetheless, the applicability of the pH sensitive sensor has been clearly demonstrated through assessments within suitable complex solutions of TPN and laked horse blood. Evidently, the sensing rationale could act as a vital stepping stone towards the development and manufacture of novel technologies that could be regularly used in clinical practice. The materials used here are disposable, inexpensive, readily adaptable for mass manufacturing and are therefore economically viable for implementation within the cost-conscious healthcare industry. Despite the considerable advances in miniaturised pH sensitive probes over recent years, this work provides invaluable research which stands at the forefront of novel and clinically applicable smart sensor systems.

References

1. WHO. WHO | The burden of health care-associated infection worldwide [Internet]. 2011 [cited 2020 Jan 20]. Available from: https://www.who.int/gpsc/country_work/burden_hcai/en/

2. Center for Disease Control and Prevention. Bloodstream Infection Event (Central Line-Associated Bloodstream Infection and Non-central line-associated Bloodstream Infection). Centers Dis Control (CDC)/National Healthc Saf Netw [Internet]. 2016 [cited 2020 Jan 21];(January):1–32. Available from: http://www.cdc.gov/nhsn/PDFs/pscM

3. Gahlot R, Nigam C, Kumar V, Yadav G, Anupurba S. Catheter-related bloodstream infections. Int J Crit Illn Inj Sci [Internet]. 2014 Apr [cited 2017 Dec 7];4(2):162–7. Available from: http://www.ncbi.nlm.nih.gov/pubmed/25024944

4. Drews FA, Bakdash JZ, Gleed JR. Improving central line maintenance to reduce central line-associated bloodstream infections. Am J Infect Control [Internet]. 2017 Nov;45(11):1224–30. Available from: https://doi.org/10.1016/j.ajic.2017.05.017

5. Raad I, Hanna H, Maki D. Intravascular catheter-related infections: advances in diagnosis, prevention, and management. Lancet Infect Dis. 2007 Oct 1;7(10):645–57.

6. Pronovost P, Needham D, Berenholtz S, Sinopoli D, Chu H, Cosgrove S, et al. An Intervention to Decrease Catheter-Related Bloodstream Infections in the ICU. N Engl J Med [Internet]. 2006 Dec 28 [cited 2018 May 6];355(26):2725–32. Available from: http://www.nejm.org/doi/abs/10.1056/NEJMoa061115

7. Dimick JB, Pelz RK, Consunji R, Swoboda SM, Hendrix CW, Lipsett PA. Increased Resource Use Associated With Catheter-Related Bloodstream Infection in the Surgical Intensive Care Unit. Arch Surg [Internet]. 2001 Feb 1 [cited 2018 May 6];136(2):229–34. Available from: http://archsurg.jamanetwork.com/article.aspx?doi=10.1001/archsurg.136.2.229

8. Rello J, Ochagavia A, Sabanes E, Roque M, Mariscal D, Reynaga E, et al. Evaluation of Outcome of Intravenous Catheter-related Infections in Critically Ill Patients. Am J Respir Crit Care Med [Internet]. 2000 Sep 14 [cited 2018 May 6];162(3):1027–30. Available from: http://www.atsjournals.org/doi/abs/10.1164/ajrccm.162.3.9911093

9. Gominet M, Compain F, Beloin C, Lebeaux D. Central venous catheters and biofilms: where do we stand in 2017? Apmis. 2017;125(4):365–75.

10. Chauhan A, Lebeaux D, Ghigo JM, Beloin C. Full and broad-spectrum in vivo eradication of catheter-associated biofilms using gentamicin-EDTA antibiotic lock therapy. Antimicrob Agents Chemother. 2012;56(12):6310–8.

11. Lebeaux D, Leflon-Guibout V, Ghigo J-M, Beloin C. In vitro activity of gentamicin, vancomycin or amikacin combined with EDTA or L-arginine as lock therapy against a wide spectrum of biofilm-forming clinical strains isolated from catheter-related infections. J Antimicrob Chemother [Internet]. 2015 Feb 23 [cited 2018 May 25];70(6):1704–12. Available from: https://academic.oup.com/jac/article-lookup/doi/10.1093/jac/dkv044

12. Alonso B, Pérez-Granda MJ, Rodríguez-Huerta A, Rodríguez C, Bouza E, Guembe M. The optimal ethanol lock therapy regimen for treatment of biofilm-associated catheter infections: an in-vitro study. J Hosp Infect. 2018;100.

13. Balestrino D, Souweine B, Charbonnel N, Lautrette A, Aumeran C, Traore O, et al. Eradication of microorganisms embedded in biofilm by an ethanol-based catheter lock solution. Nephrol Dial Transplant [Internet]. 2009 Oct 1 [cited 2018 May 15];24(10):3204–9. Available from: https://academic.oup.com/ndt/article-lookup/doi/10.1093/ndt/gfp187

14. Raad I, Chaftari AM, Zakhour R, Jordan M, Al Hamal Z, Jiang Y, et al. Successful salvage of central venous catheters in patients with catheter-related or central line-associated bloodstream infections by using a catheter lock solution consisting of minocycline, EDTA, and 25% ethanol. Antimicrob Agents Chemother. 2016;60(6):3426–32.

15. Wales PW, Kosar C, Carricato M, De Silva N, Lang K, Avitzur Y. Ethanol lock therapy to reduce the incidence of catheter-related bloodstream infections in home parenteral nutrition patients with intestinal failure: Preliminary experience. J Pediatr Surg [Internet]. 2011;46(5):951–6. Available from: http://dx.doi.org/10.1016/j.jpedsurg.2011.02.036

16. Souweine B, Lautrette A, Gruson D, Canet E, Klouche K, Argaud L, et al. Ethanol lock and risk of hemodialysis catheter infection in critically III patients a randomized controlled trial. Am J Respir Crit Care Med. 2015;191(9):1024–32.

17. Winnett G, Nolan J, Miller M, Ashman N. Trisodium citrate 46.7% selectively and safely reduces staphylococcal catheter-related bacteraemia. Nephrol Dial Transplant [Internet]. 2008 Nov 1 [cited 2018 May 21];23(11):3592–8. Available from: https://academic.oup.com/ndt/article-lookup/doi/10.1093/ndt/gfn299

18. Tribler S, Brandt CF, Petersen AH, Petersen JH, Fuglsang KA, Staun M, et al. Taurolidine-citrate-heparin lock reduces catheter-related bloodstream infections in intestinal failure patients dependent on home parenteral support: A randomized, placebo-controlled trial. Am J Clin Nutr. 2017;106(3):839–48.

19. Touré A, Lauverjat M, Peraldi C, Boncompain-Gerard M, Gelas P, Barnoud D, et al. Taurolidine lock solution in the secondary prevention of central venous catheter-associated bloodstream infection in home parenteral nutrition patients. Clin Nutr [Internet]. 2012 Aug 1 [cited 2018 May 23];31(4):567–70. Available from: https://www.sciencedirect.com/science/article/pii/S026156141200039?via%3Dihub

20. Zhang L, Cao S, Marsh N, Ray-Barruel G, Flynn J, Larsen E, et al. Infection risks associated with peripheral vascular catheters. Vol. 17, Journal of Infection Prevention. 2016. p. 207–13.

21. Frasca D, Dahyot-Fizelier C, Mimoz O. Prevention of central venous catheter-related infection in the intensive care unit. Crit Care [Internet]. 2010 Mar 9 [cited 2020 Feb 12];14(2):212. Available from: http://ccforum.biomedcentral.com/articles/10.1186/cc8853

22. Feneley RCL, Hopley IB, Wells PNT. Urinary catheters: history, current status, adverse events and research agenda. J Med Eng Technol [Internet]. 2015;39(8):459–70. Available from: http://www.tandfonline.com/doi/full/10.3109/03091902.2015.1085600

23. Barsoum N, Kleeman C. Now and Then, the History of Parenteral Fluid Administration. Am J Nephrol [Internet]. 2002 Jul [cited 2020 Feb 24];22(2–3):284–9. Available from: https://www.karger.com/Article/FullText/63775

24. Labriola L. Antibiotic locks for the treatment of catheter-related blood stream infection: Still more hope than data. Semin Dial [Internet]. 2019 Sep 1 [cited 2020 Feb 24];32(5):402–5. Available from: http://www.ncbi.nlm.nih.gov/pubmed/30950116

25. Gow KW, Tapper D, Hickman RO. Between the lines: The 50th anniversary of long-

term central venous catheters. Am J Surg [Internet]. 2017 May 1 [cited 2020 Feb 24];213(5):837–48. Available from: http://www.ncbi.nlm.nih.gov/pubmed/28364951

26. White RJ. An historical overview of the use of silver in wound management. Br J Nurs. 2001 Aug 9;10(Sup4):S3–8.

27. Farhud DD, Yeganeh MZ. A brief history of human blood groups. Iran J Public Health. 2013 Jan 1;42(1):1–6.

28. Rivera AM, Strauss KW, Van Zundert A, Mortier E. The history of peripheral intravenous catheters : How little plastic tubes revolutionized medicine. Acta Anaesthesiol Belg. 2005 Sep;56(3):271–82.

29. Future Market Insights. Central Venous Catheter Market- Global Industry Analysis, Size and Forecast, 2016 to 2026 [Internet]. Future Market Insights. 2016 [cited 2018 May 6]. Available from: https://www.futuremarketinsights.com/reports/central-venous-catheter-market

30. Raad I. Intravascular-catheter-related infections. Lancet. 1998;351(9106):893–8.

31. Dougherty L. Central venous focus access devices. Nurs Stand [Internet]. 2000 [cited 2018 May 11];14(43):45–50. Available from: https://rcni.com/sites/rcn_nspace/files/ns2000.07.14.43.45.c2876.pdf

32. Pérez-Zárate P, Aragón-Piña A, Soria-Guerra RE, González-Amaro AM, Pérez-Urizar J, Pérez-González LF, et al. Risk factors and biofilm detection on central venous catheters of patients attended at tertiary hospital. Micron. 2015;78:33–9.

33. Timsit JF. What is the best site for central venous catheter insertion in critically ill patients? Crit Care. 2003 Dec;7(6):397–9.

34. Smith RN, Nolan JP. Central venous catheters [Internet]. Vol. 347, BMJ (Online). British Medical Journal Publishing Group; 2013 [cited 2018 May 8]. p. f6570. Available from: http://www.ncbi.nlm.nih.gov/pubmed/24217269

35. Kirby DF, Corrigan ML, Hendrickson E, Emery DM. Overview of Home Parenteral Nutrition: An Update. Nutr Clin Pract. 2017;32(6):739–52.

36. Tse A, Schick MA. Central line placement. StatPearls. 2019.

37. Bannon MP, Heller SF, Rivera M. Anatomic considerations for central venous

cannulation. Risk Manag Healthc Policy. 2011;4:27–39.

38. Anthony J. Busti M. Seldinger Technique for Intravenous (IV) Line Placement [Internet]. Evidence-Based Medicine. 2015 [cited 2018 May 29]. p. 4. Available from: https://www.ebmconsult.com/articles/seldinger-technique-intravenous-iv-placement

39. Haque M, Sartelli M, McKimm J, Bakar MA. Health care-associated infections – An overview. Vol. 11, Infection and Drug Resistance. Dove Medical Press Ltd.; 2018. p. 2321–33.

40. Nuvials X, Palomar M, Alvarez-Lerma F, Olaechea P, Otero S, Uriona S, et al. Health-care associated infections. Patient characteristics and influence on the clinical outcome of patients admitted to icu. envin-helics registry data. Intensive Care Med Exp. 2015 Dec;3(S1).

41. Johnson NB, Hayes LD, Brown K, Hoo EC, Ethier KA. CDC National Health Report: leading causes of morbidity and mortality and associated behavioral risk and protective factors--United States, 2005-2013. MMWR Surveill Summ. 2014 Oct 31;63:3–27.

42. European Centre for Disease Prevention and Control. Point prevalence survey of healthcare associated infections and antimicrobial use in European hospitals 2011–2012 [Internet]. 2013 [cited 2020 Jan 20]. Available from: https://www.ecdc.europa.eu/sites/default/files/media/en/healthtopics/Healthcare-associated_infections/point-prevalence-survey/Documents/healthcare-associated-infections-antimicrobial-use-PPS-summary.pdf

43. Kärki T, Plachouras D, Cassini A, Suetens C. Burden of healthcare-associated infections in European acute care hospitals. Wiener Medizinische Wochenschrift. 2019 Feb 1;169:3–5.

44. Khan HA, Baig FK, Mehboob R. Nosocomial infections: Epidemiology, prevention, control and surveillance. Vol. 7, Asian Pacific Journal of Tropical Biomedicine. Hainan Medical University; 2017. p. 478–82.

45. Shah H, Bosch W, Thompson KM, Hellinger WC. Intravascular Catheter-Related Bloodstream Infection. The Neurohospitalist [Internet]. 2013 Jul [cited 2018 May 9];3(3):144–51. Available from: https://www.ncbi.nlm.nih.gov/pmc/articles/PMC3805442/pdf/10.1177_194187441

3476043.pdf

46. O'Grady NP, Mary A, Patchen DE, Gerberding JL, Heard SO, Maki DG, et al. Morbidity and Mortality Weekly Report Centers for Disease Control and Prevention. 2002 [cited 2018 May 23];9(51). Available from: https://www.cdc.gov/mmwr/PDF/rr/rr5110.pdf

47. Reitzel RA, Rosenblatt J, Hirsh-Ginsberg C, Murray K, Chaftari A-M, Hachem R, et al. In Vitro Assessment of the Antimicrobial Efficacy of Optimized Nitroglycerin-Citrate-Ethanol as a Nonantibiotic, Antimicrobial Catheter Lock Solution for Prevention of Central Line-Associated Bloodstream Infections. Antimicrob Agents Chemother [Internet]. 2016 Sep 1 [cited 2018 May 21];60(9):5175–81. Available from: http://www.ncbi.nlm.nih.gov/pubmed/27297475

48. Tacconelli E, Smith G, Hieke K, Lafuma A, Bastide P. Epidemiology, medical outcomes and costs of catheter-related bloodstream infections in intensive care units of four European countries: literature- and registry-based estimates. J Hosp Infect [Internet]. 2009 Jun 1 [cited 2018 May 23];72(2):97–103. Available from: https://www.sciencedirect.com/science/article/pii/S0195670109000048?_rdoc=1&_fmt=high&_origin=gateway&_docanchor=&md5=b8429449ccfc9c30159a5f9aeaa92ffb

49. Eggimann P, Pittet D. Overview of catheter-related infections with special emphasis on prevention based on educational programs. Clin Microbiol Infect [Internet]. 2002 May 1 [cited 2018 May 16];8(5):295–309. Available from: https://www.sciencedirect.com/science/article/pii/S1198743X1462797X

50. A report from the NNIS System. National Nosocomial Infections Surveillance (NNIS) System Report, data summary from January 1992 through June 2004, issued October 2004. Am J Infect Control [Internet]. 2004 Dec 1 [cited 2018 May 11];32(8):470–85. Available from: https://www.sciencedirect.com/science/article/pii/S0196655304005425?via%3Dihub

51. Fletcher S. Catheter-related bloodstream infection. Contin Educ Anaesthesia, Crit Care Pain [Internet]. 2005;5(2):49–51. Available from: https://academic.oup.com/bjaed/article-lookup/doi/10.1093/bjaceaccp/mki011

52. Lorente L, Henry C, Martín MM, Jiménez A, Mora ML. Central venous catheter-related infection in a prospective and observational study of 2,595 catheters. 2005 [cited

2018 May 9]; Available from: http://ccforum.com/content/9/6/R631

53. Merrer J, De Jonghe B, Golliot F, Lefrant JY, Raffy B, Barre E, et al. Complications of femoral and subclavian venous catheterization in critically III patients: A randomized controlled trial. J Am Med Assoc. 2001 Aug 8;286(6):700–7.

54. Parienti JJ, Thirion M, Mégarbane B, Souweine B, Ouchikhe A, Polito A, et al. Femoral vs jugular venous catheterization and risk of nosocomial events in adults requiring acute renal replacement therapy: A randomized controlled trial. JAMA - J Am Med Assoc [Internet]. 2008 May 28 [cited 2020 Feb 12];299(20):2413–22. Available from: http://www.ncbi.nlm.nih.gov/pubmed/18505951

55. Goetz AM, Wagener MM, Miller JM, Muder RR. Risk of Infection Due to Central Venous Catheters: Effect of Site of Placement and Catheter Type. Infect Control Hosp Epidemiol. 1998 Nov;19(11):842–5.

56. O'Grady NP, Alexander M, Burns LA, Dellinger EP, Garland J, Heard SO, et al. Guidelines for the prevention of intravascular catheter-related infections. Clin Infect Dis. 2011 May 1;52(9):e162–93.

57. Templeton A, Schlegel M, Fleisch F, Rettenmund G, Schöbi B, Henz S, et al. Multilumen central venous catheters increase risk for catheter-related bloodstream infection: Prospective surveillance study. Infection [Internet]. 2008 Aug [cited 2020 Feb 12];36(4):322–7. Available from: https://link.springer.com/article/10.1007%2Fs15010-008-7314-x#citeas

58. O'Grady NP, Alexander M, Burns LA, Patchen Dellinger E, Garland J, Heard SO, et al. Guidelines for the Prevention of Intravascular Catheter-Related Infections, 2011. Clin Infect Dis [Internet]. 2011 [cited 2018 May 9];52(9):e162–93. Available from: https://www.cdc.gov/infectioncontrol/guidelines/pdf/bsi/bsi-guidelines-H.pdf

59. Trerotola SO, Kuhn-Fulton J, Johnson MS, Shah H, Ambrosius WT, Kneebone PH. Tunneled infusion catheters: Increased incidence of symptomatic venous thrombosis after subclavian versus internal jugular venous access. Radiology [Internet]. 2000 Oct [cited 2020 Feb 12];217(1):89–93. Available from: http://www.ncbi.nlm.nih.gov/pubmed/11012428

60. Schillinger F, Schillinger D, Montagnac R, Milcent T. Post catheterisation vein stenosis in haemodialysis: Comparative angiographic study of 50 subclavian and 50 internal jugular accesses. Nephrol Dial Transplant. 1991;6(10):722–4.

61. Barrett N, Spencer S, Mclovor J, Brown EA. Subclavian Stenosis: A Major Complication of Subclavian Dialysis Catheters. Nephrol Dial Transplant [Internet]. 1988 Jan 1 [cited 2020 Feb 12];3(4):423–5. Available from: https://academic.oup.com/ndt/article/1806660/Subclavian

62. Chernecky C, Waller J. In vitro comparisons of two antimicrobial intravenous connectors. Clin Nurs Res [Internet]. 2011 Feb [cited 2020 Feb 21];20(1):101–9. Available from: http://www.ncbi.nlm.nih.gov/pubmed/20709995

63. Moureau NL, Flynn J. Disinfection of Needleless Connector Hubs: Clinical Evidence Systematic Review. Nurs Res Pract. 2015;2015:1–20.

64. Hadaway L. Needleless connectors: Improving practice, reducing risks. JAVA - J Assoc Vasc Access. 2011 Aug 8;16(1):20–4.

65. Hadaway L, Richardson D. Needleless connectors: A primer on terminology. J Infus Nurs. 2010;33(1):22–31.

66. Curran E. Needleless connectors: the vascular access catheter's microbial gatekeeper. J Infect Prev. 2016 Sep 1;17(5):234–40.

67. Hull GJ, Moureau NL, Sengupta S. Quantitative assessment of reflux in commercially available needle-free IV connectors. J Vasc Access. 2018;19(1):12–22.

68. Khanna V, Mukhopadhayay C, K. E. V, Verma M, Dabke P. Evaluation of Central Venous Catheter Associated Blood Stream Infections: A Microbiological Observational Study. J Pathog. 2013;2013:1–6.

69. Holroyd JL, Vasilopoulos T, Rice MJ, Rand KH, Fahy BG. Incidence of central venous catheter hub contamination. J Crit Care [Internet]. 2017 Jun 1 [cited 2018 Nov 13];39:162–8. Available from: https://www.sciencedirect.com/science/article/pii/S0883944116306797?via%3Dihub

70. Pandit P, Sahni AK, Grover N, Dudhat V, Das NK, Biswas AK. Catheter-related blood stream infections: prevalence, risk factors and antimicrobial resistance pattern. Med J Armed Forces India. 2019 Oct 15;

71. Jayne MB, Bellknap DC, Flournoy DJ. The relationship of immunity and nutrition to the acquisition of methicillin-resistant Staphylococcus aureus. J Natl Med Assoc [Internet]. 1991;83(7):593–9. Available from:

http://www.ncbi.nlm.nih.gov/entrez/query.fcgi?cmd=Retrieve&db=PubMed&dopt=Citation&list_uids=1920516

72. Nair S, Ramaswamy R, Corpuz M. Central Venous Catheter Infections Identification of High-Risk Patients. Infect Dis Clin Pract. 1997;6(5):334–9.

73. M.G. B, J. V, L. T. Parenteral nutrition as a risk factor for central venous catheter-related infection. J Parenter Enter Nutr [Internet]. 2005;29(5):367–73. Available from: http://ovidsp.ovid.com/ovidweb.cgi?T=JS&PAGE=reference&D=emed10&NEWS=N&AN=44296705

74. Gonzalez-Hernandez J, Daoud Y, Styers J, Journeycake JM, Channabasappa N, Piper HG. Central venous thrombosis in children with intestinal failure on long-term parenteral nutrition. J Pediatr Surg [Internet]. 2016;51(5):790–3. Available from: http://dx.doi.org/10.1016/j.jpedsurg.2016.02.024

75. Santarpia L, Buonomo A, Pagano MC, Alfonsi L, Foggia M, Mottola M, et al. Central venous catheter related bloodstream infections in adult patients on home parenteral nutrition: Prevalence, predictive factors, therapeutic outcome. Clin Nutr [Internet]. 2016;35(6):1394–8. Available from: http://dx.doi.org/10.1016/j.clnu.2016.03.009

76. Dibb MJ, Abraham A, Chadwick PR, Shaffer JL, Teubner A, Carlson GL, et al. Central venous catheter salvage in home parenteral nutrition catheter-related bloodstream infections: Long-term safety and efficacy data. J Parenter Enter Nutr. 2016;40(5):699–704.

77. Duesing LA, Fawley JA, Wagner AJ. Central Venous Access in the Pediatric Population with Emphasis on Complications and Prevention Strategies. Nutr Clin Pract. 2016;31(4):490–501.

78. Marcos M, Soriano A, Iñurrieta A, Martínez JA, Romero A, Cobos N, et al. Changing epidemiology of central venous catheter-related bloodstream infections: Increasing prevalence of Gram-negative pathogens. J Antimicrob Chemother. 2011;66(9):2119–25.

79. Raad I, Hachem R, Hanna H, Bahna P, Chatzinikolaou I, Fang X, et al. Sources and outcome of bloodstream infections in cancer patients: the role of central venous catheters. Eur J Clin Microbiol Infect Dis [Internet]. 2007 Jul 24 [cited 2018 May 9];26(8):549–56. Available from: http://link.springer.com/10.1007/s10096-007-0320-6

80. Lake JG, Weiner LM, Milstone AM, Saiman L, Magill SS, See I. Pathogen distribution and antimicrobial resistance among pediatric healthcare-associated infections reported to the National Healthcare Safety Network, 2011-2014. Infect Control Hosp Epidemiol. 2018 Jan 1;39(1):1–11.

81. Sadoyma G, Filho AG, Gontijo Filho PP. Central venous catheter-related bloodstream infection caused by Staphylococcus aureus: Microbiology and risk factors. Brazilian J Infect Dis. 2006 Apr;10(2):100–6.

82. Donlan RM. Biofilms: Microbial life on surfaces. Emerg Infect Dis. 2002 Sep;8(9):881–90.

83. DiGIOVINE B, CHENOWETH C, WATTS C, HIGGINS M. The Attributable Mortality and Costs of Primary Nosocomial Bloodstream Infections in the Intensive Care Unit. Am J Respir Crit Care Med [Internet]. 1999 Sep 14 [cited 2018 May 9];160(3):976–81. Available from: http://www.atsjournals.org/doi/abs/10.1164/ajrccm.160.3.9808145

84. Chandra J, Kuhn DM, Mukherjee PK, Hoyer LL, McCormick T, Ghannoum MA. Biofilm formation by the fungal pathogen Candida albicans: development, architecture, and drug resistance. J Bacteriol [Internet]. 2001 Sep 15 [cited 2018 May 9];183(18):5385–94. Available from: http://www.ncbi.nlm.nih.gov/pubmed/11514524

85. Spoering AL, Lewis K. Biofilms and Planktonic Cells of Pseudomonas aeruginosa Have Similar Resistance to Killing by Antimicrobials. J Bacteriol [Internet]. 2001 [cited 2018 May 9];183(23):6746–51. Available from: https://www.ncbi.nlm.nih.gov/pmc/articles/PMC95513/pdf/jb2301006746.pdf

86. Rittmann BE. Biofilms, active substrata, and me. Water Res [Internet]. 2018 Apr [cited 2018 May 9];132:135–45. Available from: http://linkinghub.elsevier.com/retrieve/pii/S0043135417310382

87. Rabin N, Zheng Y, Opoku-Temeng C, Du Y, Bonsu E, Sintim HO. Medicinal Chemistry Biofilm formation mechanisms and targets for developing antibiofilm agents. Futur Med Chem [Internet]. 2015 [cited 2018 May 11];7(4):493–512. Available from: https://www.future-science.com/doi/pdf/10.4155/fmc.15.6

88. Jamal M, Ahmad W, Andleeb S, Jalil F, Imran M, Nawaz MA, et al. Bacterial biofilm and associated infections. J Chin Med Assoc [Internet]. 2018 Jan 1 [cited 2018 May 23];81(1):7–11. Available from: http://www.ncbi.nlm.nih.gov/pubmed/29042186

89. Donlan RM. Biofilm Formation: A Clinically Relevant Microbiological Process. 2001;33.

90. Kaplan JB. Biofilm dispersal: mechanisms, clinical implications, and potential therapeutic uses. J Dent Res [Internet]. 2010 Mar [cited 2018 May 11];89(3):205–18. Available from: http://www.ncbi.nlm.nih.gov/pubmed/20139339

91. Carratalà J. The antibiotic-lock technique for therapy of 'highly needed' infected catheters. Clin Microbiol Infect [Internet]. 2002 May 1 [cited 2018 May 30];8(5):282–9. Available from: https://www.sciencedirect.com/science/article/pii/S1198743X14627956

92. Cunningham AB, Lennox JE, Ross RJ. Biofilms: The hypertextbook [Internet]. 2008 [cited 2018 May 25]. Available from: http://biofilmbook.hypertextbookshop.com/public_version/contents/chapters/chapter002/section003/blue/page002.html

93. Lee K-H, Park SJ, Choi S, Uh Y, Park JY, Han K-H. The Influence of Urinary Catheter Materials on Forming Biofilms of Microorganisms. J Bacteriol Virol [Internet]. 2017 Mar 1 [cited 2018 May 9];47(1):32. Available from: https://synapse.koreamed.org/DOIx.php?id=10.4167/jbv.2017.47.1.32

94. Dantas LC de M, Silva-Neto JP da, Dantas TS, Naves LZ, Neves FD das, Mota AS da. Bacterial Adhesion and Surface Roughness for Different Clinical Techniques for Acrylic Polymethyl Methacrylate. Int J Dent [Internet]. 2016 [cited 2020 Jul 6];2016. Available from: /pmc/articles/PMC4969518/?report=abstract

95. Safdar N, Maki DG. Inflammation at the insertion site is not predictive of catheter-related bloodstream infection with short-term, noncuffed central venous catheters. Crit Care Med. 2002 Dec 1;30(12):2632–5.

96. Vanholder R, Canaud B, Fluck R, Jadoul M, Labriola L, Marti-Monros A, et al. Catheter-related blood stream infections (CRBSI): a European view. Sci Nephrol Dial Transpl. 2006;312(25):212–7.

97. Mermel LA, Allon M, Bouza E, Craven DE, Flynn P, O'Grady NP, et al. Clinical practice guidelines for the diagnosis and management of intravascular catheter-related infection: 2009 update by the Infectious Diseases Society of America. Clin Infect Dis [Internet]. 2009 Jul 1 [cited 2020 Feb 22];49(1):1–45. Available from: https://academic.oup.com/cid/article/49/1/1/369414

98. Peters BM, Ward RM, Rane HS, Lee SA, Noverr MC. Efficacy of Ethanol against Candida albicans and Staphylococcus aureus Polymicrobial Biofilms. Antimicrob Agents Chemother [Internet]. 2013 [cited 2018 May 15];57(1):74–82. Available from: https://www.ncbi.nlm.nih.gov/pmc/articles/PMC3535989/pdf/zac74.pdf

99. Bleasdale SC, Trick WE, Gonzalez IM, Lyles RD, Hayden MK, Weinstein RA. Effectiveness of chlorhexidine bathing to reduce catheter-associated bloodstream infections in medical intensive care unit patients. Arch Intern Med [Internet]. 2007 Oct 22 [cited 2020 Feb 12];167(19):2073–9. Available from: http://www.ncbi.nlm.nih.gov/pubmed/17954801

100. Munoz-Price LS, Hota B, Stemer A, Weinstein RA. Prevention of Bloodstream Infections by Use of Daily Chlorhexidine Baths for Patients at a Long-Term Acute Care Hospital. Infect Control Hosp Epidemiol [Internet]. 2009 Nov [cited 2020 Feb 12];30(11):1031–5. Available from: http://www.ncbi.nlm.nih.gov/pubmed/19751155

101. Popovich KJ, Hota B, Hayes R, Weinstein RA, Hayden MK. Effectiveness of Routine Patient Cleansing with Chlorhexidine Gluconate for Infection Prevention in the Medical Intensive Care Unit. Infect Control Hosp Epidemiol [Internet]. 2009 Oct [cited 2020 Feb 12];30(10):959–63. Available from: http://www.ncbi.nlm.nih.gov/pubmed/19712033

102. Devries M, Mancos PS, Valentine MJ. Reducing bloodstream infection risk in central and peripheral intravenous lines: Initial data on passive intravenous connector disinfection. JAVA - J Assoc Vasc Access. 2014;19(2):87–93.

103. Menyhay SZ, Maki DG. Preventing central venous catheter-associated bloodstream infections: Development of an antiseptic barrier cap for needleless connectors. Am J Infect Control. 2008 Dec 1;36(10):S174.e1-S174.e5.

104. Mazher MA, Kallen A, Edwards JR, Donlan RM. An In Vitro evaluation of disinfection protocols used for needleless connectors of central venous catheters. Lett Appl Microbiol. 2013 Oct;57(4):282–7.

105. Kaler W, Chinn R. Successful disinfection of needleless access ports: A matter of time and friction. J Assoc Vasc Access. 2007 Aug 9;12(3):140–2.

106. Soothill JS, Bravery K, Ho A, Macqueen S, Collins J, Lock P. A fall in bloodstream infections followed a change to 2% chlorhexidine in 70% isopropanol for catheter

connection antisepsis: A pediatric single center before/after study on a hemopoietic stem cell transplant ward. Am J Infect Control. 2009 Oct 1;37(8):626–30.

107. Rupp ME, Yu S, Huerta T, Cavalieri RJ, Alter R, Fey PD, et al. Adequate Disinfection of a Split-Septum Needleless Intravascular Connector with a 5-Second Alcohol Scrub. Infect Control Hosp Epidemiol [Internet]. 2012 Jul [cited 2020 May 5];33(7):661–5. Available from: http://www.ncbi.nlm.nih.gov/pubmed/22669226

108. Simmons S, Bryson C, Porter S. "Scrub the hub": Cleaning duration and reduction in bacterial load on central venous catheters. Crit Care Nurs Q. 2011 Jan;34(1):31–5.

109. Loveday HP, Wilson JA, Pratt RJ, Golsorkhi M, Tingle A, Bak A, et al. Epic3: National evidence-based guidelines for preventing healthcare-associated infections in nhs hospitals in england. J Hosp Infect. 2014 Jan 1;86(S1):S1–70.

110. Pérez-Granda MJ, Guembe M, Cruces R, Bouza E. Vascular catheter colonization: surveillance based on culture of needleless connectors. Crit care [Internet]. 2016 May 28 [cited 2020 Feb 22];20(1):166. Available from: http://www.ncbi.nlm.nih.gov/pubmed/27234944

111. Pérez-Granda MJ, Guembe M, Cruces R, Barrio JM, Bouza E. Assessment of central venous catheter colonization using surveillance culture of withdrawn connectors and insertion site skin. Crit Care. 2016 Feb 2;20(1).

112. Guembe M, Pérez-Granda MJ, Cruces R, Martín-Rabadán P, Bouza E. Cultures of needleless connectors are useful for ruling out central venous catheter colonization. J Clin Microbiol [Internet]. 2015 Jul 1 [cited 2020 Feb 22];53(7):2068–71. Available from: http://www.ncbi.nlm.nih.gov/pubmed/25878353

113. Guembe M, Martín-Rabadán P, Echenagusia A, Camúñez F, Rodríguez-Rosales G, Simó G, et al. Value of superficial cultures for prediction of catheter-related bloodstream infection in long-term catheters: A prospective study. J Clin Microbiol. 2013 Aug 1;51(9):3025–30.

114. Golestaneh L, Mokrzycki MH. Prevention of hemodialysis catheter infections: Ointments, dressings, locks, and catheter hub devices. Hemodial Int [Internet]. 2018 Oct 1 [cited 2020 May 6];22(S2):S75–82. Available from: http://doi.wiley.com/10.1111/hdi.12703

115. Nicolás FG, Casariego GJN, Romero MMV, García JG, Diaz RR, Perez JAP. Reducing the

degree of colonisation of venous access catheters by continuous passive disinfection. Eur J Hosp Pharm . 2016 May 1;23(3):131–3.

116. Kamboj M, Blair R, Bell N, Son C, Huang YT, Dowling M, et al. Use of disinfection cap to reduce central-line—associated bloodstream infection and blood culture contamination among hematology—oncology patients. Infect Control Hosp Epidemiol. 2015 Dec 1;36(12):1401–8.

117. Voor in 't holt AF, Helder OK, Vos MC, Schafthuizen L, Sülz S, van den Hoogen A, et al. Antiseptic barrier cap effective in reducing central line-associated bloodstream infections: A systematic review and meta-analysis. Int J Nurs Stud. 2017 Apr 1;69:34–40.

118. Oto J, Imanaka H, Konno M, Nakataki E, Nishimura M. A prospective clinical trial on prevention of catheter contamination using the hub protection cap for needleless injection device. Am J Infect Control. 2011 May 1;39(4):309–13.

119. Buchman AL, Spapperi J, Leopold P. A new central venous catheter cap: Decreased microbial growth and risk for catheter-related bloodstream infection. J Vasc Access [Internet]. 2009 Jan 24 [cited 2020 May 6];10(1):11–21. Available from: http://journals.sagepub.com/doi/10.1177/112972980901000103

120. Mariyaselvam M, Hodges E, Richardson J, Steel A, Moondi P, Young P. The coated antiseptic tip (CAT) syringe. J Med Eng Technol [Internet]. 2015 Jul 1 [cited 2020 May 6];39(5):259–63. Available from: http://www.ncbi.nlm.nih.gov/pubmed/25970696

121. Brunelli SM, Van Wyck DB, Njord L, Ziebol RJ, Lynch LE, Killion DP. Cluster-randomized trial of devices to prevent catheter-related bloodstream infection. J Am Soc Nephrol [Internet]. 2018 Apr 1 [cited 2020 May 6];29(4):1336–43. Available from: http://www.ncbi.nlm.nih.gov/pubmed/29472415

122. Wallace A, Albadawi H, Patel N, Khademhosseini A, Zhang YS, Naidu S, et al. Anti-fouling strategies for central venous catheters. Cardiovasc Diagn Ther. 2017 Dec 1;7(Suppl 3):S246–57.

123. Zander ZK, Becker ML. Antimicrobial and Antifouling Strategies for Polymeric Medical Devices. ACS Macro Lett. 2018;7(1):16–25.

124. Falde EJ, Yohe ST, Colson YL, Grinstaff MW. Superhydrophobic materials for biomedical applications. Biomaterials. 2016 Oct;104:87–103.

125. Zhang H, Chiao M. Anti-fouling coatings of poly(dimethylsiloxane) devices for biological and biomedical applications. J Med Biol Eng. 2015;35(2):143–55.

126. May RM, Magin CM, Mann EE, Drinker MC, Fraser JC, Siedlecki CA, et al. An engineered micropattern to reduce bacterial colonization, platelet adhesion and fibrin sheath formation for improved biocompatibility of central venous catheters. Clin Transl Med [Internet]. 2015 Dec [cited 2020 May 8];4(1):9–16. Available from: http://www.ncbi.nlm.nih.gov/pubmed/25852825

127. Crnich CJJ, Maki DGG. The Promise of Novel Technology for the Prevention of Intravascular Device–Related Bloodstream Infection. II. Long-Term Devices. Clin Infect Dis. 2002;34(10):1362–8.

128. Maki DG, Kluger DM, Crnich CJ. The risk of bloodstream infection in adults with different intravascular devices: A systematic review of 200 published prospective studies. Mayo Clin Proc. 2006 Sep;81(9):1159–71.

129. Groeger JS, Lucas AB, Coit D, LaQuaglia M, Arthur Brown IE, Turnbull A, et al. Evaluation of the Effect of Silver Impregnated Subcutaneous Cuffs for Preventing Tunneled Chronic Venous Access Catheter Infections in Cancer Patients. Ann Surg [Internet]. [cited 2018 May 24];218(2):206–10. Available from: https://www.ncbi.nlm.nih.gov/pmc/articles/PMC1242932/pdf/annsurg00066-0112.pdf

130. Maki DG, Cobb L, Garman JK, Shapiro JM, Ringer M, Helgerson RB. An attachable silver-impregnated cuff for prevention of infection with central venous catheters: A prospective randomized multicenter trial. Am J Med [Internet]. 1988 Sep 1 [cited 2018 May 24];85(3):307–14. Available from: https://www.sciencedirect.com/science/article/pii/0002934388905797

131. Cicalini S, Palmieri F, Petrosillo N. Clinical review: New technologies for prevention of intravascular catheter-related infections. Vol. 8, Critical Care. BioMed Central; 2004. p. 157–62.

132. Randolph AG, Cook DJ, Gonzalez CA, Andrew M. Benefit of heparin in central venous and pulmonary artery catheters: A meta-analysis of randomized controlled trials. Chest. 1998 Jan 1;113(1):165–71.

133. Chong HY, Lai NM, Apisarnthanarak A, Chaiyakunapruk N. Comparative efficacy of antimicrobial central venous catheters in reducing catheter-related bloodstream

infections in adults: Abridged cochrane systematic review and network meta-analysis. Clin Infect Dis. 2017;64:S131–40.

134. Cheung H-Y, Wong MM-K, Cheung S-H, Liang LY, Lam Y-W, Chiu S-K. Differential Actions of Chlorhexidine on the Cell Wall of Bacillus subtilis and Escherichia coli. Msadek T, editor. PLoS One [Internet]. 2012 May 11 [cited 2020 Feb 22];7(5):36659. Available from: http://dx.plos.org/10.1371/journal.pone.0036659

135. Chlorhexidine Facts: Mechanism of Action [Internet]. [cited 2020 Feb 22]. Available from: https://chlorhexidinefacts.com/mechanism-of-action.html

136. Silver sulfadiazine | C10H9AgN4O2S [Internet]. U.S. National Library of Medicine - PubChem. [cited 2020 Feb 22]. Available from: https://pubchem.ncbi.nlm.nih.gov/compound/Silver-sulfadiazine

137. Minocycline | C23H27N3O7 [Internet]. U.S. National Library of Medicine - PubChem. [cited 2020 Feb 22]. Available from: https://pubchem.ncbi.nlm.nih.gov/compound/Minocycline

138. Garrido-Mesa N, Zarzuelo A, Gálvez J. Minocycline: Far beyond an antibiotic. Vol. 169, British Journal of Pharmacology. Wiley-Blackwell; 2013. p. 337–52.

139. Campbell EA, Korzheva N, Mustaev A, Murakami K, Nair S, Goldfarb A, et al. Structural mechanism for rifampicin inhibition of bacterial RNA polymerase. Cell. 2001 Mar 23;104(6):901–12.

140. Thevissen K, Ayscough KR, Aerts AM, Du W, De Brucker K, Meert EMK, et al. Miconazole induces changes in actin cytoskeleton prior to reactive oxygen species induction in yeast. J Biol Chem [Internet]. 2007 Jul 27 [cited 2020 Feb 22];282(30):21592–7. Available from: http://www.ncbi.nlm.nih.gov/pubmed/17553796

141. Kobayashi D, Kondo K, Uehara N, Otokozawa S, Tsuji N, Yagihashi A, et al. Endogenous reactive oxygen species is an important mediator of miconazole antifungal effect. Antimicrob Agents Chemother [Internet]. 2002 Oct [cited 2020 Feb 22];46(10):3117. Available from: http://www.ncbi.nlm.nih.gov/pubmed/12234832

142. Barasch A, Griffin AV. Miconazole revisited: New evidence of antifungal efficacy from laboratory and clinical trials. Future Microbiol. 2008 May 28;3(3):265–9.

143. Maki DG, Stolz SM, Wheeler S, Mermel LA. Prevention of central venous catheter-

related bloodstream infection by use of an antiseptic-impregnated catheter: A randomized, controlled trial. Ann Intern Med [Internet]. 1997 Aug 15 [cited 2018 May 12];127(4):257–66. Available from: http://annals.org/article.aspx?doi=10.7326/0003-4819-127-4-199708150-00001

144. Lorente L, Lecuona M, Jiménez A, Raja L, Cabrera J, Gonzalez O, et al. Chlorhexidine-silver sulfadiazine- or rifampicin-miconazole-impregnated venous catheters decrease the risk of catheter-related bloodstream infection similarly. Am J Infect Control [Internet]. 2016 Jan 1 [cited 2020 Feb 22];44(1):50–3. Available from: http://www.ncbi.nlm.nih.gov/pubmed/26412482

145. Veenstra DL, Saint S, Sullivan SD. Cost-effectiveness of antiseptic-impregnated central venous catheters for the prevention of catheter-related bloodstream infection. J Am Med Assoc [Internet]. 1999 Aug 11 [cited 2018 May 16];282(6):554–60. Available from: http://jama.jamanetwork.com/article.aspx?doi=10.1001/jama.282.6.554

146. Bischoff SC, Austin P, Boeykens K, Chourdakis M, Cuerda C, Jonkers-Schuitema C, et al. ESPEN guideline on home enteral nutrition. Clin Nutr. 2020 Jan 1;39(1):5–22.

147. Pittiruti M, Hamilton H, Biffi R, MacFie J, Pertkiewicz M, ESPEN. ESPEN Guidelines on Parenteral Nutrition: Central Venous Catheters (access, care, diagnosis and therapy of complications). Clin Nutr. 2009 Aug 28;28(4):365–77.

148. Shanks RMQ, Donegan NP, Graber ML, Buckingham SE, Zegans ME, Cheung AL, et al. Heparin stimulates Staphylococcus aureus biofilm formation. Infect Immun [Internet]. 2005 Aug [cited 2020 Jul 6];73(8):4596–606. Available from: https://pubmed.ncbi.nlm.nih.gov/16040971/

149. Safdar N, Maki DG. Use of vancomycin-containing lock or flush solutions for prevention of bloodstream infection associated with central venous access devices: a meta-analysis of prospective, randomized trials. Clin Infect Dis [Internet]. 2006;43(4):474–84. Available from: http://www.ncbi.nlm.nih.gov/pubmed/16838237

150. Bookstaver PB, Williamson JC, Tucker BK, Raad II, Sherertz RJ. Activity of novel antibiotic lock solutions in a model against isolates of catheter-related bloodstream infections. Ann Pharmacother. 2009;43(2):210–9.

151. Weijmer MC, Marinus #, Van Den Dorpel A, Van De Ven PJG, Ter Wee PM, Van Geelen JACA, et al. Randomized, Clinical Trial Comparison of Trisodium Citrate 30% and

Heparin as Catheter-Locking Solution in Hemodialysis Patients. J Am Soc Nephrol [Internet]. 2005 [cited 2018 May 17];16:2769–77. Available from: http://jasn.asnjournals.org/content/16/9/2769.full.pdf

152. Olthof ED, Nijland R, Gülich AF, Wanten GJA. Microbiocidal effects of various taurolidine containing catheter lock solutions. Clin Nutr [Internet]. 2015 Apr 1 [cited 2018 May 23];34(2):309–14. Available from: https://www.sciencedirect.com/science/article/pii/S0261561414001319?via%3Dihub#bib23

153. Bradshaw JH, Puntis JW. Taurolidine and Catheter-related Bloodstream Infection: A Systematic Review of the Literature. J Pediatr Gastroenterol Nutr. 2008;47(2):179–86.

154. Shah CB, Mittelman MW, Costerton JW, Parenteau S, Pelak M, Arsenault R, et al. Antimicrobial Activity of a Novel Catheter Lock Solution. Antimicrob Agents Chemother [Internet]. 2002 Jun 1 [cited 2018 May 23];46(6):1674–9. Available from: http://www.ncbi.nlm.nih.gov/pubmed/12019075

155. Olthof ED, Versleijen MW, Huisman-de Waal G, Feuth T, Kievit W, Wanten GJA. Taurolidine lock is superior to heparin lock in the prevention of catheter related bloodstream infections and occlusions. PLoS One [Internet]. 2014 [cited 2018 May 23];9(11):e111216. Available from: http://www.ncbi.nlm.nih.gov/pubmed/25379781

156. Rane HS, Bernardo SM, Walraven CJ, Lee SA. In Vitro Analyses of Ethanol Activity against Candida albicans Biofilms. Antimicrob Agents Chemother [Internet]. 2012 [cited 2018 May 15];56:4487–9. Available from: http://aac.asm.org/

157. Laird J, Soutar R, Butcher I. Complications of the ethanol-lock technique in the treatment of central venous catheter sepsis. J Infect [Internet]. 2005 Nov 1 [cited 2018 May 15];51(4):338. Available from: https://www.sciencedirect.com/science/article/pii/S0163445305000393?via%3Dihub

158. Mermel LA, Alang N. Adverse effects associated with ethanol catheter lock solutions: A systematic review. J Antimicrob Chemother [Internet]. 2014 Oct 1 [cited 2018 May 16];69(10):2611–9. Available from: https://academic.oup.com/jac/article-lookup/doi/10.1093/jac/dku182

159. Meckmongkol TT, Costanzo C, Ciullo S, Prasad R, Arthur LG. Hidden morbidity of ethanol lock therapy. Pediatr Surg Int. 2018 Jan 1;34(1):71–4.

160. Milisavljevic V, Tran LP, Batmalle C, Bootsma HJ. Benzyl alcohol and ethanol can enhance the pathogenic potential of clinical Staphylococcus epidermidis strains. Am J Infect Control [Internet]. 2008 Oct 1 [cited 2018 May 16];36(8):552–8. Available from: https://www.sciencedirect.com/science/article/pii/S0196655308000928

161. Redelman C V., Maduakolam C, Anderson GG. Alcohol treatment enhances Staphylococcus aureus biofilm development. FEMS Immunol Med Microbiol. 2012;66(3):411–8.

162. El-Hennawy AS, Frolova E, Romney WA. Sodium bicarbonate catheter lock solution reduces hemodialysis catheter loss due to catheter-related thrombosis and blood stream infection: An open-label clinical trial. Nephrol Dial Transplant. 2019;34(10):1739–45.

163. Farha MA, French S, Stokes JM, Brown ED. Bicarbonate Alters Bacterial Susceptibility to Antibiotics by Targeting the Proton Motive Force. ACS Infect Dis [Internet]. 2018 Mar 9 [cited 2020 Feb 13];4(3):382–90. Available from: https://pubs.acs.org/doi/10.1021/acsinfecdis.7b00194

164. Dobay O, Laub K, Stercz B, Kéri A, Balázs B, Tóthpál A, et al. Bicarbonate inhibits bacterial growth and biofilm formation of prevalent cystic fibrosis pathogens. Front Microbiol. 2018 Sep 19;9(SEP).

165. Letscher-Bru V, Obszynski CM, Samsoen M, Sabou M, Waller J, Candolfi E. Antifungal Activity of Sodium Bicarbonate Against Fungal Agents Causing Superficial Infections. Mycopathologia [Internet]. 2013 Feb [cited 2020 Feb 14];175(1–2):153–8. Available from: http://www.ncbi.nlm.nih.gov/pubmed/22991095

166. Memar MY, Ghotaslou R, Samiei M, Adibkia K. Antimicrobial use of reactive oxygen therapy: Current insights. Infect Drug Resist. 2018 Apr 24;11:567–76.

167. Dunnill C, Patton T, Brennan J, Barrett J, Dryden M, Cooke J, et al. Reactive oxygen species (ROS) and wound healing: the functional role of ROS and emerging ROS-modulating technologies for augmentation of the healing process. Int Wound J [Internet]. 2017 Feb 1 [cited 2017 Dec 5];14(1):89–96. Available from: http://doi.wiley.com/10.1111/iwj.12557

168. Ray PD, Huang B-W, Tsuji Y. Reactive oxygen species (ROS) homeostasis and redox regulation in cellular signaling. Cell Signal. 2012 May;24(5):981–90.

169. Nair S V., Baranwal G, Chatterjee M, Sachu A, Vasudevan AK, Bose C, et al. Antimicrobial activity of plumbagin, a naturally occurring naphthoquinone from Plumbago rosea, against Staphylococcus aureus and Candida albicans. Int J Med Microbiol. 2016 Jun 1;306(4):237–48.

170. Dryden MS, Cooke J, Salib RJ, Holding RE, Biggs T, Salamat AA, et al. Reactive oxygen: A novel antimicrobial mechanism for targeting biofilm-associated infection. J Glob Antimicrob Resist [Internet]. 2017;8:186–91. Available from: http://dx.doi.org/10.1016/j.jgar.2016.12.006

171. Lu J, Cokcetin NN, Burke CM, Turnbull L, Liu M, Carter DA, et al. Honey can inhibit and eliminate biofilms produced by Pseudomonas aeruginosa. Sci Rep. 2019 Dec 3;9(1):1–13.

172. Dryden M, Cooke J, Salib R, Holding R, Pender SLF, Brooks J. Hot topics in reactive oxygen therapy: Antimicrobial and immunological mechanisms, safety and clinical applications. J Glob Antimicrob Resist. 2017 Mar 1;8:194–8.

173. Cokcetin NN, Pappalardo M, Campbell LT, Brooks P, Carter DA, Blair SE, et al. The Antibacterial Activity of Australian Leptospermum Honey Correlates with Methylglyoxal Levels. Gan SH, editor. PLoS One [Internet]. 2016 Dec 28 [cited 2020 Feb 23];11(12):e0167780. Available from: https://dx.plos.org/10.1371/journal.pone.0167780

174. Maddocks SE, Jenkins RE, Rowlands RS, Purdy KJ, Cooper RA. Manuka honey inhibits adhesion and invasion of medically important wound bacteria in vitro. Future Microbiol. 2013 Nov 22;8(12):1523–36.

175. Irish J, Blair S, Carter DA. The Antibacterial Activity of Honey Derived from Australian Flora. Otto M, editor. PLoS One [Internet]. 2011 Mar 28 [cited 2020 Feb 23];6(3):e18229. Available from: http://dx.plos.org/10.1371/journal.pone.0018229

176. Sherlock O, Dolan A, Athman R, Power A, Gethin G, Cowman S, et al. Comparison of the antimicrobial activity of Ulmo honey from Chile and Manuka honey against methicillin-resistant Staphylococcus aureus, Escherichia coli and Pseudomonas aeruginosa. BMC Complement Altern Med [Internet]. 2010 Sep 2 [cited 2020 Feb 23];10(1):47. Available from:

http://bmccomplementalternmed.biomedcentral.com/articles/10.1186/1472-6882-10-47

177. Blair SE, Cokcetin NN, Harry EJ, Carter DA. The unusual antibacterial activity of medical-grade Leptospermum honey: Antibacterial spectrum, resistance and transcriptome analysis. Eur J Clin Microbiol Infect Dis. 2009 Oct;28(10):1199–208.

178. Anand S, Deighton M, Livanos G, Pang ECK, Mantri N. Agastache honey has superior antifungal activity in comparison with important commercial honeys. Sci Rep. 2019 Dec 3;9(1):1–14.

179. Yusoff NYN, Mohamad S, Abdullah H, Rahman NA. Antifungal activity of Malaysian honey and propolis extracts against pathogens implicated in denture stomatitis. In: AIP Conference Proceedings [Internet]. American Institute of Physics Inc.; 2016 [cited 2020 Feb 23]. p. 020006. Available from: https://doi.org/10.1063/1.4968861

180. Irish J, Carter DA, Shokohi T, Blair SE. Honey has an antifungal effect against Candida species. Med Mycol [Internet]. 2006 May [cited 2020 Feb 23];44(3):289–91. Available from: https://academic.oup.com/mmy/article-lookup/doi/10.1080/13693780500417037

181. Alandejani T, Marsan J, Ferris W, Slinger R, Chan F. Effectiveness of honey on Staphylococcus aureus and Pseudomonas aeruginosa biofilms. J Am Acad Otolaryngol Neck Surg [Internet]. 2009 Jul 1 [cited 2020 Feb 23];141(1):118. Available from: http://www.ncbi.nlm.nih.gov/pubmed/19559969

182. Merckoll P, Jonassen TØ, Vad ME, Jeansson SL, Melby KK. Bacteria, biofilm and honey: A study of the effects of honey on “planktonic” and biofilm-embedded chronic wound bacteria. Scand J Infect Dis. 2009 Jul 8;41(5):341–7.

183. Cooper R, Jenkins L, Hooper S. Inhibition of biofilms of Pseudomonas aeruginosa by Medihoney in vitro. J Wound Care. 2014 Mar 26;23(3):93–104.

184. Dryden M, Lockyer G, Saeed K, Cooke J. Engineered honey: In vitro antimicrobial activity of a novel topical wound care treatment. J Glob Antimicrob Resist. 2014 Sep;2(3):168–72.

185. Halstead FD, Webber MA, Rauf M, Burt R, Dryden M, Oppenheim BA. In vitro activity of an engineered honey, medical-grade honeys, and antimicrobial wound dressings against biofilm-producing clinical bacterial isolates. J Wound Care [Internet]. 2016

Feb 2 [cited 2017 Dec 5];25(2):93–102. Available from: http://www.magonlinelibrary.com/doi/10.12968/jowc.2016.25.2.93

186. Cooke J, Dryden M, Patton T, Brennan J, Barrett J. The antimicrobial activity of prototype modified honeys that generate reactive oxygen species (ROS) hydrogen peroxide. BMC Res Notes [Internet]. 2015 [cited 2020 Feb 23];8(1):20. Available from: http://www.biomedcentral.com/1756-0500/8/20

187. Halstead FD, Webber MA, Oppenheim BA. Use of an engineered honey to eradicate preformed biofilms of important wound pathogens: An in vitro study. J Wound Care [Internet]. 2017 Aug 2 [cited 2020 Feb 23];26(8):442–50. Available from: http://www.ncbi.nlm.nih.gov/pubmed/28795889

188. Widhalm JR, Rhodes D. Biosynthesis and molecular actions of specialized 1,4-naphthoquinone natural products produced by horticultural plants. Hortic Res [Internet]. 2016 Dec 21 [cited 2018 May 24];3(1):16046. Available from: http://www.nature.com/articles/hortres201646

189. Davis J, Molina MT, Leach CP, Cardosi MF. Plasma-polyplumbagin-modified microfiber probes: A functional material approach to monitoring vascular access line contamination. ACS Appl Mater Interfaces [Internet]. 2013 Sep 17 [cited 2020 Jul 7];5(19):9367–71. Available from: https://pubs.acs.org/doi/abs/10.1021/am402821c

190. Sameni S, Hande MP. Plumbagin triggers DNA damage response, telomere dysfunction and genome instability of human breast cancer cells. Biomed Pharmacother. 2016;82:256–68.

191. Khaw AK, Sameni S, Venkatesan S, Kalthur G, Hande MP. Plumbagin alters telomere dynamics, induces DNA damage and cell death in human brain tumour cells. Mutat Res - Genet Toxicol Environ Mutagen. 2015;793:86–95.

192. Segura M, Alvarez-Lerma F, Tellado JM, Jiménez-Ferreres J, Oms L, Rello J, et al. A clinical trial on the prevention of catheter-related sepsis using a new hub model. Ann Surg. 1996;223(4):363–9.

193. Luna J, Masdeu G, Pérez M, Claramonte R, Forcadell I, Barrachina F, et al. Clinical trial evaluating a new hub device designed to prevent catheter-related sepsis. Eur J Clin Microbiol Infect Dis. 2000;19(9):655–62.

194. Paredes J, Alonso-Arce M, Schmidt C, Valderas D, Sedano B, Legarda J, et al. Smart

central venous port for early detection of bacterial biofilm related infections. Biomed Microdevices. 2014 Feb 11;16(3):365–74.

195. Bernstein M, Woods M. “Smart catheters” for the major problem of catheter-related infections [Internet]. American Chemical Society. 2012 [cited 2020 Feb 23]. Available from: https://www.acs.org/content/acs/en/pressroom/newsreleases/2012/august/smart-catheters-for-the-major-problem-of-catheter-related-infections.html

196. Pant J, Goudie MJ, Chaji SM, Johnson BW, Handa H. Nitric oxide releasing vascular catheters for eradicating bacterial infection. J Biomed Mater Res - Part B Appl Biomater. 2018 Nov 1;106(8):2849–57.

197. Mihu MR, Cabral V, Pattabhi R, Tar MM, Davies KK, Friedman AJ, et al. Sustained Nitric Oxide-Releasing Nanoparticles Interfere with Methicillin-Resistant Staphylococcus aureus Adhesion and Biofilm Formation in a Rat Central Venous Catheter Model. Antimicrob Agents Chemother [Internet]. 2017 Jan 1 [cited 2020 May 5];61(1):e02020-16. Available from: http://aac.asm.org/content/61/1/e02020-16.abstract

198. Xiong L, Batchelor-Mcauley C, Compton RG. Calibrationless pH sensors based on nitrosophenyl and ferrocenyl co-modified screen printed electrodes. Sensors Actuators, B Chem. 2011 Nov 28;159(1):251–5.

199. ANB Sensors. Calibration free pH Sensing | ANB Sensors Next Generation Sensors [Internet]. [cited 2020 Nov 11]. Available from: http://www.anbsensors.com/calibration-free-ph-sensor/

200. Robinson KL, Lawrence NS. A Vinylanthracene and Vinylferrocene-Containing Copolymer: A New Dual pH/Sulfide Sensor. Electroanalysis [Internet]. 2006 Apr [cited 2020 Jul 7];18(7):677–83. Available from: http://doi.wiley.com/10.1002/elan.200503456

201. Lawrence NS, Robinson KL. Molecular anchoring of anthracene-based copolymers onto carbon nanotubes: Enhanced pH sensing. Talanta. 2007 Dec 15;74(3):365–9.

202. Lawrence NS, Pagels M, Hackett SFJ, McCormack S, Meredith A, Jones TGJ, et al. Triple Component Carbon Epoxy pH Probe. Electroanalysis [Internet]. 2007 Feb [cited 2020 Jul 7];19(4):424–8. Available from: http://doi.wiley.com/10.1002/elan.200603725

203. Lafitte VGH, Wang W, Yashina AS, Lawrence NS. Anthraquinone-ferrocene film electrodes: Utility in pH and oxygen sensing. Electrochem commun. 2008 Dec 1;10(12):1831–4.

204. Gao X, Dai C, Xu ZJ, Lawrence NS, Fisher AC. An Electrochemical Method for Monitoring the Acidity of Water for Fuel Cell and Environmental Applications. Energy Technol [Internet]. 2018 Jan 1 [cited 2020 Jul 7];6(1):94–9. Available from: http://doi.wiley.com/10.1002/ente.201700617

205. Dai C, Chan CWI, Barrow W, Smith A, Song P, Potier F, et al. A Route to Unbuffered pH Monitoring: A Novel Electrochemical Approach. Electrochim Acta. 2016 Feb 1;190:879–86.

206. Lawrence N, ANB Sensors. Reference electrode using local environment pH control. United States Patent Application Publication; US 2019 0293592 A1, 2019.

207. Makos MA, Omiatek DM, Ewing AG, Heien ML. Development and characterization of a voltammetric carbon-fiber microelectrode pH sensor. Langmuir. 2010 Jun 15;26(12):10386–91.

208. McLister A, Lowry N, Anderson A, McHugh J, Davis J. Novel pH sensing redox wire based on a polyamide homopolymer of L-tryptophan. Fibers Polym. 2015 Oct 29;16(10):2294–7.

209. McLister A, Davis J. Molecular Wiring in Smart Dressings: Opening a New Route to Monitoring Wound pH. Healthcare [Internet]. 2015 Jun 25 [cited 2020 Feb 14];3(3):466–77. Available from: http://www.ncbi.nlm.nih.gov/pubmed/27417774

210. Li M, Phair J, Cardosi MFMF, Davis J. Nanostructuring carbon fibre probes for use in central venous catheters. Anal Chim Acta. 2014 Feb 17;812:1–5.

211. Chaisiwamongkhol K, Batchelor-Mcauley C, Compton RG. Amperometric micro pH measurements in oxygenated saliva. Analyst [Internet]. 2017 [cited 2020 Feb 14];142(15):2828–35. Available from: http://www.ncbi.nlm.nih.gov/pubmed/28702560

212. Jamal M, Razeeb KM, Shao H, Islam J, Akhter I, Furukawa H, et al. Development of Tungsten Oxide Nanoparticle Modified Carbon Fibre Cloth as Flexible pH Sensor. Sci Rep. 2019 Dec 1;9(1):1–9.

213. Park HJ, Yoon JH, Lee KG, Choi BG. Potentiometric performance of flexible pH sensor

based on polyaniline nanofiber arrays. Nano Converg [Internet]. 2019 Dec 18 [cited 2020 Feb 14];6(1):9. Available from: https://nanoconvergencejournal.springeropen.com/articles/10.1186/s40580-019-0179-0

214. Dai C, Song P, Wadhawan JD, Fisher AC, Lawrence NS. Screen Printed Alizarin-Based Carbon Electrodes: Monitoring pH in Unbuffered Media. Electroanalysis [Internet]. 2015 Apr 1 [cited 2020 Jul 7];27(4):917–23. Available from: http://doi.wiley.com/10.1002/elan.201400704

215. Huang WD, Cao H, Deb S, Chiao M, Chiao JC. A flexible pH sensor based on the iridium oxide sensing film. Sensors Actuators, A Phys. 2011;169(1):1–11.

216. Yang J, Kwak TJ, Zhang X, McClain R, Chang WJ, Gunasekaran S. Digital pH Test Strips for In-Field pH Monitoring Using Iridium Oxide-Reduced Graphene Oxide Hybrid Thin Films. ACS Sensors. 2016;1(10):1235–43.

217. Maiolo L, Mirabella S, Maita F, Alberti A, Minotti A, Strano V, et al. Flexible pH sensors based on polysilicon thin film transistors and ZnO nanowalls. Appl Phys Lett. 2014;105(9).

218. Dai C, Crawford LP, Song P, Fisher AC, Lawrence NS. A novel sensor based on electropolymerized substituted-phenols for pH detection in unbuffered systems. RSC Adv. 2015 Dec 1;5(126):104048–53.

219. Hu K, Li Y, Rotenberg SA, Amatore C, Mirkin M V. Electrochemical Measurements of Reactive Oxygen and Nitrogen Species inside Single Phagolysosomes of Living Macrophages. J Am Chem Soc. 2019 Mar 3;141(11):4564–8.

220. Thirumalai D, Kathiresan V, Lee J, Jin SH, Chang SC. Electrochemical reactive oxygen species detection by cytochrome: C immobilized with vertically aligned and electrochemically reduced graphene oxide on a glassy carbon electrode. Analyst. 2017 Dec 7;142(23):4544–52.

221. Li Y, Hu K, Yu Y, Rotenberg SA, Amatore C, Mirkin M V. Direct Electrochemical Measurements of Reactive Oxygen and Nitrogen Species in Nontransformed and Metastatic Human Breast Cells. J Am Chem Soc. 2017 Aug 28;139(37):13055–62.

222. Rawson FJ, Hicks J, Dodd N, Abate W, Garrett DJ, Yip N, et al. Fast, Ultrasensitive Detection of Reactive Oxygen Species Using a Carbon Nanotube Based-

Electrocatalytic Intracellular Sensor. ACS Appl Mater Interfaces. 2015 Oct 28;7(42):23527–37.

223. Enomoto J, Matharu Z, Revzin A. Electrochemical biosensors for on-chip detection of oxidative stress from cells. In: Methods in Enzymology [Internet]. Academic Press Inc.; 2013 [cited 2020 Feb 24]. p. 107–21. Available from: http://www.ncbi.nlm.nih.gov/pubmed/23791096

224. Sultana ST, Babauta JT, Beyenal H. Electrochemical biofilm control: A review. Biofouling. 2015 Oct;31(9):745–58.

225. Liu WK, Brown MRW, Elliott TSJ. Mechanisms of the bactericidal activity of low amperage electric current (DC). J Antimicrob Chemother. 1997;39(6):687–95.

226. del Pozo JL, Rouse MS, Patel R. Bioelectric effect and bacterial biofilms. A systematic review. Int J Artif Organs. 2008 Sep;31(9):786–95.

227. Asadi MR, Torkaman G. Bacterial Inhibition by Electrical Stimulation. Adv Wound Care. 2014 Feb 1;3(2):91–7.

228. Czerwińska-Główka D, Krukiewicz K. A journey in the complex interactions between electrochemistry and bacteriology: From electroactivity to electromodulation of bacterial biofilms. Bioelectrochemistry. 2020;131.

229. Gottenbos B, Grijpma DW, van der Mei HC, Feijen J, Busscher HJ. Antimicrobial effects of positively charged surfaces on adhering Gram-positive and Gram-negative bacteria. J Antimicrob Chemother. 2001;48(1):7–13.

230. Abbaszadegan A, Ghahramani Y, Gholami A, Hemmateenejad B, Dorostkar S, Nabavizadeh M, et al. The Effect of Charge at the Surface of Silver Nanoparticles on Antimicrobial Activity against Gram-Positive and Gram-Negative Bacteria: A Preliminary Study. J Nanomater [Internet]. 2015 Sep [cited 2020 Jun 2];2015:1–8. Available from: http://dx.doi.org/10.1155/2015/720654

231. Malanovic N, Lohner K. Gram-positive bacterial cell envelopes: The impact on the activity of antimicrobial peptides. Biochim Biophys Acta - Biomembr. 2016 May 1;1858(5):936–46.

232. Sandvik EL, McLeod BR, Parker AE, Stewart PS. Direct Electric Current Treatment under Physiologic Saline Conditions Kills Staphylococcus epidermidis Biofilms via Electrolytic Generation of Hypochlorous Acid. PLoS One. 2013 Feb 4;8(2):e55118.

233. Bard Allen J., Faulkner Larry R. Electrochemical Instrumentation. In: Electrochemical Methods: Fundamentals and Applications, 2nd Edition. 2nd ed. Austin: John Wiley and Sons Inc.; 2001. p. 632–58.

234. Kissinger PT, Heineman WR. Laboratory Techniques in Electroanalytical Chemistry, Revised and Expanded. 2nd ed. Kissinger PT, Heineman WR, editors. Laboratory Techniques in Electroanalytical Chemistry, Revised and Expanded. CRC Press; 1996. 1008 p.

235. Zoski C. Handbook of Electrochemistry. First. Zoski C, editor. Handbook of Electrochemistry. Elsevier B.V.; 2006. 1–847 p.

236. Skoog DA, Holler FJ, Crouch SR. Principles of Instrumental Analysis. 7th ed. Cengage Learning; 2017.

237. Pletcher D. A First Course in Electrode Processes. 2nd ed. Royal Society of Chemistry; 2009.

238. Marioli JM, Kuwana T. Electrochemical characterization of carbohydrate oxidation at copper electrodes. Electrochim Acta. 1992 Jun 1;37(7):1187–97.

239. Compton RG, Banks CE. Understanding Voltammetry. 3rd ed. Understanding Voltammetry. World Scientific Publishing Europe Ltd.; 2018.

240. Brett C, Brett AMO. Electroanalysis. Oxford: Oxford University Press; 1998. 88 p.

241. Fisher AC. Electrode Dynamics. Oxford: Oxford University Press; 1996. 1–84 p.

242. Prasad K, Muthuraman G, Zen JM. The role of oxygen functionalities and edge plane sites on screen-printed carbon electrodes for simultaneous determination of dopamine, uric acid and ascorbic acid. Electrochem commun. 2008;10(4):559–63.

243. Anderson A, Phair J, Benson J, Meenan B, Davis J. Investigating the use of endogenous quinoid moieties on carbon fibre as means of developing micro pH sensors. Mater Sci Eng C [Internet]. 2014 Oct 1 [cited 2018 Oct 19];43:533–7. Available from: https://www.sciencedirect.com/science/article/pii/S0928493114004457

244. Mohammadzadeh Kakhki R. A review to recent developments in modification of carbon fiber electrodes. Arab J Chem. 2014 Nov 1;12(7):1783–94.

245. Elgrishi N, Rountree KJ, McCarthy BD, Rountree ES, Eisenhart TT, Dempsey JL. A Practical Beginner's Guide to Cyclic Voltammetry. J Chem Educ. 2018;95(2):197–206.

246. Brownson DAC, Banks CE. The Handbook of Graphene Electrochemistry. The Handbook of Graphene Electrochemistry. 2014. 1–201 p.

247. Dias LG, Meirinho SG, Veloso ACA, Rodrigues LR, Peres AM. Electronic tongues and aptasensors. In: Bioinspired Materials for Medical Applications. Elsevier Inc.; 2017. p. 371–402.

248. Biesheuvel PM, Porada S, Dykstra JE. The difference between Faradaic and non-Faradaic electrode processes [Internet]. 2018 Sep [cited 2020 Nov 11]. Available from: http://arxiv.org/abs/1809.02930

249. Singh AK. Experimental Methodologies for the Characterization of Nanoparticles. In: Engineered Nanoparticles. Elsevier; 2016. p. 125–70.

250. Watts JF, Wolstenholme J. An Introduction to Surface Analysis by XPS and AES. An Introduction to Surface Analysis by XPS and AES. John Wiley & Sons, Ltd; 2003. 1–15 p.

251. Embong Z. XPS, AES and Laser Raman Spectroscopy: a Fingerprint for a Materials Surface Characterisation. J Sains Nukl Malaysia. 2011;(January 2011):26–45.

252. Ferrari AC, Robertson J. Interpretation of Raman spectra of disordered and amorphous carbon. Phys Rev B [Internet]. 2000 [cited 2020 Feb 10];61(20):14095–107. Available from: https://link.aps.org/doi/10.1103/PhysRevB.61.14095

253. Lohumi S, Kim MS, Qin J, Cho BK. Raman imaging from microscopy to macroscopy: Quality and safety control of biological materials. TrAC - Trends Anal Chem [Internet]. 2017;93(June):183–98. Available from: http://dx.doi.org/10.1016/j.trac.2017.06.002

254. Marcelli A, Cricenti A, Kwiatek WM, Petibois C. Biological applications of synchrotron radiation infrared spectromicroscopy. Biotechnol Adv. 2012;30(6):1390–404.

255. Bumbrah GS, Sharma RM. Raman spectroscopy – Basic principle, instrumentation and selected applications for the characterization of drugs of abuse. Vol. 6, Egyptian Journal of Forensic Sciences. Egyptian Forensic Medicine Authority; 2016. p. 209–15.

256. Mohammad KA, Zekry A, Abouelatta M. LED Based Spectrophotometer can compete with conventional one. Int J Eng Technol. 2015;4(2):399.

257. Clark J. UV-visible absorption spectra [Internet]. Chemguide. 2016 [cited 2020 Feb 11]. Available from: https://www.chemguide.co.uk/analysis/uvvisible/theory.html

258. Banks CE, Compton RG. Exploring the electrocatalytic sites of carbon nanotubes for NADH detection: An edge plane pyrolytic graphite electrode study. Analyst [Internet]. 2005 Aug 11 [cited 2020 Jul 24];130(9):1232–9. Available from: www.rsc.org/analyst

259. Phair J, Newton L, McCormac C, Cardosi MF, Leslie R, Davis J. A disposable sensor for point of care wound pH monitoring. Analyst [Internet]. 2011 Nov 21 [cited 2020 Jul 24];136(22):4692–5. Available from: www.rsc.org/analyst

260. Alkire R, Bartlett P. Electrochemistry of Carbon Electrodes - Advances in Electrochemical Sciences and Engineering. Wiley-VCH; 2015.

261. Zhang W, Zhu S, Luque R, Han S, Hu L, Xu G. Recent development of carbon electrode materials and their bioanalytical and environmental applications. Chem Soc Rev [Internet]. 2016 Feb 7 [cited 2020 Jul 24];45(3):715–52. Available from: https://pubs.rsc.org/en/content/articlehtml/2016/cs/c5cs00297d

262. Fletcher S. Screen-Printed Carbon Electrodes. In: Advances in Electrochemical Science and Engineering. wiley; 2016. p. 425–43.

263. Pasakon P, Mensing JP, Phokaratkul D, Karuwan C, Lomas T, Wisitsoraat A, et al. A high-performance, disposable screen-printed carbon electrode modified with multi-walled carbon nanotubes/graphene for ultratrace level electrochemical sensors. J Appl Electrochem [Internet]. 2019 Feb 15 [cited 2020 Jul 24];49(2):217–27. Available from: https://link.springer.com/article/10.1007/s10800-018-1268-1

264. Rawlinson S, McLister A, Kanyong P, Davis J. Rapid determination of salicylic acid at screen printed electrodes. Microchem J [Internet]. 2018 Mar 1 [cited 2018 Oct 19];137:71–7. Available from: http://uir.ulster.ac.uk/39043/2/170807

265. Eng AYS, Chua CK, Pumera M. Intrinsic electrochemical performance and precise control of surface porosity of graphene-modified electrodes using the drop-casting technique. Electrochem commun. 2015 Aug 1;59:86–90.

266. Spătaru N, Calderon-Moreno JM, Osiceanu P, Kondo T, Terashima C, Popa M, et al. Conductive diamond powder inclusion in drop-casted graphene for enhanced effectiveness as electrocatalyst substrate. Chem Eng J. 2020 Dec 15;402:126258.

267. Valentine CJ, Takagishi K, Umezu S, Daly R, De Volder M. Paper-Based Electrochemical Sensors Using Paper as a Scaffold to Create Porous Carbon Nanotube Electrodes. ACS Appl Mater Interfaces [Internet]. 2020 Jun 25 [cited 2020 Jul 24];12:30685. Available

from: https://dx.doi.org/10.1021/acsami.0c04896

268. Qin Y. A brief description of textile fibers. In: Medical Textile Materials. Elsevier; 2016. p. 23–42.

269. Mercante LA, Scagion VP, Migliorini FL, Mattoso LHC, Correa DS. Electrospinning-based (bio)sensors for food and agricultural applications: A review. TrAC - Trends Anal Chem. 2017 Jun 1;91:91–103.

270. Ribeiro RF, Pardini LC, Alves NP, Júnior CARB. Thermal Stabilization study of polyacrylonitrile fiber obtained by extrusion. Polimeros. 2015 Nov 1;25(6):523–30.

271. Wang Y, Tong Y, Zhang B, Su H, Xu L. Formation of Surface Morphology in Polyacrylonitrile (PAN) Fibers during Wet-Spinning. J Eng Fiber Fabr [Internet]. 2018 Jun 15 [cited 2020 Jul 24];13(2):52–7. Available from: http://journals.sagepub.com/doi/10.1177/155892501801300208

272. Choi D, Kil HS, Lee S. Fabrication of low-cost carbon fibers using economical precursors and advanced processing technologies. Carbon N Y. 2019;142:610–49.

273. Morgan P. Carbon Fibers and Their Composites. Taylor & Francis; 2005.

274. Chung DDL. Carbon Composites: Composites with Carbon Fibers, Nanofibers, and Nanotubes. Butterworth-Heinemann; 2017.

275. Kahoush M, Behary N, Cayla A, Mutel B, Guan J, Nierstrasz V. Surface modification of carbon felt by cold remote plasma for glucose oxidase enzyme immobilization. Appl Surf Sci. 2019 May 15;476(August 2018):1016–24.

276. Zhao L, Liu W, Liu P, Tian J, Xu M, Sun S, et al. Study on atmospheric air glow discharge plasma generation and surface modification of carbon fiber fabric. Plasma Process Polym [Internet]. 2020 Jan 22 [cited 2020 Mar 30];1–11. Available from: https://onlinelibrary.wiley.com/doi/abs/10.1002/ppap.201900148

277. Sharma M, Gao S, Mäder E, Sharma H, Wei LY, Bijwe J. Carbon fiber surfaces and composite interphases. Compos Sci Technol. 2014;102:35–50.

278. Tiwari S, Bijwe J. Surface Treatment of Carbon Fibers - A Review. Procedia Technol. 2014;14:505–12.

279. Almeida DAL, Couto AB, Oishi SS, Ferreira NG. Chemical and electrochemical treatment effects on the morphology, structure, and electrochemical performance of

carbon fiber with different graphitization indexes. J Solid State Electrochem. 2018;22(11):3493–505.

280. Wang Y, Liu Y, Wang K, Song S, Tsiakaras P, Liu H. Preparation and characterization of a novel KOH activated graphite felt cathode for the electro-Fenton process. Appl Catal B Environ. 2015;165:360–8.

281. Kim NH, Mishra AK, Lee JH, Kuila T, Khanra P, Bose S. Chemical functionalization of graphene and its applications. Prog Mater Sci. 2012;57(7):1061–105.

282. Matos I, Bernardo M, Fonseca I. Porous carbon: A versatile material for catalysis. Catal Today. 2017;285:194–203.

283. Boehm H. Surface oxides on carbon and their analysis: a critical assessment. Carbon N Y. 2002;40(2):145–9.

284. Huang X. Fabrication and properties of carbon fibers. Materials (Basel). 2009;2(4):2369–403.

285. Compton R, Eklund J, Marken F. Sonoelectrochemical Processes: A Review Richard. Electroanal. 1997;9:509–22.

286. González-García J, Esclapez MD, Bonete P, Hernández YV, Garretón LG, Sáez V. Current topics on sonoelectrochemistry. Ultrasonics. 2010;50(2):318–22.

287. Xie J, Ding J, Attenburrow G, Mason T. Influence of power ultrasound on leather processing. Part I: Dyeing. J Am Leather Chem Assoc. 1999;94:146–57.

288. Murphy MA, Marken F, Mocak J. Sonoelectrochemistry of molecular and colloidal redox systems at carbon nanofiber-ceramic composite electrodes. Electrochim Acta. 2003;48(23):3411–7.

289. Liu J, Tian Y, Chen Y, Liang J, Zhang L, Fong H. A surface treatment technique of electrochemical oxidation to simultaneously improve the interfacial bonding strength and the tensile strength of PAN-based carbon fibers. Mater Chem Phys. 2010;122(2–3):548–55.

290. Dutt JSN, Cardosi MF, Wilkins S, Livingstone C, Davis J. Characterisation of carbon fibre composites for decentralised biomedical testing. Mater Chem Phys. 2006;97(2–3):267–72.

291. Banks C, Davies T, Wildgoose G, Compton R. Electrocatalysis at graphite and carbon

nanotube modified electrodes: edge-plane sites and tube ends are the reactive sitesNo Title. Chem Commun. 2005;(7):829–41.

292. Hyde M, Davies T, Compton R. Fabrication of random assemblies of metal nanobands: A general method. Angew Chemie-International Ed. 2005;44(40):6491–6.

293. Velický M, Toth PS, Woods CR, Novoselov KS, Dryfe RAW. Electrochemistry of the Basal Plane versus Edge Plane of Graphite Revisited. J Phys Chem C. 2019 May 9;123(18):11677–85.

294. Cline K, McDermott M, McCreery R. Anomalously Slow-Electron Transfer at Ordered Graphite-Electrodes - Influence of Electronic Factors and Reactive Sites. J Phys Chem. 1994;98(20):5314–9.

295. McDermott C, Kneten K, McCreery R. Electron-Transfer Kinetics of Aquated Fe+3/+2, Eu+3/+2, And V+3/+2 at Carbon Electrodes - Inner-Sphere Catalysis By Surface Oxides. J Electrochem Soc. 1993;140(9):2593–9.

296. Ranganathan S, Kuo T, McCreery R. Facile preparation of active glassy carbon electrodes with activated carbon and organic solvents. Anal Chem. 1999;71(16):3574–80.

297. Xiong L, Batchelor-Mcauley C, Ward KR, Downing C, Hartshorne RS, Lawrence NS, et al. Voltammetry at graphite electrodes: The oxidation of hexacyanoferrate (II) (ferrocyanide) does not exhibit pure outer-sphere electron transfer kinetics and is sensitive to pre-exposure of the electrode to organic solvents. J Electroanal Chem. 2011;661(1):144–9.

298. Ji X, Banks CE, Crossley A, Compton RG. Oxygenated edge plane sites slow the electron transfer of the ferro-/ferricyanide redox couple at graphite electrodes. ChemPhysChem. 2006;7(6):1337–44.

299. Chou A, Bocking T, Singh N, Gooding J. Demonstration of the importance of oxygenated species at the ends of carbon nanotubes for their favourable electrochemical properties. Chem Commun. 2005;(7):842–4.

300. Zhang G, Sun S, Yang D, Dodelet JP, Sacher E. The surface analytical characterization of carbon fibers functionalized by H2SO4/HNO3 treatment. Carbon N Y. 2008;46(2):196–205.

301. Bismarck A, Kumru ME, Springer J, Simitzis J. Surface properties of PAN-based carbon

fibers tuned by anodic oxidation in different alkaline electrolyte systems. Appl Surf Sci. 1999;143(1):45–55.

302. Zhang Z, Xi J, Zhou H, Qiu X. KOH etched graphite felt with improved wettability and activity for vanadium flow batteries. Electrochim Acta. 2016;218:15–23.

303. Mani GK, Morohoshi M, Yasoda Y, Yokoyama S, Kimura H, Tsuchiya K. ZnO-Based Microfluidic pH Sensor: A Versatile Approach for Quick Recognition of Circulating Tumor Cells in Blood. ACS Appl Mater Interfaces. 2017;9(6):5193–203.

304. Salvo P, Calisi N, Melai B, Cortigiani B, Mannini M, Caneschi A, et al. Temperature and pH sensors based on graphenic materials. Biosens Bioelectron. 2017;91(October 2016):870–7.

305. Northrop-Clewes CA, Thurnham DI. The discovery and characterization of riboflavin. Ann Nutr Metab. 2012 Nov;61(3):224–30.

306. Suwannasom N, Kao I, Pruß A, Georgieva R, Bäumler H. Riboflavin: The health benefits of a forgotten natural vitamin. Int J Mol Sci. 2020 Feb 1;21(3):950.

307. Mielgo-Ayuso J, Aparicio-Ugarriza R, Olza J, Aranceta-Bartrina J, Gil Á, Ortega RM, et al. Dietary intake and food sources of niacin, riboflavin, thiamin and vitamin B6 in a representative sample of the spanish population. The anthropometry, intake, and energy balance in Spain (ANIBES) study. Nutrients. 2018 Jul 1;10(7):846.

308. Toyosawa T, Suzuki M, Kodama K, Araki S. Effects of intravenous infusion of highly purified vitamin B2 on lipopolysaccharide-induced shock and bacterial infection in mice. Eur J Pharmacol [Internet]. 2004 May 25 [cited 2020 Feb 26];492(2–3):273–80. Available from: http://www.ncbi.nlm.nih.gov/pubmed/15178375

309. Martins SAR, Combs JC, Noguera G, Camacho W, Wittmann P, Walther R, et al. Antimicrobial efficacy of riboflavin/UVA combination (365 nm) in vitro for bacterial and fungal isolates: A potential new treatment for infectious keratitis. Investig Ophthalmol Vis Sci. 2008 Aug 1;49(8):3402–8.

310. Ahgilan A, Sabaratnam V, Periasamy V. Antimicrobial Properties of Vitamin B2. Int J Food Prop [Internet]. 2016 May 3 [cited 2020 Feb 26];19(5):1173–81. Available from: http://www.tandfonline.com/doi/full/10.1080/10942912.2015.1076459

311. Khan S, P MR, Rizvi A, Alam MM, Rizvi M, Naseem I. ROS mediated antibacterial activity of photoilluminated riboflavin: A photodynamic mechanism against

nosocomial infections. Toxicol Reports. 2019 Jan 9;6:136–42.

312. Antal IP, Bazel YR, Kormosh ZA. Electrochemical methods for determining group B vitamins. J Anal Chem. 2013 Jul;68(7):565–76.

313. Gribat LC, Babauta JT, Beyenal H, Wall NA. New rotating disk hematite film electrode for riboflavin detection. J Electroanal Chem. 2017;798(May):42–50.

314. Yu YY, Wang JX, Si RW, Yang Y, Zhang CL, Yong YC. Sensitive amperometric detection of riboflavin with a whole-cell electrochemical sensor. Anal Chim Acta. 2017;985:148–54.

315. Bao H, Zheng Z, Yang B, Liu D, Li F, Zhang X, et al. In situ monitoring of Shewanella oneidensis MR-1 biofilm growth on gold electrodes by using a Pt microelectrode. Bioelectrochemistry. 2016;109:95–100.

316. Celiešiūtė R, Radzevič A, Žukauskas A, Vaitekonis Š, Pauliukaite R. A Strategy to Employ Polymerised Riboflavin in the Development of Electrochemical Biosensors. Electroanalysis. 2017;29(9):2071–82.

317. Roushani M, Abdi Z. Novel electrochemical sensor based on graphene quantum dots/riboflavin nanocomposite for the detection of persulfate. Sensors Actuators, B Chem. 2014;201:503–10.

318. Valipour A, Roushani M. Using silver nanoparticle and thiol graphene quantum dots nanocomposite as a substratum to load antibody for detection of hepatitis C virus core antigen: Electrochemical oxidation of riboflavin was used as redox probe. Biosens Bioelectron. 2017;89(August 2016):946–51.

319. Roushani M, Valipour A. Voltammetric immunosensor for human chorionic gonadotropin using a glassy carbon electrode modified with silver nanoparticles and a nanocomposite composed of graphene, chitosan and ionic liquid, and using riboflavin as a redox probe. Microchim Acta. 2016;183(2):845–53.

320. Roushani M, Shahdost-Fard F. A novel ultrasensitive aptasensor based on silver nanoparticles measured via enhanced voltammetric response of electrochemical reduction of riboflavin as redox probe for cocaine detection. Sensors Actuators, B Chem. 2015;207(PartA):764–71.

321. Wu S, Xiao Y, Song P, Wang C, Yang Z, Slade RCT, et al. Riboflavin-mediated extracellular electron transfer process involving Pachysolen tannophilus. Electrochim

Acta. 2016;210:117–21.

322. Meng Y, Hun X, Zhang Y, Luo X. Toehold-aided DNA recycling amplification using hemin and G-quadruplex reporter DNA on magnetic beads as tags for chemiluminescent determination of riboflavin. Microchim Acta. 2016;183(11):2965–71.

323. Song N, Dares CJ, Sheridan M V., Meyer TJ. Proton-Coupled Electron Transfer Reduction of a Quinone by an Oxide-Bound Riboflavin Derivative. J Phys Chem C. 2016;120(42):23984–8.

324. Tan SLJ, Webster RD. Electrochemically induced chemically reversible proton-coupled electron transfer reactions of riboflavin (Vitamin B 2). J Am Chem Soc. 2012;134(13):5954–64.

325. Kormányos A, Hossain MS, Ghadimkhani G, Johnson JJ, Janáky C, de Tacconi NR, et al. Flavin Derivatives with Tailored Redox Properties: Synthesis, Characterization, and Electrochemical Behavior. Chem - A Eur J. 2016;22(27):9209–17.

326. Leite AM de O, Miguel MAL, Peixoto RS, Rosado AS, Silva JT, Paschoalin VMF. Microbiological, technological and therapeutic properties of kefir: A natural probiotic beverage. Brazilian J Microbiol. 2013 Oct 30;44(2):341–9.

327. Plessas S, Nouska C, Mantzourani I, Kourkoutas Y, Alexopoulos A, Bezirtzoglou E. Microbiological exploration of different types of Kefir grains. Fermentation. 2017;3(1):1–10.

328. Rosa DD, Dias MMSS, Grześkowiak ŁM, Reis SA, Conceição LL, Peluzio M do CGDCG. Milk kefir: Nutritional, microbiological and health benefits. Nutr Res Rev. 2017 Jun 1;30(1):82–96.

329. Piermaria JA, Pinotti A, Garcia MA, Abraham AG. Films based on kefiran, an exopolysaccharide obtained from kefir grain: Development and characterization. Food Hydrocoll. 2009 May;23(3):684–90.

330. Witthuhn RC, Schoeman T, Britz TJ. Characterisation of the microbial population at different stages of Kefir production and Kefir grain mass cultivation. Int Dairy J. 2005 Apr 1;15(4):383–9.

331. Prado MR, Blandón LM, Vandenberghe LPS, Rodrigues C, Castro GR, Thomaz-Soccol V, et al. Milk kefir: Composition, microbial cultures, biological activities, and related

products. Front Microbiol [Internet]. 2015 Oct 30 [cited 2020 Feb 26];6:1177. Available from: /pmc/articles/PMC4626640/?report=abstract

332. Fiorda FA, Vinicius de Melo Pereira G, Thomaz-Soccol V, Rakshit SK, Pagnoncelli MGB, Vandenberghe LP de S, et al. Microbiological, biochemical, and functional aspects of sugary kefir fermentation - A review. Food Microbiol. 2017 Sep 1;66:86–95.

333. Satir G, Guzel-Seydim ZB. How kefir fermentation can affect product composition? Small Rumin Res. 2016;134:1–7.

334. Streeter I, Leventis H, Wildgoose G, Pandurangappa M, Lawrence N, Jiang L, et al. A sensitive reagentless pH probe with a ca. 120 mV/pH unit response. J Solid State Electrochem. 2004 Aug;8(10).

335. Anderson A, Davis J. Next generation transdermal drug delivery – An electrochemical approach to ph manipulation for controlled release within smart patch technologies. In: IFMBE Proceedings. Springer Verlag; 2015. p. 919–22.

336. Bejugam M, Sewitz S, Shirude PS, Rodriguez R, Shahid R, Balasubramanian S. Trisubstituted isoalloxazines as a new class of G-quadruplex binding ligands: Small molecule regulation of c-kit oncogene expression. J Am Chem Soc. 2007;129(43):12926–7.

337. Cowden, W.B., Halladay, P.K, Cunningham, R.B, Hunt, N.H, Clark IA. Flavins as Potential Antimalarials. 2. 3-Methyl-lO-(substituted-phenyl)flavins. J Med Chem. 1991;34(6):1819.

338. Faki H. The development & evaluation of photoantimicrobial isoalloxazine dyes towards infection control. University of Central Lancashire; 2017.

339. Radzevič A, Niaura G, Ignatjev I, Rakickas T, Celieš iūtė R, Pauliukaite R. Electropolymerisation of the natural monomer riboflavin and its characterisation. Electrochim Acta. 2016;222:1818–30.

340. Yang Y, Wu Y, Hu Y, Cao Y, Poh CL, Cao B, et al. Engineering Electrode-Attached Microbial Consortia for High-Performance Xylose-Fed Microbial Fuel Cell. ACS Catal. 2015;5(11):6937–45.

341. Laureys D, De Vuyst L. Microbial species diversity, community dynamics, and metabolite kinetics of water Kefir fermentation. Appl Environ Microbiol. 2014;80(8):2564–72.

342. Pan TM, Wang CW, Mondal S, Pang ST. Super-Nernstian sensitivity in microfabricated electrochemical pH sensor based on CeTixOyfilm for biofluid monitoring. Electrochim Acta. 2018;261:482–90.

343. Lonsdale W, Wajrak M, Alameh K. Manufacture and application of RuO2solid-state metal-oxide pH sensor to common beverages. Talanta. 2018;180(December 2017):277–81.

344. Zhu Z, Liu X, Ye Z, Zhang J, Cao F, Zhang J. A fabrication of iridium oxide film pH micro-sensor on Pt ultramicroelectrode and its application on in-situ pH distribution of 316L stainless steel corrosion at open circuit potential. Sensors Actuators, B Chem. 2018;255:1974–82.

345. Chinnathambi S, Euverink GJW. Polyaniline functionalized electrochemically reduced graphene oxide chemiresistive sensor to monitor the pH in real time during microbial fermentations. Sensors Actuators, B Chem. 2018;264:38–44.

346. Manjakkal L, Sakthivel B, Gopalakrishnan N, Dahiya R. Printed flexible electrochemical pH sensors based on CuO nanorods. Sensors Actuators, B Chem. 2018;263:50–8.

347. Dang W, Manjakkal L, Navaraj WT, Lorenzelli L, Vinciguerra V, Dahiya R. Stretchable wireless system for sweat pH monitoring. Biosens Bioelectron. 2018;107(December 2017):192–202.

348. Cisternas R, Ballesteros L, Valenzuela ML, Kahlert H, Scholz F. Decreasing the time response of calibration-free pH sensors based on tungsten bronze nanocrystals. J Electroanal Chem. 2017;801(August):315–8.

349. Sha R, Komori K, Badhulika S. Amperometric pH Sensor Based on Graphene-Polyaniline Composite. IEEE Sens J. 2017;17(16):5038–43.

350. Chou J, Yan S, Liao Y, Lai C. Characterization of Flexible Arrayed pH Sensor Based on Nickel Oxide Films. 2018;18(2):605–12.

351. Mani GK, Miyakoda K, Saito A, Yasoda Y, Kajiwara K, Kimura M, et al. Microneedle pH Sensor: Direct, Label-Free, Real-Time Detection of Cerebrospinal Fluid and Bladder pH. ACS Appl Mater Interfaces. 2017;9(26):21651–9.

352. Padmanathan N, Shao H, Razeeb KM. Multifunctional Nickel Phosphate Nano/Microflakes 3D Electrode for Electrochemical Energy Storage, Nonenzymatic Glucose, and Sweat pH Sensors. ACS Appl Mater Interfaces. 2018;10(10):8599–610.

353. Bause S, Decker M, Gerlach F, Näther J, Köster F, Neubauer P, et al. Development of an iridium-based pH sensor for bioanalytical applications. J Solid State Electrochem. 2017;1–10.

354. Ahmed NM, Kabaa EA, Jaafar MS, Omar AF. Characteristics of Extended-Gate Field-Effect Transistor (EGFET) Based on Porous n-Type (111) Silicon for Use in pH Sensors. J Electron Mater. 2017;46(10):5804–13.

355. Rahimi R, Ochoa M, Parupudi T, Zhao X, Yazdi IK, Dokmeci MR, et al. A low-cost flexible pH sensor array for wound assessment. Sensors Actuators, B Chem. 2016;229:609–17.

356. Amiri M, Amali E, Nematollahzadeh A, Salehniya H. Poly-dopamine films: Voltammetric sensor for pH monitoring. Sensors Actuators, B Chem. 2016;228:53–8.

357. Phair J, Joshi M, Benson J, McDonald D, Davis J. Laser patterned carbon-polyethylene mesh electrodes for wound diagnostics. Mater Chem Phys. 2014 Feb 14;143(3):991–5.

358. Phair J, Benson J, McCormac C, Cundell J, Gracheva S, Wilkinson D, et al. Butyl grafted polyethylene films doped with carbon black: A foundation for the development of smart bandages. Sensors Actuators, B Chem. 2014 Mar 31;193:764–9.

359. Fava EL, Martimiano do Prado T, Almeida Silva T, Cruz de Moraes F, Censi Faria R, Fatibello-Filho O. New Disposable Electrochemical Paper-based Microfluidic Device with Multiplexed Electrodes for Biomarkers Determination in Urine Sample. Electroanalysis [Internet]. 2020 Mar 11 [cited 2020 Mar 11]; Available from: https://onlinelibrary.wiley.com/doi/abs/10.1002/elan.201900641

360. Nsabimana A, Lan Y, Du F, Wang C, Zhang W, Xu G. Alkaline phosphatase-based electrochemical sensors for health applications. Vol. 11, Analytical Methods. Royal Society of Chemistry; 2019. p. 1996–2006.

361. Cincotto FH, Fava EL, Moraes FC, Fatibello-Filho O, Faria RC. A new disposable microfluidic electrochemical paper-based device for the simultaneous determination of clinical biomarkers. Talanta. 2019 Apr 1;195:62–8.

362. Yang C, Feng W, Li Y, Tian X, Zhou Z, Lu L, et al. A promising method for diabetes early diagnosis via sensitive detection of urine glucose by Fe–Pd/rGO. Dye Pigment. 2019 May 1;164:20–6.

363. Kim HY, Jang KJ, Veerapandian M, Kim HC, Seo YT, Lee KN, et al. Reusable urine glucose sensor based on functionalized graphene oxide conjugated Au electrode with protective layers. Biotechnol Reports. 2014 Sep;3:49–53.

364. Arya SK, Estrela P. Electrochemical ELISA-based platform for bladder cancer protein biomarker detection in urine. Biosens Bioelectron. 2018 Oct 15;117:620–7.

365. Singh S, Gill AAS, Nlooto M, Karpoormath R. Prostate cancer biomarkers detection using nanoparticles based electrochemical biosensors. Biosens Bioelectron. 2019 Jul 15;137:213–21.

366. Pan Y, Sonn GA, Sin MLY, Mach KE, Shih MC, Gau V, et al. Electrochemical immunosensor detection of urinary lactoferrin in clinical samples for urinary tract infection diagnosis. Biosens Bioelectron. 2010 Oct 15;26(2):649–54.

367. Altobelli E, Mohan R, Mach KE, Sin MLY, Anikst V, Buscarini M, et al. Integrated Biosensor Assay for Rapid Uropathogen Identification and Phenotypic Antimicrobial Susceptibility Testing. Eur Urol Focus. 2017 Apr 1;3(2–3):293–9.

368. Milo S, Thet NT, Liu D, Nzakizwanayo J, Jones B V., Jenkins ATA. An in-situ infection detection sensor coating for urinary catheters. Biosens Bioelectron. 2016 Jul 15;81:166–72.

369. Chaudhari R, Joshi A, Srivastava R. pH and Urea Estimation in Urine Samples using Single Fluorophore and Ratiometric Fluorescent Biosensors. Sci Rep. 2017 Jul 19;7(1):1–9.

370. Fischbach FT, Dunning MB. Overview of Chemistry Studies. In: A Manual of Laboratory and Diagnostic Tests. 8th ed. Philadelphia: Wolters Kluwer Health/Lippincott Williams & Wilkins; 2009. p. 378.

371. Haddadin Y, Regunath H. Central Line Associated Blood Stream Infections (CLABSI) [Internet]. StatPearls. StatPearls Publishing; 2018 [cited 2018 Nov 13]. Available from: http://www.ncbi.nlm.nih.gov/pubmed/28613641

372. Bouza E, Alvarado N, Alcala L, Perez MJ, Rincon C, Munoz P. A Randomized and Prospective Study of 3 Procedures for the Diagnosis of Catheter-Related Bloodstream Infection without Catheter Withdrawal. Clin Infect Dis [Internet]. 2007 Mar 15 [cited 2018 Nov 13];44(6):820–6. Available from: https://academic.oup.com/cid/article-lookup/doi/10.1086/511865

373. O'Grady NPP, Alexander M, Dellinger EPP, Gerberding JLL, Heard SOO, Maki DGG, et al. Guidelines for the Prevention of Intravascular Catheter–Related Infections. Clin Infect Dis. 2002 Dec;35(11):1281–307.

374. Rowley-Neale SJ, Brownson DAC, Smith G, Banks CE. Graphene Oxide Bulk-Modified Screen-Printed Electrodes Provide Beneficial Electroanalytical Sensing Capabilities. Biosensors [Internet]. 2020 Mar 12 [cited 2020 Mar 26];10(3):27. Available from: https://www.mdpi.com/2079-6374/10/3/27

375. Metto M, Eramias S, Gelagay B, Washe AP. Voltammetric Determination of Uric Acid in Clinical Serum Samples Using DMF Modified Screen Printed Carbon Electrodes. Int J Electrochem [Internet]. 2019 Feb 3 [cited 2020 Mar 26];2019:1–8. Available from: https://doi.org/10.1155/2019/6318515

376. Kamanina OA, Kamanin SS, Kharkova AS, Arlyapov VA. Glucose biosensor based on screen-printed electrode modified with silicone sol–gel conducting matrix containing carbon nanotubes. 3 Biotech. 2019 Jul 1;9(7):1–7.

377. Chou JC, Lin SH, Kuo PY, Lai CH, Nien YH, Lai TY, et al. Integrating a Plastic Glucose Biosensor Based on Arrayed Screen-Printed Electrodes Utilizing Magnetic Beads with a Microfluidic Device. IEEE J Electron Devices Soc. 2019 Nov 12;7:1151–60.

378. Aller-Pellitero M, Fremeau J, Villa R, Guirado G, Lakard B, Hihn JY, et al. Electrochromic biosensors based on screen-printed Prussian Blue electrodes. Sensors Actuators, B Chem. 2019 Jul 1;290:591–7.

379. Müller A, Sachse S, Decker M, Matysik F-M, Vonau W. Comparison of H2O2 screen-printed sensors with different Prussian blue nanoparticles as electrode material. J Electrochem Sci Eng. 2020 Mar 9;10(2):207.

380. Lorenzetti AS, Sierra T, Domini CE, Lista AG, Crevillen AG, Escarpa A. Electrochemically Reduced Graphene Oxide-Based Screen-Printed Electrodes for Total Tetracycline Determination by Adsorptive Transfer Stripping Differential Pulse Voltammetry. Sensors [Internet]. 2019 Dec 13 [cited 2020 Mar 26];20(1):76. Available from: https://www.mdpi.com/1424-8220/20/1/76

381. Beitollahi H, Garkani-Nejad F, Tajik S, Ganjali MR. Voltammetric determination of acetaminophen and tryptophan using a graphite screen printed electrode modified with functionalized graphene oxide nanosheets within a Fe3O4SiO2 nanocomposite. Iran J Pharm Res. 2019 Dec 1;18(1):80–90.

382. Su JY, Jin GP, Chen T, Liu XD, Chen CN, Tian JJ. The characterization and application of prussian blue at graphene coated carbon fibers in a separated adsorption and electrically switched ion exchange desorption processes of cesium. Electrochim Acta. 2017;230:399–406.

383. Jirakunakorn R, Khumngern S, Choosang J, Thavarungkul P, Kanatharana P, Numnuam A. Uric acid enzyme biosensor based on a screen-printed electrode coated with Prussian blue and modified with chitosan-graphene composite cryogel. Microchem J. 2020 May 1;154:104624.

384. Tajik S, Safaei M, Beitollahi H. A sensitive voltammetric sertraline nanosensor based on ZnFe2O4 nanoparticles modified screen printed electrode. Meas J Int Meas Confed. 2019 Sep 1;143:51–7.

385. Motaharian A, Hosseini MRM, Naseri K. Determination of psychotropic drug chlorpromazine using screen printed carbon electrodes modified with novel MIP-MWCNTs nano-composite prepared by suspension polymerization method. Sensors Actuators, B Chem. 2019 Jun 1;288:356–62.

386. Ibáñez-Redín G, Furuta RHM, Wilson D, Shimizu FM, Materon EM, Arantes LMRB, et al. Screen-printed interdigitated electrodes modified with nanostructured carbon nano-onion films for detecting the cancer biomarker CA19-9. Mater Sci Eng C. 2019 Jun 1;99:1502–8.

387. Zubko EI, Zubko MK. Co-operative inhibitory effects of hydrogen peroxide and iodine against bacterial and yeast species. BMC Res Notes [Internet]. 2013 Jul 15 [cited 2018 Nov 26];6(1):272. Available from: http://www.ncbi.nlm.nih.gov/pubmed/23856115

388. Perumal PK, Wand ME, Sutton JM, Bock LJ. Evaluation of the effectiveness of hydrogen-peroxide-based disinfectants on biofilms formed by Gram-negative pathogens. J Hosp Infect [Internet]. 2014;87(4):227–33. Available from: http://dx.doi.org/10.1016/j.jhin.2014.05.004

389. Chua SL, Ding Y, Liu Y, Cai Z, Zhou J, Swarup S, et al. Reactive oxygen species drive evolution of pro-biofilm variants in pathogens by modulating cyclic-di-GMP levels. Open Biol [Internet]. 2016 Nov 1 [cited 2020 Jul 28];6(11). Available from: /pmc/articles/PMC5133437/?report=abstract

390. The Joint Commission. CVC Maintenance Bundles. CLABSI Toolkit – Prev Cent Assoc Bloodstream Infect Useful Tools, An Int Perspect [Internet]. 2013;1–7. Available from:

https://www.jointcommission.org/assets/1/6/CLABSI_Toolkit_Tool_3-22_CVC_Maintenance_Bundles.pdf

391. Seymou VM, Dhallu TS, Mos HA, Tebb SE, Elliot TSJ. A prospective clinical study to investigate the microbial contamination of a needleless connector. J Hosp Infect [Internet]. 2000 Jun 1 [cited 2020 Jul 30];45(2):165–8. Available from: http://www.journalofhospitalinfection.com/article/S0195670100907266/fulltext

392. Korsak N, Taminiau B, Leclercq M, Nezer C, Crevecoeur S, Ferauche C, et al. Short communication: Evaluation of the microbiota of kefir samples using metagenetic analysis targeting the 16S and 26S ribosomal DNA fragments. J Dairy Sci. 2015 Jun 1;98(6):3684–9.

393. Fiorda FA, de Melo Pereira GV, Thomaz-Soccol V, Medeiros AP, Rakshit SK, Soccol CR. Development of kefir-based probiotic beverages with DNA protection and antioxidant activities using soybean hydrolyzed extract, colostrum and honey. LWT - Food Sci Technol. 2016 May 1;68:690–7.

394. BioAssay. Peroxide Assay Kit [Internet]. 2007 [cited 2020 Mar 23]. Available from: https://www.sigmaaldrich.com/catalog/product/sigma/mak311

Publications Resulting from this Research

Casimero C, McConville A, Fearon J, Lawrence C, Taylor C, Smith R et al. Sensor systems for bacterial reactors: A new flavin-phenol composite film for the in situ voltammetric measurement of pH. Analytica Chimica Acta. 2018;1027:1-8.

Bigham T, **Casimero C**, Dooley J, Ternan N, Snelling W, Davis J. Microbial water quality: Voltammetric detection of coliforms based on riboflavin–ferrocyanide redox couples. Electrochemistry Communications. 2019;101:99-103.

Casimero C, Bigham T, McGlynn R, Dooley J, Ternan N, Snelling W et al. Electroanalytical properties of chlorophenol red at disposable carbon electrodes: Implications for Escherichia coli detection. Bioelectrochemistry. 2019;130:107321.

McLister A, **Casimero C**, McConville A, Taylor C, Lawrence C, Smith R et al. Design of a smart sensor mesh for the measurement of pH in ostomy applications. Journal of Materials Science. 2019;54(14):10410-10419.

Anderson A, Hegarty C, **Casimero C**, Davis J. Electrochemically controlled dissolution of nanocarbon–cellulose acetate phthalate microneedle arrays. ACS Applied Materials & Interfaces. 2019;11(39):35540-35547.

Cameron S, Barber R, Scott C, **Casimero C**, Hegarty C, O'Loughlin L, et al. Laser scribed polyimide as a platform for monitoring pH within smart bandages. In: 2020 7th International Conference on Signal Processing and Integrated Networks, SPIN 2020. Institute of Electrical and Electronics Engineers Inc.; 2020. p. 654–658.

Devine A, Hegarty C, **Casimero C**, Molyneaux RL, Smith RB, Cardosi MF, et al. Electrochemically initiated release: exploring new modalities for controlled drug release. J Electroanal Chem. 2020 Feb 4;113926.

Casimero C, Hegarty C, McGlynn R, Davis J. Ultrasonic exfoliation of carbon fiber: electroanalytical perspectives. Journal of Applied Electrochemistry. 2020;50(3):383-394.

Casimero C, Ruddock T, Hegarty C, Barber R, Devine A, Davis J. Minimising Blood Stream Infection: Developing New Materials for Intravascular Catheters. Medicines. 2020;7(9):49.